ULTRA SHORT LASER PULSES AND COUPLED-CAVITY MODE LOCKING IN A KCI:TI COLOUR-CENTRE LASER

Xiaonong Zhu

A Thesis Submitted for the Degree of PhD
at the
University of St Andrews

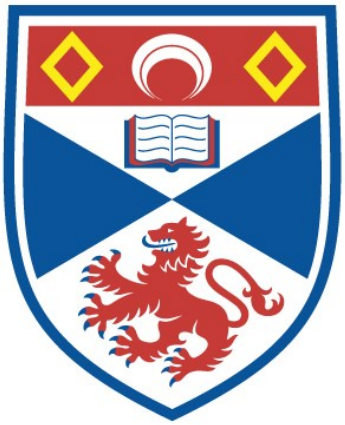

1991

Ultrashort Laser Pulses and Coupled-Cavity Mode Locking in a KCl:Tl Colour-Centre Laser

Xiaonong Zhu, B.Sc., M.Sc.

— A thesis submitted for the degree of Doctor of Philosophy to the University of St. Andrews

Department of Physics and Astronomy

University of St. Andrews

North Haugh, St. Andrews

Fife, KY16 9SS

Scotland, U. K.

1 May 1991

ProQuest LLC.
789 East Eisenhower Parkway
P.O. Box 1346
Ann Arbor, MI 48106 – 1346

Declaration

I, Xiaonong Zhu, hereby certify that this thesis has been composed by myself, that it is a record of my own work and that it has not been presented in partial or complete fulfilment for any other degree or prefessional qualification. I was admitted to the Faculty of Science of the University of St. Andrews as a candidate for the degree of Ph.D under ordinance general No. 12 on 1st October 1987.

Signed Date 1st May 1991

Certificate

I hereby certify that the candidate, Xiaonong Zhu, has fulfilled the conditions of the Resolution and Regulations appropriate to the degree of Ph. D..

Signature of supervisor Date 1st May 1991.

Copyright

In submitting this thesis to the University of St. Andrews I understand that I am giving permission for it to be made available for use in accordance with the regulations of the University Library for the time being in force, subject to any copyright vested in the work not being affected thereby. I also understand that the title and abstract will be published, and that a copy of the work may be made and supplied to any bona fide library or research worker.

To the world, to my motherland.

献给世界，献给祖国。

Acknowledgements

I would like to thank my supervisor, Professor Wilson Sibbett, for his persistently encouraging supervision during the course of this work, and in particular for his many valuable comments and suggestions on the contents of this thesis.

I am indebted to David Crust, Dr. Peter Kean, Dr. Andrew Finch and Dr. Bill Sleat for their help and collaboration.

I would also like to thank all other colleagues and friends for assistance, understanding and constructive discussions directly or indirectly related to my study.

Finally, financial support from the Sino-British Friendship Scholarship Scheme is gratefully acknowledged.

Abstract

The basic principles of generation, characterisation and propagation of ultrashort laser pulses and related experimental studies of mode locking of a coupled-cavity KCl:Tl colour-centre laser are presented. Extensive experimental investigations of mode locking with a two-cavity arrangement similar to a previously reported soliton laser has indicated that such a scheme is a very general technique for the generation of picosecond-femtosecond pulses. With or without the formation of optical solitons in the control fibre a variety of spectral and temporal features for the laser output pulses can be obtained. This new type of pulse generation technique has thus been named as "coupled-cavity mode locking" and it has been shown in this work that the coupled-cavity mode-locked KCl:Tl colour-centre laser is a very useful femtosecond laser source.

Through replacing the traditional electron-optical streak camera tube by an optical Kerr material and using the optical (pulse) beam to scan the pulse(s) to be measured, a novel pulse measurement method have been proposed. For this new measurement scheme no electron-photon transformation and any other electronic systems are involved, and therefore it is expected to have the advantages of easy operation and high resolution.

Study of the relationship between the temporal and the spectral features of an optical field suggests that a Fourier transform of a first-order spectral autocorrelation of a femtosecond pulse will give rise to the intensity profile of the pulse. A schematic for the measurement of the first-order spectral autocorrelation is also configurated.

A strong similarity between the impact of dispersion on the temporal feature and that of self-phase modulation on the spectral feature of optical pulses has been found. This leads to two important inferences: first, the spectral extension induced by self-phase modulation is linearly proportional to the peak optical intensity only when the associated nonlinear phase shift is sufficiently large, second, if the incident pulses are appropriately chirped a suitable length of SPM-medium can be used to compress the incident spectrum (rather than broaden it).

To initiate coupled-cavity mode locking a minimum optical power coupled into the control cavity is required. The specific value of this threshold is not only dependent on the properties of the nonlinear medium such as the length of the fibre, the magnitude of the Kerr coefficient, but also on the main cavity parameters, e. g. the main cavity power level and the effective gain bandwidth. Such a fact simply illustrates that to understand the physical mechanisms involved in the coupled-cavity mode locking the interactive function of various factors in both cavities must be considered. The upper-limit of the nonlinear phase shift, Φ_{NL}, experienced by the pulses coupled into the control cavity is found to be $\Phi_{NL} \leq 2\pi$. Above this value, further increase of the intrafibre power would lead to the laser operation in an unstable regime. In addtion, if the peak optical intensity inside the fibre core is sufficiently high the other nonlinear effects such as modulational instability and self-Raman action can occur besides self-phase modulation. In these cases the process of mode locking enhancement may be frustrated.

By incorporating an Er-doped mono-mode optical fibre in the control cavity of such a coupled-cavity mode-locked KCl:Tl laser has led to the generation of 75 fs pulses at 1.5 μm. This result represents the shortest pulses produced with this method in a non-soliton regime. The influence of spectral control on the coupled-cavity mode locking process has been thoroughly examined. It is clearly indicated that an optimum value of the effective gain bandwidth exists. While there is excess band the output pulses from the CCM, KCl:Tl laser will become frequency-chirped. By using an appropriate length of glass rod either inside or outside the laser cavities the frequency chirp can be effectively removed and in either cases sub-100 fs, near bandwidth limited pulses can be obtained.

Direct application of the CCM, KCl:Tl laser has been made in the study of femtosecond pulse propagation in various optical fibre types. In the single pass experiments the incident pulses from the CCM laser with a variable power level is controlled to have a duration of 120 fs and a bandwidth-duration product ~0.35. Interestingly, in two fibre samples where bright optical solitons can be formed spectral narrowing has been recorded for the exiting pulses. For one of the Er-doped fibre sample extreme spectral extension covering a wavelength of 1.3 - 1.7 μm was measured. Within

such a spectral range the longer wavelength components show the typical SPM-related spectral profile whereas in the shorter wavelength region a distinct feature at ~1.35 μm exists. Such a novel feature of spectral extension has been attributed to a new type of nonlinear process, which is designeted as *self-phase-modulation mediated four wave mixing*. It has been explained that this observation may lead to a new scheme by which ultrashort pulses around 1.3 μm may be generated.

Contents

Part I
Field Review

Chapter 1

General Introduction

The year 1990 is the 30 year anniversary of the operation of the first laser (Maiman 1960). In looking back over the past three decades it is clear that tremendous achievements have been made in this field. The influence of lasers, together with other related scientific and technical inventions on human society continues to grow (Ausubel and Langford 1987). Among the many significant laser and laser-related research areas, one particularly fast advancing branch is the generation and the application of ultrashort laser pulses (Shapiro 1977, Grischkowsky, Fork, Shank, Mourou, Diels 1985, Sibbett 1991).

1.1 Ultrashort laser pulses

Although it is common that, in many textbooks and other introductionary publications, lasers are often mainly described as special light sources which can generate "monochromatic" light beams having very high emission intensity. Their capability for producing ultrashort pulses is another striking feature of a laser system which offers advantages over purely electronic devices (Siegman 1987).

In contrast to the ordinary single frequency or pure colour laser beam, ultrashort laser pulses of duration equal or less than a few tens of picoseconds (1 ps = 10^{-12} s) can have broad spectral bandwidths that extend in some cases to as much as several teraHertz (Zhu *et al* 1989b). These ultrashort laser pulse sources represent a very useful diagnostics in the study of various transient events encountered within fields of photophysics, photochemistry, photobiology and optoelectronics (Alfano 1982, Doust and West 1983, Sibbett 1987). The decay and dephasing of excited states of atoms and molecules (Shank *et al* 1979, Weiner and Ippen 1984), the moleculeur vibration and rotation (Robbins *et al* 1980, Zewail 1990), the relaxation of optically induced birefringence (Eisenthal 1977), the intramolecular charge transfer (Barbara 1990, Okada *et al* 1990) and the primary

process of photosynthsis (Campillo and Shapiro 1977) are some of the examples of the ultrafast dynamical processes in nature. A more extensive list of various sorts of fast dynamics in the timescale of 10^{-8} - 10^{-15} s is shown as Fig. 1.1 The majority of these ultrafast phenomena would not be accessible to study without the availability of ultrashort laser pulses[1] (Shank 1983, 1987, Gruebele and Zewail 1990). In an analogy as to how the telescopes and microscopes invented two centuries ago have influenced almost every aspect of science, the far-reaching impact of the ultrashort pulse laser sources on the expansion of scientific knowledge propably can be only partially imagined at the moment. However, if we say that telescopes enable one to see things far away and microscopes to see small things, then the ultrashort pulses laser sources help us to observe events that occur in ultrafast regimes.

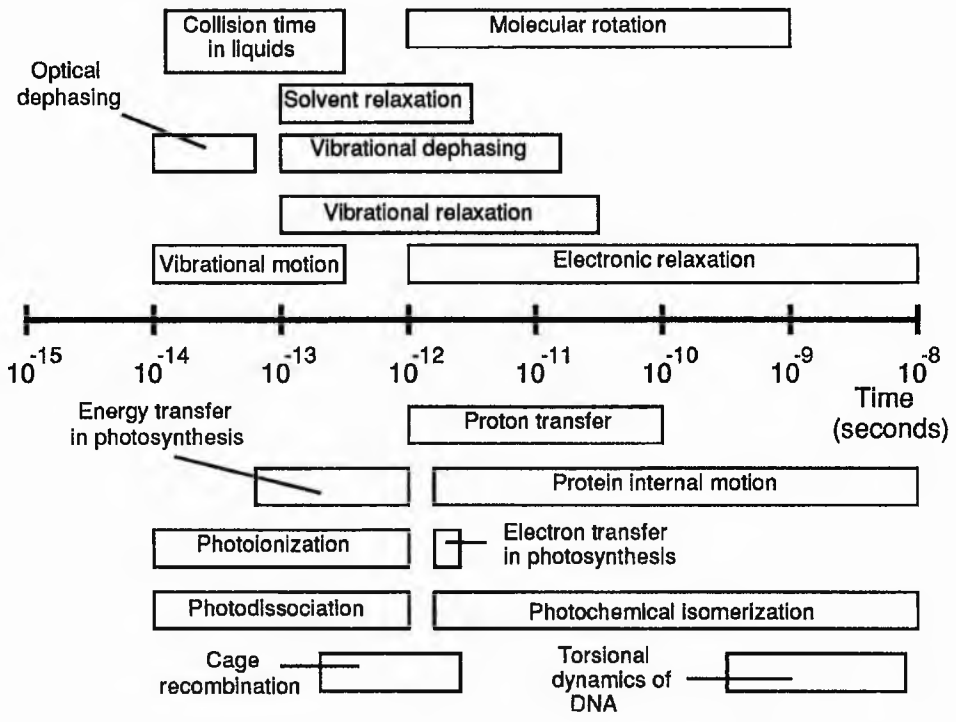

Fig. 1.1. Timescales of various ultrafast phenomena in physics, chemistry and biology. The box lengths indicate the time ranges (from Fleming and Wolynes 1990).

[1] As scientists take more and more of their research interests in the microscopic respect of nature, it would be expected that they will meet increasing amount of ultrafast processes, because the events under their study in these situations often occur within a very small spatial range (in an order of the size of atoms or part of molecules).

To certain extent, an ultrashort laser pulse can be viewed as a δ-function in the time domain and a special kind of "white light" in the sense of its large spectral extension in the frequency domain. As light impulses, ultrashort pulses have been used to test the response time of new generation fast photodetectors (Parker 1990) and in the development of high-speed electronic devices as well as the associated electronical measuring systems (Valdmanis 1978, Auston *et al* 1980, DeFonzo 1988). Pulses having durations around 20 ps have also been used to measure the spatial distances between the earth and satellites with a precision of ~ 1cm (Krause *et al* 1984).

Another important feature of ultrashort light pulses is that of high peak optical power. Using the technique called chirped pulse amplification, pulses having durations of several picoseconds have been amplified to a peak power in excess of 10^{13} W (Bado *et al* 1990). Such intense pulses under optimum focusing conditions can produce extremely high energy density in a small volume of a medium and are able to tear atoms apart and thereafter to induce many new interesting phenomena (Hutchinson 1989). Also, using high power ultrashort laser pulses to realize the controlled and efficient nuclear fusion continues to be one of the major technical objectives of scientists and engineers (Nuckolls *et al* 1972). Picosecond - femtosecond pulses output directly from a laser, at relatively low average power, have substantial peak power and are largely used in the study of many nonlinear optical effects[2] (Auston 1977). Given that the repetition rate is high for such lower power systems then good signal-to-noise diagnostics can be exploited.

Ultrashort laser pulses can be also taken as optical digits to be used in communication and information systems. In this case, because the extent of signal "1"s is so narrow (say ~ 10 ps) that the time interval between the successive bits can be very small (100 ps) and so the bit rate can be higher than 10 GHz. This will improve that of the current communication system at least by two orders (Mollenauer 1985). Because the studies of the non-dispersive ultrashort pulses (optical solitons) and optical fibre amplifiers have

[2] On the other hand, once the pulse inside a laser cavity is sufficiently short the effects of optical nonlinearities will inevitably take place. The interplay between ultrashort laser pulses and various kinds of nonlinear effects such as self-phase-modulation, self Raman effect etc. is actually a part of highlight in the current study of the ultrafast optical technique.

been making significant progress (Mollenauer *et al* 1986, Nakazawa 1990, Baker 1990) the new generation of digital optical communication may come into public service during this decade.

1.2 Brief overview of the development of ultrashort pulse laser sources

Pulses having different durations can generally be produced by employing different methods. Short pulse generation techniques and the associated typical pulse durations are shown in Table 1, where the cavity period, T, is used to be a timescale reference. The precise pulse duration relating to each particular technique is dependent on the characteristics of laser medium and the operational status.

Table 1.1 Laser pulse generation techniques and the corresponding pulse durations

Technique	Pulse duration	
Q-switching	10-100 ns	(> T)*
Cavity-dumping	1-10 ns	(T)
Intracavity-injection	0.1-1 ns	(T/10)
Gain-switching†	10 ps - 0.1 ns	(≥ T)
Mode-locking	20 fs - 100 ps	(T/[10^2-10^5])

* T ≡ round-trip period of laser resonator.

† Suitable for short cavities (T ≤ 10 ps), mainly used for semiconductor lasers.

From Table 1.1, it can be seen that the major means for producing ps-fs pulses is the technique called *mode-locking*. This technique which was developed in the mid 1960's and has been implemented in a varity of ways (see Table 1.2), including *active mode locking*, *passive mode locking*, *synchronous mode locking*, *colliding-pulse mode locking* and *coupled-cavity mode locking*, or a mixture of some of them, often named as *hybrid mode locking*[3]. In the consideration of achieving enough energy for individual pulses,

[3] It is worth mentioning that nowadays people tend to use the words "active" and "passive" in a more general sense. If mode locking is achieved without any modulational drive to any devices inside a laser system it can be termed as "passive", otherwise it will be regarded as "active". Therefore, it follows that all the mode-locking methods can be divided into the two groups, either "passive" or "active". The synchronous mode locking belongs to active, the colliding-pulse mode locking is passive and the coupled-cavity mode locking can be either active or passive depending on individual systems.

each of these mode locking schemes can be combined with the other techniques shown in Table 1.1. For example, this is the case when *Q-switched mode-locked* or *cavity-dumped mode-locked* lasers are involved. The term *CW mode locking* is taken to indicate that the laser is not operated in these combined schemes and the pump beam is a continuous wave.

Table 1.2 Mode-locking family

Member	Main characteristics
Spontaneous mode locking	Without using any modulational devices, unreliable performance (self-pulsing condition not under control), pulse duration varies, largely depends on the properties of gain media.
Active mode locking	Pulse duration normally longer than 10 ps, available for high output power, requires external modulational driver, prone to phase jitter problems.
Passive mode locking	Pulse duration easily shorter than 1 ps, wavelength tunable in certain range, lower phase jitter, applicability limited by available saturable absorbers*, low average output power.
Synchronous mode locking	Pulse duration shorter than pump pulses, high energy efficiency, requires a mode-locked pump laser, critically dependent on cavity lengths.
Colliding-pulse mode locking	Able to generate shortest pulses (< 100 fs), having drawbacks of passive mode locking.
Coupled-cavity mode locking	Pulse duration comparable to colliding-pulse mode locking, applicable to variety of laser types, no specific requirements on the type of nonlinearities used in control cavity, sacrifice ~50% laser out put power, cavity length servo system required.

*When liquid dyes are used as absorbers it is cumbersome to change them regularly. This is also true for synchronous mode-locking dye lasers.

As shown in Table 1.2, in addition to the various mode-locking approaches mentioned above there is another special kind of mode locking, called spontaneous mode locking or self (mode) locking. This mode locking is achieved without using any modulational devices either active or passive inside laser cavity and the whole mode locking process is

completely self-starting and sustaining. A great many of discussions about spontaneous mode locking were carried out in the period of 1965-1970, first on He-Ne laser (Crowell 1965) and then on the other laser types (Statz and Tang 1965, Gaddy and Schaefer 1966, Duguay *et al* 1967). Because spontaneous mode locking is essentially not a controllable process and often relates to unreliable performance, it would be better to regard it as a common phenomenon which occurs in many multimode lasers rather than to treat it as a particular mode-locking technique.

The active mode locking first achieved by DiDomenico (1964) and Hargrove *et al* (1964), and passive mode locking by Mocker and Collins (1965) and DeMaria *et al* (1966) are the two oldest members in the mode-locking family. The development of these two mode-locking techniques benefited a lot from the studies of the mechanisms behind spontaneous mode locking (Lamb 1964, Sargent *et al* 1974). Nowadays, both active and passive mode lockings, or the conbinations of them, have been well developed and incorporated in most of commercial ultrashort pulse laser sources. The synchronous mode locking reported initially in 1968 (Soffer and Linn 1968) was intensively studied in the 1970's and as more different types of mode-locked lasers became commercially available this technique that needs a mode-locked master laser to pump a slave laser has become widely used in many research laboratories. The colliding-pulse mode locking, which can be regarded as a new generation of traditional passive mode locking, was first reported by Fork *et al* (1981). It has played a major role in the generation of femtosecond pulses in the last few years and using this technique in a dye laser, the shortest ever laser pulses of 19 fs have been produced (Finch *et al* 1988). The coupled-cavity mode locking is the youngest member in the mode locking family at the moment. This new mode locking scheme is, in fact, a generalization of the soliton laser (Mollenauer and Stolen 1984). It has been developed dramatically since it was first operated two years ago by Kean *et al* (1988, 1989), and independently by Blow and Wood (1988). The main subject of this thesis will be devoted to the study of this new mode locking technique.

At this stage, it is necessary to point it out that all types of mode locking described above, no matter what they are and being conducted on what sort of laser system, are

related to locking of longitudinal modes in a laser. In another words, these locked modes all have the same transverse pattern, which in most of cases is limited to be a fundamental transverse mode. In practice, mode locking can be also achieved for a set of transverse modes which corresponding to the same longitudinal pattern (Auston 1968). This kind of mode locking is named as *transverse mode locking* in contrast to those listed in Table 1.2, which all belong to *longitudinal mode locking*. In the cases where several longitudinal and transverse modes exist it is possible to achieve *simultaneous longitudinal and transverse mode locking* (Smitch 1968). Nevertheless, in spite of the interesting physics encountered in the mode locking which involves different transverse modes, the sophisticates of these methods have actually got them out the way to any practical uses. In this thesis wherever the term mode locking occurs it will implicitly mean longitudinal mode locking.

The early history of the research on the generation, measurement of short laser pulses, as well as some of their uses can be found in the review article by Harris (1966), the texts edited by Goodwin (1974) and that by Shapiro (1977). The series of proceedings of the conferences on *Picosecond Phenomena* (Shank *et al* 1978, Hochstrasser *et al* 1980 and Eisenthal *et al* 1982) and then on *Ultrafast Phenomena* (Auston and Eisenthal 1984, Fleming and Siegman 1986, Yajima *et al* 1988, Harris *et al* 1990) are certainly the best literature where an overview of the development of picosecond to femtosecond techniques and their applications can be obtained. A more comprehensive review on the generation of ultrashort laser pulses in both theoretical and experimental respects was given by New (1983). Introductions to some of the more recent advances, particularly that related with the newly developed coupled-cavity mode locking, has been addressed by Miller and Sibbett (1988), Sibbett (1990).

It is known that efforts towards producing short and ultrashort laser pulses were made soon after the invention of the first laser. The recorded shortest pulse duration has dropped from just below 1 ns in the mid 1960's to subpicosecond in 1974, and to several tens of femtoseconds in the early 1980's (Fork *et al* 1983 and New 1990). If we say that the years of the 1970's can be taken as an era of picosecond pulses then since 1980 we

have entered the femtosecond-pulse decade (Shank *et al* 1984)[4]. Up to now, the shortest light pulses which thus have been obtained are around 20 fs directly from a laser and 6 fs after extracavity compression (Fork *et al* 1987).

A survey of the total publications has been carried out for each year after 1981 on the subject of mode locking as shown in Fig. 1.2 [This figure was based on counting the number of the articles under the subject word of "Laser mode locking" assembled in the Physics Abstracts (INSPEC)]. It can be seen that the annual publication numbers since 1985 are substantially larger than those in the 1980-84 period. Studies of the different mode locking techniques used in diverse types of laser systems, like solid-state lasers, dye lasers, semiconductor diode lasers and gas lasers, are still ongoing world-wide on a major scale. On the other hand, the slight decrease in research publications after 1986 indicated in Fig. 1.2 probably means that the mode-locking methodologies are now reaching a state of some maturity.

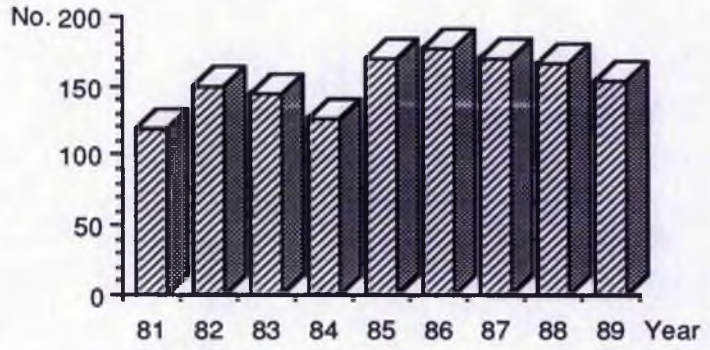

Fig. 1.2. Number of publications under the subject of "laser mode locking."

The main objectives of much of the current reseach are not in the pursuit of the shortest ever pulse durations but rather more, towards (i) improving the performance of the existing ultrashort pulse laser sources and (ii) developing new systems which can have high output power, broad wavelength coverage and tunability, and good structural quality. Also for these aims, studies of frequency chirp compensation (Dietel *et al* 1983, Diels *et al* 1985) and extracavity compression (Grischkowsky and Balant 1982, Kafka *et*

[4] This is also illustrated by the fact that the biennial conference on "Picosecond Phenomena" initiated in 1978 had to change its title to "Ultrafast Phenomena" in 1984 in order to cover the new advances in the generation and applications of femtosecond laser pulses.

al 1984, and Piche and Ouelette 1986) have become critically important research subjects in ultrashort pulse geneation. In addition, the exploitation of nonlinear effects such as harmonic generation (Yakymyshyn and Pollock 1989), parametric oscillators (Vanherzeele 1990) and optical continua (Penzkofer and Kaiser 1977) has become a key complementary means of achieving ultrashort pulses at selected wavelength regions.

The two pie charts shown in Fig. 1.3, 1.4 were obtained by categorizing the amount of the publications in 1989 (again under the subject words "laser mode locking" assembled in the Physics Abstracts) according to laser types and wavelengths respectively. In Fig. 1.3, the solid-state lasers mainly include Nd:YAG, Nd:Glass, Nd:YLF and all kinds of colour centre lasers (under various pumping schemes), the gas lasers consist of Ar^+, Kr^+, CO_2 and excimer lasers. The class termed as "others" covers fibre lasers, general discussions on mode-locking theories or techniques and so forth. Because most of solid-state lasers and fibre lasers operate at near-infrared and dye lasers in the visible region, it would be expected from Fig. 1.3 that a wavlength distribution like that shown in Fig. 1.4 would emerge. Nevertheless, it should be emphasised that either the tendency shown in Fig. 1.2 or the distributions given in Fig. 1.3, 1.4 can only be taken as a very rough estimation. The purpose of presenting them here is not to provide accurate statistics of this active research area but rather to give some idea of how the current studies of mode locking are proceeding.

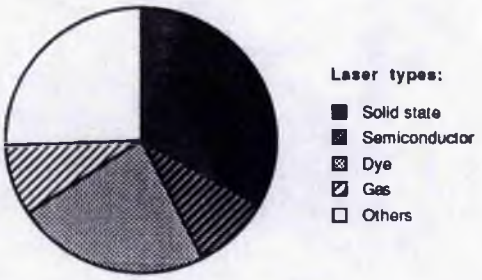

Fig. 1.3. Distribution of research papers on mode locking for different laser types.

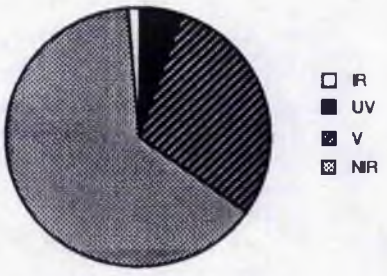

Fig. 1.4. Distribution of wavelength coverage for mode-locked lasers. V: visible; UV: ultraviolet; NIR: near-infrared; IR: infrared.

1.3 Subject-matter of this thesis

The work presented in this thesis relates to the study of the general principles of optical pulses and the coupled-cavity mode locking in a KCl:Tl colour-centre laser. Similar to that of many other research subjects the motivation of this work has two respects: one is an inherent interest in the subject itself, where some new and unknown physics always arises, the other is the practical objective of developing ultrashort pulse laser sources with better performance.

For the sake of clarity, the contents of the thesis is devided into three parts. Following this first chapter which forms Part I, Part II includes all the descriptions and the discussions on the fundamental principles of ultrashort laser pulses, and Part III is devoted to the study of coupled-cavity mode locking. The second part consists of four chapers, including the definition or mathematical characterisation of light pulses (Ch. 2), pulse measurement (Ch. 3), pulse generation (Ch. 4) and pulse propagation (Ch. 5). In Part III, a specific introduction to the development of coupled-cavity mode locking is presented in Ch. 6, a detailed analysis of the key elements in the coupled-cavity mode-locked KCl:Tl colour-centre laser in Ch. 7 and the major experimental results of this laser's performances in Ch. 8, Ch. 9, several direct applications of the coupled-cavity mode-locked laser are demonstrated in Ch. 10 and some general conclusions are presented in Ch. 11.

Part II
Basic Principles of Ultrashort Laser Pulses

This second part is a review of some fundamental principles of ultrashort laser pulses. Important aspects relating to characterization, generation, measurement and propagation of optical pulses are discussed in detail. This should give a relatively complete description of the essential knowledge used in this area and, on the other hand, provide the relevant theoretical background which is needed in the interpretation of the experimental data presented in the third part of this thesis.

Chapter 2

Mathematical Description of Light Pulses

2.1 Optical field and its complex representation

It is known that, using Fourier expansion, an arbitrary optical signal E(t) at a fixed point in space can always be decomposed into a group of harmonic fields

$$E(t) = \frac{1}{\sqrt{2\pi}} \int_{-\infty}^{+\infty} e(\omega) e^{-i\omega t} d\omega \tag{2.1a}$$

where $e(\omega)$ is the weight function for different harmonics and determined by

$$e(\omega) = \frac{1}{\sqrt{2\pi}} \int_{-\infty}^{+\infty} E(t) e^{i\omega t} dt \tag{2.1b}$$

For simlicity, we can reexpress the above two equations as

$$E(t) = \mathcal{F}\{e(\omega)\} \tag{2.2a}$$

$$e(\omega) = \mathcal{F}^{-1}\{E(t)\} \tag{2.2b}$$

or, even more simply

$$E(t) \leftrightarrow e(\omega) \tag{2.3}$$

which means E(t) and $e(\omega)$ are a Fourier transform pair.

Since E(t) is a real function, associated with which a complex variable, V(t), often called *complex analytic signal,* can thus be introduced. It satisfies

$$\mathrm{Re}[V(t)] = E(t) \tag{2.4}$$

where Re[ ] means taking the real part. Similar to Eqs. (2.2), we have

$$V(t) = \mathcal{F}\{\upsilon(\omega)\} \tag{2.5a}$$

$$\upsilon(\omega) = \mathcal{F}^{-1}\{V(t)\} \tag{2.5b}$$

or

$$V(t) \leftrightarrow \upsilon(\omega) \tag{2.6a}$$

where

$$\upsilon(\omega) = \begin{cases} 2e(\omega) & (\omega > 0) \\ 0 & (\omega < 0) \end{cases} \tag{2.6b}$$

Eq. (2.6b) represents a very important feature of the complex analytic signal, which is that V(t) does not possess any negative frequency components. In many theoretical analyses or derivations relating to electromagnetic fields, using the complex representation has proved much more convenient and simpler than using its real signal counterpart (Yariv 1976).

In the cases where optical fields have a relatively small bandwidth so that the condition

$$\frac{\Delta\omega_\upsilon}{\omega_o} << 1 \tag{2.7}$$

exists, where ω_o is the mean optical frequency and $\Delta\omega_\upsilon$ is the bandwidth of $\upsilon(\omega)$, or $e(\omega)$ Eq. (2.5a) can be approximated as (Born and Wolf 1980)

$$V(t) = \mathcal{A}(t)e^{-i\omega_o t} \tag{2.8a}$$

with

$$\mathcal{A}(t) = A(t)e^{i\phi(t)} \tag{2.8b}$$

Eq. (2.7) is known as the *quasi-monchromatic condition* and Eqs. (2.8a) can be taken as a general expression of a wave packet, with $e^{i\omega_o t}$ being the carrier wave and $\mathcal{A}(t)$ representing the slowly varing envelope[1]. Provided that $\upsilon_A(\omega)$ is the associated frequency spectrum of $\mathcal{A}(t)$, i. e.

$$\mathcal{A}(t) \leftrightarrow \upsilon_A(\omega) \tag{2.9}$$

then from the Fourier frequency shift theorem, it can be verified that

$$\upsilon_A(\omega) = \upsilon(\omega + \omega_o) \tag{2.10}$$

or, equivalently,

$$\upsilon(\omega) = \upsilon_A(\omega - \omega_o) \tag{2.11}$$

In practice, the Fourier transform given by Eq. (2.9) is easy to perform and so, instead of using Eq. (2.5b), the complex field spectrum $\upsilon(\omega)$ can be determined by first using Eq. (2.9) to obtain $\upsilon_A(\omega)$ and then making a frequency shift in accordance with Eq. (2.11).

In most of cases, an ultrashort optical pulse can be described by Eqs. (2.8). Different forms of A(t) lead to different pulse shapes (see Table 2.1) while the phase term, $\phi(t)$,

---

[1] The meaning of "slowly varing envelope" here only makes sense when it is in a comparision with the changing speed of the carrier wave. To be more precise, A(t) and $\phi(t)$ satisfy

$$\frac{dA}{Adt}, \frac{d\phi}{dt} << \omega_o$$

describes both the slower phase changing of the envelope and the charateristics of the carrier. For instance, provided that $\phi(t)$ is not a constant, we can always make a Taylor expansion of it, which yields

$$\phi(t) = \phi_o + \phi^{(1)}t + \phi^{(2)}t^2 + \cdots \tag{2.12}$$

where ϕ_o is the constant phase, $\phi^{(n)}$ is the n^{th} order derivate of $\phi(t)$ with respective to time t. Substituting Eq. (2.12) into Eqs. (2.8), we have (neglecting all the high order derivative terms)

$$V(t) = A(t)e^{i\phi_o}\, e^{-i[(\omega_o - \phi^{(1)})t - \phi^{(2)}t^2]} \tag{2.13}$$

or, equivalently, in another form

$$V(t) = A(t)e^{i\phi_o}\, e^{-i\omega t} \tag{2.14a}$$

with

$$\omega = \omega(t) = [\omega_o - \phi^{(1)}] - 2\phi^{(2)}t \tag{2.14b}$$

Both Eqs. (2.13) and (2.14b) indicate a carrier which has a chirped frequency. ($\phi^{(1)}$ induces a frequency shift and $\phi^{(2)}$ represents a linear frequency chirp). $\phi^{(2)} < 0$ corresponds to a positive or up chirp and $\phi^{(2)} > 0$ relates to a negative or down chirp. If $\phi(t)$ equals to a constant, i. e. $[\phi^{(n)}]_{n\geq 2} = 0$, the pulse will be regarded as a coherent pulse. Discussions on how coherent optical pulses can become frequency chirped will be presented in Sec. 2.4.

Table 2.1 Typical pulseshapes and associated amplitude spectra*

Pulseshape	A(t)	$\upsilon_A(\omega)$
Gaussian	$e^{-2\ln 2(t/\Delta t)^2}$	$\frac{\Delta t}{2\sqrt{\ln 2}} e^{-(\omega\Delta t)^2/8\ln 2}$
Hyperbolic sech	$\mathrm{Sech}(1.76t/\Delta t)$	$\frac{\Delta t}{1.76}\sqrt{\frac{\pi}{2}}\,\mathrm{sech}\left(\frac{\pi\omega\Delta t}{3.52}\right)$
Square	$1 \quad (\lvert t\rvert \leq \frac{\Delta t}{2})$	$\frac{\Delta t}{\sqrt{2\pi}}\,\mathrm{sinc}\left(\frac{\omega\Delta t}{2}\right)$
Single-sided exponential	$e^{-\ln 2(t/2\Delta t)} \quad (t \geq 0)$	$\frac{\Delta t}{\sqrt{2\pi}} \frac{1}{-\ln 2/2 + i\omega\Delta t}$
Lorentzian	$\frac{1}{\sqrt{1+(2t/\Delta t)^2}}$	$\Delta t\sqrt{\frac{\pi}{2}}\, e^{-\omega\Delta t/2} \quad (\omega \geq 0)$
Asymmetrical sech	$\frac{1}{e^{-t/(1+b)} + e^{t/(1-b)}}$	———

* Assuming that $\phi(t) = 0$;
Δt is FWHM pulse duration defined from $A^2(t)$; b is a parameter for pulseshape asymmetry.

It is interesting to point it out that the wave packet expression of optical pulses given in Eq. (2.8a) also provides a useful approach to understand how a light pulse may be constructed. If a single frequency plane wave with unit amplitude is modified by a modulator which has a time variation function described by $\mathcal{A}(t)$ then the output light becomes a wavepacket (see Fig. 2.1). [In practice, pulses having durations greater than 1 ps, can be generated in this way although it is often not very effecient. In such cases, the modulator could be an electro-optical switch, or an optical Kerr switch (Duguay and Hansen 1971), or a combination of a phase modulator with a dispersive line (Wigmore and Grischkowsky 1978, Kobayashi *et al* 1988). For even shorter pulses, however, the requirement on the switching speed or modulation frequency in this simple scheme becomes too high to realize and so other methods have to be considered.]

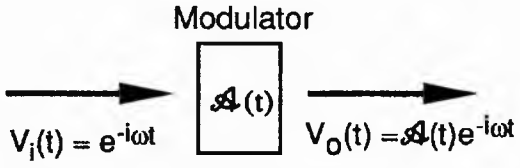

Fig. 2.1. A simple way to convert a cw harmonic wave into optical pulses.

2.2 Intensity and power spectrum

Strictly speaking, the real instantaneous intensity of an optical field E(t) should be defined as the modulus of the Poynting vector for the associated electromagnetic wave. Among most of optical problems this simplifies to

$$I = a\,E^2 \tag{2.15}$$

where a is a constant relating to the dielectric coefficient, the velocity of light in the medium and the effective beam cross section. However, in practice, because no available detectors are capable of following the changes at the optical frequency (at ~10^{14} Hz), a time average over many optical cycles always takes place during measurements. Therefore, the commonly used definition of the instaneous intensity is

$$I \equiv a\,(E^2)_{\text{average over optical period}} \tag{2.16}$$

Neglecting the constant coefficient, this leads to

$$I(t) = V(t)V^*(t) = \mathcal{A}(t)\mathcal{A}^*(t) = A^2(t) \tag{2.17}$$

Thereafter, it can be seen that the instantaneous intensity given by Eq. (2.17) only reflects the time variation of the profile or the amplitude of a wave packet. It does not provide any information about the phase and the characteristics of the carrier.

Similarly, in the spectral domain, a *power spectrum* can be defined

$$i(\omega) \equiv \upsilon(\omega)\upsilon^*(\omega) \tag{2.18}$$

Sometimes, $i(\omega)$ is also called *spectral intensity*. Both $I(t)$ and $i(\omega)$ are measurable and because of energy conservation they satisfy

$$\int_{-\infty}^{+\infty} I(t)dt = \int_{-\infty}^{+\infty} i(\omega)d\omega \tag{2.19}$$

Note that $I(t)$ and $i(\omega)$ do not form a Fourier transform pair although a relation between the full widths at half maxima (FWHM) of $I(t)$ and $i(\omega)$ is often addressed (For detailed discussions see section 2.3.)

2.3 Linear autocorrelation and coherence

Through an analogy of power spectrum, $i(\omega)$, to its corresponding optical field spectrum $\upsilon(\omega)$, a question of what the Fourier transform of $i(\omega)$ is may arise. If we denote

$$G_1(\tau) = \int_{-\infty}^{+\infty} i(\omega)e^{i\omega\tau}d\omega \tag{2.20a}$$

from Eqs. (2.5a) and (2.18), it can be derived that (Bradley and New 1974)

$$G_1(\tau) = \int_{-\infty}^{+\infty} V(t)V^*(t+\tau)dt \tag{2.20b}$$

$G_1(\tau)$ is called the *first order*, or *linear autocorrelation* of the analytic signal[2]. Eqs (2.20a), (2.20b) indicate that

$$i(\omega) \leftrightarrow G_1(\tau) \tag{2.21}$$

---

[2] A more thorough description of various cross- and auto-correlations of optical fields should be found in the subject of photostatistics, where both $E(t)$ and $V(t)$ are taken as stochastic processes and the definitions of all the measurable vriables like $I(t)$, $i(\omega)$, $G_1(\tau)$ involve an ensemble average. This average in the cases of stationary process is equvalent to a time average (Walker 1975). For details see the text by Saleh (1978).

For a quasi-monochromatic wave, i. e. Eqs. (2.8) hold, then substituting into Eq. (2.20b) yields

$$G_1(\tau) = | G_1(\tau) | e^{i\Phi(\tau)} e^{-i\omega_0\tau} \tag{2.22}$$

where $| G_1(\tau) |$, $\Phi(t)$ are slowly varing functions of τ and can be determined by

$$| G_1(\tau) | e^{i\Phi(\tau)} = \int_{-\infty}^{+\infty} A(t)A(t+\tau)e^{i[\phi(t) - \phi(t+\tau)]}dt \tag{2.23}$$

As an example, if

$$\phi(t) - \phi(t + \tau) \approx - \frac{d\phi}{dt}\tau \tag{2.24}$$

and assuming $d\phi/dt \approx$ constant, then

$$| G_1(\tau) | = \int_{-\infty}^{+\infty} A(t)A(t+\tau)dt \tag{2.25}$$

$$\Phi(\tau) = - \frac{d\phi}{dt}\tau \tag{2.26}$$

In many applications, a normalized form for $G_1(t)$ is used, which is given by

$$g_1(\tau) \equiv \frac{G_1(\tau)}{G_1(0)} \tag{2.27}$$

From Eq. (2.22), it is easy to derive that

$$g_1(\tau) = | g_1(\tau) | e^{i[\Phi(\tau) - \Phi(0) - \omega_0\tau]} \tag{2.28}$$

where

$$| g_1(\tau) | = \frac{\int_{-\infty}^{+\infty} A(t)A(t+\tau)dt}{\int_{-\infty}^{+\infty} A(t)A(t)dt} \tag{2.29}$$

With $| g_1(\tau) |$ representing the envelope and $e^{i[\Phi(\tau) - \Phi(0) - \omega_0\tau]}$ describing the temporal fringes, $g_1(\tau)$ determines the whole interferometric pattern detected in a Michelson interferometer (Demtroder 1981, also see Appendix B).

From Eq. (2.27), it is obvious that

$$| g_1(\tau = 0) | = 1 \tag{2.30}$$

and for optical pulses, suppose Δt is the pulse duration, then

$$| g_1(\tau>2\Delta t) | \approx 0 \tag{2.31}$$

The FWHM duration of $| g_1(\tau) |$ is known as the *coherence time*, τ_c, and it should be noted that it is τ_c (not the pulse duration Δt) that has a standard reciprocal relation with the bandwidth of power spectrum determined by Fourier transform, i. e.

$$\tau_c \frac{\Delta\omega}{2\pi} = P \tag{2.32}$$

where P is a constant of the order of unity, the exact value of which is dependent on pulseshapes (see Table 2.2).

Table 2.2 Bandwidth-duration product for different pulseshapes

Pulseshape	$\tau_c \Delta\omega/2\pi$	$\Delta t \Delta\omega/2\pi$
Gaussian	0.882	0.441
Hyperbolic sech	0.778	0.315
Square	1.772	0.886
Lorentzian	0.382	0.221

In general, for coherent pulses a fixed ratio between the pulse duration Δt, which is defined as the FWHM of I(t), to the coherence time τ_c exists, although it again varies for different pulseshapes (see Table 2.2). For symmetrical coherent pulses, as an approximation, we have

$$\Delta t \approx \frac{\tau_c}{2} \tag{2.33}$$

thus

$$\Delta t \frac{\Delta\omega}{2\pi} \approx \frac{P}{2} \tag{2.34}$$

The product on the left-hand-side of the above formula (known as *pulse duration bandwidth product*) is commonly used in evaluating characteristics of the pulses interested. However, such judgement whenever possible should be carried out in conjunction with related spectral data for the measured pulses or eqivalently their first order autocorrelation traces.

Normally, if the value of this product is close to one of those listed in Table 2.2 and the spectrum is smooth and symmetric a particular pulse shape may then be assigned to the pulse. If it is too small (say less than 0.3) and the spectrum is asymmetric this most likely implies that the pulse has an asymmetrical shape (Finch, 1989). For the cases where large values of $\Delta t\Delta\omega/2\pi$ apply (e. g. larger than 0.5) and the spectra do not show any symmetrical satellite peaks (i. e. the pulses do not have square profiles) it is an indication that the pulses are not completely coherent. They may be either frequency-chirped or temporally scrambled like a noise burst. For the former two cases, however, pulses are coherent and also the shortest for the associated spectral bandwidth. They are thus termed as *bandwidth-limited* or *transform-limited* pulses.

Experimental determination of τ_c can be made by monitoring the intensity change at one point on the reception screen while one of the two arms in a Michelson interferometer is being alterred, or instead, by measuring the visibility of the interference pattern following Eqs. (B.1) and (B.2) in Appendix B. The former method is rather convenient in that it normally gives a direct display $g_1(\tau)$ on the screen of an oscilloscope. It is, however, restricted by the maximum translation distance that can be achieved in practice and thus only suitable for measuring small τ_c or the coherence time of short pulses. Alternative methods of involving intensity autocorrelation measurements and then deducing τ_c (Ou *et al* 1989), or by coupling the two replica beams in a photorefractive crystal and then measuring the gain profile experienced by one of them (Dominic *et al* 1990) have been reported. In the latter case, the gain profile is proportional to $| g_1(\tau) |$ and one of its main advantages is that it is capable of measuring τ_c for weak laser pulses.

It is important to know that, normally, the coherence time of a pulse sequence from a mode-locked laser is not the same as that of associated individual pulses (Rush and Ho 1984). This can be simply demonstrated by lengthening one of the Michelson interferometer arms and thus enabling one pulse in the train to be added with a later pulse in the sequence. It can be found that some coherence may be retained between different pulses from the mode-locked pulse train and as the time separation between the two added pulses increases the curve of $| g_1(\tau) |$ rolls off.

Based on both theoretical and experimental results, Ruch and Ho have claimed that mode-locked pulse train is as coherent as a single mode source operating at the same average power. To understand this, one may need to be reminded that for a multimode laser, when all the modes are locked, it means that from the status of one mode the status of all the other modes can be determined. In such a situation the laser would no longer behave like an ordinary multimode system. In fact, in the time domain, the total optical field becomes a wave packet like the one described by Eq. (2.8a). It is this wavepacket that circulates within the laser cavity, giving an output of a sequence of pulses. Hence, although the whole bandwidth contributes to individual pulse profile the coherence of the pulse train is in fact determined by the linewidth of the carrier, which is normally approximated by the central lasing mode. Provided that $\Delta\omega_m$ is the actual linewidth of this mode (see Appendix B), we have

$$\tau_s \approx \frac{2\pi}{\Delta\omega_m} \tag{2.35}$$

where τ_s is the coherence time of a pulse train. Combining Eq. (2.35) with Eq. (2.32) yeilds

$$\tau_s \approx \frac{\Delta\omega}{\Delta\omega_m}\tau_c \tag{2.36}$$

Eq. (2.36) shows the relation between the coherence time of a pulse train and that of individual pulses. It should be pointed out that most of reported experimental results relating to the measurement of the coherence time for mode-locked pulses are that for individual pulses not the whole pulse train. In practice, for a sequence of frequency-chirped pulses, in addition to the expected decrease of τ_c, the linewidth of the carrier mode increases (Siegman 1986). From Eq. (2.36) this will result in a sharper decrease of τ_s. In such a sense, it is justified to say that τ_s is more sensitive to the phase change than τ_c and therefore can be used to identify the quality of mode-locked pulses. It is significant that Bradley *et al* (1970) used to measure the cross-correlation for the pulses of noise burst type output from a mode-locked Nd:glass laser, showing that there is no coherent relation between two nearest neighbouring pulses. This is a clear indicaton of the poor coherent quality of the associated pulse train.

2.4 Three basic types of optical pulses

Based on the general descriptions about optical field given above, we are now able to deal with some specific forms of optical pulses. In many applications three types of light pulses can be identified through appropriate measurement. They are *bandwidth-limited pulses*, *chirped pulses* and *noise bursts* (see Fig. 2.2). Of course, all of them may be accompanied with some non-zero background in practice if the associated pulse generation process is not very efficient. The former two types, both of which are described by Eq. (2.8), belong to the category of determinative optical field, while the latter is related to the random process in light emission.

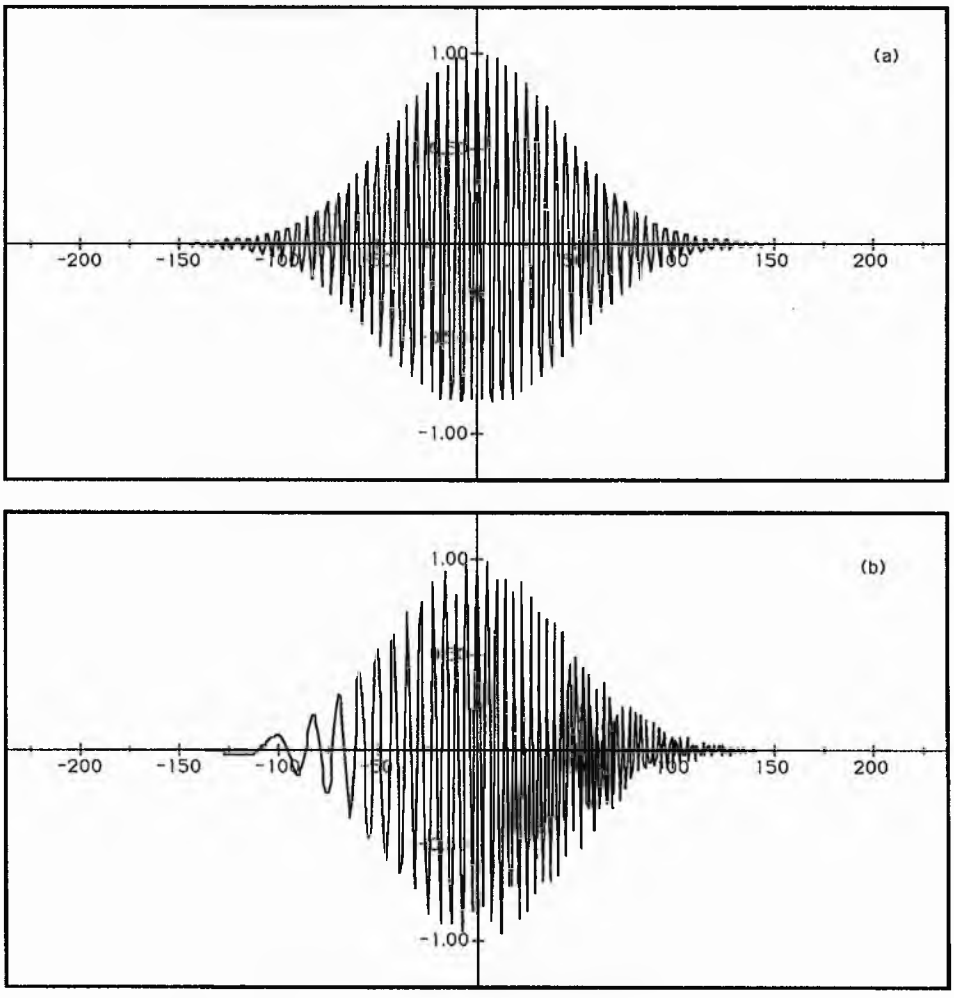

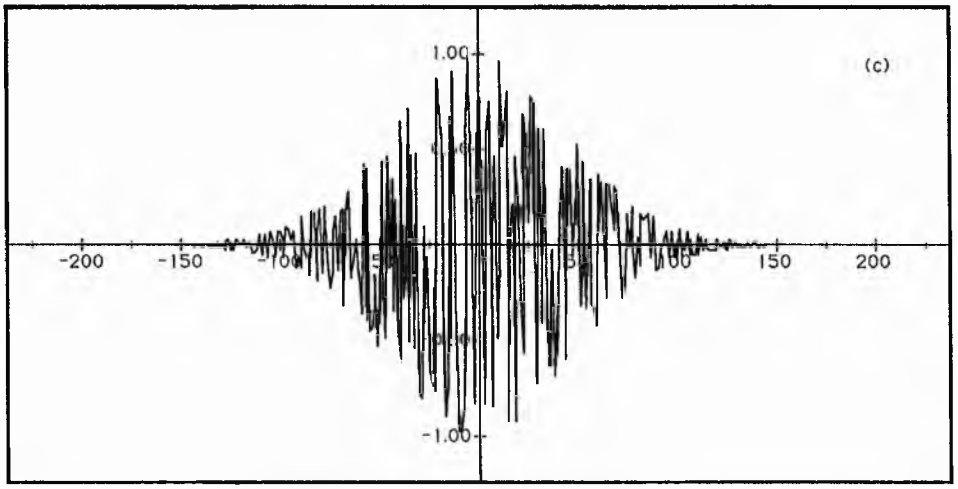

Fig. 2.2. Optical fields for three types of light pulses; (a) coherent (or bandwidth- limited) (b) frequency-chirped (c) noise burst. (All in the same time scale of 50 fs/div.)

A noise burst can be expressed in time domain as a Gaussian-distributed random variable R(t) multiplied by a real envelope function $A_T(t)$ (Pike and Hercher 1970),

$$V_b(t) = A_T(t)R(t) \tag{2.37}$$

Note that the random variable R(t) represents a steady-state thermal radiation with a finite spectral width and $A_T(t)$ can be regarded as a truncating function. An example of a noise burst is that from a Q-switched laser. A Q-switched pulse develops from noise in a very short time after a sudden change of lasing threshold and so the modes included in it are often unrelated. This leads to the pulse having poor phase coherence. For transient mode-locked lasers, when incomplete phase locking occurs amongst the oscillating longitudinal modes, the output pulses also tend to be like noise bursts (see Section 3.4). In contrast with coherent pulses, a significant feature for a noise burst is the inconsistency of its coherence time with the duration of its envelope. This implies that Eq. (2.33) is no longer valid for noise bursts, but it should be rewritten as

$$\Delta t > \frac{\tau}{2} \tag{2. 38}$$

It thus follows that in such cases Eq. (2.34) also does not hold. However, there is evidence showing that when noise bursts appear Eq. (2.32) remains valid (McDonald *et al* 1984). Further characterization of the three types of pulses regarding to the differences among their autocorrelation traces will be discussed in Sec. 4.3.

2.5 Intensity autocorrelation

For optical pulses shorter than 1 ps, it becomes difficult to directly measure the intensity function I(t). Under these circumstances, autocorrelation techniques have been utilized (Ippen and Shank 1977). Because the linear autocorrelation of the optical field does not provide any extra information except a Fourier transform of the power spectrum, (i. e. $G_1(\tau)$ and $i(\omega)$ can be derived from each other), in order to obtain further information of I(t) higher order autocorrelation (Sala *et al* 1980) has to be exploited. Among these higher order autocorrelations, the most commonly used one is the *second order autocorrelation*, i. e. the *intensity autocorrelation*, which is defined by

$$G_2(\tau) = \int_{-\infty}^{+\infty} I(t)I(t+\tau)dt \tag{2.39}$$

Using Eqs. (2.8) and (2.17), we obtain

$$G_2(\tau) = \int_{-\infty}^{+\infty} A^2(t)A^2(t+\tau)dt \tag{2.40}$$

Similar to $G_1(\tau)$, a normalized form of $G_2(\tau)$ can be introduced

$$g_2(\tau) = \frac{G_2(\tau)}{G_2(0)} = \frac{\int_{-\infty}^{+\infty} I(t)I(t+\tau)dt}{\int_{-\infty}^{+\infty} I^2(t)dt} \tag{2.41}$$

Note that, in contrast to $g_1(\tau)$, $g_2(\tau)$ is a real function. Practical measurement of $G_2(\tau)$ is often achieved through the generation of second harmonics of the pulses to be measured, thus intensity autocorrelation is also called *SHG autocorrelation*. In many experiments relating to femtosecond pulses, the FWHM of $g_2(\tau)$, noted as τ_I, is measured and the pulse durations are deduced from this.

2.6 Summary

In the previous subsections, several physical variables which describe optical pulses from different respects have been introduced. To avoid any confusion, a brief summary of the

relationships between these quantities is given in a form of a flow chart as show in Fig. 2.3. Accompanied with this is an example of various expressions for a Gaussian coherent pulse as included in Table 2.3. Compared with the connection between V(t), $g_1(\tau)$ and I(ω) shown in Fig. 2.3, a first order autocorrelation in the spectral domain, $g_1(\Omega)$, (derived from υ(ω) and indicated by dashed lines) is proposed, where Ω is the frequency shift. Since a Fourier transform of $g_1(\Omega)$ leads to I(t), $g_1(\Omega)$ should be of practical value in pulse measurements. For further discussions, see Section 4.4.

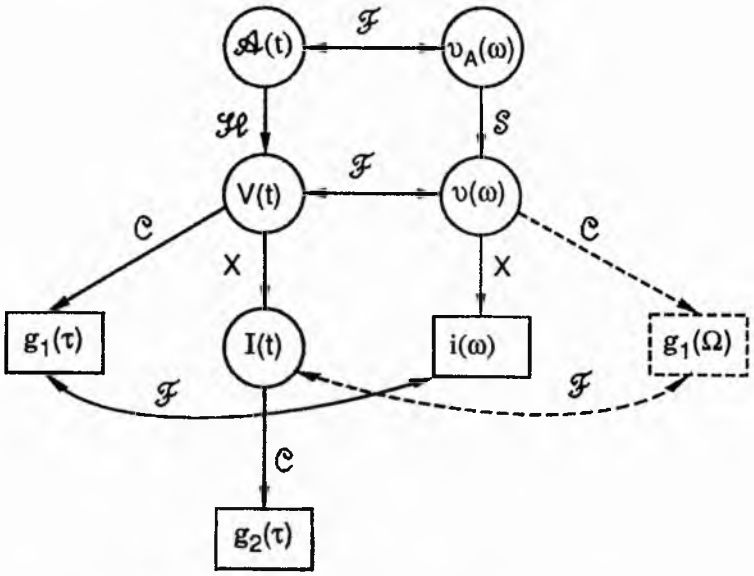

Fig. 2.3. Relationships among various descriptive variables of optical field. $\mathcal{F}$: Fourier transform; $\mathcal{H}$: multiply harmonic term $e^{-i\omega_0 t}$; $\mathcal{S}$: frequency shift; $\mathcal{C}$: autocorrelation; X: multiply by conjugate term; Those quantities enclosed in boxes are directly measurable for femtosecond pulses.

Table 2.3 Various expressions for a Gaussian pulse

$[\, E(t) = A_o e^{-at^2} \cos(\omega t)]$

Time domain	Spectral domain
$A(t) = A_o e^{-at^2}$	$\upsilon_A(\omega) = \frac{A_o}{\sqrt{2a}} e^{-\omega^2/4a}$
$V(t) = A_o e^{-at^2} e^{-i\omega_o t}$	$\upsilon(\omega) = \frac{A_o}{\sqrt{2a}} e^{-(\omega - \omega_o)^2/4a}$
$I(t) = A_o^2 e^{-2at^2} \Rightarrow (\Delta t)$	$i(\omega) = A_o^2 \frac{1}{\sqrt{2a}} e^{-2(\omega - \omega_o)^2/4a}$
$g_1(\tau) = A_o^2 e^{-a\tau^2/2} \Rightarrow (\tau_c)$	↓
$g_2(\tau) = A_o^4 e^{-a\tau^2} \Rightarrow (\tau_I)$	$(\Delta\omega)$

$a = 2\ln 2/(\Delta t)^2$; $\tau_c = 2\Delta t$; $\tau_I = 1.414\Delta t$; $\Delta\omega = 2\ln 2/\Delta t$.

Chapter 3

Pulse Generation

As outlined in Chapter 1, the major approaches in the generation of ultrashort laser pulses are the various mode-locking schemes. These may be accompanied by some alternatives, like gain switching, a combination of phase modulation and chirp compensation, and so on. In this chapter the state of the art for all of these techniques will be addressed.

3.1 Modes and laser modes

From classical electromagnetic (e-m) theory (Jackson 1975) it is well known that, in contrast to the case of free space, e-m fields in restrained circumstances must have particular distribution patterns in both space and time domains in order to meet relevant boundary conditions. These patterns, often relating to different discrete oscillating frequencies (or wavelengths), are called *modes* of the e-m wave. A typical example of e-m wave modes are those enclosed in a rectangular cavity (see Fig. 3.1), where the frequencies of these modes are fixed and given by

$$\omega_{\ell,m,n} = c\sqrt{\left(\frac{\ell\pi}{L_x}\right)^2 + \left(\frac{m\pi}{L_y}\right)^2 + \left(\frac{n\pi}{L_z}\right)^2} \tag{3.1}$$

ℓ, m, n, are integral indices, different values of which correspond to distinct modes. In this case the number of modes per unit volume and per unit frequency range is

$$p(\nu) = \frac{8\pi\nu^2}{c^3} \tag{3.2}$$

where $\nu = \omega/2\pi$. $p(\nu)$ is called mode density.

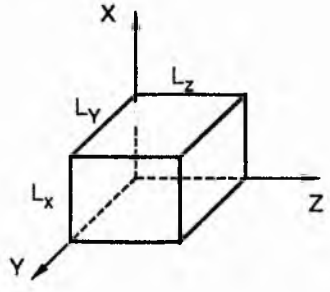

Fig. 3.1. A closed rectangular cavity.

Now consider the modes in a laser cavity, which is, in general, simply constructed by two parallel mirrors separated by a distance L (see Fig. 3.2). Since there are no boundaries on the sides of the laser cavity, (i. e. an open cavity), it can be understood that significant losses are introduced. Therefore, compared with a closed cavity, there should be a substantial reduction in the mode number for an open cavity. The frequencies for these modes are (Svelto 1982)

$$\nu_{\ell,m,n} = \frac{c}{2L}\left[\ell + \frac{m+n+1}{\pi}\cos^{-1}\sqrt{\left(1-\frac{L}{R_1}\right)\left(1-\frac{L}{R_2}\right)}\right] \tag{3.3}$$

where R_1, R_2 are the radii of the two mirrors M_1 and M_2 respectively. Modes with different values of m and n but the same ℓ value usually have distinct distributions in the plane perpendicular to the cavity axis and so they are regarded as transverse modes. Axial or standing-wave modes also exist and these are generally referred to as longitudinal modes. The most commonly encountered longitudinal modes in laser research are those with $m = n = 0$ but different ℓ values. These modes are also called fundamental, or TEM_{00} modes. In the majority of literature on lasers wherever the term of mode locking is used it implicitly refers to the phase locking between these modes. Their frequencies, from Eq. (3.3) can be written as

$$\nu_{\ell,} = \frac{c}{2L}\left[\ell + \frac{1}{\pi}\cos^{-1}\sqrt{\left(1-\frac{L}{R_1}\right)\left(1-\frac{L}{R_2}\right)}\right] \tag{3.4}$$

where we omit the indices m and n, which are equal to zero.

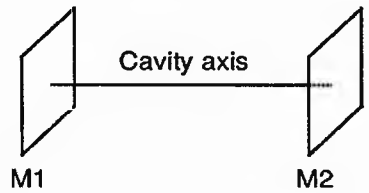

Fig. 3.2. A two-mirror laser cavity.

The actual number of modes in a laser is determined by several factors such as the fluorescence bandwidth of the gain medium, the lasing threshold, and the frequency separation between two nerghbouring modes (see Fig. 3.2). The last one, also called *mode separation*, can be derived from Eq. (3.4), namely

$$\Delta\nu_o = \frac{c}{2L} \tag{3.5}$$

From Fig. 3.3, the number of lasing modes may be evaluated by using

$$N = \frac{\Delta\nu_g}{\Delta\nu_o} \tag{3.6}$$

where $\Delta\nu_g$ is the laser bandwidth[1]. Assign $\Delta\nu_f$ to be the fluorescence bandwidth, then we have

$$\Delta\nu_g = b_o\Delta\nu_f \tag{3.7}$$

where $b_o \leq 1$, is determined by the characteristics of gain material and the degree of pumping.

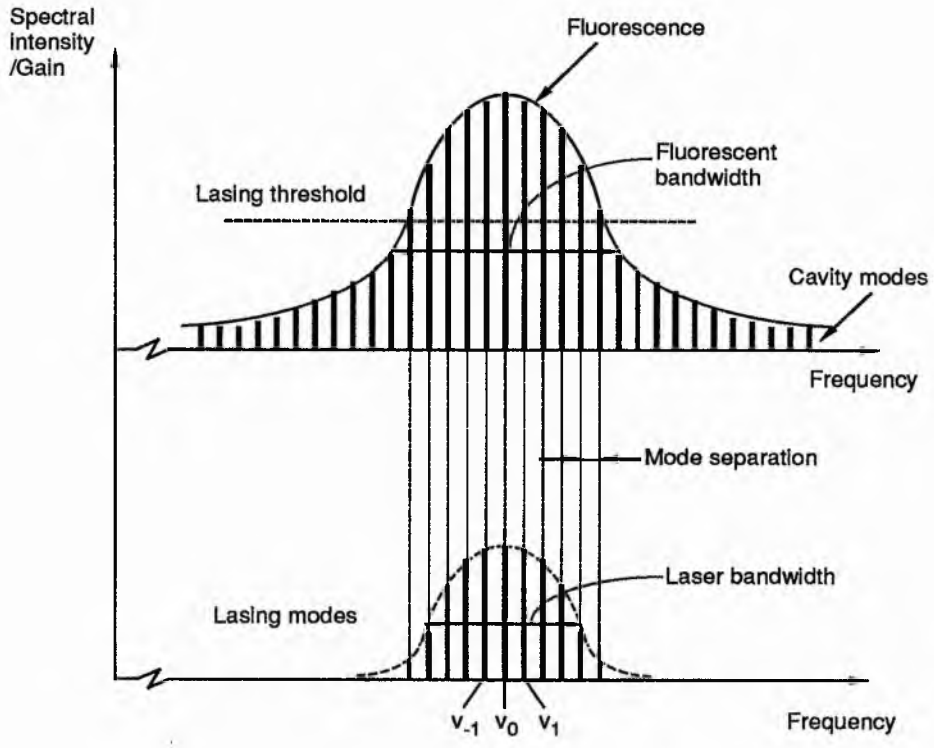

Fig. 3.3. Illustration of longitudinal modes in a laser cavity.

3.2 General relationship among laser axial modes

From experimental observations, it is known that a free running multimode laser often has an unstable output (Linde 1973). This has been taken as a clear indication of that no

[1] Note that although it is common to regard the gain bandwidth as an approximation of the actual laser bandwidth, in some cases these two may be quite different. This occurs when the spectral distribution of losses in a cavity are significant.

fixed phase relationship exists among the oscillating axial modes[2]. Such a phase independence among the different lasing modes can be attributed to the following two effects: (i) different modes normally do not start lasing at the same time so that their initial phases are most likely to be random and (ii) because of dispersion effect in a laser system, the mode separation is actually not a constant, instead, it varies for different modes according to the following equation (Yariv 1975)

$$\Delta\nu_\ell = \frac{\Delta\nu_0}{n\left(1 + \frac{\chi'(\nu_\ell)}{2n^2}\right)} \tag{3.8}$$

where $\Delta\nu_0$ is the mode separation for the sourceless cavity [the one given in Eq. (3.6)], n is the normal refractive index of the gain medium, χ' is the real part of the dielectric coefficient contributed by resonant atoms. Generally speaking, both n and χ' are the functions of frequency, but since χ' corresponds to the refractive index in an anomalously dispersive region the change of χ' with frequency is normally much greater than that of n. Thus, to stress this, χ' in Eq. (3.8) is written in a functional form. The subscript index ℓ is used to specify that the mode separation is for the ℓ_{th} mode.

Despite of the effects mentioned above, which causes laser modes not to have a fixed phase relationship, for laser systems where the gain medium has a homogeneously broadened fluorescence an important factor which enables different modes to be related to certain extent also exists. This factor is that all the modes are enveloped by the same gain profile and the existence of one mode often influences the properties of another mode. If one mode accesses more gain the other modes will experience less. In most circumstances such a mode competition, merely couples the amplitudes of different modes together and seems nothing to do with the phases of mode, but it can lead to the suppression of a noticeable number of modes and so the entire laser bandwidth will be

[2] Actually, an interesting similarity between the light from a multimode laser and that scattered when a coherent beam illuminates a rough surface can be found. For the latter, because the individual point sources on the scattering screen do not have a fixed phase relationship relative to each other it leads to the resultant scattered field having irregular spatial speckles, while the output of a free running multimode laser, fluctuating in the time domain, can be treated as an one dimensional speckle in the time domain.

decreased. Obviously this will not be desirable for a laser which is used to produce ultrashort optical pulses.

For some low gain and narrow band lasers only a few modes are established above the lasing threshold and in these cases the competition between modes in the use of gain tends to cause the laser to operate on a single mode (Smith 1972). However, this picture may not be true for the intensely pumped broadband lasers, where a dynamic balance between the suppressed modes and the newly established modes is reached. Also, for a standing wave laser cavity the spatial hole burning effect in the gain medium will counteract mode competition effect efficiently. At the positions where the central intense mode has wave nodes the side band modes can easily get enough gain to reach laser threshold.

3.3 Mode locking

The phase for the q_{th} mode in a multimode laser can be expressed as

$$\phi_q(t) = 2\pi\nu_q t + \phi_{0q} \tag{3.9}$$

where ϕ_{0q} is the initial phase, which is a fixed value for each mode. Suppose a total of $2n+1$ modes reach threshold, then the total optical field and the associated intensity can then be written respectively as

$$V(t) = \sum_{q=-n}^{n} A_q e^{i\phi_q} = \sum_{q=-n}^{n} A_q e^{i(\omega_q t + \phi_{0q})} \tag{3.10}$$

$$I(t) = \sum_{q=-n}^{n} A_q^2 + \sum_{-n(q\neq m)}^{n} 2A_q A_m \cos(\phi_q - \phi_m) \tag{3.11}$$

where A_q is the amplitude of the q_{th} mode. For simplicity, we ignore the linewidth of each mode, i.e. all the modes are treated as ideal harmonic waves. In this case, A_q is a constant although its value may vary for different modes (see Fig. 3.3). The summations in Eqs. (3.10) and (3.11) are critically dependent on the properties of phase terms. Normally, for a free-running multimode laser, because no fixed relation exists among the phases of different modes, Eq. (3.11) is simply an addition of many sinusoidal waves with

randomly distributed phases. A numerical example of the intensity output from the laser operating under such a random situation is shown in Fig. 3.4(a), where the total number of lasing modes is assumed to be 7 and their amplitude follows a Gaussian distribution. It can be seen that I(t) has a repetitive irregular pattern, the period of which equals to the cavity roundtrip time.

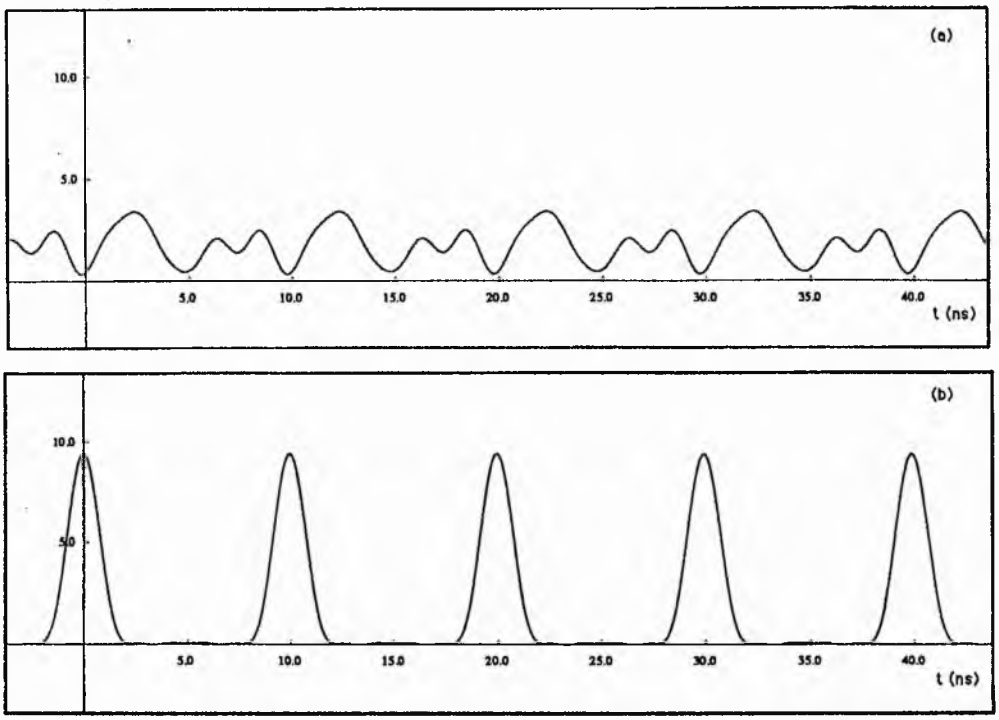

Fig. 3.4. Intensity output of a multimode laser with 7 oscillating modes in lasing. (a) With random initial phases; (b) All the initial phases are equal to zero. [The amplitudes for these modes have the normalized values 0.21, 0.5, 0.97, 1, 0.97, 0.5, 0.21 repectively and for simplicity the frequency separation between any two neighbouring modes is kept the same (100 MHz)].

In contrast to this, if the phase difference between any neighbouring modes becomes the same for all the lasing modes, distinct results can be obtained. These are the cases which the term *mode locking* describes. Mode locking occurs when

$$\Delta\phi_\ell = \Delta\phi_{\ell+1} = \Delta\phi \tag{3.12}$$

where

$$\Delta\phi_\ell \equiv \phi_{\ell+1} - \phi_\ell \tag{3.13}$$

Using Eq. (3.9) $\Delta\phi_\ell$ can be written as

$$\Delta\phi_\ell(t) = 2\pi(\Delta\nu_\ell)t + \Delta\phi_{0\ell} \tag{3.14}$$

It is clear that the phase difference is contributed by two parts: one is the mode separation and the other is the the initial phase difference. Because Eq. (3.12) should hold at any time during mode locking, associated with a constant $\Delta\phi$ an even $\Delta\nu_\ell$ and a uniform $\Delta\phi_{0\ell}$ must exist simultaneously. That is equivalent to Eq. (3.12) for the mode-locking condition there should be

$$\Delta\nu_\ell = \Delta\nu_{\ell+1} = \Delta\nu \tag{3.15a}$$

$$\Delta\phi_{0\ell} = \Delta\phi_{0(\ell+1)} = \Delta\phi_o \tag{3.15b}$$

A similar calculation to that given in Fig. 3.4(a) except that in this case where the phases of all the modes satisfy Eq. (3.15) is shown in Fig. 3.4(b). The substantial distinction between the two results is very illustrative. With the mode phases unlocked, the laser output has a random fluctuation [Fig. 3.4(a)], but with the mode phases locked stable and regular, high peak power pulses are generated [Fig. 3.4(b)].

In practice, no matter what kind of action occurs or is taken as long as the equivalences in Eqs. (3.15) hold, Eqs. (3.10) and (3.11) can be then respectively rewritten as

$$V(t) = \sum_{\ell=-n}^{n} A_\ell e^{i(\phi_0 + \ell\,\Delta\phi)} \tag{3.16}$$

where ϕ_0 is the phase of the central mode (corresponding to $\ell = 0$),

$$I(t) = \sum_{\ell=-n}^{n} A_\ell^2 + \sum_{-n(\ell\neq m)}^{n} 2A_\ell A_m \cos[(\ell-m)(\Delta\phi)] \tag{3.17}$$

Taking $A_\ell = A_{\ell+1} = A_o$, the above two equations are reduced to

$$V(t) = A_o \frac{\sin\dfrac{2n+1}{2}\Delta\phi(t)}{\sin\dfrac{\Delta\phi(t)}{2}} e^{i\phi_0} \tag{3.18}$$

$$I(t) = A_o^2 \left(\frac{\sin\dfrac{2n+1}{2}\Delta\phi(t)}{\sin\dfrac{\Delta\phi(t)}{2}} \right)^2 \tag{3.19}$$

It can be seen that Eq. (3.18) has a form of a wave packet [see Eq. (2.8)] with an amplitude given by

$$A(t) = A_0 \frac{\sin\frac{2n+1}{2}\Delta\phi(t)}{\sin\frac{\Delta\phi(t)}{2}} \tag{3.20}$$

A simple analysis of Eq. (3.19) will show that I(t) represents a regular sequence of pulses with a time interval equal to the laser cavity roundtrip time

$$T = \frac{1}{\Delta\nu} \tag{3.21}$$

This pulse train (viewed at any selected space point along the laser cavity axis) in fact relates to a single pulse which travels back and forth in the laser cavity (Crowell 1965). The pulse duration is given by

$$\Delta t = \frac{1}{(2n+1)\Delta\nu} = \frac{1}{\Delta\nu_g} = \frac{T}{2n+1} \tag{3.22}$$

where $(2n + 1)\Delta\nu$ represents the full lasing bandwidth. Thus, it illustrates that to achieve shorter pulses then broadband lasers must be used. By taking $\Delta\phi = 2n\pi$ in Eq. (3.19), the peak intensity of the pulse can be derived to be

$$I_p = A_0^2(2n+1)^2 = (2n + 1)\langle I\rangle \tag{3.23a}$$

This value, as shown, is $(2n + 1)$ times greater than the associated average intensity[3]. For a practical laser system, due to the fluorescence profile of gain medium, different modes normally have unequal amplitudes (see Fig. 3.3), an effective lasing mode number can be introduced, which satisfies

$$I_p = N_{eff}\langle I\rangle \tag{3.23b}$$

(For instance, for the mode amplitude distribution shown in Fig. 3.4, $N_{eff} \approx 5$) In these cases, strictly speaking, no simple analytic function like those given in Eqs. (3.18) and

---

[3] For Eq. (3.10), the time average over the second term on the right hand of the formula equals zero and thus

$$\langle I(t)\rangle = \sum_{\ell=-n}^{n} A_\ell^2 = (2n + 1)A_0^2$$

(3.19) can be derived. When the mode number is large enough, however, the summation in Eq. (3.16) can be approximated as an integral (Svelto 1982) and so that the temporal amplitude A(t) is proportional to the Fourier transform of the mode amplitude profile. In another word, A(t) can be solved using Eq. (2.9) in Sec. 2.1.

3.4 Incomplete mode locking

In practice, the mode relationship in a multimode laser system may not just be like one of those two extreme situations mentioned above, i. e. either all locked or all unrelated, instead, it is more likely to be a mixture of both. Such a mixed state can be called *incomplete mode locking*, or *partial mode locking*, and as shown in Fig. 3.5 it has two basic forms: (a) Two sets of interplaced modes exist, one set is locked and the other is not [Fig. 3.5(a)]; (b) Only those modes having frequencies in the central spectral region are phase locked while those in the other regions are not [Fig. 3.5(b)].

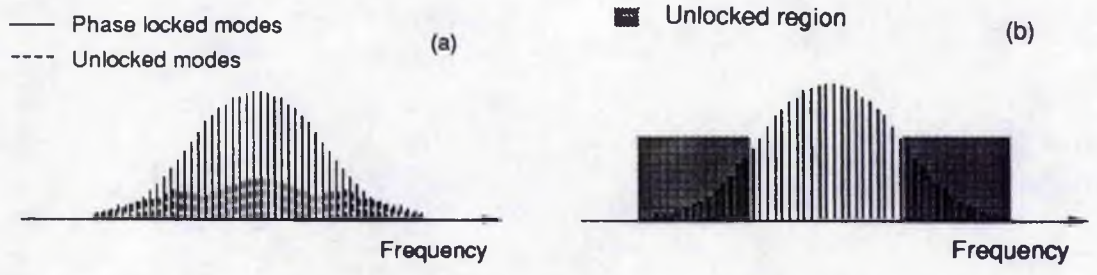

Fig. 3.5. Incomplete mode locking. (a) There coexist two sets of interplaced modes, one set is phase locked the other is not; (b) Mode locking only occurs in one part of laser spectrum.

In the first circumstance, the entire output can be taken as a simple combination of certain percentage of completely mode-locked pulses with some other percentage of noise fluctuation. This leads to the generation of the pulses which have a significant background (Bradley and New 1974). The second type of incomplete mode locking is liable to be observed for mode-locked lasers which are under a pulsed pumping scheme. In these cases, if there is not sufficient time for all the modes to be properly coupled together before pumping ceases, many modes, especially those in the wings of the laser spectrum, will remain in a random phase distribution. In another words, this is like an

incomplete dynamic process, during which the intracavity optical field only partially develops into pulses that could ultimately be completely mode locked. At such a stage the amplitude of the total field takes a pulse form, and perhaps with some satellite peaks, but the phases of the modes are still far from the status of complete locking (Siegman and Kuizenga 1974). This is just what a noise burst looks like. (As discussed previously, for a noise burst, although the pulse envelope is formed the coherence is still poor because the mode phases are not appropriately coupled). Therefore, this second type of incomplete mode locking leads to the production of noise bursts. In SHG autocorrelation measurements, this gives rise to a narrow spike on the top of the traces (see Ch. 4). Furthermore, because of the uncertainty in the phase term of a noise burst, [speaking of Fig. 3.5(b), this means there is not a clear demarcation between the locked region and the unlocked region and the phases of all the modes are still changing], a "wobbling" of the temporal envelope may occur. This contributes to a relatively large temporal phase jitter in the output pulse train.

For broadband lasers, if they are pumped above threshold by substantial amounts, or for laser systems there are considerable amount of Fabry-Perot effects, it is possible that mode locking occurs in different section of the laser spectrum (Siegman and Kuizenga 1974). This may be regarded as another special type of incomplete mode locking which leads to the generation of multiple pulses per cavity roundtrip. These pulses are, in general, not evenly separated in time and also do not have the same carrier frequency.

When the pulses in a laser cavity become short enough (e. g. less than 1 ps) considerable dispersion and nonlinear effects may take place. These two effects can distort the mode locking process through introducing a large amount of frequency chirp in the pulses. Under this circumstance, the pulses stop experiencing any further shortening and meanwhile have a large bandwidth-pulse duration value. For such pulses the SHG autocorrelation traces do not show any coherent spikes and also there is no deviation from the standard peak to background ratio. However, as discussed in the section 4.3, these frequency-chirped pulses can be efficiently diagnosed by making a measurement of their interferometric autocorrelation traces.

In the above, we have described several typical cases of incomplete mode locking which results in the production of pulses having backgrounds, noise bursts, multiple pulses and chirped pulses. Understandably, in a more general sense, incomplete mode locking could lead to an output which is a mixture of the above types of pulses, for example, a chirped burst of noise (Bradley and New 1974) or chirped multiple pulses and so on.

3.5 Mode locking techniques

Many methods can be used to enable the multimode laser to operate in a mode-locking status. Strictly speaking, this is not achieved by striving to lock those unrelated modes which may already be above the laser threshold but, instead, to take special measures to introduce newly phase-coupled modes and make them lase while suppressing the unrelated modes are suppressed. Therefore, at every moment of a mode-locking process exists a competition between inherent tendency for free running and mode coupling action. In such a sense, by good quality of mode locking it should mean the predominant of mode coupling effect over the random nature in a multimode laser.

3.5.1 Active mode locking[4]

The way to generate phase-coupled modes with uniform phase separation is to modulate the optical field inside a laser cavity at a frequency equal to the reciprocal of cavity period. Such periodic modulation represents the key part for all sorts of mode-locking techniques. Since it can be applied to either the amplitude or the phase of the field, mode locking thus achieved is explicitly named as *amplitude modulation* (AM) mode locking or *frequency modulation* (FM) mode locking.

Amplitude modulation

As an example, let us first examine the function of a sinusoidal amplitude modulator. Suppose the modulation function of an amplitude modulator can be expressed as

$$M_A(t) = 1 + M\cos(\Omega t + \phi) \tag{3.24}$$

[4] Here we use the word "active" in its more general sense (see footnote 3 in chapter 1).

where M is the modulation index ($|M| \leq 1$) that describes the modulation depth, Ω is the modulation frequency and ϕ represents the initial phase shift. After passing through this modulator, a plane wave becomes

$$\begin{aligned} V_1(t) &= M_A(t)V_i(t) \\ &= [1+ M\cos(\Omega t + \phi)]\, A_0 e^{-i\omega t} \\ &= A_0 e^{-i\omega t} + \frac{A_0 M}{2} e^{-i[(\omega + \Omega)t + \phi]} + \frac{A_0 M}{2} e^{-i[(\omega - \Omega)t - \phi]} \end{aligned} \tag{3.25}$$

It can be seen that the modulated wave is composed of three different frequency components: one original and two new sidebands (see Fig. 3.6). If such a modulated wave passes through the modulator again, then we have

$$\begin{aligned} V_2(t) &= M_A(t)V_1(t) \\ &= A_0\left[1 + 2\left(\frac{M}{2}\right)^2\right]e^{-i\omega t} + A_0 M\, e^{-i[(\omega + \Omega)t + \phi]} + A_0 M\, e^{-i[(\omega - \Omega)t - \phi]} \\ &\quad + A_0\left(\frac{M}{2}\right)^2 e^{-i[(\omega + 2\Omega)t + 2\phi]} + A_0\left(\frac{M}{2}\right)^2 e^{-i[(\omega - 2\Omega)t - 2\phi]} \end{aligned} \tag{3.26}$$

Thus another two new components at frequencies $(\omega + 2\Omega)$, $(\omega - 2\Omega)$ are introduced. If a modulator like the one described by Eq. (3.24) is inserted in a laser cavity where a light beam bounces back and forth between the mirrors, it can be imagined that the multipass effect will lead to many sidebands. These sidebands do not necessarily have the same phase with the original carrier and also among themselves, but the phase difference between any neighbouring components (including the central carrier) remains constant. This is just what the mode-locking condition requires [see Eq. (3.12)].

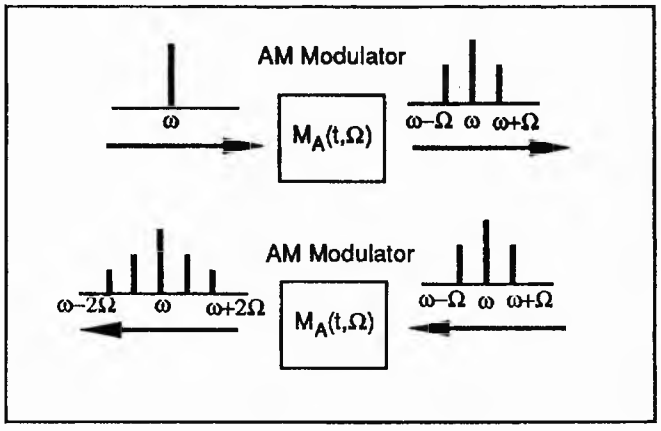

Fig. 3.6. Amplitude modulation.

Frequency modulation

For a frequency modulator, the modulating action is on the phase of the incident wave. A typical FM function can be written as

$$M_F(t) = e^{-i(\beta \sin \Omega t)} \tag{3.27}$$

where β is the modulation index. (Here for simplicity we ignore any existing constant phase shift). Again, assuming that the incident wave is a plane wave, after modulation, the beam becomes

$$\begin{aligned} V_1(t) &= A_o M_F(t) e^{-i\omega t} \\ &= A_o e^{-i(\omega t + \beta \sin \Omega t)} \\ &= A_o \{ J_o(\beta) e^{-i\omega t} + J_1(\beta)[e^{-i(\omega + \Omega)t} - e^{-i(\omega - \Omega)t}] \\ &\quad + J_2(\beta)[e^{-i(\omega + 2\Omega)t} + e^{-i(\omega - 2\Omega)t}] \\ &\quad + J_3(\beta)[e^{-i(\omega + 3\Omega)t} - e^{-i(\omega - 3\Omega)t}] \ldots\ldots \} \end{aligned} \tag{3.28}$$

where $J_n(\beta)$ are Bessel function. Different from amplitude modulation, FM leads to infinite number of sidebands after a single pass. These sidebands are located symmetrically at a frequency interval of Ω on each side of the incident wave frequency. It may be noticed that the resultant field after frequency modulation has a chirped frequency, which is, from Eq. (3.28), given by

$$\omega(t) = \omega + \beta\Omega \cos(\Omega t) \tag{3.29}$$

Obviously, the zero chirp occurs at a time period,

$$T = \frac{2\pi}{\Omega} \tag{3.30}$$

Since $| \omega(t) - \omega |_{max} = \beta\Omega$, the product $\beta\Omega$ in Eq. (3.29) represents the frequency variation range caused by modulation. As far as the magnitude for various sidebands is concerned, it can be verified that most of energy lies in the components which are within the frequency range of $2\beta\Omega$ (Jones 1988). Therefore, $2\beta\Omega$ can be taken as an approximation of the extended bandwidth induced by FM (see Fig. 3.7).

Suppose that the modulated wave is repropagated through modulator. The wave after the second FM becomes

$$V_2(t) = M_F(t)V_1(t) = A_0 e^{-i(\omega t + 2\beta \sin\Omega t)} \tag{3.31}$$

for which the total frequency is

$$\omega(t) = \omega + 2\beta\Omega\cos(\Omega t) \tag{3.32}$$

As a comparision of the above formula with Eq. (3.29), we can see that the effective bandwidth of the wave is simply doubled, i. e. it becomes $4\beta\Omega$ (Fig. 3.7).

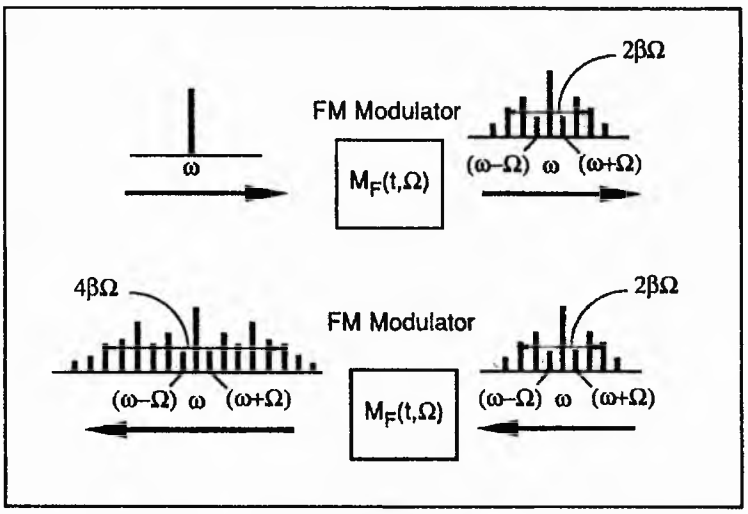

Fig. 3.7. Frequency modulation.

To summarize, a commonly important characteristic for AM and FM modulation types described above is that they both lead to the generation of symmetrically distributed sideband frequency components. These new sideband components have frequencies given by

$$\omega_n = n\Omega + \omega \tag{3.33}$$

where Ω is the modulation frequency, ω is the frequency for the optical wave to be modulated and n is an integer. It is clear that these sidebands are uniformly displaced in frequency domain and within a laser cavity such a frequency spreading will be enhanced or multiplied due to multipass effect. Suppose the index n takes the value among the range of -N, ··· -1, 0, 1, ··· N, then the maximum feasible value of n can be estimated by $N\Omega = \Delta\nu_g/2$. For the purpose of mode locking, Ω is chosen in such a way that

$$\Omega = (\Delta\nu_g)_{\text{average}} \tag{3.34}$$

and so, closely beside every laser mode there is a sideband signal. (If the linewidth for both local modes and the sidebands are considered, this should be pictured as a partial

overlap in the two spectra). Through the frequency pulling (or alternatively, injection locking) effect the sideband signal forces its neighbouring mode to oscillate at the same frequency and with the same phase. Thereafter, the mode-locking condition is met and short pulses are thus generated. Such a physical process involved in either AM mode locking or FM mode locking can also be viewed in time domain equivalently, as demonstrated in Fig. 3.8.

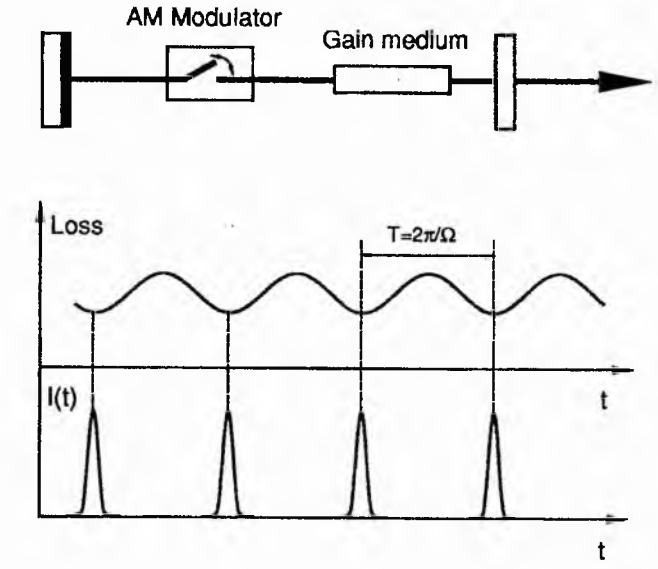

Fig. 3.8(a). Time domain view of active mode locking by amplitude modulation. The AM modulator acts as an imperfect shutter which opens and closes alternatively at a frequency $\Omega = 2\pi/T$, and so the cavity loss is modulated and the intracavity optical field is pulsed. (The pulse passes the modulator every time when the shutter is opened, which corresponds to the minimum loss).

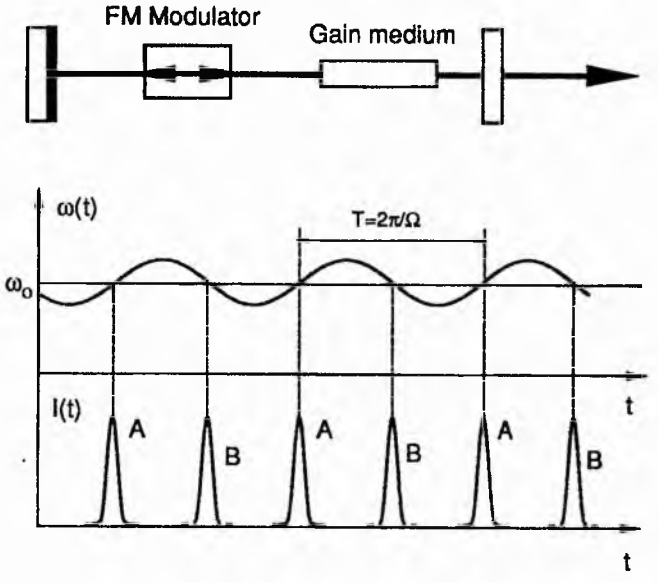

Fig. 3.8(b). Time domain view of active mode locking by frequency modulation. The FM modulator periodically alters the effective optical pass of the cavity, and thus introduces a variable frequency chirp into the intracavity optical field. The accumulation of this chirping effect during multipass leads the associated frequency components out of the gain profile and so only the light that passes the modulator at the chirp-free time can be established. As shown in the graph, during every modulation period which is also the cavity roundtrip time, there are two occasions at which the pulse can pass the modulator without experiencing frequency chirp. Therefore two sequences of pulses as marked A and B in the graph may exist.

Modulation devices

As far as the practical modulation devices are concerned, the two most commonly used modulators are electro-optic switches and acousto-optic switches. The acousto-optic switch is mainly used in AM mode locking while the electro-optic switch, e. g. a Pockels cell, can be used for either AM or FM purposes. (The only difference for the latter AM application is that an additional polariser is included[5]). The working principles and the merits of these two types of modulators have been included in many scientific publications (e. g. Demokan 1982, Yariv and Yeh 1984) and very useful instructions relating to the selection criteria based on rather practical consideration can be found in the article by Mourou (1990).

As an alternative to incorporating a switching device into a laser cavity to modulate cavity loss, amplitude modulation of intracavity optical field can be also realized by pulsing the laser pumping sources, which leads to a modulation of intracavity gain. Practically, this pulsed pumping scheme can be implemented by either employing a mode-locked laser as the pump source or, for semiconductor diode lasers, using RF electronic wave to drive the laser. In accepted jargon, the former method is named as synchronously pumping mode locking (or briefly *synchronous mode locking*) while the latter is often called *gain modulation mode locking*. Nevertheless, no matter whether the modulation is applied to the gain or the loss, or the frequency, all the mode-locking approaches described above have a common feature which is that they are all actively initiated and driven by another periodic signal either electrical or optical. Thus, they can be grouped into the same and a more general type of mode locking - *active mode locking*.

To achieve proper performance with any arrangement of the active mode locking category, a critical synchronization between the driving signal and the cavity period is required. In another words, if any detuning between the driving frequency and the cavity repetition frequency occurs appropriate mode locking will not normally be obtained. (If detuning is only in a fairly small range it may lead to the generation of broader pulses or

[5] Such a polarizer is inserted inside laser cavity together with the Pockels cell. Each time when the polarization of the beam is changed to a perpendicular direction because of the action of Pockels cell the beam will be dumped by the polarizer.

unstable performance, while for larger detuning mode locking may not be established). However, an exception to this is that if the modulation frequency is an integral multiple of the cavity repetition frequency then multiple pulses with even time separation can be generated (Demokan 1982). The number of the pulses per cavity roundtrip is equal to the number of switching actions taken within the time interval of one cavity period. In the frequency domain, this corresponds to the existence of different sets of modes, e. g. like those shown in Fig. 3.5(a), but in this case, the modes in each set are phase locked, although there is still no relationship between the modes in the different groups. Since the mode groups are interplaced among each other, this means that a given mode may not be coupled with its neighbouring modes, and so the mode locking appears to have a rather channeling effect whithin the whole spectrum.

Self-consistency theory

A well known theory about AM and FM mode locking is the one called *self-consistency* model presented by Kuizenga and Siegman (1970). The essential point of the model lies in the recognition of the fact that at the steady state of a mode-locked laser, the pulse circulating in the cavity must reproduce itself after every roundtrip. This can be equivalently viewed as that at steady state, the spectral extension caused by modulator in either an AM or FM mode locked laser is always balanced by the spectral shortening due to the gain medium therein in one cavity roundtrip. Such a picture simplifies the analysis to become a matter of studying the pulse propagation through the gain medium and modulator in the cavity and then equalizing the field after one roundtrip with the original one at a time shift equal to cavity period. This gives rise to the relationship between pulse duration and system parameters, which is

$$\Delta t = \frac{(2\sqrt{2}\ln 2)^{1/2}}{\pi}\left(\frac{g_o}{\delta}\right)^{1/4}\left(\frac{2\pi}{\Omega\Delta\nu_g}\right)^{1/2} \tag{3.35}$$

where g_o is the roundtrip saturated amplitude gain at the central frequency of the gain spectrum, Ω is the modulation frequency, $\Delta\nu_g$ is the gain bandwidth and δ is the modulation index. [Note that such a pulse duration is proportional to $(\Delta\nu_g)^{-1/2}$ rather than

$(\Delta\nu_g)^{-1}]$. Eq. (3.35) is valid for both AM and FM mode locking but it should be remembered that the modulation index in these two cases is defined differently. For AM, the single pass transform function is given by (Siegman and Kuizenga 1974)

$$M_A(t) \approx e^{-\delta\Omega^2 t^2/4} \tag{3.36a}$$

For FM,

$$M_F(t) \approx e^{-i\,\delta\Omega^2 t^2/2} \tag{3.36b}$$

In many applications, an AM modulator usually has a transmission function form given by

$$M_A = \cos[\delta_A \sin(\Omega t)] \tag{3.37a}$$

where δ_A is the modulational index used in practice. Through some mathematical manipulation Eq. (3.37) can be approximated as

$$M_A \approx e^{-(\delta_A)^2 \Omega^2 t^2/2} \tag{3.37b}$$

therefore, compared with Eq. (3.36a), it follows that $\delta = 2(\delta_A)^2$.

While for an FM modulator

$$\begin{aligned} M_F &= e^{-i\delta_F \cos\Omega t} \\ &\approx e^{-i(\delta_F)}\, e^{i\,\delta_F \Omega^2 t^2/2} \end{aligned} \tag{2.38}$$

Neglecting the constant phase term in the above formula and comparing it with Eq. (3.36b) yields $\delta = \delta_F$.

The relation presented in Eq. (3.35) between pulse duration and the modulational index is of practical value because the latter parameter is adjustable by varying the RF power applied to the modulator. In general,

$$\delta_A,\ \delta_F \propto (P_{RF})^{1/2} \tag{3.39}$$

from the relationships between δ_A, δ_F and δ given above, we have

$$\text{for AM} \quad \Delta t \propto (P_{RF})^{1/4} \tag{3.40a}$$

$$\text{for FM} \quad \Delta t \propto (P_{RF})^{1/8} \tag{3.40b}$$

In the derivation of Eq. (3.35) a steady state Gaussian pulse shape is assumed. This pulse circulates in the laser cavity, having an expression given by

$$\text{for AM} \quad V(t) = e^{-2\ln 2(t/\Delta t)^2}\, e^{-i\omega t} \tag{3.41a}$$

$$\text{for FM} \quad V(t) = e^{-2\ln 2(t/\Delta t)^2(1+i)}\, e^{-i\omega t} \tag{3.41b}$$

where Δt is the pulse duration given by Eq. (3.35). It is thus readily shown that for AM operation the bandwidth-pulse duration product is

$$\Delta t \Delta \nu = 0.441 \tag{3.42}$$

In contrast, for FM mode locking, because of the presence of frequency chirp in the pulses such a product is enlarged by a factor of $\sqrt{2}$, i. e.

$$\Delta t \Delta \nu = 0.441\sqrt{2} = 0.624 \tag{3.43}$$

Interestingly, through comparing the above results with Eq. (3.35) we can find that the actual pulse bandwidth $\Delta\nu$ is proportional to $(\Delta\nu_g)^{1/2}$.

The dynamic process in actively mode-locked lasers either in a transient state or cw operation has also been widely studied (Siegman and Kuizenga 1974, Demokan 1982, Aechtner *et al* 1986). It is worth mentioning that both analytic studies and numerical simulations on AM mode locking have shown that it usually takes a considerable period to reach the final steady state. Typically, 10^4 - 10^5 cavity roundtrips may be needed before the regular phase relationship is established between all the modes. It is thus concluded that the active mode locking is a quite slow process. Such a feature in fact also represents a weakness of this type mode locking, because the longer the process takes more rigorous requirements are placed upon the synchronization of the circulating pulse and the RF driving frequency to the modulator. When the pulses to be produced become very short, e. g. 1 ps, the condition of stability and the accuracy on both RF driving source and the cavity length will be extremely difficult to meet with the existing servo-based techniques. It is thus now well accepted that active mode locking is not suitable for producing ultrashort pulses with durations significantly shorter than 1 ps.

Nevertheless, there is a very important feature revealed in the simulation on the dynamic process for a AM-type active mode locking by Chong and Lindsay (1978). That is, although it needs about 50,000 roundtrip time for the mode phases to be completely related (with a perfect π phase shift from any two nerghbouring modes) the formation of a cluster of pulses in the time domain only takes 100 roundtrips. This a clear indication of

that it does not have much requirement on the phases of the modes to produce the pulses which do not have very high quality in terms of coherence. In another words, compared with the complete mode locking, from which a perfect coherent pulse is generated, the incomplete mode locking is much more easily attained. To a certain extent, such observations and the related arguement may help one to understand the ease of the appearance of spontaneous mode locking in a laser, where a regular pulse train is generated but it does not necessarily mean the modes involved are all in a good phase-locked status.

3.5.2 Passive mode locking

Amplitude modulation of the optical field inside a laser cavity can also be realized by using a nonlinear, or saturable absorber (Bradley 1977). Because of the difference in the mechanism involved in obtaining modulational effect, a completely different mode locking approach is demonstrated with this method, which is named as *passive mode locking*. Under this scheme, the nonlinear absorber bleaches automatically every time when a strong peak pulse arrives while for low power level signals it simply presents high attenuation. Such discriminating absorption behaviour reflects the key function of a nonlinear absorber and represents a fundamental feature of all kinds of passive mode-locking techniques. It enables the effective amplitude modulation to be achieved through utilizing the inherent fluctuation nature in a laser and so the modulation is much more efficient and without any synchronization problems. This is a significant advantage over the active mode locking techniques mentioned above. Moreover, because of no RF driving source is needed, the complexity and the cost of the system is also substantially reduced. Practically, the nonlinear absorber used for passive mode locking can be one of many different kinds of materials such as particular gases (Fox *et al* 1968), colour centre crystals (Chen 1985) or multi-quantum well semiconductor (Silberberg *et al* 1984), but those most commonly used are liquid organic dyes (Bradley 1977, French and Taylor 1984). The selection of the absorber is mainly dependent on the characteristics of the

laser system involved, especially the operating wavelength and the power level, as well as the upper lasing level lifetime of the gain medium.

Main characteristics of saturable absorbers

For various saturable absorbers, the time dependence of absorption can be described by (Hercher 1967)

$$\xi(t) = \xi_o\left[1 + \frac{\sigma_{24}/\sigma_{13} - 1}{1 + I/I_s}\frac{I}{I_s}(1 - e^{-(1 + I/Is)t/\tau_{21})}\right] \tag{3.44}$$

where ξ_o is the so-called small signal, or unsaturated absorption coefficient, σ_{24}, σ_{13} are the absorption cross-sections for the excited and ground states respectively, τ_{21} is the relaxation time and I_s is the saturation intensity defined by

$$I_s \equiv \frac{h\nu}{\sigma_{13}\tau_{21}} \tag{3.45}$$

It is readily shown that a system characterized by Eq. (3.44) has a response time (corresponding to absorption lifetime)

$$t_r = \frac{\tau_{21}}{1 + I/I_s} \tag{3.46}$$

and the decay time (the fluorescence lifetime)

$$\tau_d = \tau_{21} \tag{3.47}$$

If the incident light flux has durations much longer than t_r, the steady state value of $\xi(t)$ can be employed, which is equivalent to setting $t \rightarrow \infty$ in Eq. (3.44)

$$\xi_s = \xi_o\left[1 + \frac{\sigma_{24}/\sigma_{13} - 1}{1 + I/I_s}\frac{I}{I_s}\right] \tag{3.48}$$

Neglecting any excited state absorption, the above equation is reduced to

$$\xi_s = \frac{\xi_o}{1 + I/I_s} \tag{3.49}$$

Eq. (3.49) is the commonly used saturable absorption equation for a two level fast nonlinear absorber. It clearly indicates that as intensity increases to a value comparable to I_s the absorption will decrease severely. An equivalent view of this nonlinear effect can also be obtained through consideration of the transmission equation of such a absorber having a thickness of l_b. This is

$$\ln T - \ln T_0 = \frac{I}{I_s}(T - 1) \tag{3.50}$$

where T_0 is small signal transmission given by $T_0 = e^{-\xi_0 l_b}$. Obviously, as $I/I_s \rightarrow 0$, $T \approx T_0$ and as $I/I_s >> 1$, $T \rightarrow 1$, i. e. when the incident intensity is sufficiently large the absorber will be bleached or becomes transparent.

For the purpose of passive mode locking the two most important parameters within a saturable absorber are the relaxation time, τ_{21} and the saturation intensity, I_s. The former determines how much detailed temporal structures of the fluctuating field in the cavity can be effectively isolated and the latter is the reference or threshold intensity level which provides the discriminating action that initiates the process. For practical laser systems, due to the differences among the various characteristic time parameters, which lead to distinct features of pulse evolution process, passive mode locking is further divided into two essential categories:

(i) Passive mode locking of solid-state lasers: $\tau_{21} \leq \Delta t < T << \tau_{32}$

(ii) Passive mode locking of dye lasers: $\Delta t << \tau_{21} < \tau_{32} \approx T$

where τ_{32} is the upper lasing level lifetime of gain medium. As it will be discussed in the following text, the first type relates to transient state operation while the second is usually in the steady or quasi-steady state.

Giant-pulse lasers ($\tau_{21} \leq \Delta t < T << \tau_{32}$)

The passive mode locking of solid-state lasers such as Nd:YAG, Nd:glass and ruby lasers leads to the generation of a train of giant ultrashort pulses under a temporal envelope of several tens or hundreds of ns (Letokhov 1969, Fleck 1970). The distinct features for these pulses are their high pulse energy (typically ~1mJ/per pulse) and nonsteady-state behaviour (the pulses in the wings of the envelope has low energy while the most energetic pulses appear in the centre). The relatively long lifetime of the upper lasing level for these solid-state lasers determines that a large amount of energy can be stored in the gain medium and the saturation of gain is such a slow process that it does not have significant influence on the process of pulse formation. The pulses normally evolve in the following three phases (see Fig. 3.9): (i) the linear amplification; (ii) the nonlinear

absorption; (iii) the nonlinear amplification. During phase (i) the initial intensity fluctuations, which is not strong enough to saturate the absorption, is linearly amplified and correspondingly the pulses among the fluctuation are broadened because of the bandwidth limitation of gain medium. Based on a four-level gain system, the pulse duration at the end of the linear phase was derived (Demokan 1982) to be

$$\Delta t_1 = \frac{4\ln 2}{\pi}\sqrt{\frac{\alpha_0 t_1}{T}}\left[1+\sqrt{\frac{\Delta\alpha}{\alpha_0 W_r}}\right]\Delta t_0 \qquad (3.51)$$

where α_0 is the gain threshold, t_1 is the time interval of the linear phase, which can be estimated by the following formula

$$t_1 = \sqrt{\frac{2T\ln(i_1/i_0)}{(d\alpha/dt)|_{t=t_a}}}$$

where i_1, i_0 are normalized intensities with respect to I_s at the end and the beginning of the linear phase accordingly, $(d\alpha/dt)|_{t=t_a}$ is the gain slope rate at the starting time of the linear phase (see Fig. 3.9). T is the cavity period, $\Delta\alpha$ is the increment of the net gain, W_r is the relative pumping rate and Δt_0 is the initial pulse width determined by the lasing bandwidth.

The second phase starts once the maximum intensity peak reaches the level at which significant absorption saturation occurs. Such saturation enables the largest fluctuation peak to be gradually isolated and also enhanced because it experiences less loss. Therefore, at the end of this nonlinear absorption period the maximum pulse is selected while the low intensity fluctuations are suppressed. Meanwhile, the selected peak pulse itself is also compressed due to the large absorption in the wings and less absorption in the centre during each transit.

When the nonlinear absorption is completely saturated the pulse evolution enters the third phase, during which a dramatic amplification of the selected pulse(s) occurs. This is accompanied by rapid depletion of gain. [Such a gain depletion also helps to suppress any secondary pulses which may possibly appear because of inefficient pulse selection in the previous phase (Glenn 1975)]. Once the gain drops below the associated threshold the

rest of process becomes a decay of the most intense pulse which is bouncing back and forth in the laser cavity. During this last phase, the pulse is sufficiently short and intense that other intensity-dependent nonlinear effects such as self-phase-modulation are likely to take effect, such that in conjunction with the influence of group-velocity dispersion this may cause the pulse to be distorted. Therefore it is generally recognized that for giant pulse mode-locked lasers the pulses in the initial part of the train tend to be narrower and cleaner than those in the trailing part.

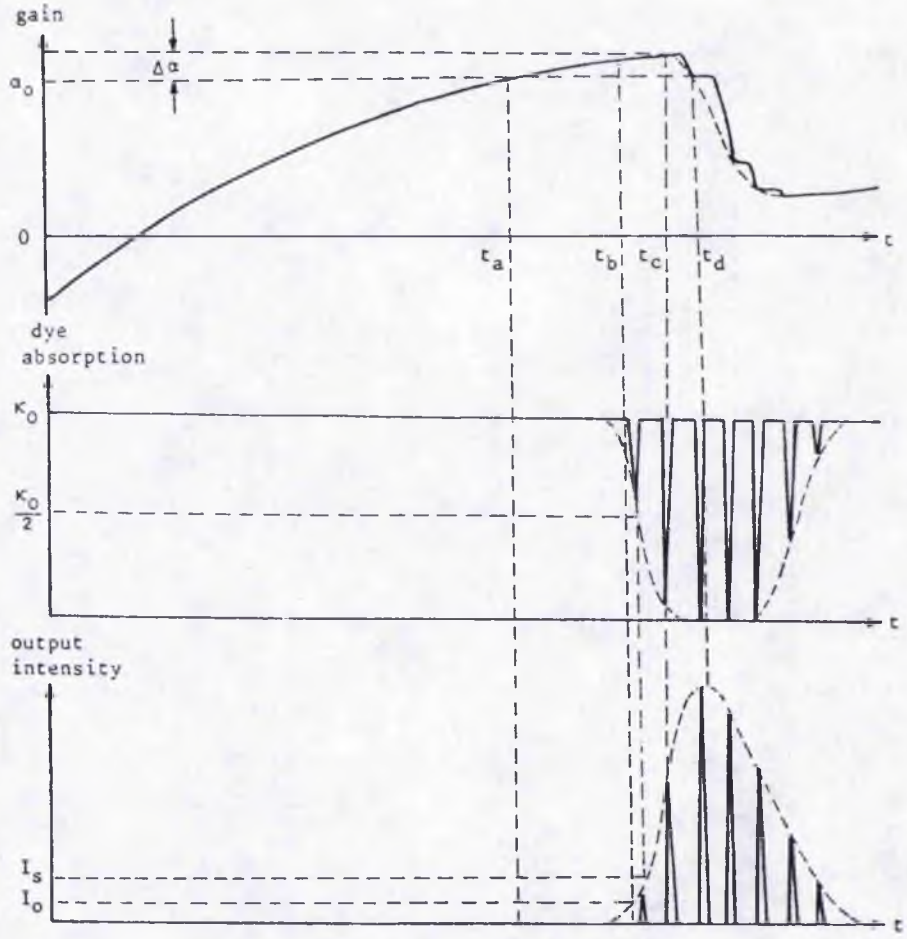

Fig. 3.9. Dynamic process in passively mode-locked giant pulse lasers (after Demokan).
t_a - t_b: linear amplification phase,
t_b - t_c: nonlinear absorption phase,
t_c - t_d: nonlinear amplification phase.
(t_a is the time when the first lasing mode occurs; t_b the time when the absorption saturation is initiated, t_c represents the starting time for gain saturation; t_d the time when gain falls below threshold value, associated with which the maximum intensity is reached).

However, if the pulse distortion in the phase of nonlinear amplification can be appropriately avoided, the pulse duration in this last phase may be estimated by using the following empirical equation (Demokan 1982)

$$\Delta t_f = \Delta t_l \left[\frac{\Delta\alpha}{\kappa_0(1 + 1/W_r)}\right]^{1/4} \tag{3.52}$$

where $\kappa_0 = 2L\xi_0$ is the absorption coefficient per roundtrip (excluding the loss caused by mirrors, γ). Combining the above equation with Eq. (3.51), we obtain

$$\Delta t_f = \frac{4\ln 2}{\pi}\sqrt{\frac{\alpha_0 t_l}{T}}\left[\frac{\Delta\alpha}{\kappa_0(1 + 1/W_r)}\right]^{1/4}\left[1 + \sqrt{\frac{\Delta\alpha}{\alpha_0 W_r}}\right]\Delta t_0 \tag{3.53}$$

Example I. Timescale of the dynamic process in a giant pulse laser (from Demokan)
Suppose: $\kappa_0 = 1.0$, $\alpha_0 = \kappa_0 + \gamma = 1.4$, $\Delta\alpha = 0.1$, $T = 5$ ns, $W_r = 5$, $(d\alpha/dt)_{t=t_a} = 4.5 \times 10^4$ /s,

$i_1 = 10^{-3}$, $i_0 = 3.6 \times 10^{-12}$,

Substitution of these values into Eqs. (3.51) to (3.53) yields

$$\Delta t_l = 24.5\Delta t_0 \tag{3.54a}$$

$$\Delta t_f = \Delta t_l / 1.86 \tag{3.54b}$$

$$\Delta t_f = 13.2\Delta t_0 \tag{3.54c}$$

From the above values it can be seen that the pulse shortening in the nonlinear phases is less than the pulse broadening in the linear phase, and so the final pulse duration is still much larger than the minimum allowed value.

Based on the three-phase picture described above, for passive mode locking within solid state lasers a critical requirement relates to the ratio of the transition cross section of the gain medium, σ_a to that of the absorber, σ_b. Generally speaking, σ_a/σ_b must be in an appropriate range so that, in one respect, the absorption saturation can start before gain saturation and in another respect the absorption saturation does not start too soon. If gain saturation starts immediately before absorption saturation (this could happen whenever I_s is too high to reach in a practical system) there would be an insufficient pulse selection process and the laser is more likely to operate in a regime of free-running oscillation. Associated with such an understanding, an idea of the existence of a second threshold, or, the mode locking threshold was proposed (Wilbrandt and Weber 1975). Such a threshold relates to achieving a minimum intensity required to saturate the absorber (for the largest

fluctuating peak at the end of the linear phase). Therefore, only if the pumping is above this second threshold can an acceptable pulse train be generated. While if the absorption saturation is too easy to reach, which means even very small fluctuating peaks can pass the absorber without experiencing much loss, there will be a high probability of generating multiple pulses. In addition, the premature bleaching of the absorber also reduces the amount of energy which can be stored and thus the amplification for the pulses in the later phases would be decreased. In practice, to achieve the desired operating regime, the effective intensities at the gain medium and the absorber are adjusted. This is done by careful design of the cavity structure so that the two beam cross sections are different in the gain and loss medium. Nevertheless, because of the initiation of the whole mode-locking process is based on the nature of a large amount of intensity fluctuations, despite of the various positive efforts which can be made for achieving better performance, the stochastic feature in these passively mode locked solid-state lasers can not be completely ruled out (New 1982).

It is worth mentioning that for all the discussions given above, it is implicitly assumed that the absorber has an infinitely fast recovery time (i. e. $\tau_{21} \approx 0$). Obviously this is not true in practice. If the absorber is taken as an automatic switch, the recovery time τ_{21} will represents the minimum switching time, which is not only responsible for isolating the largest fluctuating peaks during the pulse selection phase (the second phase) but also sets a practical limitation of the minimum pulse duration that can be obtained (i. e. there is always $\Delta t \geq \tau_{21}$). Apparently, if τ_{21} is longer than the time separation of two adjacent fluctuating pulses, the picture of pulse selection described in the previous part has to be either abandoned or revised. This is what happened in passively mode-locked dye lasers, as discussed in the next.

Passive mode locking of dye lasers ($\Delta t << \tau_{21} < \tau_{32} \approx T$)

When the passive mode-locking technique is applied to various dye lasers, it is found that the produced pulses may have durations much smaller than the correponding relaxation time of the saturable absorber employed (Ippen *et al* 1972). Such results have been

attributed to the combined action of both gain saturation and absorption saturation (New 1974). In dye laser systems, the gain medium has much shorter upper lasing level lifetime (e. g. for rhodamine 6G $\tau_{32} \sim 5$ ns) compared with that for solid-state lasers where τ_{32} is typically in an order of several hundred microseconds. Therefore, in these cases it is easier for the gain to be saturated during the mode locking process. (Meanwhile, the laser also favours cw operation since there is less energy being stored and so the Q-switch effect becomes small). However, because the time durations of the fluctuating peaks are much shorter than the response times of either gain or absorber dyes, both gain and absorption saturations are energy related rather than intensity-related. This makes a substantial difference from the case in giant pulse lasers. Through appropriate selection of parameters of both gain and absorber dyes, it is possible that a combination of absorption saturation and gain saturation can give rise to a net gain with narrow peak, thus only the central part of the circulating pulse is effectively amplified. In terms of pulse compression, this corresponds to a process of the leading edge of the circulating pulse is compressed by the absorber while the trailing edge is shortened by the gain medium. This is again in a clear contrast to the giant pulse lasers where both pulse selection and compression is dominated by the saturable absorber alone. Therefore, it is concluded from both theoretical and experimental aspects that the pulse formation is much more efficient in passively mode-locked dye lasers, where the pulse evolution process is fast and pulses shorter than 1 ps can be readily produced. Through introducing a dispersive element in his theoretical model, Haus (1975) has obtained a closed-form solution from the equations which describes pulse evolution process, showing that a steady state pulse can have a sech^2 pulse shape.

Due to the involvement of gain saturation, it is expected that in addition to the request on the transition cross-sections for getting a right time sequence of saturation, in order to achieve appropriate compression effect in passively mode-locked dye lasers, a particular requirement on the upper lasing lifetime of the gain dye also needs to be satisfied. Based on a detailed numerical analysis for some typical experimental conditions, such a

requirement has been expressed to be that the ratio of cavity period to the upper lasing level lifetime must be in a suitable range (Herrmann and Wilhelmi 1987), that is

$$\frac{T}{\tau_{32}} \in (0.1, 10) \tag{3.55}$$

If T/τ_{32} is so large that it is above the range, it means that the gain may recover completely within two successive transits, and so there is too much amplification for the leading edge of the pulse while the pulse is passing through the gain medium. This is obviously not desired because it causes the leading edge of the pulse to be broadened or even distorted. On the other hand, however, if T/τ_{32} is too small, less than the minimum limit given in Eq. (3.55), it will take too long time for gain to recover and so there will be a lack of gain. The gain depletion effect will then be reduced and the shortening of the pulse trailing edge is diminished.

3.5.3 Colliding pulse mode locking

During the early development of passive mode locking it was found that the location of the absorber in a cavity had significant impact on the mode-locking performance. This is due to the fact that when the absorber is placed at particular positions and the counterpropagating flux signals pulses meet each other inside the absorber. Under these circumstances, the absorption saturation effect is enhanced and so a better operational behaviour is observed. Such observations and associated understanding soon led to an effort to deliberately utilize this pulse addition effect. A direct and simple way to do this in a standing-wave cavity is to put the saturable absorber as close as possible to the high refrection end mirror (Bradley 1977) so that the leading edge reflected can meet the trailing edge of the same pulse in the absorber. Such an idea is further exploited in ring cavity structures, where a proper arrangement enables that the two counterpropagating pulses always collide with each other inside the absorber. This is the so-called colliding pulse mode locking scheme. A colliding pulse mode-locked laser can operate much more stably compared with the other passive mode locking schemes and with appropriate intracavity dispersion compensation, it is possible to generate pulses having durations of a

few tens of femtoseconds without employing any external compression (Kuhlke *et al* 1983).

3.6 Gain switching and ultrashort cavity

The importance of all sorts of mode-locking techniques in the generation of picosecond to femtosecond pulses has been addressed in a great deal of research work. However, it is also beneficial to know that mode locking is not the only way for producing ultrashort pulses. According to Eq. (2.34) in Section 2.3, ultrashort pulses may be generated even for a single mode laser as long as the mode linewidth of this laser is broad enough.

One technique, which has been well employed in semiconductor diode lasers (Demokan 1982) and liquid dye lasers (Miyazoe and Maeda 1971, Cox *et al* 1978), is *gain switching*. Similar to the mode locking by gain modulation, gain switching can be implemented by modulating the injection current for diode lasers or using light pulse train as pumping source for dye lasers. The only substantial difference under the gain switching scheme is that no synchronization exists between pumping signal and cavity period. This is rather like driving an oscillator at a non-resonant frequency. The relaxation oscillation of the oscillator leads to the production of pulses, the duration of which can be estimated by (Yariv 1975, 273-277)

$$\Delta t \approx \frac{2\pi}{\omega_r} = \frac{2\pi}{\sqrt{W_r - 1}} \sqrt{t_c \tau} \tag{3.56}$$

where ω_r is the frequency of the relaxation oscillation for the laser oscillator, W_r is the relative pumping rate (for semiconductor diode, W_r is the ratio of injection current density to the threshold current density), t_c is the cavity photon lifetime and τ is the relaxation time of upper lasing level (or the free electron lifetime for laser diodes).

From Eq. (3.56) it can be seen that for obtaining short Δt high W_r and small t_c are demanded. In order to prevent the laser from producing multiple relaxation peaks during each pumping cycle an upper limit for W_r exists. (Suppose ω_p is the pumping, or gain-switching frequency, the maximum value of W_r can be simply derived from $\omega_r = \omega_p$). From Eq. (B.6) in Appendix B, it is readily shown that the cavity photon lifetime is

proportional to cavity period and inversely proportional to cavity loss. Therefore, for producing short pulses with this gain switching method the shortest possible laser cavities are preferred. This is therefore very suitable for semiconductor lasers and also applicable for high gain liquid dye lasers. (It is known that there is not any severe difficulties to construct a dye laser having a cavity length less than 1 mm). Generally speaking, pulses produced through gain switching can have durations comparable to the cavity period, which is often shorter than that of pumping pulses. As an example, for a 400 μm long semiconductor laser, the associated cavity period is ~10 ps.

In contrast to those involved in synchronous mode locking, pulse evolution under the action of gain switching is essentially a non steady-state process, where little connection exists between successive pulses. It is thus expected that normally the gain switching pulses have relatively poor coherence. In addition, due to the limited size of gain medium the output power from gain switching laser would be at a quite low level. Nevertheless, an advantage of the gain switching approach is that it is very easy to employ this technique without suffering any synchronization problems. Another attractive feature of gain switching laser is that the central laser wavelength can be tuned conveniently through adjusting the cavity length. (Note that there could be only one mode, or at most several unlocked modes, in lasing for a short cavity gain switching laser).

For dye lasers, a special type of short cavity structure can be created by using two coherent pump beams separated at an proper angle to excite the gain medium such that a distributed fringe pattern of inversion population and refractive index is formed. The Bragg reflection of this spatial pattern plays the role of feedback and so no cavity mirrors are required. This is so called *distributed feedback dye laser* (Herrmann and Wilhelmi 1987), which has both properties of short cavity and high loss and therefore have been exploited to generate ultrashort pulses with the incorporation of gain switching technique (Bor *et al* 1982).

3.7 Combination of phase modulation and chirp compensation

All the pulse generation methods discussed above relate to taking various actions in altering the operating parameters of a laser, so that pulses having durations as short as the bandwidth-limit can be produced. It is clear that these techniques are not very suitable for narrow linewidth lasers because the final pulse duration is determined by laser bandwidth. The technique of combined phase modulation and chirp compensation, which is implemented outside laser cavity, do not suffer such a limitation.

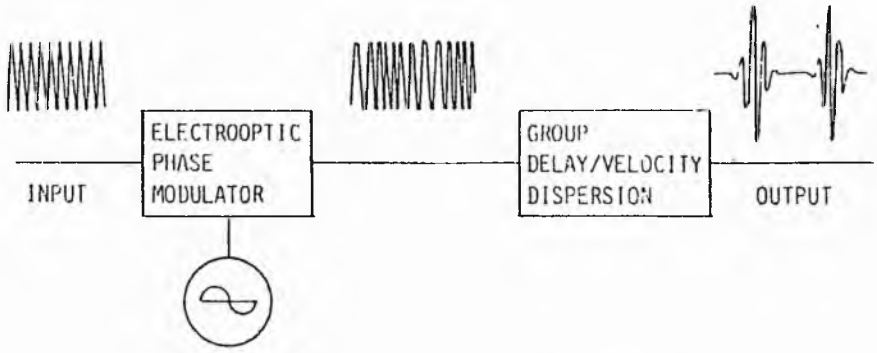

Fig. 3.10. Technique of combined phase modulation and chirp compensation (from Kobayashi *et al*).

As shown in Fig. 3.10, a beam from a single frequency laser is first sent through a phase modulator where the carrier frequency is chirped (corresponding to a spectral broadening). After this, the chirped signal is directed through a dispersive delay line such as a grating pair or an optical fibre, among which the modulated signal is pulsed as a result of different frequency components propagating at different velocities (e. g. the low frequency components drag backwards relatively while the high frequency components catch up). If the parameters for both modulator and the dispersive device are appropriately selected, near-bandwidth-limited pulses can be produced. From previous discussions on FM modulator, it is known that the bandwidth extension after the modulator is given by

$$\Delta\nu \approx \frac{2\beta\Omega}{2\pi} \tag{3.57a}$$

Under the optimum condition, it has been shown by Kobayashi *et al* (1988) that the pulses after the dispersive delay line have durations given by

$$\Delta t \approx \frac{0.7}{\Delta v} \tag{3.57b}$$

In an experiment also conducted by Kobayashi *et al* (1988), pulses having durations of less than 8 ps were generated by converting a single frequency cw beam from an Ar^+ laser with such a method.

In order to enhance the frequency modulation effect to achieve a larger spectral extension, the modulator can be placed in a Fabry-Perot (FP) cavity, the repetition frequency of which is an integer multiple of the modulation frequency. With this arrangement pulses of less than 1 ps have been produced (Kobayashi *et al* 1972). Nevertheless a disadvantage of the FP modulator is that it has a very low energy efficiency in terms of conversion from a cw beam to the pulse train (as demonstrated in Fig. 3.11). A further improvement on this is to replace the front mirror of the FP with another high finesse FP filter, which named as input Fabry-Perot filter (IFPF) as shown in Fig. 3.11 (Kobayashi *et al* 1990). Such a new structure is expected to have energy conversion efficiency as high as ~ 60%.

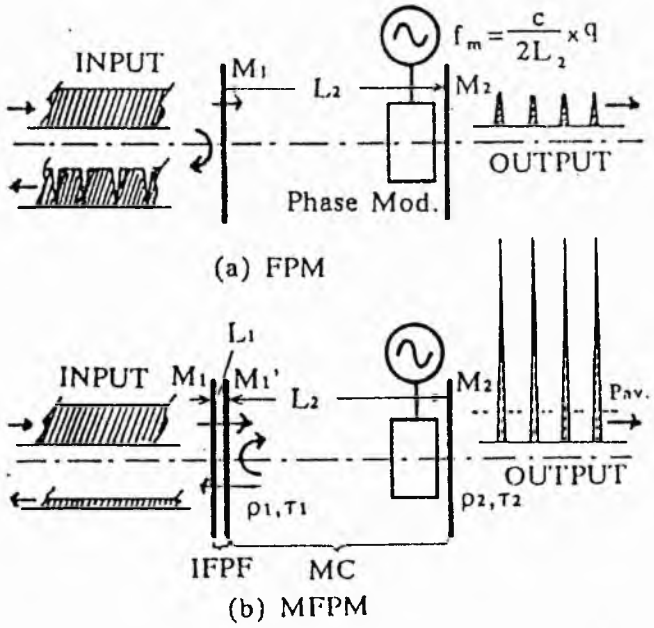

Fig. 3.11. Fabry-Perot electrooptic modulator and modified Fabry-Perot electrooptic modulator as optical pulse generators (from Kobayashi *et al*).

Chapter 4

Pulse Measurement

As in many other scientific research areas, measurement techniques in the *ultrafast phenomenon* field are especially significant. This is because new methods of measurement often results in further insight into temporal structure of ultrashort pulses, which undoubtedly helps to improve pulse generation techniques (Bradley and New 1974). Also stringent requirements apply to the many applications which rely upon precise characterisation of the diagnostic pulses (Ippen and Shank 1977, Sibbett *et al* 1983). As the light pulses generated either from laser sources or optical compressors become shorter and while there is more attention being paid to pulse structure rather than just the FWHM duration of the intensity profile the need of developing new pulse measurement technique retains a high priority in research.

In this chapter we will summarize some of the most important techniques which have ever been developed for the purpose of ultrashort pulse measurement. The concentrations are focused on the principles of the two most widely used instrument: electron-optical streak camera and SHG autocorrelator. Meanwhile two new methods are presented, one is based on a *photon-optical streak camera* and the other on *the first-order spectral autocorrelator*.

4.1 Introduction

To date, since the temporal range covered by ultrashort light pulse durations has been so large, from sub-nanosecond to several femtoseconds, there is not a universal method which can be adopted for the measurement of all such pulses. Instead, according to the timescale of the pulses to be measured different methods should be selected. A summary of these methods together with some brief comments is given in Table 4.1. Two experimental results of laser pulses that were monitored by a real-time oscilloscope and sampling oscilloscope respectively are shown in Fig. 4.1 and Fig. 4.2.

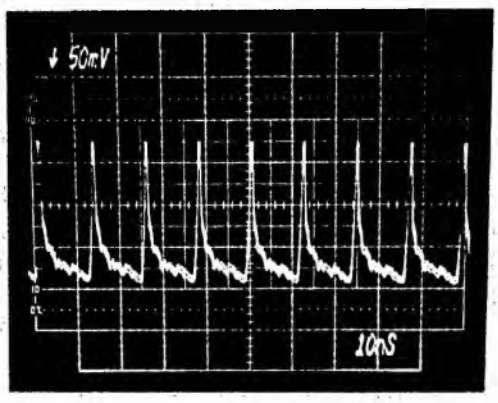

Fig. 4.1. Oscillogram for optical pulses from a cw mode-locked Nd:YAG laser.

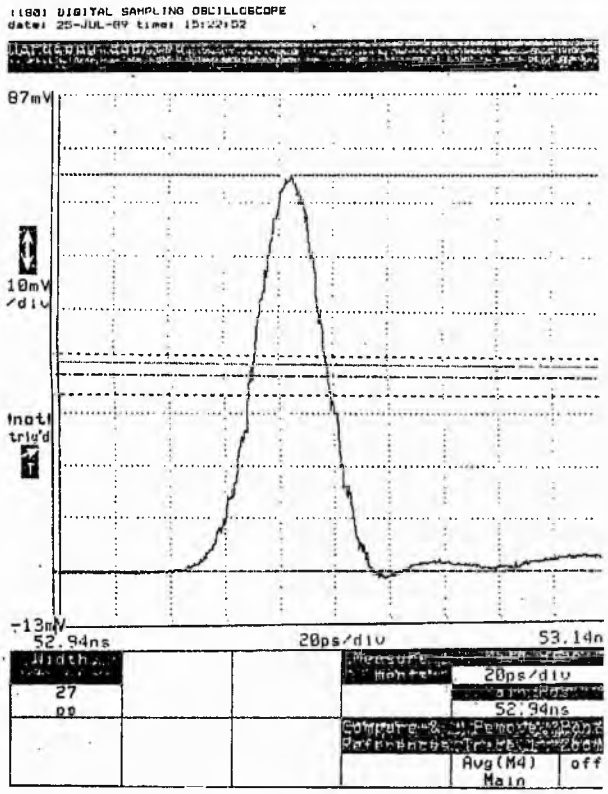

Fig. 4.2. Trace of an optical pulse from a coupled-cavity mode-locked KCl:Tl laser displayed on a sampling scope connected with a fast p-i-n photodiode.

In the years between 1967 and the mid 1970s, the technique called *two-photon fluorescence* (TPF) was widely used for the measurement of pulse durations. This method which represents an indirect approach has the same mathematical description as that for the non-background-free SHG technique. With TPF, the pulse to be measured is split into two identical replica and then the two replica meet each other from opposite directions within a liquid dye, where the fluorescence thus produced is photographed. Since each time two photons are absorbed to reach an upper atomic enery level of the dye molecules

the relaxation of this excited state leads to the generation of the fluorescence at 2ω with an intensity proportional to $(I_\omega)^2$. An apparent advantage of TPF is that it does not need a pulse train to implement. (This is unlike that in SHG method). However, because of this, a very energetic pulse is required and accordingly serious problems may arise. Under excitation of intense laser radiation the fluorescence quenching effect occurs, which can lead to some inaccuracy in the analysis (Bradley and New 1974). In the following the principles and characteristics of the electron-optical streak camera and the SHG autocorrelator are reviewed.

Table 4.1 A brief outline of light pulse measurement

Devices	Suitable timescales	Comments
Avalanche photodiode + Real-time oscilloscope	≥ 1 ns	Insufficient time resolution for ultrashort pulse measurements.
Fast p-i-n photodiode + Sampling oscilloscope	1 ns ~ 10 ps	Stable pulse trains are needed for sampling.
Electron-optical streak camera (Two modes: Single-shot and synchronous scan)	1 ns ~ 0.1 ps	Practically obtained time resolution is several times larger than theoretical limit.
SHG autocorrelator (Intensity or interferometric, with background or background free)	0.1 ns ~ 5 fs*	Indirect measurement, The interferometric autocorrlation traces provides some phase information.

* In a more general sense this should be one optical cycle; 5 fs is for $\lambda = 1.5$ μm.

4.2 Electron-optical streak cameras

As implied by its name, an electron-optical streak camera is a device which first transfers a packet of photons (an optical pulse) into a packet of electrons and then this electron packet is rapidly scanned to become a spatial streak on a phosphor screen (see Fig. 4.3). The first step is based on the well known electron-optical effect and the second can be achieved with the electron beam scanning technique similar to those used in oscilloscopes.

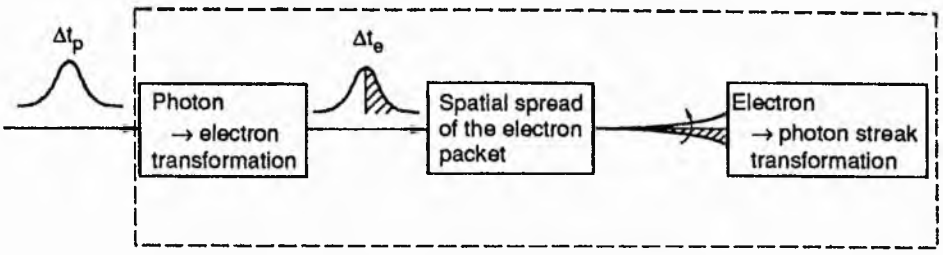

Fig. 4.3. Basic principle of an electron-optical streak camera.

Although, the history of streak cameras to measure the ultrafast events can be traced back to the mid 1950s (Zavoiskii and Fanchenko 1956), the main exploitation of such devices in the measurement of ultrashort laser pulses did not take place until a breakthrough on the time resolution of the streak tube was obtained in 1969 (Bradley 1970). Such an achievement was realized by placing a mesh (see Fig. 4.4) with very high accelerating voltage close to the photocathode so that the effect of initial speed diffusion of the photoelectrons (caused by scattering and collisions inside the cathode) could be substantially diminished. This led to a substantial improvements in the time resolution of streak cameras from several tens of picosecond to around 1 ps (Bradley *et al* 1971). Further effort towards improving the time resolution of streak camera has been still making steady progress and with new designs of streak tube structure a time resolution of ~100 fs is predicted for single-shot cameras (Finch *et al* 1988, Niu *et al* 1988). However, because of the practical time jitter problem in synchronization between the scan voltage and the pulses to be measured this theoretically predicted time resolution is not readily obtained for the repetitively operating or "synchronous" streak camera. (For the mode-locked cw lasers discussed in this thesis the overall time resolution also includes the resolution of pulse time jitter in the laser output).

In the Gaussian approximation, a measured pulse duration from a single-shot streak camera can be expressed as

$$\Delta t_{ms} = \sqrt{(\Delta t_p)^2 + (\Delta t_s)^2 + (\Delta t_d)^2} \tag{4.1}$$

where Δt_p is actual pulse duration, Δt_s is the time resolution limit arising from the finite spatial resolution of the streak tube and Δt_d relates to the time dispersion of the

photoelectrons. Suppose the minimum spatial dispersion which can be resolved by the streak camera is δx, then we have

$$\Delta t_s = \frac{\delta x}{v_s} \tag{4.2}$$

where v_s is the scanning or "streak" velocity of photoelectrons. To a good approximation, Δt_d is mainly attributed to the initial velocity spread of photoelectrons and it can be expressed as (Bradley 1977)

$$\Delta t_d = \frac{m\Delta u}{eE} \tag{4.3}$$

where Δu is the half width of the initial photoelectron velocity distribution (in a direction along the tube axis), m and e are the electronic mass and charge respectively, E is the electric field near the photocathode.

Example I. Typical time resolution of an electron-optical streak camera
Supposing that $\delta x = 0.02$ mm, $v_s = c/3$, $\Delta u = 7.0 \times 10^4$ m/s, $E = 10$ kV/cm
then the substitution of these values into Eqs (4.2) and (4.3) respectively yields
$\Delta t_s = 200$ fs, $\Delta t_d = 400$ fs. For $\Delta t_p = 150$ fs, according to Eq. (4.1), we have $\Delta t_{ms} = 472$ fs.

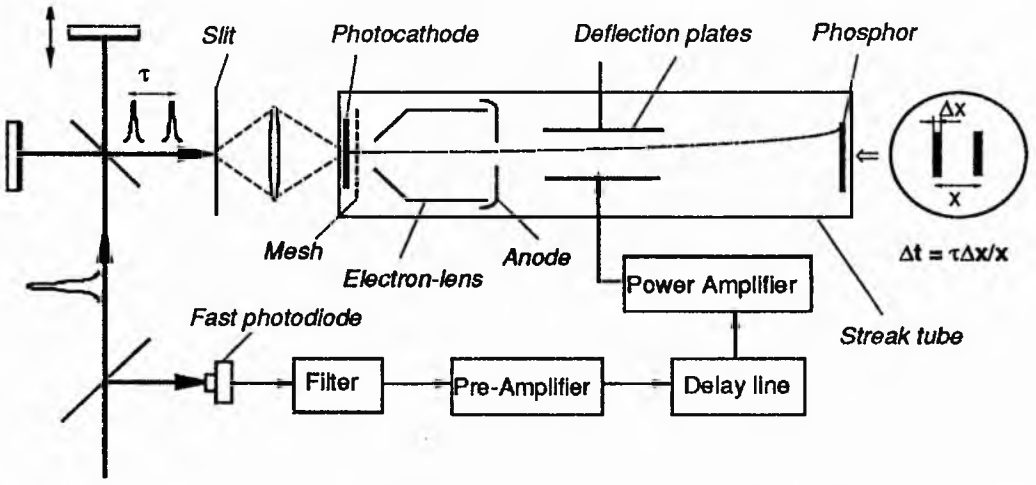

Fig. 4.4. Experimental arrangement for pulse measurement with an electron-optical streak camera.

For the illustration of Fig. 4.4, the practical operation of a streak camera is relatively straight forward. The pulse(s) to be measured is first sent to a Michelson interferometer arrangement where a single pulse is split into two replicas. (The time delay between them

can be accurately controlled by altering the length of one arm of the interferometer. Otherwise a glass plate with calibrated thickness can be used to provide a known time delay). These two temporally separated pulses then illuminate a slit, which is imaged onto the photocathode. The photoelectrons thus produced are accelerated by the mesh and subsequent electrodes which constitute the static electron lens system. During the time when the electrons pass between the two deflection plates a high speed voltage ramp is applied such that the electrons are swept from their straight line trajectory and streaked across the phosphor screen to form two spatially separated streaks. Each of the streaks corresponds to one pulse component. For a single-shot measurement the above actions only occur once while for the synchronous-scan mode the process will be periodically repeated (Sibbett 1982). The measured pulse duration can then be deduced from the spatial width of each streak and the separation between them (see Fig. 4.4), i. e.

$$\Delta t_{ms} = \frac{\Delta x}{x}\tau \tag{4.4}$$

where τ is the time delay between the two replicas. An experimental result of the streak traces associated with the pulses from a coupled-cavity mode-locked KCl:Tl colour-centre laser (details given in Chs. 6, 7) is reproduced in Fig. 4.5.

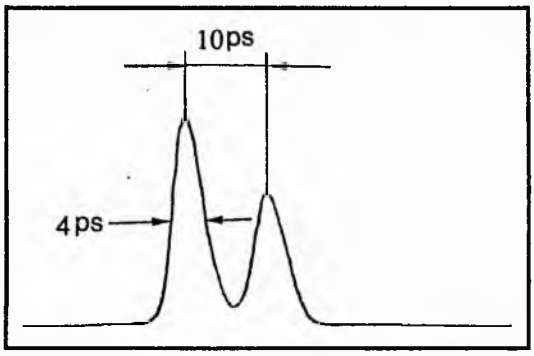

Fig. 4.5. Streak camera records for pulses from a coupled-cavity mode-locked KCl:Tl colour-centre laser. Note that this measured result is much longer than the actual pulse duration. This is not only because of the limited time resolution of the camera system itself but also due to the time jitter problem arising during the course of measurement (see text).

From the above descriptions, it can be recognised that to achieve proper measurement data, the action of applying the ramp voltage to the deflecter must be synchronised to the arrival of the packet of electrons. Failure to attaining this synchronization between these two events will mean either that no streaks are produced for the single-shot measurement,

or that the recorded streaks are blurred because of the jitter during the sequential streaking in the synchronous scan mode. (In practice, the number of repeat streaks can be readily reduced by placing a mechanical shutter with an opening duration of several milliseconds in front of the camera).

Although significant improvements have been made to the deflection circuits (Thomas *et al* 1981) and the triggering method for overcoming the time jitter problem, the best measured results are just under 1 ps for synchronous scan (Finch 1989) and about 300 fs for the single-shot operation (Finch *et al* 1988). Both of resolutions are still several times worse than those predicted for the particular devices by Eq. (4.1). It is, therefore, justified to say that the main uses of streak cameras still remain in picosecond (at most to the demarcation of the subpicosecond) regime[1]. As the researches of ultrafast phenomena enter the femtosecond regime, the capacity of the streak camera for ultrashort pulse measurement rather lags behind the resolution requirements.

Moreover, the process of pulse duration measurement using electron-optical streak cameras may lead one to realize that two fundamental limitations exist for such devices. The first is that the transformation from photons to electrons based on the photo-electric effect can depart from the essentially distortion-free process. From the basic equation $h\nu = \Phi_v + \frac{1}{2} m v_e^2$ where Φ_v represents the escape energy, electrons excited by the photons of different frequencies will have different speeds. A cutoff wavelength which exists ($\lambda_{cutoff} = hc/\Phi_v$) also limits the wavelengths of the photons to be measured. The second limitation is that the photon-electron transformation is an energy process, during which the phase information included in optical pulses is lost. In another words, whether the pulse to be measured is coherent or chirped, or is indeed solely a noise burst, such features will normally not be clear by performing a measurement on a streak camera.

Photon-optical streak camera ?

In a consideration about how to get rid of the limitations of an electron-optical streak camera and also to facilitate the synchronization between the scanning action and the

[1] Useful informations about some detailed commercial streak cameras can be found in the papers given by Doukas *et al* (1982).

pulses, an alternative approach by which the pulses can be scanned with optical pulses via the optical Kerr effect has been considered by the author. In this scheme, no photon-electron transformation is needed. The basic principle of this "photon-optical streak camera" is illustrated in Fig. 4.6 and can be described in the following manner.

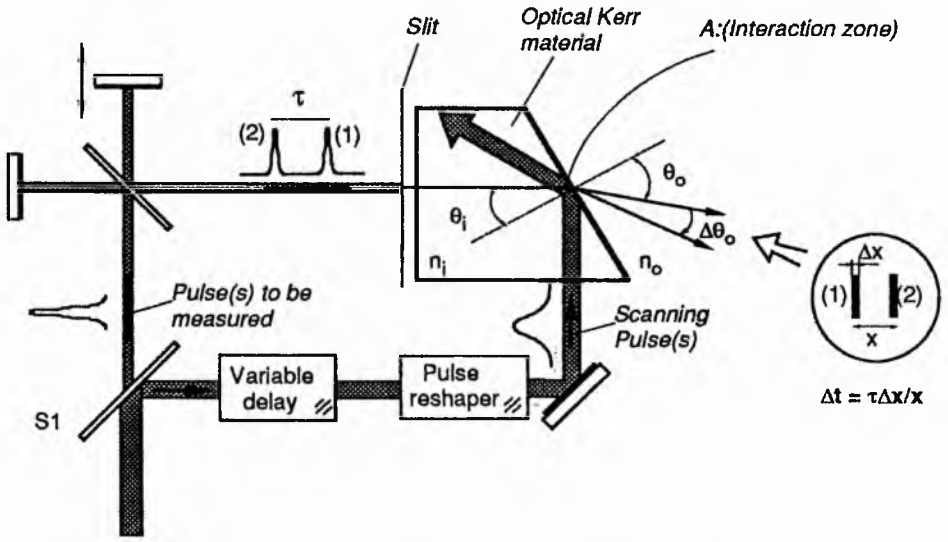

Fig. 4.6. Schematic of a photon-optical streak camera.

At the beam splitter S1, the incident beam is divided into two components. One represents the signal to be measured is directed via a caliberated time delay arrangement, and the other more intense portion is used for scanning purposes. This scanning beam passes through a delay line, temporally stretched to an appropriate duration and subsequently directed into an optical Kerr crystal at an angle of incidence which exceeds the critical angle. In the absence of the scanning beam, the pulses (1), (2) to be measured will be refracted at the oblique surface of the optical Kerr device at an output angle θ_o, which satisfies

$$\sin\theta_o = \frac{n_i}{n_o}\sin\theta_i \tag{4.5}$$

If the scanning pulse arrives at the region (indicated by the letter *A* in the graph) when the leading pulse (1) is just about to be refracted, it will be subjected to a dynamic change of refractive index of n_i due to the optical Kerr effect. This will give rise to a deflection of this refracted pulse. The angular range of the deflection may be expressed as

$$\Delta\theta_o \approx \frac{d\theta_o}{dn_i}\Delta n_i \tag{4.6}$$

where $d\theta_o/dn_i$ represents the variation of the refractive angle caused by per unit change in refractive index and Δn_i is the refractive index change. Δn_i can be written as

$$\Delta n_i = n_i(I) - n_i(0) \tag{4.7}$$

Using Eq. (4.5), then

$$\frac{d\theta_o}{dn_i} = \frac{\sin\theta_i}{n_o\cos\theta} = \frac{\tan\theta_o}{n_i} \tag{4.8}$$

It follows that for larger values of $d\theta_o/dn_i$ then smaller n_o and larger θ_i are required. Thus, we can simply let $n_o = 1$ and $\theta_i = \sin^{-1}[1/(n_i + \Delta n_i)]$. The latter value is chosen such that the total reflection can be just avoided while the refractive index is increased to the maximum[2].

From Eq. (4.8) it can be estimated that, in general, $d\theta_o/dn_i \sim 1$. Thus to make this system practicable, material with a high optical Kerr coefficient must be used and a tight focus for the scanning pulses is needed. (The scanning pulses may come from another high power short pulse laser, if necessary). To reduce undesired dispersion effects the device should be made as thin as possible when used with femtosecond pulses. This does not place any particular restrictions on interaction length because this scheme is based on an interface phenomenon. If such a pulse measurement scheme can be implemented[3], it could offer quite distinct advantages. For example it would be easy to operate, have excellent time resolution, minimal jitter problems in synchronization and it should be compact and relatively inexpenssive.

4.3 SHG autocorrelator

As mentioned in Section 2.5, the autocorrelation technique is a very important method in the duration-measurement of optical pulses. It was not widely employed during the years

---

[2] Interestingly, if this unexpected total reflection occurs the device will be acting as an optical switch.

[3] The feasibility of such a whole optical pulse measurement device is really dependent on whether a material with a Kerr coefficient $\Delta n/n = 10^{-1}$~10^{-2} at a peak power density level of 10 GW/cm^2 can be found. [One possible candidate material could be the Chinese tea, which has been shown to have a Kerr coefficient 10^6 larger than that of CS_2 (Zhang *et al* 1989)].

soon after its invention (Maier *et al* 1966, Weber 1967, Armstrong 1967), partially because of its inconvenience in applying it to pulsed lasers (Ippen and Shank 1977), and partially because the TPF method (Giordmaine *et al* 1967), had exactly the same measuring function as the SHG autocorrelation but was much easier to perform[4]. As more cw mode-locked lasers were developed to have pulse durations less than 0.1 ps, the SHG autocorrelation scheme gained a greater prominence for pulse measurement in the picosecond and femtosecond regimes. This was especially true when a real-time display of the autocorrelation traces was demonstrated (Fork and Beisser 1978), where the repetitive time delay was obtained through mounting a corner reflector on a commercial shaker assembly.

The SHG autocorrelation does not directly provide the pulse profile, but in many cases it is possible to deduce reasonably close estimates for the pulse durations. With slight increase of the time resolution of the detecting system and some improvement on the precision and the stability of the delay system, the interferometric (or fringe-resolved) autocorrelation traces can be obtained, which provides the phase information that the intensity autocorrelation does not include for the measured pulses (Diels *et al* 1978).

4.3.1 Experimental arrangement

An experimental set-up of a SHG autocorrelator is shown in Fig. 4.7. Basically, it is composed up of two parts: one is a Michelson interferometer which serves as a pulse divider and delay control; the other part is simply a SHG crystal together with a focusing lens. The detector (e. g. photomultiplier) behind the crystal is selected to be either only sensitive to the frequency-double signal or an optical filter which blocks the fundamental frequency light is placed in front of the detector. One of the corner reflectors C_1 is mounted on a speaker which is translated by the output of a triangular wave drive oscillator. At each position of C_1 one particular delay between the two replica pulses is

[4] Besides these techniques, the advantages of streak cameras as direct linear measurement devices still had major attractions in 1970s because their time resolution capabilities were competible with the durations of the pulses generated at that stage.

obtained and thus one point in the autocorrelation trace is recorded. With every half of the translation period of the speaker an entire autocorrelation trace is formed.

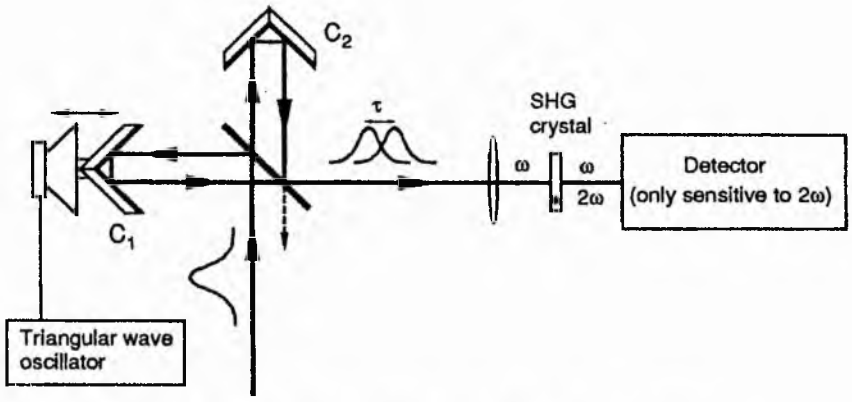

Fig. 4.7. Experimental set-up for a SHG autocorrelator.

In general, the translation amplitude of the speaker is chosen according to the pulse duration regime. For longer pulses larger time delays ($\tau_{max} \geq 10\Delta t$) and so greater amplitudes are needed. The translation frequency is dependent upon the response time of the detector system and the necessity for a stationary display of the autocorrelation trace on an oscilloscope. These two requirements set an upper and lower limits for the shaker frequency. Normally a compromise value is used, which is typically around 200 Hz. Assuming that the cw mode-locked pulse trains have a pulse repetition period ~12 ns, it is readily estimated that to construct one complete autocorrelation trace a total of 10^5 pulses are required in a typically averaged autocorrelation profile[5]. As C_1 is moved back and forth overwriting of the autocorrelation traces happens and this gives rise to a stationary display on the oscilloscope screen. The time calibration of the measured autocorrelation trace can be implemented by moving another corner reflector C_2 mounted on a translation stage by a known displacement.

---

[5] Imagine that if the pulse duration, or even pulse shape, varies noticeablely within the time interval of one shaking period, the recorded autocorrelation trace will be a mixed contribution of these different pulses. By assuming the existence of a pulse duration distribution, Van Stryland (1979) showed that owing to the averaging effect over the pulses having different durations the observed autocorrelation will always tend to have an exponential profile. Such a profile led some researchers to erroneously assume that the measured pulses had an exponential shape, from which rather shorter pulse durations were optimistically deduced.

4.3.2 Theoretical analyses

If the influence of the group velocity dispersion in the SHG crystal is neglected and by assuming that the pattern of the spatial distribution of the field is time-independent (Mindl *et al* 1983), the detected second harmonic signal from a SHG autocorrelator can be expressed as

$$I_{2\omega}(\tau) \propto G_I \equiv \int_{-\infty}^{+\infty} I^2(t,\tau)dt \tag{4.9}$$

where $I(t,\tau)$ is given by

$$I(t,\tau) = [V(t) + V(t+\tau)]\,[V(t) + V(t+\tau)]^* \tag{4.10}$$

The time integral in Eq. (4.9) represents the accumulating effect caused by the limited response time of the detector. Provided that the measured pulses are coherent, i. e.

$$V(t) = A(t)e^{i\phi_o}e^{-i\omega t} \tag{4.11}$$

where ϕ_o is a constant, substitution of Eq. (4.11) into Eq. (4.10) and then bringing the resultant expression for $I(t,\tau)$ into Eq. (4.9), it can be deduced that:

$$G_I(\tau,\omega) = G_{2B}(\tau) + G_f(\omega,\tau) \tag{4.12a}$$

where

$$G_{2B}(\tau) = \int_{-\infty}^{+\infty} [A^4(t) + A^4(t+\tau) + 4A^2(t)A^2(t+\tau)]dt \tag{4.12b}$$

$$G_f(\omega,\tau) = \int_{-\infty}^{+\infty} \{2\cos(2\omega\tau)A^2(t)A^2(t+\tau) + 4\cos(\omega\tau)[A^3(t)A(t+\tau) + A^3(t+\tau)A(t)]\}dt \tag{4.12c}$$

Eq. (4.12a) is the general expression of the so-called *interferometric autocorrelation*, which contains two components. The first one expressed by Eq. (4.12b) is solely a function of time delay, while the second given by Eq. (4.12c) relies on both the time delay and the carrier frequency. If the detector system cannot follow the oscillations characterised by $\cos(\omega\tau)$, the second component will be averaged out, i. e. $(G_f)_{avg.} = 0$, and so only the slowly changing portion, $G_{2B}(\tau)$, is recorded. $G_{2B}(\tau)$ is widely referred to

as the *intensity autocorrelation* (the non-background-free type)[6], which can be rewritten as

$$G_{2B}(\tau) = 2\int I^2(t)dt\left[1 + \frac{2\int I(t)I(t+\tau)dt}{\int I^2(t)dt}\right] = C[1 + 2g_2(\tau)] \qquad (4.13)$$

where $I(t) = A^2(t)$ and the indices for integral range (from $-\infty$ to $+\infty$) are omitted. Since $g_2(0) = 1$ and $g_2(\tau >> 2\Delta t) = 0$, $G_{2B}(\tau)$ has a peak-to-background ratio of 3:1. In some experimental arrangements only $g_2(\tau)$ is recorded. This was achieved by either polarizing the two replica pulses orthogonally (Weber 1967) or making them have a noncollinear incident angle (Ippen and Shank 1977). To differ from G_{2B} in names, $g_2(\tau)$ is termed as *background-free intensity autocorrelation.* In a form similar to Eq. (4.13), Eq. (4.12a) can be reexpressed as

$$G_I = C\left\{1 + [2 + \cos(2\omega\tau)]g_2(\tau) + 2\cos(\omega\tau)\left(\frac{2\int A^3(t)A(t+\tau)dt}{\int A^4(t)dt} + \frac{2\int A^3(t+\tau)A(t)dt}{\int A^4(t)dt}\right)\right\} \qquad (4.14)$$

It is straightforward to derive that the interferometric autocorrelation function G_I has a peak-to-background ratio [$G_I(0)/G_I(\tau >> 2\Delta t)$] of 8:1. The fringes have maxima when $\omega\tau = 2n\pi$ and minimas at $\omega\tau = (2n+1)\pi$. For the first minimum value ($n = 0$), $\omega\tau = \pi$ and $G \approx 0$. As $|\tau|$ increases the maxima decrease while the minima increase. They finally merge at the background level. The period of the fringes displayed on the time delay axis is given by $T_f = 2\pi/\omega$, which corresponds to one optical cycle of the carrier. This feature leads to a special use of interferometric autocorrelation which is that the timescale on the screen can be conveniently calibrated by counting the number of the fringes in each division.

If the pulses to be measured are frequency chirped, it can be shown that Eqs. (4.12) are still valid except that in these cases ω is a function of both t and τ, and consequently,

$$\omega = \omega(t, \tau) = \omega_0 + \frac{d}{d\tau}[\phi(t+\tau) - \phi(t)] = \omega_0 + \frac{d\phi}{dt} + \frac{d^2\phi}{dt^2}\tau + \cdots \qquad (4.15)$$

---

6 It should be pointed out that the designations of interferometric autocorrelation and intensity autocorrelation sometimes give rise to some confusion. They are both autocorrelations of optical intensity, the only difference between them is simply that one has fringes resolved with better time resolution whereas the other is fringe-averaged and therefore only sensitive to the pulse profiles.

The oscillatory terms $\cos(2\omega\tau)$, $\cos(\omega\tau)$ thus cannot be taken out of the time integral as in Eq. (4.14). An interesting feature implied by Eq. (4.15) is that for chirped pulses the fringes within the interferometric autocorrelation trace are no longer uniform. Instead, the variation of the fringe frequency with respect to the delay time follows the same pattern as the carrier chirp in the time domain. This is the basic reason why Diels *et al* (1985) concluded that the characteristics of the pulse phase or the carrier can be included in the interferometric autocorrelation.

Example II. Interferometric autocorrelations for chirped and unchirped pulses

For a linear chirped Gaussian pulse, suppose

$$V(t) = e^{-at^2} e^{i\phi(t)} e^{-i\omega_0 t} \tag{4.16}$$

where $a = 2\ln 2/(\Delta t)^2$, $\phi(t) = bt^2$ (b is the chirp parameter), and so

$$\omega(t, \tau) = \omega_0 + 2bt + 2b\tau \tag{4.17}$$

Bringing Eq. (4.16) into Eq. (4.12) produces (Sala *et al* 1980):

$$g_I \equiv \frac{G_I(\tau)}{C} = 1 + 2e^{-a\tau^2} + \cos(2\omega_0\tau)e^{-(1+b^2/a^2)a\tau^2} + 4\cos(\omega_0\tau)\cos(b^2\tau^2/4a)e^{-(3+b^2/a^2)a\tau^2/4} \tag{4.18}$$

The corresponding intensity autocorrelation is given by

$$g_{2B} \equiv \frac{G_{2B}(\tau)}{C} = 1 + 2e^{-a\tau^2} \tag{4.19}$$

Note that the intensity autocorrelation does not indicate whether the pulse is chirped or not. In Eq. (4.18), let b = 0, the interferometric autocorrelation for a chirp-free Gaussian pulse can be obtained, which is

$$g_I' = 1 + e^{-a\tau^2}[2 + \cos(2\omega_0\tau)] + 4\cos(\omega_0\tau)e^{-3a\tau^2/4} \tag{4.20}$$

Two calculated results following Eq. (4.18) and Eq. (4.20) for $\Delta t = 75$ fs, $b/a = 20$, $\omega_0 = 1.25 \times 10^{15}$ Hz (for $\lambda = 1.5$ μm) are shown in Fig. 4.8(a), (b) respectively, where corresponding intensity autocorrelation traces are also shown. As it is expected, for both the chirped and unchirped pulses, whose electric fields have been shown in Fig. 2.2, the intensity autocorrelations are the same while the interferometric counterparts are dramatically different. For the chirped case, because a large value has been assumed for the chirp parameter, the interferometric fringes are only visible in the central part of the traces. If we reassume $b/a = 2$ the corresponding interferometric autocorrelation trace will be the one reproduced in Fig. 4.8(c). Two experimentally recorded autocorrelation traces, one for unchirped pulses and one for chirped pulses, are presented in Fig. 4.9(a) and (b) respectively. A qualititive comparision of these traces with the calculated data in Fig. 4.8(a), (c) shows satisfactory agreement.

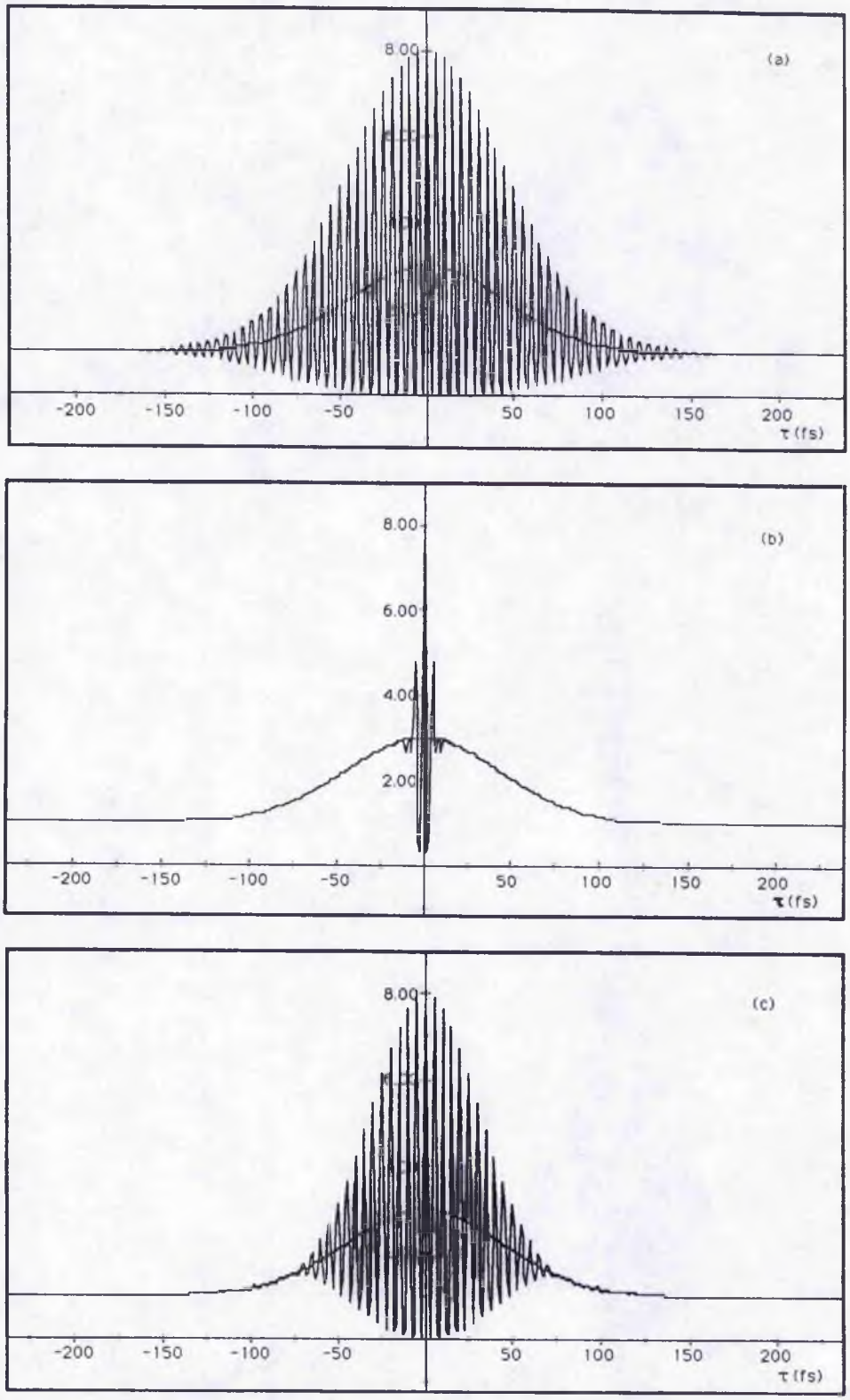

Fig. 4.8. Calculated intensity and interferometric autocorrelation traces for 75 fsec Gaussian pulses. (a) chirp-free, (b), (c) chirped, where the chirp parameter b = 20a, 2a respectively.

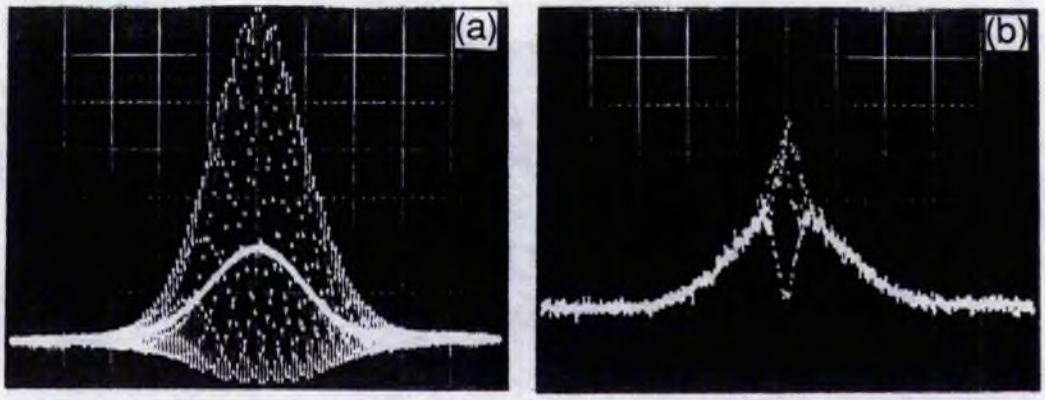

Fig. 4.9. Experimentally recorded autocorrelation traces for the coupled-cavity mode-locked KCl:Tl colour centre laser pulses. (a) for main output pulses, (b) for pulses out of the control fibre.

The upper and lower envelopes of the interferometric autocorrelation traces can be obtained simply by setting $\omega\tau$ in Eq. (4.12c) equal to $2n\pi$ and $(2n+1)\pi$ respectively. For the traces shown in Fig. 4.8, we have

$$(g_I)_{\text{external-envelope}} = 1 + 2e^{-a\tau^2} + e^{-(1+b^2/a^2)a\tau^2} + 4e^{-(3+b^2/a^2)a\tau^2/4} \qquad (4.21a)$$

$$(g_I)_{\text{internal-envelope}} = 1 + 2e^{-a\tau^2} + e^{-(1+b^2/a^2)a\tau^2} - 4e^{-(3+b^2/a^2)a\tau^2/4} \qquad (4.21b)$$

Thus, the width of the interferometric autocorrelation can be estimated from Eq. (4.21a). With the left-hand-side of Eq. (4.21a) equal to 4, we obtain

$$3 = 2e^{-a(\tau_{2c}/2)^2} + e^{-a(1+b^2/a^2)(\tau_{2c}/2)^2} + 4e^{-a(3+b^2/a^2)(\tau_{2c}/2)^2/4} \qquad (4.22)$$

where τ_{2c} is the FWHM of the interferometric autocorrelation trace. From Eq. (4.22), it can be seen that τ_{2c} is frequency-chirp dependent, and for a given pulse duration a fixed relationship between τ_{2c} and the chirp parameter b can be established. In general, as demonstrated in Fig. 4.10, the larger the frequency chirp the smaller is the FWHM duration of the interferometric autocorrelation. (This can be understood by the fact that as the pulses become heavily chirped in a linear form, the leading part and the trailing part are no longer coherent, which leads to a wash-out of the fringe visibility in the wings of the interferometric autocorrelation trace and so a decrease of τ_{2c}). For a known pulse shape, such a feature can be used to evaluate the magnitude of the chirp in the pulses, when a linear chirp is assumed. From Eq. 4.21(a), if b = 0, we have $\tau_{2c} = 1.696\Delta t$ (For chirp-free sech^2 pulse shape, $\tau_{2c} = 1.897\Delta t$), otherwise $\tau_{2c} < 1.696\Delta t$.

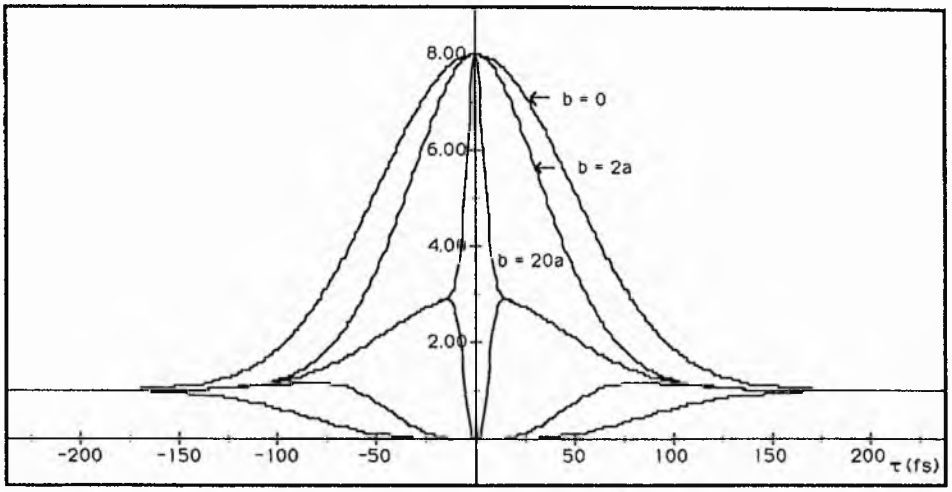

Fig. 4.10. Envelopes of interferometric autocorrelation traces for the Gaussian pulses which have the chirp parameters b = 0, 2a, 20a.

As a measure of interference, τ_{2c} can be taken as a second-order coherence time, which may be compared with the parameter τ_c described in Section 2.1. A common property of τ_{2c} and τ_c is that they are both frequency-chirp related, except that τ_{2c} is expected to be more sensitive owing to the fact that it describes a higher coherence order. (As far as the statistical feature of the field is concerned, it is possible that for two sequence of pulses they may have the same τ_c but their τ_{2c}'s may be quite different). A similar argument applies for yet higher-order coherence times, which may be derived from the n_{th} order autocorrelation ($n > 2$) (Sala *et al* 1980). However, in practice, the high order autocorrelations are often difficult to achieve because of the requirement on higher pulse power and more complicated optical arrangements.

Finally, it needs to be emphasised that because τ_{2c} is dependent upon both frequency-chirp and pulse phase, the actual duration of the measured pulses should be always deduced from the FWHM width of the intensity autocorrelation rather than the envelope of the interferometric one. In the cases where the pulse coherence is wanted to be checked, a comparison of Δt's deduced respectively from intensity and the interferometric autocorrelations can be made. If the two values are the same the pulses are coherent, otherwise, (the one derived from τ_{2c} is smaller than that from τ_I), implying that the pulses are not perfectly coherent.

4.3.3 Problems of deviations from the standard peak-to-background ratio

Sometimes in experiments, it has been found that the recorded autocorrelation traces do not have the theoretically expected peak-to-background ratio. This may be due to misalignment of the autocorrelator so that the two replica pulses entering the SHG crystal do not have equal intensities. Assuming that I_1, I_2 are the intensities for the two replica pulses and $I_1/I_2 = h$. It can be shown that the peak-to-background ratio in these cases is given by,

(i) for intensity autocorrelation,

$$r = 1 + \frac{4h}{1+h^2} \tag{4.23}$$

and

(ii) for interferometric autocorrelation,

$$r_f = 1 + \frac{6h + 4h^{3/2} + 4h^{1/2}}{1+h^2} \tag{4.24}$$

A plot of both r and r_f versus h is given in Fig. 4.11. It is clearly shown that the ratios 3:1 and 8:1 only exist when $h = 1$, otherwise, $r < 3/1$ and $r_f < 8/1$.

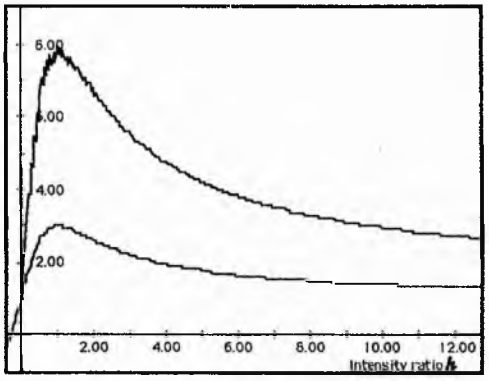

Fig. 4.11. Variations of the peak-to-background ratios of the intensity and interferometric autocorrelation traces as a function of the ratio between the two replica pulse intensities.

During experiments, whether the two replica pulses have equal intensity or not can be checked by alternatively blocking one of the two arms of the interferometer and then comparing the corresponding SHG signal levels. If $I_1 = I_2$, but the measured SHG autocorrelation traces still do not have the predicted peak-to-background ratio, it will be most likely that the pulses themselves are not discrete, or in another words, they are mixed with some background light (Mindl *et al* 1983). [Of course, the laser should

always be properly aligned so that only single transverse mode exists, otherwise, the spatial coherence of the measured pulses needs to be considerred (Weber and Danielmeyer 1970)].

4.3.4 Intensity autocorrelation of noise bursts

In the discussions given above we have limited our consideration to the autocorrelations of the discrete pulses, either chirped or unchirped. In practice, since the optical pulses generated by various mode-locked techniques (see Section 3.4) often comprise incoherent components, there has been a great deal of interest in the characteristics of the SHG autocorrelation for noise bursts.

The general expression for the intensity autocorrelation relating to a noise burst can be obtatined by substituting Eq. (2.37) given in Section 2.4 into Eq. (4.12b), which gives rise to (Pike and Hercher 1970)

$$g_b = 1 + (1 + |g_{1R}(\tau)|^2)\, g_{2A}(\tau) \tag{4.25}$$

where

$$g_{1R}(\tau) = \frac{\int R(t)R^*(t+\tau)dt}{\int R^2(t)dt} \tag{4.26a}$$

$$g_{2A}(\tau) = \frac{\int [A_T(t)A_T^*(t+\tau)]^2 dt}{\int A_T^4(t)dt} \tag{4.26b}$$

It should be remembered that in the above equations R(t) is a random variable relating to the thermal noise and $A_T(t)$ is the amplitude profile function of the noise burst. Suppose that a noise burst has an amplitude profile of Gaussian shape

$$A_T(t) = e^{-at^2} \tag{4.27}$$

and the thermal noise, has a normalized spectral distribution given by

$$i_n(\omega) = e^{-\ln 2[(\omega - \omega_o)^2/\Delta\omega_n^2]} \tag{4.28}$$

where $\Delta\omega_n$ is the bandwidth and ω_o is the mean frequency, from Eqs. (4.27) and (4.28) and noting that a Fourier transform of $i_n(\omega)$ gives rise to $g_{1R}(\tau)$ [see Eq. (2.21)], then:

$$g_{1R}(\tau) = e^{-4\ln 2\,[\tau/\tau_c]^2} \tag{4.29a}$$

$$g_{2A}(\tau) = e^{-a\tau^2} \tag{4.29b}$$

τ_c is given by

$$\tau_c = \frac{4\ln 2}{\Delta\omega_n} \tag{4.30}$$

which is the coherence time of R(t). Substituting Eqs. (4.29) into Eq. (4.25) yields

$$g_b = 1 + e^{-a\tau^2}(1 + e^{-4\ln 2\,[\tau/\tau_c]^2}) \tag{4.31}$$

Example III. Intensity autocorrelation for noise bursts

Assuming that Δt = 60 ps, τ_c= 6ps = Δt/10, then according to Eq. (4.31) where a = 2ln2/Δt^2, we have

$$g_b = 1 + e^{-3.85\times10^{-4}\tau^2}(1 + e^{-0.077\tau^2}) \tag{4.32}$$

where τ is in a unit of ps. A plot of Eq. (4.32) is shown in Fig. 4.12(a). For comparison, an experimentally recorded SHG intensity autocorrelation trace, obtained for the pulses from a synchronously mode-locked KCl:Tl colour centrelaser is reproduced in Fig. 4.12(b).

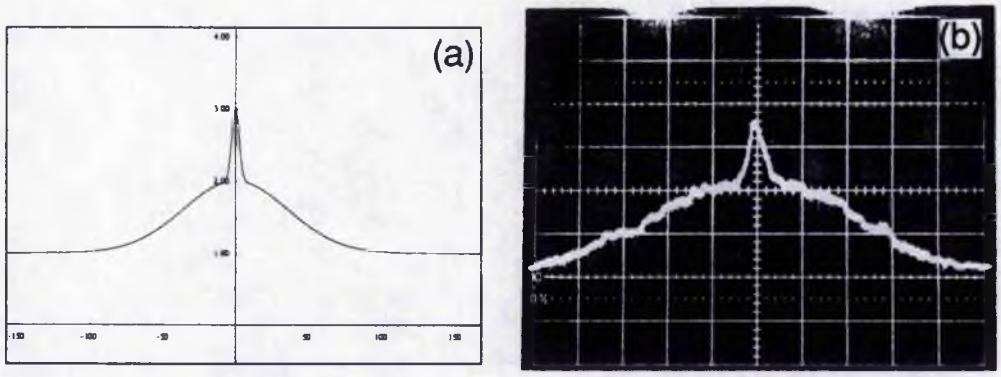

Fig. 4.12. Calculated (a) and experimental (b) intensity autocorrelation traces for 60 ps noise-burst pulses with a central wavelength around 1.5 μm.

It can be recognized that g_b given by Eq. (4.31) is characterized by the parameters for two temporal extents: one is the pulse duration Δt [= $(a/2\ln 2)^{1/2}$], and the other is related to the first order coherence time τ_c of the thermal carrier. It is this feature that leads to the general profile of g_b frequently having a shoulder - like one envelope sitting on the top of the other (see Fig. 4.12). Moreover, two extreme forms of g_b can be derived from Eq. (4.31). The first one is that, if $\tau_c \approx 0$ ($\Delta\omega \to \infty$), then this implies that R(t) is completely incoherent so that $|g_{1R}(\tau)| = 0$ and:

$$g_b = g_w = 1 + g_{2A}(\tau) \tag{4.33}$$

In contrast, if $\tau_c \to \infty$ ($\Delta\omega \approx 0$), which means the carrier has a well defined ("single") frequency so that $|g_{1R}(\tau)| = 1$, then the second extreme form of g_b exists:

$$g_b = g_c = 1 + 2g_{2A}(\tau) \tag{4.34a}$$

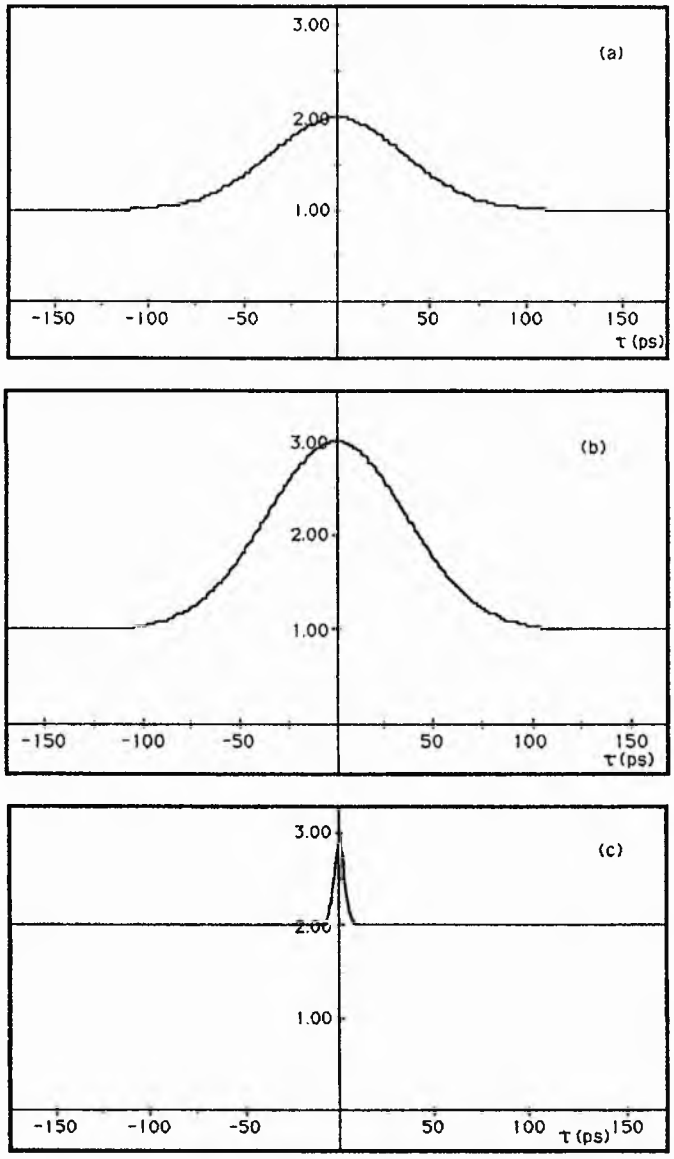

Fig. 4.13. Intensity autocorrelations for (a) "white noise burst", (b) coherent pulses, (c) continuous noise.

Eq. (4.33) gives the intensity autocorrelation of a "white" noise burst, while Eq. (4.34a), as expected, is for a coherent pulse. Plots made on the basis of these two equations with $\Delta t = 60$ ps is shown in Fig. 4.13 (a), (b) respectively, which should be compared with the

trace given in Fig. 4.12(a). Another extreme situation of Eq. (4.31) is that for a = 0, which means the thermal noise is not truncated at all. Therefore

$$g_b = g_n = 2 + e^{-4\ln 2\,[\tau/\tau_c]^2} \qquad (4.34b)$$

where g_n is the intensity autocorrelation for continuous noise. A plot of Eq. (4.34b), again with τ_c = 6 ps, is shown in Fig. 4.13(c).

4.3.5 Combination of intensity autocorrelation, interferometric autocorrelation and the spectrum measurement

As a final comment on the autocorrelation pulse measurement technique, it should be pointed out that the dependence of the intensity autocorrelation profile on the pulse shape is not governed by a one-to-one relationship. A pulse shape, therefore, can not be unambiguously determined from the autocorrelation measurements. (Further evidence for this is that the SHG autocorrelation is always symmetric and so any asymmetry in the pulses to be measured will not be shown). A similar arguement is also true for the relationship between the interferometric autocorrelation and the pulse phases. All of these features indicate that with the autocorrelation measurement, the pulse duration and the frequency chirping characteristics can only be derived for an assumed pulse shape and a given type of chirp. This more or less represents the primary drawback of this type of measurement. However, as demonstrated by Diels *et al* (1985), by the iterative fitting of the intensity autocorrelation, the pulse spectrum and the interferometric autocorrelation of a trial pulse to experimentally measured data, the pulse shape and phase can be determined to a reasonably accurate extent.

4.4 Other techniques

As a consequence of the inadequate time resolution of streak cameras and the inherent ambiguity in the SHG autocorrelation measurement, many new techniques for the pulse shape and phase determination have been under consideration for picosecond-to-femtosecond regime. According to the physical principles involved, these new techniques can be grouped into two types: one is the *heterodyne technique* and the other is the *spectral filtering - time delay* technique.

For the heterodyne technique, the key point is to derive a suitable reference pulse and so after the heterodyne measurement the information included in the signal pulse can be appropriately inferred. A general schematic of this approach is shown in Fig. 4.14. Based on some special modifications on the general arrangement and the difference in the directly recorded physical quantities, this scheme has been further specified as *the cross-correlation* (Nakatsuka and Grischkowsky), or *the time-domain interferometry* (Rothenberg and Grischkowsky 1985, Rothenberg 1986), or *the spectral-interferometry* methods (Reynaud *et al* 1989).

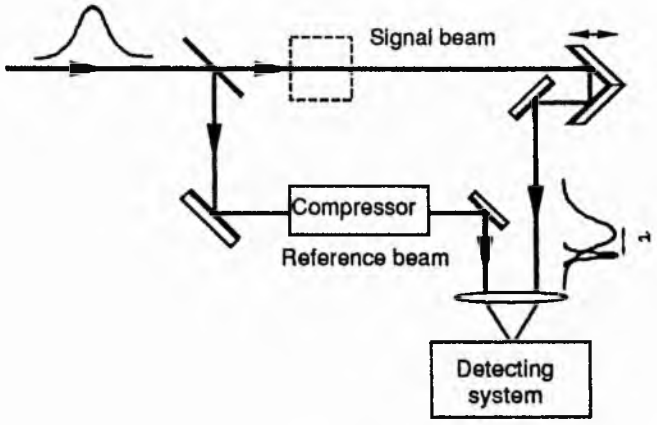

Fig. 4.14. Typical experimental arrangement used in heterodyne pulse measurement technique.

With the cross-correlation, the pulse to be measured is divided into two intensity components where one is the signal pulse and the other is directed to a temporal compressor and taken as the reference pulse. The cross-correlation between the signal pulse and the reference pulse enables the signal pulse shape to be deduced. In the time-domain interferometry arrangement, one additional Mach-Zehnder interferometer, or a resonant vapour cell, is inserted in the signal pass (at the position marked by the dash line block in Fig. 4.14). This Mach-Zehnder interferometer in which one of its arms includes an etalon filter for the carrier functions to convert the phase information of the signal pulse into a modulated intensity pattern. The subsequent cross-correlation resolves this interference pattern, from which the phase of the signal pulse can be determined. For the spectral-interferometry method, instead of measuring the temporal cross-correlation the

spectral interferogram is recorded. Such a spectral interferogram has a modulated pattern which is a record of the spectral phase difference between the signal pulse and the reference pulse. From the number of the spectral fringes, the relative spectral phase shift of the signal pulse can be found. In the cases where the phase of the reference pulse is known, the complete spectral components of the measured pulses will be obtainable, which is given by

$$\upsilon(\omega) = \sqrt{i(\omega)}\, e^{i\phi(\omega)} \tag{4.35}$$

By Fourier transforming $\upsilon(\omega)$, the temporal features of the measured pulses in both shape and phase can be obtained[7].

The spectral filtering - time delay technique is based on the fact that for chirped pulses, different time sections within a pulse have correspondingly different frequency constituents. Therefore, if a tunable spectral filter is used to select particular sections of the spectrum, a time delay between these spectral segments can be detected (see Fig. 4.15). For example, either the low frequency group lead the high frequency group, or vice versa. The curve of this delay time versus frequency (τ - ω) therefore will indicate which frequency components are at any specified time locations in the pulses and so the pulse phase can be determined uniquely. It has been shown that (Martinez and Chilla 1990),

$$\tau(\omega) = \frac{d\phi}{d\omega} \tag{4.36a}$$

and so,

$$\phi(\omega) = \int \tau(\omega) d\omega \tag{4.36b}$$

A more straightforward use of the τ - ω curve involves a derivate of ω with respect to τ, which gives both the sign and the magnitude of linear frequency chirp.

In practice, the delay time measurements have been carried out by using a streak camera (Gomes *et al* 1985), a sampling oscilloscope (Johnson *et al* 1986) and an autocorrelator (Martinez and Chilla 1990). For the first two systems the delay time can be self-referenced where for the autocorrelator a reference pulse sequence is needed. The

---

[7] For the spectral phase measurement, a method of determining the first three Taylor expansion coefficients of $\phi(\omega)$ through conducting a fitting process to both the recorded intensity autocorrelation and the spectrum was demonstrated by Kobayashi *et al* (1986).

tunable filter could be a spectrometer, or a grating-slit combination. One important point in performing this spectral filtering - time delay measurement is that special care must be taken to make sure that no extra dispersion is introduced during the spectral selection process.

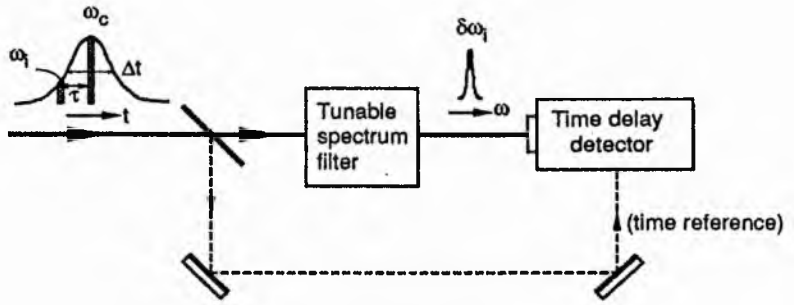

Fig. 4.15. Schematic of spectral filtering - time delay technique for optical pulse measurement.

First-order spectral autocorrelator

In the summary of Section 2.6, it was mentioned that the autocorrelation of the Fourier components of optical pulses is given by:

$$G_1(\Omega) = \int_{-\infty}^{+\infty} \upsilon(\omega)\upsilon^*(\omega+\Omega)d\omega \qquad (4.37)$$

The significance of this spectral autocorrelation is that a reverse Fourier transform of it gives the pulse intensity profile I(t). In the following, one possible way to attain this spectral autocorrelation experimentally is described.

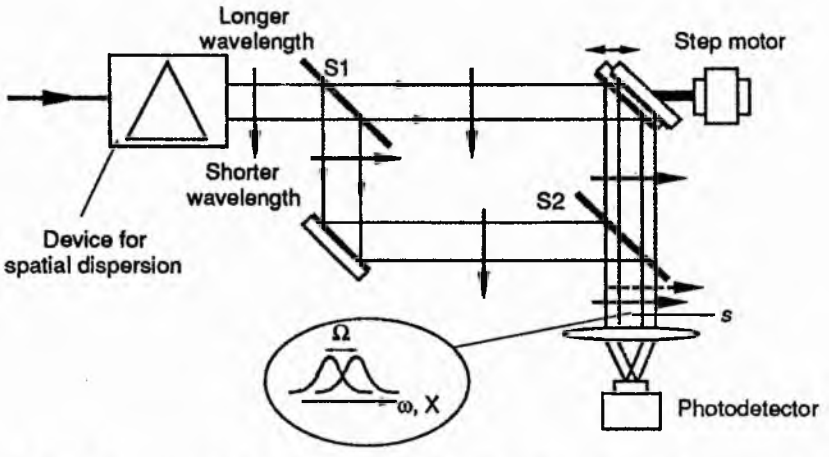

Fig. 4.16. Schematic for the measurement of the first-order spectral autocorrelation.

As shown in Fig. 4.16, the proposed arrangement consists of two parts: one spatial dispersion device and a Mach-Zehnder interferometer. The pulse is first sent to the spatial dispersion device, (e.g. a prism or grating,) so that the pulse spectrum can be spatially extended. The arrows in Fig. 4.16 across the beam means that the wavelength decreases along the designated direction. This spatially spread spectrum is divided in intensity at the beam splitter S1 into two identical parts, which meet each other at the beam splitter S2 after travelling an equal optical distance only different paths. In this case, these two spectral replicas match precisely in space in front of the detector. However, if we shift one of the reflectors, say the the one on the up-right corner of the interferometer, along the direction parallel to the incident beam, there will be a spatial (and thus spectral) displacement of the two spectral replicas at the position marked by the letter *s*. Thus, the signal received by the detector, which is chosen to have a suitable detecting area, will be

$$I(\Omega) \propto \int_{-\infty}^{+\infty} [\upsilon(\omega) + \upsilon(\omega+\Omega)][\upsilon(\omega) + \upsilon(\omega+\Omega)]^* d\omega$$

$$= \int_{-\infty}^{+\infty} \{\, i(\omega) + i(\omega+\Omega) + 2\mathrm{Re}[\upsilon(\omega)\upsilon^*(\omega+\Omega)] \,\} d\omega \qquad (4.38)$$

The integrals on $i(\omega)$ and $i(\omega+\Omega)$ contribute to a background level while the third integration term leads to $G_1(\Omega)$. Note that a real-time display of $G_1(\Omega)$ is also achievable if the method of shifting the mirror by an speaker (as demonstrated in ordinary autocorrelators) is adopted here. This will certainly enable Friouer transforms of $G_1(\Omega)$ to be repeated at relatively shor-term time intervals such that any pulse shape change during this period can be monitored.

Chapter 5

Pulse Propagation

With the advent of the development in both generation and measurement techniques of ultrashort laser pulses, the subject of optical pulse propagation in various media has been of much research interest (Garrett and McCumber 1970, Davis and Lin 1973, Bendow *et al* 1980, Crosignani *et al* 1981, Maimistov and Manykin 1983, Smith *et al* 1985, Menyuk 1987, and Christov 1988). It is not only directly involved in many applications of laser pulses but also closely related to the study of laser sources that produce short pulses.

Owing to the existence of the finite response times and so the limited transformation bandwidth of the various media, optical pulses having durations in picosecond-femtosecond range can be readily modified in phase and amplitude during their propagation. In particular, pulse propagation in linear, dispersive media involves the process of pulse broadening or pulse shortening without generation of any new frequency components while in nonlinear media frequency shifts or spectral extension may become prominent effects. Studies of pulse propagation are generally directed towards two distinct objectives: one relates to scheme by which undesired pulse distortions can be avoided and the other is the exploration of effective means for either producing pulses at new frequencies or reshaping the pulses into required forms. In this chapter, the fundamental physics involved in pulse propagation, as well as some basic principles used in pulse compression techniques, are presented. These are given in the order of pulse propagation in linear media, nonlinear media and a summary of the basic propagation equations that can be applied under different circumstances.

5.1 Linear media

5.1.1 Expression of dispersion

For lossless linear media, the feature of the propagating pulses will be solely dependent on the material dispersion, which is defined as the frequency-dependence of the

susceptibility, $\chi(\omega)$. [χ relates the polarization of a medium to the incident field (see Appendix A)]. χ is related to the dielectric constant ε_r ($\varepsilon_r = 1 + \chi$), ε_r is related to the refractive index n ($n = \sqrt{\varepsilon_r}$) and n is related to the propagation constant $\beta = kn$ ($k = 2\pi/\lambda$), so there are many ways to describe dispersive parameters. For example, $\varepsilon_r(\omega)$, $n(\lambda)$, $\beta(\omega)$ etc.. In optics, the two most commonly used forms are $n(\lambda)$ and $\beta(\omega)$. In the cases where the material properties of the media are of primary concern, the expressions for the wavelength dependence of refractive index are often used. One of these is known as Sellmeier dispersion formula for solid and liquid materials and may be expressed as:

$$n^2 - 1 = \sum_{j=1}^{n} - \frac{B_j \lambda^2}{\lambda^2 - \lambda_j^2} \tag{5.1}$$

where the coefficients B_j, λ_j can be determined through a fitting process to the experimentally measured $n(\lambda)$ curve[1]. From Eq. (5.1), the first three differentiation orders of n with respect to λ can be obtained to be (Marcuse 1980):

$$\frac{dn}{d\lambda} = -\frac{\lambda}{n} \sum_{j=1}^{n} \frac{B_j \lambda_j^2}{(\lambda^2 - \lambda_j^2)^2} \tag{5.2a}$$

$$\frac{d^2n}{d\lambda^2} = \frac{1}{n} \sum_{j=1}^{n} \frac{B_j \lambda_j^2 (3\lambda^2 + \lambda_j^2)}{(\lambda^2 - \lambda_j^2)^3} - \frac{1}{n} \left(\frac{dn}{d\lambda}\right)^2 \tag{5.2b}$$

$$\frac{d^3n}{d\lambda^3} = -\frac{12\lambda}{n} \sum_{j=1}^{n} \frac{B_j \lambda_j^2 (\lambda^2 + \lambda_j^2)}{(\lambda^2 - \lambda_j^2)^4} - \frac{3}{n} \frac{dn}{d\lambda} \frac{d^2n}{d\lambda^2} \tag{5.2c}$$

It has been established that for many materials simple approximate relations exist in most of the visible region between the i_{th} and the $(i\text{-}1)_{th}$ order derivatives ($i = 4,3,2$) of the

---

[1] As an example, for pure silica, the coefficients for a three term Sellmeier expansion are (Kobayashi *et al* 1977)

$B_1 = 0.6961663$ $B_2 = 0.4079426$ $B_3 = 0.8974994$

$\lambda_1^2 = 0.004679148\ \mu m^2$ $\lambda_2^2 = 0.01351206\ \mu m^2$ $\lambda_3^2 = 97.934002\ \mu m^2$

[Information about the material dispersion for the glasses with different dopants can be found in the paper by Fleming (1978)].

refractive index (Bor and Rácz 1985). For example:

$$\frac{d^2n}{d\lambda^2} = -\frac{3}{\lambda}\frac{dn}{d\lambda} \tag{5.2d}$$

$$\frac{d^3n}{d\lambda^3} = -\frac{4}{\lambda}\frac{d^2n}{d\lambda^2} \tag{5.2e}$$

These relations can be useful in simplifing the associated calculations, especially, in the circumstances where only the estimate is needed.

Describing dispersion in terms of a frequency dependence of the propagation constant is common in the situations where the features of the propagating optical wave are the main issue to be dealt with. In many analyses, $\beta(\omega)$ is expanded into a Taylor series,

$$\beta(\omega) = \beta(\omega_0) + \beta'(\omega - \omega_0) + \frac{1}{2}\beta''(\omega - \omega_0)^2 + \frac{1}{6}\beta'''(\omega - \omega_0)^3 + \cdots \tag{5.3}$$

ω_0 is the central frequency of the propagating pulses, $\beta' = \frac{d\beta}{d\omega}$, $\beta'' = \frac{d^2\beta}{d\omega^2}$, $\beta''' = \frac{d^3\beta}{d\omega^3}$ are all evaluated at $\omega = \omega_0$. If $\beta(\omega)$ varies slowly with ω, or ω is very close to ω_0, Eq. (5.3) can be approximated by retaining the terms up to the the second order. Significantly, the three lowest coefficients, β, β' and β'' have specific physical meanings. This is that, β is related to the phase velocity, β' to the group velocity and β'' to the *group velocity dispersion* (GVD). (Further details about these three parameters are listed in Table 5.1, where their respective physical units are also included).

Table 5.1 Physical meanings of β, β' and β''

$\beta(\omega_0) = \frac{\omega_0}{v_\phi(\omega_0)} = \frac{\omega_0}{\text{Phase velocity}}$	($[s]^0/[m]$)
$\beta'(\omega_0) = \left(\frac{d\omega}{d\beta}\right)^{-1} = \frac{1}{v_g(\omega_0)} = \frac{1}{\text{Group velocity}}$	($[s]^1/[m]$)
$\beta''(\omega_0) = \frac{d}{d\omega}\left(\frac{1}{v_g(\omega)}\right) = \text{Group velocity dispersion}$	($[s]^2/[m]$)

Useful relationships between β, β', β'', β''' and $n(\lambda)$, $\frac{dn}{d\lambda}$, $\frac{d^2n}{d\lambda^2}$, $\frac{d^3n}{d\lambda^3}$ are given as follows

$$\beta = \frac{2\pi n}{\lambda} \tag{5.4a}$$

$$\beta' = \frac{1}{c}\left(n - \lambda\frac{dn}{d\lambda}\right) \tag{5.4b}$$

$$\beta'' = \frac{\lambda^3}{2\pi c^2}\frac{d^2n}{d\lambda^2} \tag{5.4c}$$

$$\beta''' = -\frac{\lambda^2}{(2\pi)^2 c^3}\left(3\lambda^2\frac{d^2n}{d\lambda^2} + \lambda^3\frac{d^3n}{d\lambda^3}\right) \tag{5.4d}$$

5.1.2 Group velocity dispersion

In some theoretical analyses, β' ($=1/v_g$) is also termed as *group delay* (per unit length). This is because for an optical wave packet, the phase velocity describes the speed of the carrier (or the phase), whereas the group velocity v_g relates to the propagation speed of the pulse envelope (Siegman 1986; Ch. 9). (The term $1/v_g$ simply represents the time delay required for the pulse profile travelling unit distance). Generally speaking, group delay is frequency dependent and so a temporal spread of the propagating pulses arises due to this effect. From Table 5.1, it is known that β'' is equal to the differential of group delay with respect to frequency and, therefore, it represents the amount of time spread of an impulse of light within a unit distance and for unit frequency extent. An equivalent parameter which carries the same meaning as β'' except being related to the temporal spread of the light impulse for per unit wavelength rather than per unit frequency can be introduced. That is the commonly used group velocity dispersion parameter $D(\lambda)$. The full expression for $D(\lambda)$ in terms of the wavelength dependence of refractive index is given in Table 5.2, where a comparison of different forms of group delay and group velocity dispersion (GVD) is also listed[2]. In some other cases a dimensionless group-velocity dispersion parameter is used, which is defined as

$$Y \equiv \lambda^2\frac{d^2n}{d\lambda^2} \tag{5.5}$$

It can be readily shown that

$$D = -\frac{1}{c\lambda}Y \tag{5.6}$$

---

[2] In literature, there is often an arbitrary choice of GVD expression by different authors and confusion can arise in figuring out the relation between the formulae given and those favoured by the readers. In such circumstances, Table 5.2 may be of some help.

Table 5.2 Group delay and group velocity dispersion

	In terms of ω	In terms of λ
Group delay	$\tau = \frac{1}{v_g} = \frac{1}{c}(n + \omega\frac{dn}{d\omega})$ ------ $\Rightarrow$	$= \frac{1}{c}(n - \lambda\frac{dn}{d\lambda})$
Group velocity dispersion	$\beta'' = \frac{d\tau}{d\omega} = \frac{d}{d\omega}\left(\frac{1}{v_g}\right) = \frac{1}{c}(2\frac{dn}{d\omega} + \omega\frac{d^2n}{d\omega^2})$	$D = \frac{d\tau}{d\lambda} = \frac{d}{d\lambda}\left(\frac{1}{v_g}\right) = -\frac{\lambda}{c}\frac{d^2n}{d\lambda^2}$
	— Pulse spread per unit length and per unit frequency ([s]/ [m][s]$^{-1}$)	— Pulse spread per unit length and per unit wavelength ([s]/ [m][m])
	$\beta'' \Delta\omega = D\Delta\lambda$ $-\frac{2\pi c}{\lambda^2}\beta'' = D$	

5.1.3 Normal and anomalous dispersion

For a given material, in addition to the variation of the magnitude, each GVD parameter such as β'', D and Y, etc. may also possess different signs within different frequency or wavelength region. To specify this difference in sign the terms *normal dispersion* and *anomalous dispersion* are commonly used. Note that for normal dispersion β'' is positive while D and $(dv_g/d\omega)$, negative (see Table 5.3).

Table 5.3 Signs of various GVD parameters

Parameters / Dispersion types	β''	$\frac{dv_g}{d\omega}$	D	$\frac{d^2n}{d\lambda^2}$	Y
Normal dispersion	+	–	–	+	+
Anomalous dispersion	–	+	+	–	–

In the region of normal dispersion the longer wavelength components propagate faster than the shorter wavelength components and so accordingly a positive frequency chirp develops for bandwidth limited input pulses. In anomalously dispersive region, the opposite applies. Most optical materials exhibit normal dispersion in the visible spectral region but have anomalous dispersion in the near infrared. The wavelength at which the

sign of GVD switches is called the zero dispersion wavelength, λ_{zero}, although in these cases higher order dispersion terms may not be zero. For fused silica, $\lambda_{zero} = 1.3\ \mu m$ (Ainslie and Day 1986).

5.1.4 Effect of dispersion on propagating pulses

As for the study of any other linear systems, pulse propagation in a linear optical medium can be analysed by using the concept of a *transform function*. An optical transform function h(ω), which specifies the modification impact of the medium on an incident harmonic wave at frequency ω, connects the Fourier frequency components of the output signal to the corresponding input ones. In the cases where pulses propagate along the spatial axis z, this can be expressed as

$$\upsilon_o(\omega, z_o) = h(\omega, z_i, z_o)\upsilon_i(\omega, z_i) \tag{5.7}$$

where $\upsilon_o(\omega, z_o)$, $\upsilon_i(\omega, z_i)$ are the Fourier components for output and input optical field. The transform function $h(\omega, z_i, z_o)$ is given by

$$h(\omega, z_i, z_o) = e^{i\beta(\omega)(z_o - z_i)} \tag{5.8}$$

In many applications the propagation constant β(ω) is often approximated with terms up to the second differential in the Taylor expansion, i. e.

$$\beta(\omega) \approx \beta_{2T}(\omega) \equiv \beta(\omega_o) + \beta'(\omega - \omega_o) + \frac{1}{2}\beta''(\omega - \omega_o)^2 \tag{5.9}$$

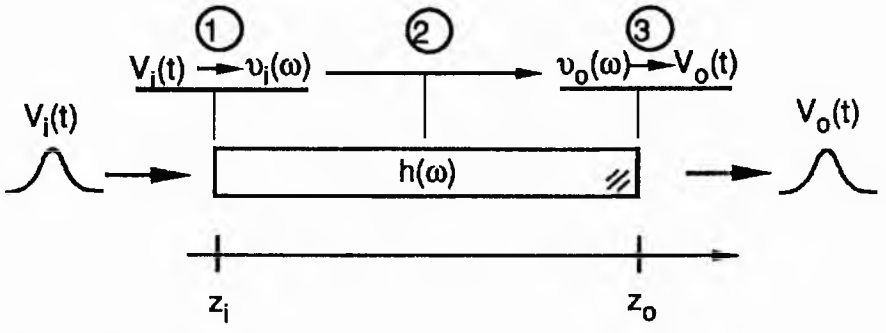

Fig. 5.1. Three-steps for analysing pulse propagation in dispersive media (see text).

Based on Eq. (5.8) and as demonstrated in Fig. 5.1 a general procedure for investigating pulse propagation in a linear, dispersive medium characterized by Eq. (5.8)

includes just three steps. Firstly, make a Fourier transform of incident field $V_i(t)$ to obtain $\upsilon_i(\omega)$, secondly, using Eq. (5.7) find the output Fourier components $\upsilon_o(\omega)$ and thirdly, by making an inverse Fourier transform of $\upsilon_o(\omega)$ then $V_o(t)$ can be determined. Following such a three-step procedure, the results obtained for a frequency-chirped Gaussian pulse propagating through a dispersive line by a distance z (= z_o - z_i) are as shown in Table 5.4.

Table 5.4 Propagating characteristics of a Gaussian pulse in a dispersive medium

Input ($z_i = 0$)			Output ($z_o = z$)	
$V_i(t)$	$e^{-\Gamma_o t^2} e^{-i\omega_o t}$	$h(\omega) = e^{-i\beta_T(\omega)z}$ ⟶	$V_o(t)$	$e^{-\Gamma(z)(t - \beta' z)^2} e^{-i[\omega_o t - \beta(\omega_o)z]}$
$\upsilon_i(\omega)$	$e^{-(\omega - \omega_o)^2/4\Gamma_o}$		$\upsilon_o(\omega)$	$e^{-i\beta_T(\omega)z}\, e^{-(\omega - \omega_o)^2/4\Gamma_o}$
Γ_i	$\Gamma_o \equiv a_o - ib_o$		$\Gamma(z)$	$\Gamma(z) \equiv a(z) - ib(z)$
$I_i(t)$	$e^{-2a_o t^2}$		$I_o(t)$	$e^{-2a(z)t^2}$
Δt_i	$\sqrt{\frac{2\ln 2}{a_o}}$		Δt_o	$\sqrt{\frac{2\ln 2}{a(z)}}$
$I_i(\omega)$	$e^{-4\ln 2(\omega - \omega_o)^2/(\Delta\omega)^2}$		$I_o(\omega)$	$e^{-4\ln 2(\omega - \omega_o)^2/(\Delta\omega)^2}$
$\Delta\nu_i$	$\frac{\sqrt{2\ln 2}}{\pi\sqrt{a_o}}\sqrt{a_o^2 + b_o^2}$		$\Delta\nu_o$	$\frac{\sqrt{2\ln 2}}{\pi\sqrt{a(z)}}\sqrt{a^2(z) + b^2(z)}$

The relationships involving the pulse characteristic parameters a, b and Γ included in Table 5.4 for both input and output pulses are as follows (Siegman 1986; Ch. 9)

$$\frac{1}{\Gamma(z)} = \frac{1}{\Gamma_o} + i2\beta'' z \tag{5.10}$$

$$a(z) = \frac{a_o}{(1 + 2\beta'' z b_o)^2 + (2\beta'' z a_o)^2} \tag{5.11}$$

$$b(z) = \frac{b_o(1 + 2\beta'' z b_o) + 2\beta'' z a_o^2}{(1 + 2\beta'' z b_o)^2 + (2\beta'' z a_o)^2} \tag{5.12}$$

Note that $a(0) = a_o$, $b(0) = b_o$ and $\Gamma(0) = \Gamma_o$, and the pulse duration parameter "a" is always ≥ 0, the frequency chirp parameter "b", however, can have either a negative or positive value, and Γ is a complex parameter as defined in Table 5.4. From Eqs. (5.11)

and (5.12), we have

$$\frac{\Delta t_o(z)}{\Delta t_i} = \sqrt{\frac{a_o}{a(z)}} = \sqrt{1 + (2\beta'' z a_o)^2 + 4\beta'' z b_o + (2\beta'' z b_o)^2} \tag{5.13a}$$

$$\Delta\nu_o = \Delta\nu_i \tag{5.13b}$$

Eqs. (5.13) reflects the following two significantly important features of pulse propagation in dispersive media. The variation of the temporal duration for propagating pulses is dependent on the properties of the group velocity dispersion in the medium. In particular, for pulse shortening, which only occurs when $b_o \neq 0$, the condition $\beta'' b_o < 0$ must be satisfied. Secondly, the spectrum of pulses remains unchanged during propagation (physically, this is obvious because no nonlinear interactions are involved in the whole process).

If the incident pulses are bandwidth-limited, i. e. $b_o = 0$, Eq. (5.13a) is reduced to

$$\frac{\Delta t_o}{\Delta t_i} = \sqrt{1 + (2\beta'' a_o z)^2} = \sqrt{1 + (z/z_D)^2} \tag{5.14a}$$

with

$$z_D = \frac{1}{2a_o|\beta''|} = \frac{\pi c}{2\ln 2}\frac{\Delta t_i^2}{|D|\lambda_o^2} = \frac{1}{1.47}\frac{(\Delta t_i[\text{ps}])^2}{|D|[\text{ps/nm/km}]\,(\lambda_o[\mu\text{m}])^2}\,[\text{km}] \tag{5.14b}$$

Eq. (5.14a) implies that the pulse duration increases monotonically with the propagation distance. The parameter z_D, often designated as the *dispersion distance*, refers to the spatial position at which the duration of an initially chirp-free coherent pulse increases by a factor of $\sqrt{2}$. Of course, once the pulse is broadened it is no longer bandwidth limited. Letting $b_o = 0$ in Eq. (5.12) the dispersion-induced frequency chirp can be readily deducted to be:

$$b(z) = \frac{2\beta'' z a_o^2}{1 + (2\beta'' z a_o)^2} = \frac{a_o(z/z_D)}{1 + (z/z_D)^2} \tag{5.15}$$

Eq. (5.15) indicates that as z increases b(z) first increases and then decreases. A maximum value is reached at $z = z_D$, at which $b(z_D) = a_o/2$.

In the wavelength region where β'' is close to zero, or for extremely short pulses, the third-order dispersion term may need to be considered. In such circumstances, Eq. (5.14a)

should be modified into (Marcuse and Lin 1981)

$$\frac{\Delta t_o}{\Delta t_i} = \sqrt{1 + (2\beta'' a_o z)^2 + (2\beta''' a_o z)^2 a_o/2} = \sqrt{1 + (z/z_D')^2} \qquad (5.14c)$$

$$z_D' = \frac{1}{\sqrt{(2a_o\beta'')^2 + (2a_o\beta''')^2 a_o/2}} \qquad (5.14d)$$

The existence of third-order dispersion often causes the propagating pulses to be temporally distorted (Boyer and Franco 1984). In particular, associated with an input pulse having a clean, discrete profile, the exiting pulse will have a rather extended ringing wing in the trailing edge due to the effect of the third-order dispersion (Marcuse 1980). This is in contrast to the function of the second-order dispersion, which in general leads to an exiting pulse profile that is proportional to the Fourier transform of the original pulse shape (Jones 1974).

Example I. Pulse broadening caused by dispersion

For a bandwidth limited initial pulse that has a Gaussian shape, whith Δt_i = 150 fs, λ_o= 1.5 μm, and D = ±15 ps/nm/km, from Eq. (5.14b), we have z_D= 45 cm.

Variation of pulse duration ratio as a function of the propagation distance according to Eq. (5.14a) is as shown in Fig. 5.2, where the asymptote is obtained by assuming $z >> z_D$. Note that, in this case, no matter what the sign of the dispersion parameter, pulse duration always increases during propagation. This is not the case when the input pulse is frequency chirped (see Example II).

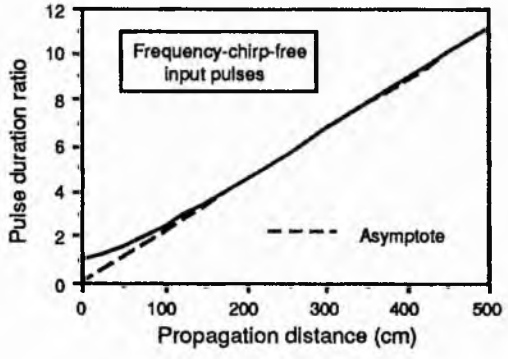

Fig. 5.2. Pulse broadening caused by dispersion. (The pulse duration ratio is $\Delta t_o/\Delta t_i$ with Δt_i = 150 fs).

If the initial pulses are frequency-chirped, i. e., $b_o \neq 0$, and suppose β'' has the opposite sign from b_o, within the initial propagation distance the pulse duration decreases until $z = z_{opt}$ (see Fig. 5.3), where

$$z_{opt} = \frac{1}{2\beta''} \frac{-b_o}{a_o^2 + b_o^2} \tag{5.16a}$$

For $b_o >> a_o$,

$$z_{opt} \approx \frac{-1}{2b_o\beta''} \tag{5.16b}$$

z_{opt} is known as *the optimum length* for pulse compression and Eq. (5.16a) can be readily derived through finding out the extreme value of a(z) in Eq. (5.11) [$a(z_{opt}) = a_{max} = (a_o^2 + b_o^2)/a_o$]. If the chirp parameter b_o is replaced by the associated pulse duration-bandwidth product, P_i ($\equiv \Delta t_i \Delta \nu_i$), then Eq. (5.16a) can be rewirtten as

$$z_{opt} = \frac{2\ln 2}{\pi} \frac{c\Delta t_i^2}{|D|P_i^2\lambda_o^2} \sqrt{\left(\frac{\pi P_i}{2\ln 2}\right)^2 - 1} = z_D \left(\frac{2\ln 2}{\pi P_i}\right)^2 \sqrt{\left(\frac{\pi P_i}{2\ln 2}\right)^2 - 1} \tag{5.17}$$

Substitution of z_{opt} into Eq. (5.13a) gives rise to

$$(\Delta t_o)_{z_{opt}} = \frac{\Delta t_i \, a_o}{\sqrt{a_o^2 + b_o^2}} = \frac{2\ln 2}{\pi} \frac{\Delta t_i}{P_i} \tag{5.18}$$

Since $\Delta \nu_o = \Delta \nu_i$, from Eq. (5.18), it follows that,

$$(\Delta t_o \Delta \nu_o)_{z_{opt}} = \frac{2\ln 2}{\pi} = 0.441 \tag{5.19}$$

Therefore, at the optimum length, the chirp in the pulse is removed and the pulse becomes bandwidth limited. (Such a feature can be also checked by bringing z_{opt} into Eq. (5.12), where this leads to $b(z_{opt}) = 0$).

After passing through z_{opt}, the duration of the propagating pulse starts to increase monotonically. At $z = 2z_{opt}$, the pulse is restored in both duration and the magnitude of frequency chirp except that the chirp parameter has an opposite sign to its initial value. That is, $a(2z_{opt}) = a_o$, $b(2z_{opt}) = -b_o$.

Example II. General features of pulse propagation in a dispersive medium

Suppose: Δt_i = 150 fs, $b_o = 10a_o$, and D = ±15 ps/nm/km, we have P_i = 4.43.

From Eqs. (5.17), (5.18), we obtain: $z_{opt} \approx 4.5$ cm and $(\Delta t_o)_{min.}$ = 15 fs.

Thus, Eq. (5.13a) can be reduced to

$$\frac{\Delta t_o}{\Delta t_i} = \sqrt{1 + 0.05\,(z[\text{cm}])^2 \pm 0.44\, z[\text{cm}]} \tag{5.20}$$

A plot of the above equation is shown in Fig. 5.3. Note that for the curve associated with $D > 0$, the pulse is compressed among the region with $z \leq z_{opt}$. When $z > z_{opt}$ the pulse duration increases as shown in Fig. 5.2 but at a much faster rate. For $D < 0$ (i. e. $\beta''b_0 > 0$), no pulse shortening occurs during the whole propagation process.

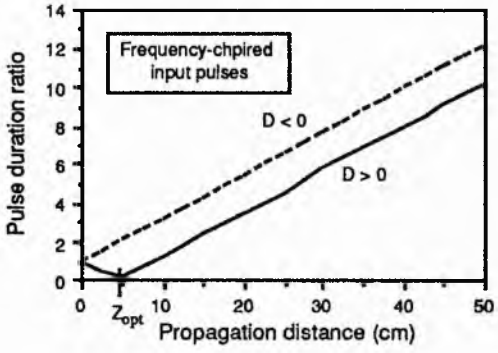

Fig. 5.3. As for Fig. 5.2 except that the incident pulses are frequency chirped (see Example II in text).

5.1.5 Typical dispersive devices

In the light of pulse compression or frequency-chirp compensation, dispersion control in terms of both sign and magnitude is of primary importance (Dietel *et al* 1983, Silvestri *et al* 1984, Fehrenbach and Salour 1984, Gordon and Fork 1984, Diels *et al* 1985, Valdmanis and Fork 1986). It is unfortunate that for a given medium where $n(\lambda)$ is a characteristic of the material, the only variable parameter that can be used in the control of the dispersive effect is the propagation distance. This in some circumstances could be rather inconvenient since cutting back the length of the medium is not always easy to do. Therefore, development of some special dispersive devices which can provide adjustable frequency-dependent phase delay for any incident light wave is necessary. To be more specific, suppose ω_1, ω_2 are the two frequency components of an incident signal and have their wavefronts overlaped, as shown in Fig. 5.4. After passing through the dispersive device, the wavefront of ω_1-componets will lag behind the ω_2-component along the propagating direction. (The exact difference in the time delay between the two frequency components can be controlled by some of the system parameters, which in Fig. 5.4 are represented by an array variable s.) In this case, if $\omega_2 > \omega_1$, the device is said to have negative dispersion, otherwise it is a positively dispersive system. In the following, the characteristics of the two most important dispersive devices are reviewed. These are the

diffraction grating pair and the four-prism sequence. Both utilize the feature of the inherent angular dispersion to construct an unequal optical pass length for different spectral components so that a frequency/wavelength-dependent group delay is introduced.

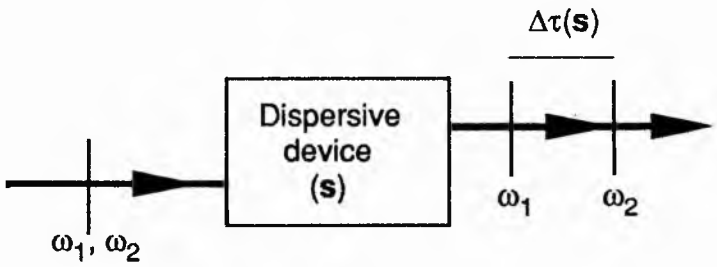

Fig. 5.4. Function of a general dispersive device. The vertical lines represent the wave fronts and the time delay difference, $\Delta\tau$, is adjustable by altering the control parameters of the device s.

Diffraction grating pair

In 1969, Fisher *et al* proposed the important idea of utilizing optical Kerr effect to stretch the spectrum of a light pulse and then use an appropriate dispersive delay line to remove the associated frequency chirp such that the pulse could be temporally compressed. In the same year, Treacy (1969) realized that a parallel displaced grating pair could be used, as an adjustable dispersive device, to fulfil Fisher's pulse compression purposes. In the next 18 years or so, there were significant developments in the manufacture of optical fibres, which represent almost ideal media for exploiting the nonlinear Kerr effect at relatively low power levels. In fact, pulse compression with a fibre-grating pair combination has become one of the most active and exciting research subjects (Shank *et al* 1982, Kafka *et al* 1984, Grischkowsky and Balant 1984, Dianov *et al* 1984, Knox *et al* 1985, Johnson *et al* 1986, Tai and Tomita 1986, Kafka and Baer 1988). Remarkable results have been reported for the compression ratios and the pulse durations, and in particularly impressive data were described where 6 fs pulses were produced through using a dispersive system of double grating pair and one four-prism sequence (Fork *et al* 1987).

In a grating pair, with their faces and rulings parallel to each other (see Fig. 5.5), the low frequency components of an incident beam experience a longer pass than the high frequency components. Therefore, the grating pair forms a negative dispersive system.

The group delay thus introduced by the grating pair can be expressed as

$$\tau = c_1 + \tau(\omega) \tag{5.21}$$

with c_1 being a frequency-independent constant and $\tau(\omega)$ given by Treacy (1969) to be:

$$\tau(\omega) = \frac{B}{\cos[\gamma - \theta(\omega)]}(1 + \cos[\theta(\omega)]) \tag{5.22}$$

B is the perpendicular distance between gratings, γ is the incidence angle and $\theta(\omega)$ is the angle between incident and diffracted rays at frequency ω. $\theta(\omega)$ can be determined by grating equation, which for the first order is:

$$\sin[\gamma - \theta(\omega)] = \frac{2\pi c}{\omega d} - \sin\gamma \tag{5.23}$$

where d is grating period. Suppose that $\phi(\omega)$ is the total phase shift introduced by the grating pair between the arbitrary chosen entrance point Q_1 and the exiting point Q_2, the associated transform function is given by:

$$h(\omega) = T_o \exp[i\phi(\omega)]$$

where $T_o(<1)$ is a constant accounting for the possible loss incurred during the transmission. Similar to Eq. (5.9), $\phi(\omega)$ can be approximated as:

$$\phi(\omega) \approx \phi_o + \phi'(\omega - \omega_o) + \frac{1}{2}\phi''(\omega - \omega_o)^2 \tag{5.24}$$

where ϕ_o is a constant phase shift, $\phi' = \frac{d\phi}{d\omega}$, $\phi'' = \frac{d^2\phi}{d\omega^2}$, all evaluated at the central carrier frequency ω_o. It is readily shown that

$$\phi'(\omega) = \tau(\omega) \tag{5.25}$$

and

$$\phi''(\omega) = \frac{-4\pi^2 cB}{\omega^3 d^2 \left[1 - (\frac{2\pi c}{\omega d} - \sin\gamma)^2\right]^{3/2}} \tag{5.26}$$

Since $\frac{2\pi c}{\omega d} = \frac{\lambda}{d}$ is of an order of 10^{-2} - 10^{-3}, which normally means that $\frac{2\pi c}{\omega d} << \sin\gamma$, and so Eq. (5.26) can be approximated as

$$\phi''(\omega) \approx \frac{-4\pi^2 cB}{\omega^3 d^2 \cos^3\gamma} \tag{5.27}$$

We can see that ϕ'' is always negative and proportional to the grating separation B.

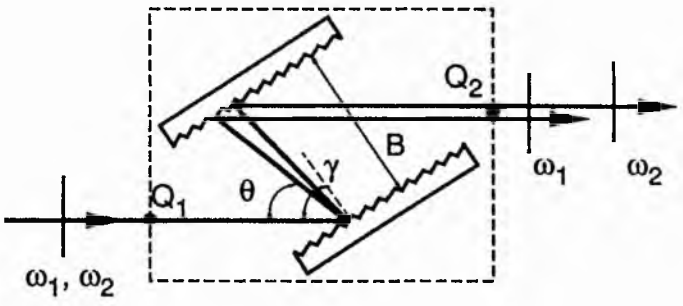

Fig. 5.5. Geometrical arrangement for a typical negative dispersive device - a grating pair. The grating separation B and the incident angle γ can be adjusted to control the amount of dispersion introduced.

At this stage, it is straightforward to understand that all the rest discussions about the influence of the grating pair on an incident optical pulse, (say, it has a Gaussian shape either chirped or not) can be deduced by substituting $\phi''(\omega_0)$ for $\beta''z$ in Eqs (5.10-13, 15, 16). The function played by the propagating distance z in the previous formulae is replaced by the grating separation B.

In the cases where the cubic term in the Taylor expansion of $\phi(\omega)$ is of interest, $\beta'''z$ in Eq. (5.15c) can be replaced by $\phi'''(\omega_0)$, which, for a grating pair, are given by (Christov and Tomov 1986)

$$\phi'''(\omega) = \frac{-3\,\phi''(\omega)}{\omega}\left[\frac{1 + (2\pi c/\omega d)\sin\gamma - \sin^2\gamma}{1 - (2\pi c/\omega d - \sin\gamma)^2}\right] \qquad (5.28)$$

Further discussions on fibre-grating pair compressor is included in Appendix D.

Four-prism sequence

The four-prism sequence comprising an arrangement as indicated in Fig. 5.6 was first proposed by Fork *et al* in 1984. Compared with a grating pair, such a prism system has the advantage of low loss and is adjustable from negative to positive dispersion value in the visible region and so is a very useful device in the precise control of dispersion. In addition to the uses in pulse compression, it is also frequently incorporated inside the colliding-pulse mode-locked laser cavities (Valdmanis and Fork 1986, Finch *et al* 1988).

In Fig. 5.6, the four prisms are identical, having a shape which allows the minimum deviation angle to be equal to the Brewster angle. The exit face of prism I is parallel to the entrance face of prism II, and prisms III and IV are symmetrically placed to prisms I and II with the line MM' as the symmetrical plane. Such an arrangement means that the exit beam is collinear with the incident beam and no transverse displacement is

introduced. (While, for a grating pair, such spatial displacement exists. Nevertheless, if another grating pair is used, placed symmetrically to the first pair, the double grating pair system will function exactly as the four-prism sequence and so the transverse displacement can be avoided).

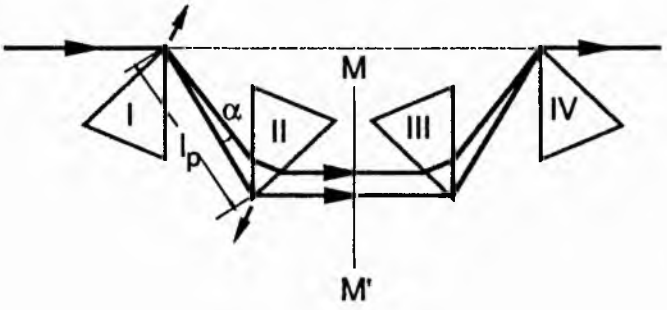

Fig. 5.6. Four-prism sequence. The control parameters are l_p and the path length inside the prisms [Through translating any of the prisms along an axis normal to its base (as shown by the arrow near the apex of prisms I and II) more positive dispersion can be introduced, otherwise the whole device provides negative dispersion]. MM' marks the central symmetrical position.

The dispersion parameter, D, for a segment medium, like the prism sequence, can be expressed as

$$D = -\frac{\lambda}{cL}\frac{d^2\mathbb{P}}{d\lambda^2} \tag{5.29}$$

where $L = \Sigma l_i$ is the total physical length of the dispersive system, $\mathbb{P} = \Sigma n_i l_i$ is the corresponding optical path length[3]. For the four-prism sequence, $\mathbb{P}$ can be expressed as

$$\mathbb{P} = \mathbb{P}_0 + \mathbb{P}(\lambda) \tag{5.30}$$

---

[3] Suppose there are m different material along the propagating path, then for the i_{th} one of a length l_i and dispersion D_i, an overall dispersion of the dispersive system can be defined as

$$D \equiv \frac{\sum_{i=1}^{m} D_i l_i}{\Sigma l_i} = \frac{\sum_{i=1}^{m} D_i l_i}{L} \tag{5.29a}$$

Substitution of $D_i = -\frac{\lambda}{c}\frac{d^2 n_i}{d\lambda^2}$ into the above equation yields

$$D = -\frac{\lambda}{cL}\frac{d^2(\Sigma n_i l_i)}{d\lambda^2} \tag{5.29b}$$

which leads to Eq. (5.29) in the text. Obviously, if the medium of interest has a dispersion that changes continuously with the spatial position, the overall group velocity dispersion and the total optical path length should be respectively rewritten as:

$$D = \frac{1}{L}\int_0^L D(z)dz \qquad \text{and} \qquad \mathbb{P} = \int_0^L n(z)dz \tag{5.29c}$$

From Eq. (5.29a), it is possible that for a sequence of different optical media the overall D value may be close to zero. Such a feature can be utilized to minimize the dispersion effect on the propagating pulses (Lin *et al* 1980).

where $\mathbb{P}_o$ is a wavelength-independent constant, $\mathbb{P}(\lambda)$ is given by

$$\mathbb{P}(\lambda) = 2l_p\cos\alpha \tag{5.31}$$

α is the relative dispersion angle for the spectral component at wavelength λ. From Eq. (5.31), the following two equations can be derived (Fork *et al* 1984)

$$\frac{d^2\mathbb{P}}{d\lambda^2} = 4l_p\left\{\left[\frac{d^2n}{d\lambda^2} + (2n - \frac{1}{n^3})\left(\frac{dn}{d\lambda}\right)^2\right]\sin\alpha - 2\left(\frac{dn}{d\lambda}\right)^2\cos\alpha\right\} \tag{5.32}$$

$$\frac{d^3\mathbb{P}}{d\lambda^3} = 4l_p\left[\frac{d^3n}{d\lambda^3}\sin\alpha - 6\frac{dn}{d\lambda}\frac{d^2n}{d\lambda^2}\cos\alpha\right] \tag{5.33}$$

Bringing Eq. (5.32) into Eq. (5.29) gives rise to the D parameter of the four prism sequence. Eq. (5.33) relates to the third-order dispersion. The associated phase shift expression for the prism system are given by

$$\frac{d^2\phi}{d\omega^2} = \beta''L = -\frac{\lambda^2}{2\pi c}DL = -\frac{\lambda^3}{2\pi c^2}\frac{d^2\mathbb{P}}{d\lambda^2} \tag{5.34}$$

$$\frac{d^3\phi}{d\omega^3} = \beta'''L = -\frac{\lambda^4}{4\pi^2c^3}(3\frac{d^2\mathbb{P}}{d\lambda^2} + \lambda\frac{d^3\mathbb{P}}{d\lambda^3}) \tag{5.35}$$

which can be compared with Eqs. (5.26) and (5.28) relating to the grating pair. Numerical examples of the magnitudes of the 2nd and the 3rd order phase shifts (for $\lambda_o = 620$ nm) introduced by a double grating pair, a four prism sequence and a glass rod respectively can be found in the paper by Fork *et al* (1987).

Finally, it is worth mentioning that the grating pair (Heritage *et al* 1985, Weiner *et al* 1986, Weiner *et al* 1988) and the prism sequence (Fork 1986, Dawson *et al* 1986) systems have also been utilized to perform spectral filtering of ultrashort pulses. In these circumstances, a variable slit or a specially designed mask is located at a proper position where the spectrum of the propagating pulses is spatially distributed. Through manipulating both the phase and the amplitude of the spectral components with the mask, various pulse shapes such as squared (Weiner *et al* 1986), beat modulated (Heritage *et al* 1986) can be conveniently achieved. This is expected to be of substantial importance in future digital optical communications and data processing systems because particular

optical digits (e. g. square pulses) could be produced.

5.2 Nonlinear media

5.2.1 Dispersion around a region of atomic resonance

It is known that dispersion in absorption (or gain) media is affected by the action of atomic transitions. This is further reflected by the fact that the susceptibility for a resonant atomic medium can be described using the complex relationship,

$$\chi = \chi' - i\chi'' \tag{5.36}$$

where χ' contributes to refractive index, χ'' relates to absorption or gain. For a two-level atomic system, from the treatment of density matrix theory (Yariv 1975; Ch. 8), χ', χ'' are given by

$$\chi'(\omega) = - \frac{2\mu^2}{\Delta\omega\varepsilon_0 h/2\pi} \frac{2(\omega_a - \omega)}{\Delta\omega} \Delta N g(\omega) \tag{5.37}$$

$$\chi''(\omega) = - \frac{2\mu^2}{\Delta\omega\varepsilon_0 h/2\pi} \Delta N g(\omega) \tag{5.38}$$

ε_0 is the electric permeability of vacuum, h is Planck constant, μ is the atomic dipole along the direction of incident field, ω_a is the central resonant frequency, ΔN ($= N_2 - N_1$) is the atom population difference, $\Delta\omega$ is the associated linewidth (FWHM) of the resonance and $g(\omega)$ is the normalized, dimensionless line shape function given by

$$g(\omega) = \frac{(\Delta\omega/2)^2}{(\omega - \omega_a)^2 + (\Delta\omega/2)^2} \tag{5.39}$$

The population difference in Eqs. (5.37), (5.38) is a function of incident intensity,

$$\Delta N = \frac{\Delta N_0}{1 + I(\omega)/I_s(\omega)} \tag{5.40}$$

where $I_s(\omega)$ is the lineshape-related saturation intensity, defined as

$$I_s(\omega) = \frac{h\omega/2\pi}{2\tau_{21}\sigma(\omega)} \tag{5.41}$$

with

$$\sigma(\omega) = \frac{\omega\mu^2}{\Delta\omega c n \varepsilon_0 h/2\pi} g(\omega) \tag{5.42}$$

representing a spectrally distributed emission cross-section. According to Eqs. (5.37) and (5.40), $\chi'(\omega)$ is also intensity dependent and thus for sufficiently high intensities $\chi'(\omega)$ will be saturated. Through introducing a small signal value of the real part of susceptibility,

$$\chi_o'(\omega) = -\frac{2\mu^2}{\Delta\omega\epsilon_o h/2\pi}\frac{2(\omega_o - \omega)}{\Delta\omega}\Delta N_o g(\omega) \tag{5.43}$$

Eq. (5.37) can be rewritten as

$$\chi'(\omega) = \frac{\chi_o'(\omega)}{1 + I(\omega)/I_s(\omega)} \tag{5.44}$$

From the above equation, the intensity-dependent refractive index caused by the atomic transitions can be readily obtained,

$$n \approx n_o(1 - \frac{\chi_o'(\omega)}{2n^2}\frac{I}{I_s}) \tag{5.45}$$

where $n_o \approx 1 + \chi_o'(\omega)/2$, represents the refractive index at the small signal level. Another noticeable feature of $\chi'(\omega)$ given in Eq. (5.37) is that it can be conveniently derived from measuring $\chi''(\omega)$. Combining Eqs. (5.37) and (5.38), we obtain

$$\chi'(\omega) = \frac{2(\omega_o - \omega)}{\Delta\omega}\chi''(\omega) \tag{5.46}$$

Since $\chi''(\omega)$ is proportional to the gain coefficient, Eq. (5.46) implies that the larger the gain the greater the influence of the atomic transition on dispersion. As ω takes the value on different sides of ω_o the sign of $\chi'(\omega)$ changes.

For the media where all the atoms are involved in the resonant process the associated propagation constant will be

$$\beta_{tr} = kn_{tr} = \frac{2\pi}{\lambda}\sqrt{1 + \chi'} \approx \frac{2\pi}{\lambda}(1 + \frac{\chi'}{2}) \tag{5.47}$$

On the other hand, if the absorption or amplification action is only associated with part of the total number of atoms, which is true for most of the absorbers and gain media that are actually used, the propagation constant will be the one relating to the host material, β_h, plus the contribution from the resonant atoms, $\Delta\beta$, namely,

$$\beta_T = \beta_h + \Delta\beta \tag{5.48}$$

For $|\chi'| << 1$, it can be shown that (Yariv 1975; Ch. 8)

$$\Delta\beta \approx \beta_h \frac{\chi'(\omega)}{2n_h^2} \tag{5.49}$$

Therefore, using Eq. (5.49), the overall propagation constant β_T can be rewritten as

$$\beta_T = \beta_h\left(1 + \frac{\chi'(\omega)}{2n_h^2}\right) = \beta_h + \frac{\beta_{tr}^2 - k^2}{2\beta_h} \tag{5.50}$$

In terms of refractive indices, Eq. (5.50) is equivalent to

$$n_T = n_h\left(1 + \frac{\chi'(\omega)}{2n_h^2}\right) = n_h + \frac{n_{tr}^2 - 1}{2n_h} \tag{5.51}$$

where n_T, n_h and n_{tr} are the refractive indices for the entire medium, the host medium and the resonant atoms respectively. [Note that there is no such relation as $n_T = n_h + n_{tr}$, or $n_T = (n_h + n_{tr})/2$.]

5.2.2 Effect of gain/absorption on propagating pulses (small signal treatment)

As far as the medium gain/absorption is concerned, the gain coefficient for the optical field is

$$\alpha(\omega) = -\frac{\beta_h \chi''(\omega)}{2n_h^2} = -\frac{k\chi''(\omega)}{2n_h} = \sigma(\omega)\Delta N \tag{5.52}$$[4]

Note that if there is a population inversion, i. e. $\Delta N > 0$, then $\chi''(\omega) < 0$ and $\alpha(\omega) > 0$, which means there is real gain. Otherwise, $\Delta N < 0$ and so $\alpha(\omega) < 0$, $\alpha(\omega)$ represents absorption. Although absorption and amplification represent nonlinear processes, under small signal conditions, pulse propagation in gain/absorption media can be treated as a linear problem. In such circumstances, both $\chi'(\omega)$ and $\chi''(\omega)$ are assigned taking their small signal values and so analyses of the influence on propagating pulses by gain or absorption can be implemented by simply replacing the transform function $e^{-i\beta(\omega)z}$ of a dispersive system by $e^{\alpha(\omega)z}$. Thus, corresponding to Eq. (5.10), the associated equation

[4] Strictly speaking, $\alpha(\omega)$ should be written as $\alpha(\omega,I)$, because it is also intensity dependent.

for a gain/absorption medium is

$$\frac{1}{\Gamma(z)} = \frac{1}{\Gamma_o} + 2\alpha'' z \tag{5.53}$$

where $\alpha'' = -\frac{d^2\alpha}{d\omega^2}$ evaluated at ω_o. The pulse duration and chirp parameters are given by[5]

$$a(z) = \frac{a_o(1 + 2\alpha'' z a_o) + 2\alpha'' z b_o^2}{(1 + 2\alpha'' z a_o)^2 + (2\alpha'' z b_o)^2} \tag{5.54}$$

$$b(z) = \frac{b_o}{(1 + 2\alpha'' z a_o)^2 + (2\alpha'' z b_o)^2} \tag{5.55}$$

For unchirped input pulses ($b_o = 0$),

$$a(z) = \frac{a_o}{1 + 2\alpha'' z a_o} \tag{5.56}$$

$$b(z) = 0 \tag{5.57}$$

Therefore,

$$\frac{\Delta t_o}{\Delta t_i} = \sqrt{1 + 2\alpha'' z a_o} \tag{5.58}$$

In contrast to Eq. (5.14a), there is no square power on the term $2\alpha'' z a_o$ in the above equation, which directly indicates for real gain media ($\alpha'' > 0$) that the propagating pulses are broadened while for absorbers ($\alpha'' < 0$) the pulse durations decrease. If a two-level atomic system is considered, from Eqs. (5.38) and (5.52) the following frequency-dependent gain coefficent can be obtained

$$\alpha(\omega) = \alpha_a\, g(\omega) \tag{5.59a}$$

where α_a is the small signal gain at the central resonsant frequency, determined by

$$\alpha_a \equiv \alpha(\omega_a) = \frac{\omega_a}{2cn^2(\omega_a)} \frac{2\mu^2 \Delta N_o}{\Delta\omega \varepsilon_o h/2\pi} \tag{5.59b}$$

If $(\omega - \omega_a) << \Delta\omega$, $g(\omega)$ can be approximated as

$$g(\omega) \approx 1 - \left(\frac{2}{\Delta\omega}\right)^2 (\omega - \omega_a)^2 \tag{5.60}$$

Combining Eq. (5.60) with Eq. (5.59a) and taking a differential of $\alpha(\omega)$ with respect to ω

---

[5] Simply swapping a(z) with b(z), a_o with b_o, and replacing β'' with α'' in Eqs. (5.11) and (5.12) will give rise to the expressions of Eqs. (5.55) and (5.54) respectively.

leads to

$$\alpha'' = 2\alpha_a \left(\frac{2}{\Delta\omega}\right)^2 \tag{5.61}$$

Substitution of Eq. (5.61) into Eq. (5.58) then yields

$$\frac{\Delta t_o}{\Delta t_i} = \sqrt{1 + \frac{(32\ln 2)\alpha_a z}{(\Delta\omega\Delta t_i)^2}} \tag{5.62}$$

Eq. (5.62) is the most simplified equation that is commonly quoted in the discussions regarding the effect of the gain medium on the propagating pulses.

Example III. Pulse broadening (narrowing) in gain (absorbing) media

Suppose: $\Delta t_i = 150$ fs, $\Delta\omega = 5 \times 2\pi/\Delta t_i = 2.1 \times 10^{14}$ Hz,

$\sigma(\omega_a) = 1.0 \times 10^{-17}$ cm^2 and $\Delta N_o = \pm 5 \times 10^{17}$/cm^3,

we have $\alpha_a = \sigma(\omega_a)\Delta N_o \approx \pm 5$ /cm. With the above values a plot of Eq. (5.62) is given in Fig. 5.7.

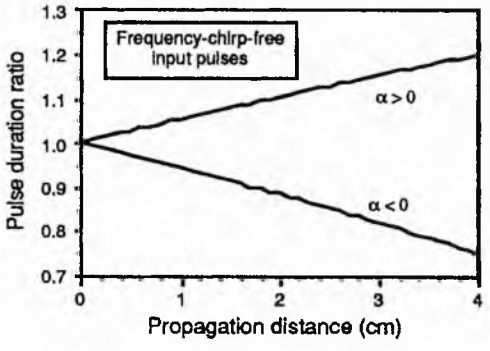

Fig. 5.7. Pulse broadening in a gain medium ($\alpha > 0$) and narrowing in an absorbing medium ($\alpha < 0$). (The pulse duration ratio is defined as $\Delta t_o/\Delta t_i$, with $\Delta t_i = 150$ fs).

For initially chirped pulses ($b_o \neq 0$), it is possible for the propagating pulses to be shortened in the gain medium ($\alpha'' > 0$), as long as the following condition is satisfied

$$2\alpha'' z < (b_0^2 - a_0^2)/a_o(b_0^2 + a_0^2) \tag{5.63}$$

The above equation implies that b_o must be larger than a_o for achieving any pulse compression.

5.2.3 Nonlinear effects in the nonresonant regime

Apart from the saturation effect involved in atomic absorption or amplification, nonlinearities in the nonresonant regime such as self-phase modulation (SPM) (Stolen and Lin 1978, Kean *et al* 1987, Alfana and Ho 1989), modulational instability (MIS)

(Hasegawa and Brinkman 1980, Anderson and Lisak 1984, Tai *et al* 1986), stimulated Raman scattering (SRS) (Stolen and Ippen 1973, Stolen *et al* 1984), four-wave mixing (FWM) (Lin *et al* 1981, Stolen and Bjorkholm 1982, Chen 1989) etc. are also of vital importance to the subject of pulse propagation. In particular, for the cases where optical fibres are used as the propagation media, the high peak intensity confined in fibre cores and long interaction distances permit the occurrence of substantial nonlinear effects (Smith 1972, Stolen 1980, Lin 1986). In general, these nonresonant nonlinear effects may occur either separately or simultaneously, depending on the magnitude of optical peak intensity and the dispersive features of the fibre.

At lower power levels only weak nonlinearities exist and self-phase modulation is often the only one that needs to be taken into account. Through an interplay between dispersion and self-phase modulation the optical solitons (for $D < 0$) or the square-like pulses with largely stretched, linear frequency chirp (for $D > 0$) (see Subsection 5.3.2) may arise. For relatively higher power levels or longer propagating distances, stimulated Raman scattering may take place, which distorts the ordinary SPM process (Gomes *et al* 1986, Schadt *et al* 1986, Kuckartz *et al* 1987, Schadt and Jaskorzynska 1987). At even higher power levels more types of nonlinearities can be involved. They interact with each other in a complex fashion and as result of such interactions, as well as the involvement of medium dispersion, the propagating pulses experience a superbroading of their spectrum. Typically, the broadened spectra can cover a range of several hundred nanometers (Lin *et al* 1978, Grigor'yants *et al* 1982, Dianov *et al* 1985, Grudinin *et al* 1987, Beaud *et al* 1987, Vodop'yanov *et al* 1987, Islam *et al* 1989, Zhu and Sibbett 1991).

In the following, some relevant features of the four nonlinear effects which are most commonly-met in pulse propagation studies will be discussed. For the sake of simplicity, it is assumed that in each case only one effect is present.

Self-phase modulation (SPM)

In any optical medium, if the propagating signal has a sufficiently high peak intensity it is

necessary that the related refractive index needs to be considered as intensity dependent, such that:

$$n = n_o + \Delta n(I) \tag{5.64}$$

n_o is the refractive index of the medium at essentially zero intensity and $\Delta n(I)$ can be expressed as (Shimizu 1967)

$$\Delta n(I) = n_{2I} I \tag{5.65}$$

where n_{2I} is the so-called *nonlinear optical Kerr coefficient*[6]. For an optical pulse, the intensity varies against time and so Eq. (5.64) simply indicates that the pulse phase will be modulated by the existence of an intensity-dependent refractive index (hence the term self-phase modulation). From Eqs. (5.64) and (5.65) the phase of the pulse at an arbitrary position, L, can be expressed as

$$\phi(t) = \phi_o + \Delta\phi = (\omega_o t - \frac{2\pi}{\lambda} n_o L) - \frac{2\pi}{\lambda}(n_{2I} I)L \tag{5.66}$$

Thus, the instantaneous frequency is given by:

$$\omega(t) = \frac{d\phi}{dt} = \omega_o + \Delta\omega(t) = \omega_o - \frac{2\pi}{\lambda} n_{2I} L \frac{dI}{dt} \tag{5.67}$$

The second term in Eq. (5.67) represents the nonlinear frequency chirp induced by SPM, and for a Gaussian pulse, it can be expressed as

---

6 If n is taken as a general function of intensity, n_2 is actually the first-order Maclaurin expansion coefficient of n(I). However, strictly speaking, the optical Kerr effect derives from the third-order nonlinearity of susceptibility, $\chi^{(3)}$. When $\chi^{(3)}$ is present, the polarization in the medium is given by

$$\mathbf{P} = \chi^{(1)}\varepsilon_o\mathbf{E} + \chi^{(3)}\mathbf{E}^2\mathbf{E}$$

and so the corresponding electric displacement is

$$\mathbf{D} = \mathbf{P} + \varepsilon_o\mathbf{E} = [(1 + \chi^{(1)}) + \frac{1}{\varepsilon_o}\chi^{(3)}\mathbf{E}^2]\,\varepsilon_o\mathbf{E}$$

Therefore, the relative dielectric constant is now

$$\varepsilon_r = \varepsilon^{(1)} + \varepsilon_I E^2$$

where $\varepsilon^{(1)} = 1 + \chi^{(1)}$, $\varepsilon_I = \chi^{(3)}/\varepsilon_o$. If an overall refractive index, defined as $n = \sqrt{\varepsilon_r}$, is introduced, the above equation leads to

$$n = \sqrt{n_o^2 + \varepsilon_I E^2} \approx n_o(1 + \frac{1}{2n_o^2}\varepsilon_I E^2) = n_o + \frac{1}{2} n_{2E} E^2$$

where $n_o = \sqrt{\varepsilon^{(1)}}$ is the ordinary refractive index, $n_{2E} = \chi^{(3)}/n_o\varepsilon_o$ is the nonlinear refractive index. Often, n_{2E} is given in esu unit, while, n_{2I} in Eq. (5.65) is in mks units. For silica, $n_{2E} = 1.14 \times 10^{-13}$ cm^2/V^2, correspondingly, $n_{2I} = 3.2 \times 10^{-16}$ cm^2/W.

$$\Delta\omega(t) = \frac{2\pi}{\lambda} n_{2I} L[4atI(t)] \tag{5.68a}$$

where $I(t) = I_o e^{-2at^2}$. A plot of $\Delta\omega(t)$ following Eq. (5.68a) together with the normalized Gaussian pulse shape is given in Fig. 5.8. It can be seen that across the pulse, from the leading edge to the trailing edge, the carrier frequency first decreases and then increases and then decreases again. Only in the central portion of the pulse does an approximate linear, positive (up) chirp exist, which can be described by[7]

$$b = 2a \frac{2\pi}{\lambda} n_{2I} L I_o = 2a\phi_{max} \tag{5.68b}$$

where $\phi_{max} = (2\pi/\lambda)n_{2I}LI_o$. The maximum frequency shifts towards both the lower and the higher frequencies (as indicated in Fig. 5.8) are given by

$$\Delta\omega_{max} = \pm 2\sqrt{\frac{2\ln 2}{e}} \frac{\Delta\phi_{max}}{\Delta t_i} \tag{5.69a}$$

From Eq. (5.69a), the corresponding FWHM bandwidth of the pure SPM spectral extension can be written as

$$\delta\omega_{SPM} = 2|\Delta\omega_{max}| = \sqrt{\frac{2}{e\ln 2}} \Delta\phi_{max}\Delta\omega_i \tag{5.69b}$$

When the initial spectral bandwidth is included, the total spectral width after self-phase-modulation is often expressed as (Gomes *et al* 1988, Kean *et al* 1989),

$$\Delta\omega_0 = \Delta\omega_i + \delta\omega_{SPM} \tag{5.70a}$$

Combining the above equation with Eq. (5.69b) gives

$$\Delta\omega_0 = \Delta\omega_i (1 + \rho\Delta\phi_{max}) \approx \Delta\omega_i(1 + \Delta\phi_{max}) \tag{5.70b}$$

where ρ is a pulseshape-related constant having a value close to 1 (for Gaussian pulse $\rho = [2/e\ln 2]^{1/2} = 1.03$). However, as shown below, in fact, Eq. (5.70a) and so Eq. (5.70b) are correct only when the condition $\Delta\phi_{max} >> 1$ is satisfied.

---

[7] If a Maclaurin expansion of I(t) to the second-order is made, Eq. (5.68a) becomes

$$\Delta\omega(t) \approx 4a\frac{2\pi}{\lambda} n_{2I} L I_o t (1 - 4at^2) = 4a\phi_{max}t(1 - 4at^2)$$

For $4at^2 << 1$, $\Delta\omega(t)$ represents a linear chirp and for $2bt = \Delta\omega(t)$, this leads to Eq. (5.68b).

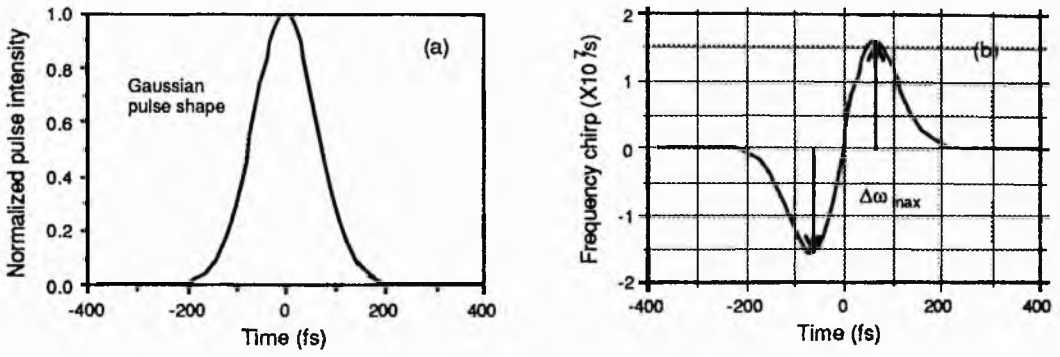

Fig. 5.8. (a) Normalized pulse intensity distribution and (b) the corresponding frequency chirp due to SPM (I_o = 1 GW/cm^2, n_{2I} = 3.2 x 10^{-16} cm^2/W, λ =1.5 μm, Δt_i = 150 fs and L = 40 cm).

Compared to the influence of the group velocity dispersion on the propagating pulses discussed in the previous section, it is interesting to note that pure SPM actually has the opposite effect on the pulses. (With dispersion, the pulse duration is broadened without any change in pulse spectrum, while with pure SPM the pulse duration remains constant but the spectrum is enlarged). These quite distinct features in fact provide a good analogy between these two effects. For dispersive media, we have $\upsilon_0(\omega,z) = [e^{i\beta(\omega)z}]\upsilon_i(\omega)$ as the spectral reation between the input and the output pulses, while for SPM media there is $V_o(t) = [e^{i\Lambda(t)z}]V_i(t)$ with $\Lambda(t) = (2\pi/\lambda)n_{2I}I(t)$ describing the temporal connection between the input and the exiting pulses. Therefore, corresponding to the parameter β'', which is used to describe the temporal spreading caused by dispersion there should be a parameter F, which characterizes the spectral spread generated by SPM. Also, in an analogy with Eq. (5.14a), the spectral broadening formula should be governed by:

$$\frac{\Delta\omega_0}{\Delta\omega_i} = \sqrt{1 + (2Fza_{o\omega})^2} \tag{5.71a}$$

where $a_{o\omega}$ is the initial spectral width parameter, which is, from Table 5.4, given by $a_{o\omega} = 1/4a_o$. An expression of the spectral-spread parameter F can be readily derived from Eq. (5.69a),

$$F \equiv \frac{2|\Delta\omega_{max}|}{z\Delta t_i} = 8\sqrt{\frac{\ln 2}{e}}\,\frac{\Delta\phi_{max}}{z(\Delta t_i)^2} \tag{5.71b}$$

where F is defined as the spectral spread for a unit length and a unit time duration. Substitution of Eq. (5.71b) into Eq. (5.71a) yields

$$\frac{\Delta\omega_0}{\Delta\omega_i} = \sqrt{1 + (\sqrt{\frac{2}{e\ln 2}}\Delta\phi_{max})^2} \qquad (5.71c)$$

which is equivalent to

$$(\Delta\omega_0)^2 = (\Delta\omega_i)^2 + (\delta\omega_{SPM})^2 \qquad (5.71d)$$

It can be seen that when $\Delta\phi_{max} >> 1$ (i.e. $\delta\omega_{SPM} >> \Delta\omega_i$) both Eq. (5.70a) and Eq. (5.71d) approximates to $\Delta\omega_0 \approx \delta\omega_{SPM}$. For small nonlinear phase shifts Eq. (5.71d) must be used instead of Eq. (5.70a).

Similar to the characteristic dispersion distance z_D, a SPM-spectral broadening characteristic length, z_s, can also be introduced, which is given by

$$z_s \equiv \frac{\lambda}{2\pi\, n_{2I}\, I_o} \qquad (5.72a)$$

With z_s Eq. (5.71c) can be rewritten as

$$\frac{\Delta\omega_0}{\Delta\omega_i} \approx \sqrt{1 + (z/z_s)^2} \qquad (5.72b)$$

At $z = z_s$, (i. e. $\Delta\phi_{max} = 1$), the overall spectral width of the propagating pulses is increased by a factor of $\sqrt{2}$. The general feature of the spectral extension in SPM media for bandwidth-limited input pulses will be similar to the the temporal spread profile given in Fig. 5.2 for purely dispersive media. For frequency-chirped incident pulses, Eq. (5.72b) should be modified into a form like Eq. (5.13a). In these cases it can be recognized that, spectral narrowing can occur in SPM media whenever the initial frequency chirp has a negative sign. (The overall variation of the spectral width as a function of the propagation distance or the optical peak intensity will be represented by a curves very much like the one shown in Fig. 5.3).

Modulational instability (MIS)

In media where dispersion-induced frequency chirps have the opposite sign to that generated by the optical Kerr effect, perturbation at certain frequencies on the propagating signal may experience gain and develop into sideband waves. Such a phenomenon has been described as modulational instability (see Fig. 5.9).

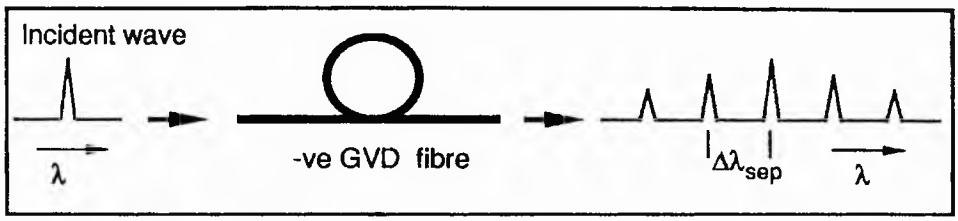

Fig. 5.9. Effect of modulational instability.

According to Tai *et al* (1986), the first sideband modulation frequency, Ω_1 is given by

$$\Omega_1 = \left[- \frac{\omega n_{2E}}{c\beta''} |E_o|^2 \right]^{1/2} \tag{5.73a}$$

where n_{2E} is the Kerr coefficient defined from $n = n_o + \frac{1}{2} n_{2E} |E_o|^2$, E_o is the electric-field amplitude for the propagating light wave. (The n_{th} sideband is given by $\Omega_n = n\Omega_1$, i.e., the sidebands are evenly separated in frequency). It is known that

$$|E_o|^2 = \frac{2P}{\varepsilon_o n_o c A} \tag{5.73b}$$

where P, A are the peak power and the cross-section parameter of the incident beam respectively, n_o is the refractive index of the medium. Bringing Eq. (5.73b) and $\beta'' = -\lambda^2 D/2\pi c$ into Eq. (5.73a) yields

$$\Omega_1 = \omega \left[\frac{2\omega n_{2E} P}{\pi n_o c^3 \lambda \varepsilon_o D A} \right]^{1/2} \tag{5.74}$$

If $\Delta\lambda_{sep.}$ is the wavelength shift associated with the modulation sideband, then

$$\frac{\Delta\lambda_{sep.}}{\lambda} = \frac{\Omega_1}{\omega} \tag{5.75}$$

Combining Eqs. (5.74), (5.75) gives

$$\Delta\lambda_{sep.} = \left[\frac{2\lambda n_{2E}}{n_o c^2 \varepsilon_o A} \right]^{1/2} \sqrt{\frac{P}{D}} \tag{5.76}$$

From Eq. (5.76), it can be seen that the sideband separation caused by the modulational instability is proportional to the square root of the optical peak power and inversely proportional to the square root of the dispersion parameter D (> 0). The gain coefficient for the modulational sideband determined by Eq. (5.76) is (Hasegawa & Brinkman 1980)

$$\alpha = \frac{n_{2E} k}{2n_o} |E_o|^2 \tag{5.77a}$$

and substitution from Eq. (5.73b), then gives

$$\alpha = \frac{n_{2E}k}{n_o^2 \varepsilon_o cA} P \tag{5.77b}$$

For $n_o = 1.5$, $\lambda = 1.5 \times 10^{-6}$ μm, $n_{2E} = 1.26 \times 10^{-22}$ $(m/V)^2$ and $A = 10^{-6}$ cm^2, then

$$\alpha = 7.5 \times 10^{-4} P(W) \; [m^{-1}] \tag{5.78}$$

Four-wave mixing (FWM)

When there are three signals of frequencies, ω_1, ω_2 and ω_3 in a medium, it is possible that these will interact with each other via the third-order nonlinear susceptibility to generate a fourth wave that has a frequency ω_4 determined by

$$\omega_1 + \omega_2 = \omega_3 + \omega_4 \tag{5.79}$$

This is so-called *four-wave mixing*, and for it to occur requires that the following phase-matching condition is satisfied,

$$\Delta\beta = \beta_1 + \beta_2 - \beta_3 - \beta_4 = 0 \tag{5.80}$$

For the degenerate cases where $\omega_1 = \omega_2 = \omega_p$, and if we denote $\omega_3 = \omega_{as}$, $\omega_4 = \omega_s$ (suppose $\omega_3 > \omega_4$), Eqs. (5.79) and (5.80) become

$$2\omega_p = \omega_{as} + \omega_s \tag{5.81}$$

$$\Delta\beta = 2\beta(\omega_p) - \beta(\omega_{as}) - \beta(\omega_s) = 0 \tag{5.82}$$

The wave relating to ω_p is called the pump (wave), those associated with ω_{as} and ω_s are referred as Stokes and anti-Stokes respectively. If the intensity of the pump wave is sufficiently high and the phase-matching condition met, then both Stokes and anti-Stokes signals can grow from noise due to the gain provided by the pump wave. On the other hand, this process can also be viewed as the "absorption" of pairs of photons at frequency ω_p whereupon the nonlinear medium immediately emits one Stokes photon at frequency ω_s and one anti-Stokes photon at frequency ω_{as}. Eq. (5.81) fulfills energy conservation and Eq. (5.82) satisfies the conservation of momentum condition.

For bulk materials, phase matching is often achieved through directing the incident waves into the medium at particular angles and one of the most important exploitations of

four-wave mixing is phase conjugation (Yariv and Yeh 1984; Ch. 13). FWM in optical fibres is usually accepted as a useful means for light frequency conversion (Sammut and Garth 1989). According to distinct fibre types phase matching is achieved in three different ways: for multimode fibres, phase matching can be realized for different waveguide modes (Stolen *et al* 1974); for birefringent fibres, phase matching is obtained for the waves which have orthogonal polarizations (Chee and Liu 1989); for monomode fibres, a particular pump wavelength (close to the zero-dispersion value, λ_o) is required to enable the matching condition to be fulfilled (Washio *et al* 1980, Lin *et al* 1981, Garth and Pask 1986). In what follows a brief discussion is included for four-wave mixing in monomode optical fibres. Some of the results included here will be quoted in Ch. 10 where experimental results regarding a novel, SPM-mediated four-wave mixing process are presented.

For a monomode optical fibre, β can be expressed as

$$\beta = k\sqrt{n_2^2 + (n_1^2 - n_2^2)b} \tag{5.83}$$

where $k = 2\pi/\lambda$, n_2, n_1 are the refractive indices of the fibre cladding and core regions respectively and b is a parameter relating to the waveguide geometry. The parameter b is a function of normalized frequency ($V = kr[n_1^2 - n_2^2]^{1/2}$ and r is the radius of fibre core). For $1.5 < V < 2.4$, the approximate expression (Gowar 1984) for $b(V)$ given below

$$b(V) = \{1.1428 - \frac{0.996}{V}\}^2 \tag{5.84}$$

is often used. If the difference in the fibre cladding and core refractive indices is small, Eq. (5.83) can be simplified to:

$$\beta \approx kn_2(1 + b\Delta) \tag{5.85}$$

with $\Delta = (n_1^2 - n_2^2)/2n_2^2 \approx (n_1 - n_2)/n_2$. From Eq. (5.85), it can be seen that β is a combination of two distinct terms. One is $\beta_m = kn_2$, known as the propagation constant of the material, and the other is $\beta_w = k(n_1 - n_2)b$, which describes the waveguide characteristic (assuming $n_1 - n_2 \approx$ const.). Eq. (5.82) can thus be re-expressed as

$$\Delta\beta = \Delta\beta_m + \Delta\beta_w = 0 \tag{5.86}$$

where $\Delta\beta_m$, $\Delta\beta_w$, are the material and waveguide contributions to the phase-matching condition (Lin *et al* 1981, Suzuki *et al* 1989).

If an effective (or overall) refractive index for the fibre is defined as

$$n = n_2 (1+ b\Delta) \tag{5.87}$$

then the phase-matching condition [Eq. (5.82)] can also be rewritten as

$$\frac{1}{c}[n(\omega_{as})\omega_{as} + n(\omega_s)\omega_s - 2n(\omega_p)\omega_p] = 0 \tag{5.88}$$

Letting $\Omega = \omega_{as} - \omega_p$ and taking $\omega_{as} = \omega_p + \Omega$ and $\omega_s = \omega_p - \Omega$ into Eq. (5.88), we obtain

$$\Omega = \{1- 2\frac{n(\omega_{as}) - n(\omega_p)}{n(\omega_{as}) - n(\omega_s)}\}\omega_p \tag{5.89}$$

Unfortunately, Eq. (5.89) is not an explicit expression of the frequency shift, because the refractive index values at the Stokes and anti-Stokes frequencies are actually dependent upon the value of Ω. Nevertheless, a necessary condition for the process of four-wave mixing can be derived from this equation, which is, for $\Omega \geq 0$, that:

$$n(\omega_{as}) + n(\omega_s) \leq 2n(\omega_p) \tag{5.90a}$$

where the equality corresponds to zero frequency shift. If a quadratic approximation is used in making a Taylor expansion of $n(\omega_{as})$ and $n(\omega_s)$ around the pump frequency, Eq. (5.90a) then becomes

$$(\frac{d^2n}{d\omega^2})|_{\omega_p} \leq 0 \tag{5.90b}$$

which implies that the four-wave-mixing process can only be achieved when the pump frequency lies in the convex part of the $n(\omega)$ versus ω curve.

Stimulated Raman scattering and self-Raman effects

Stimulated Raman Scattering (SRS) is a nonlinear effect that relates to the interaction between an input wave and one of the inherent molecular vibration modes in a medium. Normally, as a result of Raman process a new wave at the frequency

$$\omega_R = \omega_p - \Omega_R \tag{5.91}$$

is generated. In Eq. (5.91), ω_p is the frequency of the incident or pump wave, Ω_R is the molecular vibration frequency, or the Raman frequency shift (see Fig. 5. 10).

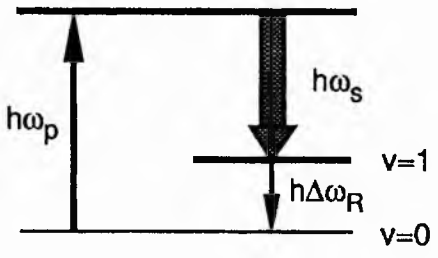

Fig. 5.10. Energy level structure responsible for the stimulated Raman process.

In optical communication techniques, the Raman process is often undesireable and is regarded as a deleterious effect, exploitation of the stimulated Raman scattering for constructing an near-infrared optical amplifier and tunable laser sources have been successively pursued in many research laboratories (Stolen 1979, Valk *et al* 1985, Lin and Glodis 1982, Mollenauer *et al* 1985, Kean *et al* 1987). In the stead-state, the intensity of the Raman wave can be written as

$$I_R = I_R(0)e^{g_R I_p z} \tag{5.92}$$

where g_R is the Raman gain coefficient, I_p is the pump intensity. A threshold condition for SRS is defined by (Smith 1972)

$$g_R I_p z \approx 16 \tag{5.93}$$

Such a value means that a Raman wave originating from noise can have an intensity that grows to be comparable to the pump intensity.

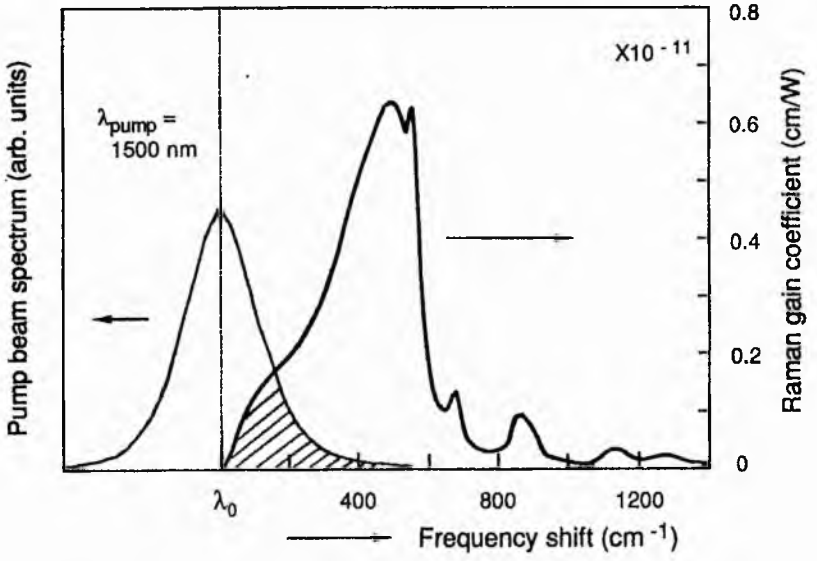

Fig. 5.11. Spectral distribution of Raman gain and the associated pump wave specturm.

A typical frequency distribution of the Raman gain coefficient adapted from the

results by Stolen *et al* (1978) is as shown in Fig. (5.11). In general, the absolute values of the Raman gain coefficient at different frequencies are approximately proportional to $1/\lambda_p$ (Stolen 1979) and changeable when different dopants are added to the materis involved (Lin 1986).

From Fig. (5.11), it can be seen that there is a continuous extension of the Raman gain due to the amorphous nature of glasses, starting from zero shift up to ~ 1000 cm^{-1}, and the peak locates at 400 cm^{-1}. Such a feature contributes to two important consequences. One is that for the pump pulses which do not have a very extended spectrum, the Raman wave appears exactly at the peak gain frequency and no detectable signal exists between the pump and Raman frequencies. In this first situation, if the pump is strong enough, the generated Raman Stokes wave achieves so much gain that it can act as a pumping source itself to generate another Raman wave (2nd Stokes). If this process is sustained, a cascade of SRS occurs, producing a series of new frequency radiations with a separation characterized by Ω_R (Valk *et al* 1985, Takahashi *et al* 1986).

The second effect occurs when the incident pulses are in the femtosecond regime. In such cases, the pump pulses have a large bandwidth so that some of the spectral components on the longer wavelength side are encompassed by the Raman gain profile (see the hatched area in Fig. 5.11). This overlaped spectral portion is thus substantially amplified by the Raman gain, leading to a continuous transfer of energy towards the longer wavelengths during propagation (Mitschke and Mollenauer 1986). This is the so-called self-Raman effect (Gordon 1986)[8]. In the presence of anomalous dispersion, it leads to an increased time delay for the propagating pulses (With normally dispersive media the effect would be opposite). Theoretical analyses have indicated that the Raman effect is essentially connected to the delayed response of the nonlinearity and the amount of frequency shift due to the self-Raman effect is governed by (Gordon 1986, Haus and Nakazawa 1987, Tai *et al* 1988)

---

[8] In the experiments of optical soliton propagation, Mitschke and Mollenauer (1986) recorded this spectral drifting phenomenon and named it as *self-soliton-frequency-shift*. The immediate theoretical analysis by Gordon (1989) attributed it to the interaction of the soliton spectral components with the distributed Raman gain.

$$\frac{d\omega}{dz} \propto \frac{1}{\Delta t_i^4} \tag{5.94}$$

For pulse propagation in the femtosecond regime, methods of using amplification-related frequency pulling effect (Blow *et al*, 1988) or constructing a new absorption band [at a wavelength appropriately located among the Raman gain region of a propagating medium (Dianov *et al* 1990)] to suppress this self-frequency shift have been investigated.

5.3 Pulse propagation equations

As a complement to the analytical discussions presented in the previous sections, there is a need for more complete features of pulse propagation in various media using he associated wave equations. A great deal of effort has been made in simplifying and numerically solving the differential equations regarding the propagating pulses under different situations (Fisher and Bischel 1975, Blow and Doran 1983, Tajima and Washio 1985, Manassah *et al* 1986, Bourkoff *et al* 1987, Golovchenko *et al* 1988, Zhao and Bourkoff 1988, Wai *et al* 1988, Boyer and Carlotti 1988, Boyer and Franco 1989). In the following, a brief description of these equations is given without involving any sophisticated derivations and then some discussions are presented on one of the most important equations - the nonlinear Schrödinger equation.

5.3.1 Wave equations under different situations

For lossless linear media, under the slow variation envelope approximation, the general wave equation given in Eq. (A.14a) in Appendix A can be reduced to (Siegman 1986)

$$\frac{\partial \mathcal{A}(z,t)}{\partial z} + \frac{1}{v_g}\frac{\partial \mathcal{A}(z,t)}{\partial t} - i\frac{\beta''}{2}\frac{\partial^2 \mathcal{A}(z,t)}{\partial t^2} = 0 \tag{5.95a}$$

$\mathcal{A}(z,t)$ is the complex pulse envelope at a spatial position z (for convenience, it will be abbreviated as $\mathcal{A}$), v_g and β'' are the group velocity and the second-order dispersion parameter respectively (as defined before, both are evaluated at the carrier frequency ω_o). Eq. (5.95a) is also known as *parabolic equation*, which describes the propagation of pulses in purely dispersive media where only the second-order dispersion is included. In a

moving coordinate system ($z = z$, $\eta = t - z/v_g$) Eq. (5.95a) can be simplified to

$$\frac{\partial \mathcal{A}}{\partial z} - i\frac{\beta''}{2}\frac{\partial^2 \mathcal{A}}{\partial \eta^2} = 0 \tag{5.95b}$$

In the cases where the third-order dispersion needs to be considered, Eq. (5.95b) is extended to (Akhmanov *et al* 1987)

$$\frac{\partial \mathcal{A}}{\partial z} - i\frac{\beta''}{2}\frac{\partial^2 \mathcal{A}}{\partial \eta^2} - \frac{1}{6}\left[\beta''' + \frac{3\beta''}{v_g k_o}\right]\frac{\partial^3 \mathcal{A}}{\partial \eta^3} = 0 \tag{5.96}$$

For high loss or very long media, where an associated attenuation coefficient is α, a loss term may be added to Eq. (5.96) and thus

$$\frac{\partial \mathcal{A}}{\partial z} + \alpha\mathcal{A} - i\frac{\beta''}{2}\frac{\partial^2 \mathcal{A}}{\partial \eta^2} - \frac{1}{6}\left[\beta''' + \frac{3\beta''}{v_g k_o}\right]\frac{\partial^3 \mathcal{A}}{\partial \eta^3} = 0 \tag{5.97}$$

To include the nonlinear effect of SPM, Eq. (5.97) should be rewritten as

$$\frac{\partial \mathcal{A}}{\partial z} + \alpha\mathcal{A} - i\frac{\beta''}{2}\frac{\partial^2 \mathcal{A}}{\partial \eta^2} - \frac{1}{6}\left[\beta''' + \frac{3\beta''}{v_g k_o}\right]\frac{\partial^3 \mathcal{A}}{\partial \eta^3} - iK|\mathcal{A}|^2\mathcal{A} = 0 \tag{5.98}$$

where $K = k_o n_{2E} / 2n_o$. Note that in deriving the nonlinear term $-iK|\mathcal{A}|^2\mathcal{A}$ in Eq. (5.98) it has been assumed that the rate of change of the nonlinear polarization is small enough to be neglected. Such an assumption will not be valid when the initial pulses have a duration equal to or less than several tens of femtosecond and the corresponding pulse peak intensity reaches the order of 10^{12} W/cm^2. Under this situation another nonlinear term (known as *shock term*) must be added to Eq. (5.98) (Anderson and Lisak 1982), such that

$$\frac{\partial \mathcal{A}}{\partial z} + \alpha\mathcal{A} - i\frac{\beta''}{2}\frac{\partial^2 \mathcal{A}}{\partial \eta^2} - \frac{1}{6}\left[\beta''' + \frac{3\beta''}{v_g k_o}\right]\frac{\partial^3 \mathcal{A}}{\partial \eta^3} - iK|\mathcal{A}|^2\mathcal{A} + K_2\frac{\partial^2|\mathcal{A}|^2\mathcal{A}}{\partial \eta^2} = 0 \tag{5.99}$$

where $K_2 = 2K/\omega_o = n_{2E}/c$. In the cases where losses and dispersive effects can be ignored then Eq. (5.99) reduces into

$$\frac{\partial \mathcal{A}}{\partial z} - iK|\mathcal{A}|^2\mathcal{A} + K_2\frac{\partial^2|\mathcal{A}|^2\mathcal{A}}{\partial \eta^2} = 0 \tag{5.100}$$

Analyses have shown that (Anderson and Lisak 1982, Yang and Shen 1984) the presence of the shock term in the above equations leads to the flattening of the leading edge and the steepening of the trailing edge of the propagating pulses. (Correspondingly, in the

frequency domain this contributes to an asymmetrical spectral extension, more to the blue than that towards the red). If the shock term is neglected, Eq. (5.100) becomes

$$\frac{\partial \mathcal{A}}{\partial z} - iK|\mathcal{A}|^2\mathcal{A} = 0 \qquad (5.101)$$

Eq. (5.101) describes one of the simplest situation of pulse propagation - only inertialless SPM is present (see Sec. 5.2.3.). If $|\mathcal{A}|^2$ is assumed to remain constant, the solution to Eq. (5.101) can be readily obtained to be $\mathcal{A}(z) = \mathcal{A}(0)e^{iK|\mathcal{A}|^2 z}$.

On the whole, Eq. (5.99) represents a very general wave equation. It can be either simplified or further extended to apply to various pulse propagation conditions. Additionally, simulations of pulse propagation at intensities above the Raman generation threshold can be performed by adding an intensity-related loss term into Eq. (5.99) (Hasegawa 1983). In this case, if the terms for the shock wave and the cubic dispersion are omitted, then

$$\frac{\partial \mathcal{A}_p}{\partial z} + (\alpha + g_{RE}|\mathcal{A}_s|^2)\mathcal{A}_p - i\frac{\beta_p''}{2}\frac{\partial^2 \mathcal{A}_p}{\partial \eta^2} - iK_p|\mathcal{A}_p|^2\mathcal{A}_p = 0 \qquad (5.102a)$$

g_{RE} is related to the Raman gain coefficient and the subscript p denotes the pump wave that provides the Raman gain. The corresponding Stokes wave can be expressed as

$$\frac{\partial \mathcal{A}_s}{\partial z} + (\alpha - g_{RE}|\mathcal{A}_p|^2)\mathcal{A}_s - i\frac{\beta_s''}{2}\frac{\partial^2 \mathcal{A}_s}{\partial \eta^2} - iK_s|\mathcal{A}_s|^2\mathcal{A}_s = 0 \qquad (5.102b)$$

5.3.2. Some important features of the nonlinear Schrödinger equation

By dropping the loss and the cubic dispersion terms from Eq. (5.98) and using appropriate transformations the following dimensionless *nonlinear Schrödinger equation* can be derived:

$$i\frac{\partial u}{\partial \xi} = \frac{1}{2}\left(\frac{-\beta''}{|\beta''|}\right)\frac{\partial^2 u}{\partial s^2} + |u|^2 u \qquad (5.103)$$

where ξ, s are the normalized spatial and (local) time variables defined by[9]

9 The physical meaning of the coefficient "a" in these given transformations can be found from Eq. (5.104b). It is actually the pulse duration parameter and, therefore, in principle can be selected according to the pulse shapes. Nevertheless, it is often defined by assuming a $sech^2$ pulse shape, i. e. $a = 1.76/\Delta t_j$ (see Sec. 2.1).

$$\xi = a^2|\beta''|z = (\Delta t_i/1.76)^{-2}\,|\beta''|z \tag{5.104a}$$

$$s = a(t - \beta' z) = (\Delta t_i/1.76)^{-1}(t - \beta' z) \tag{5.104b}$$

and

$$u = a\sqrt{\frac{K}{|\beta''|}}\,\mathcal{A} = \frac{\Delta t_i}{1.76}\sqrt{\frac{K}{|\beta''|}}\,\mathcal{A} \tag{5.104c}$$

Eq. (5.103) reflects the combined effect of the second-order group velocity dispersion and the relatively weak nonlinearity on the propagating pulses. As summarized in Table 5.5, according to the different signs that the dispersion parameter may have and the essential feature of the initial pulses, distinct solutions can be derived from this equation (Blow and Doran 1987, Tomlinson 1989).

Table 5.5 Combined effects of group velocity dispersion and nonlinearity*

Pulse types / Dispersion	Ordinary pulses ($u \to 0$ for $t >> \Delta t_i$)	Inverse pulses† ($u \to 1$ for $t >> \Delta t_i$)
$\beta'' < 0$	Solitons	Modulational instabilities
$\beta'' > 0$	Enhanced dispersion	Dark solitons

* After Blow and Doran (1987).
† This category of pulses, having a sudden drop of intensity on a continuous radiation background, may also be termed as dark pulses.

We may concentrate on the situation where the incident pulses are the ordinary pulses. [Investigations of dark solitons which only exist for the inverse pulses can be found in the papers by Weiner *et al* (1988), and Tomlinson *et al* (1989)].

For $\beta'' < 0$, Eq. (5.103) can be rewritten as

$$i\frac{\partial u}{\partial \xi} = \frac{1}{2}\frac{\partial^2 u}{\partial s^2} + |u|^2 u \tag{5.105}$$

One of the most important features of the above nonlinear Schrödinger equation is that it has analytical solutions for the initial condition (Satsuma and Yajima 1974):

$$u(0,s) = N\,\mathrm{sech}(s) \tag{5.106}$$

where N is an integral. For example, with N = 1,

$$u_1(\xi,s) = e^{-i\xi/2}\,\mathrm{sech}(s) \tag{5.107}$$

and for N = 2,

$$u_2(\xi,s) = 4e^{-i\xi/2}\,\frac{ch(3s) + 3e^{-i4\xi}ch(s)}{ch(4s) + 4ch(2s) + 3\cos(4\xi)} \tag{5.108}$$

The wave relating to the solution for $N = \eta$ ($\eta \geq 1$) is often called the η_{th}-order soliton. Solitons are stable with respect to small perturbations in the initial input condition, such as in Eq. (5.106) N is changed to $N + \zeta$ (Zakarov and Shabat 1972).

The fundamental (N = 1) soliton remains unchanged in its shape, while for higher order solitons ($N \geq 2$) the pulse shape changes periodically during propagation. In the latter case, although for different N values the pattern of the changes of pulse shape varies dramatically a common spatial period (known as *soliton period*) exists, at which the pulses are restored to their original shapes. The soliton period is given by (Satsuma and Yajima 1974)

$$\xi = \frac{\pi}{2} \tag{5.109}$$

In real space, using Eq. (5.104a), this expression leads to

$$z_o = \frac{\pi}{2}\left[\frac{\Delta t_i}{1.76}\right]^2 \frac{1}{|\beta''|} \tag{5.110a}$$

or (Mollenauer and Stolen 1982)

$$z_o = \left[\frac{\pi\Delta t_i}{\lambda 1.76}\right]^2 \frac{c}{|D|} = 0.322\,\frac{(\pi\Delta t_i)^2 c}{\lambda^2|D|} = \frac{0.322(\pi\Delta t_i c)^2}{\lambda|Y|} \tag{5.110b}$$

Solitons in the second half period make a mirror image of those in the first half and so for the purpose of calculation only the traces in $\xi \leq \pi/4$ region need to be considered. For the higher-order solitons, at the position of the exact half period (N - 1) peaks exist, all of them sitting on the top of a broader pedestal background (Tan 1987). Such a feature, obviously, may be utilized to make a judgement of the order of the solitons observed in experiments.

For producing a N = 1 soliton, from the transformation given by Eqs. (5.104), the associated actual incident optical pulse should be

$$|\mathcal{A}(0,t)| = \frac{1.76}{\Delta t_i}\sqrt{\frac{|\beta''|}{K}}\,\mathrm{sech}[(1.76/\Delta t_i)t] \tag{5.111}$$

the associated peak amplitude of which is given by

$$\hat{A}^2 = |\mathcal{A}(0,0)|^2 = \frac{\pi}{2z_0 K} \tag{5.112a}$$

The above expression is identical to

$$I_1 = \frac{\lambda_{vac}}{4n_{2I} z_0} \tag{5.112b}$$

where λ_{vac} is the vacuum wavelength for the carrier (Mollenauer and Stolen 1982).

Similarly, for the N = 2 soliton, through using Eqs. (5.108) and (5.104), it can be readily derived that

$$I_2 = 2^2 I_1 \tag{5.113}$$

In general, for the n_{th}-order soliton, the peak power for the initial optical pulses should satisfy

$$I_n = n^2 I_1 \tag{5.114}$$

A significant feature of the higher-order solitions is that they all experience a self-compression process immediately after entering the medium. The higher the soliton order, the larger the compression will be. For a N = 2 soliton, the shortest peak occurs at the half soliton period. As N increases such a peak appears earlier and earlier. After reaching the shortest peak position, the temporal profile of the solitons collapse and is involved into a complicated pulse splitting process. While N = 1 soliton is of considerable potential use in optical digital communication (Hasegawa and Tappert 1973, Mollenauer *et al* 1986), a direct application of higher order solitons is in the pulse compression scheme (Mollenauer *et al* 1983, Gouveia-Neto *et al* 1988)[10].

In the cases where $\beta'' > 0$, Eq. (5.103) becomes

$$i\frac{\partial u}{\partial \xi} = -\frac{1}{2}\frac{\partial^2 u}{\partial s^2} + |u|^2 u \tag{5.115}$$

Because for ordinary pulses $\partial^2 u/\partial s^2 < 0$, there is no possible cancellation between the two terms on the right-hand side of the above equation, and so no self-compression occurs for propagating pulses. (In some publications, to differ from the cases where only SPM is present, the coexistence of both positive GVD and SPM is also termed as *dispersed self-*

[10]However, a noticeable disadvantage of the pulse compression using higher-order solitons is that the compressed pulses are always accompanied by relatively large pedestals.

phase modulation). The frequency chirp caused by SPM and that by GVD under these situation will enhance each other, and the eventual result from the interplay between SPM and the positive GVD is that a rectangular-shaped pulse having largely stretched, linear frequency chirp is formed (Natatsaka *et al* 1981, Nelson *et al* 1983). Such a feature has been widely utilised in the fibre-grating pair pulse compression scheme (Grischowsky and Balant 1982; also see Appendix D).

Part III
Coupled-Cavity Mode Locking in a KCl:Tl Laser

The third part of this thesis presents the main experimental results for a coupled-cavity mode-locked KCl:Tl colour-centre laser. It consists of a review of the development of coupled-cavity mode locking, analyses of the key elements in a KCl:Tl laser, main mode locking performance characteristics, typical applications of the coupled-cavity KCl:Tl laser, and some general conclusions. Relevant discussions on the observed phenomena relating to the various features of coupled-cavity mode locking are also included.

Chapter 6

General Introduction to Coupled-Cavity Mode-Locked Lasers

During recent years there has been considerable research interest in the generation of ultrashort pulses using coupled-cavity arrangements. In many cases, such a system comprises an ordinary laser appended by an auxiliary (or control) cavity that incorporates a nonlinear medium. (In some particular situations, both cavities may be within a single laser). This type of mode-locking scheme which originated from the soliton laser, involves distinct physical mechanisms in producing ultrashort pulses as compared to other more traditional mode-locking techniques. It has thus been regarded as a new method of mode-locking, which offers attractive advantages over alternatives in terms of pulse duration, frequency-tuning ranges and applicability to different laser systems. In this chapter an overview of this novel type of mode locking will be presented. In section 6.1 a general description of coupled-cavity mode-locked lasers is included. This is followed by a review of the development history in section 6.2.

6.1. General description of a coupled-cavity mode-locked laser

6.1.1 Principal configuration

The schematic of a coupled-cavity mode-locked (CCM) laser configuration is shown in Fig. 6.1(a). The main cavity itself is a conventional laser configuration with M_0 as its output coupler. By passing through a beamsplitter part of the output of the main cavity laser is coupled into a nonlinear medium and then fed back to the main cavity by the retroreflector M_r. M_r, M_0 form the control cavity and the optical path between them is adjusted so that it is matched to the main cavity length.

The main cavity laser may contain any one of the KCl:Tl, LiF:F_2^+, NaCl:OH^-, Ti:Al_2O_3, Nd:YAG (either pumped by a flashlamp or a semiconductor-diode laser), Nd:YLF, Nd:glass or CO_2 gain medium. The nonlinear elements that have been

incorporated into the control cavity so far include an optical fibre (with either positive or negative group-velocity dispersion), semiconductor amplifier/absorber, second harmonic generation crystal, multi-quantum-well semiconductor structure and Ge crystal. All of these nonlinear devices can be classified into two categories that provide resonant and nonresonant nonlinearities respectively.

Combinations of the main cavity laser and the nonlinear element, which have led to successful CCM operation, are indicated in Fig. 6.1(b). Although there are a lot of options as to which kind of nonlinear devices should be used, for most of the reported CCM lasers the nonlinear elements are various optical fibres. The combination of KCl:Tl laser with a negative GVD fibre is actually the basis of the soliton laser.

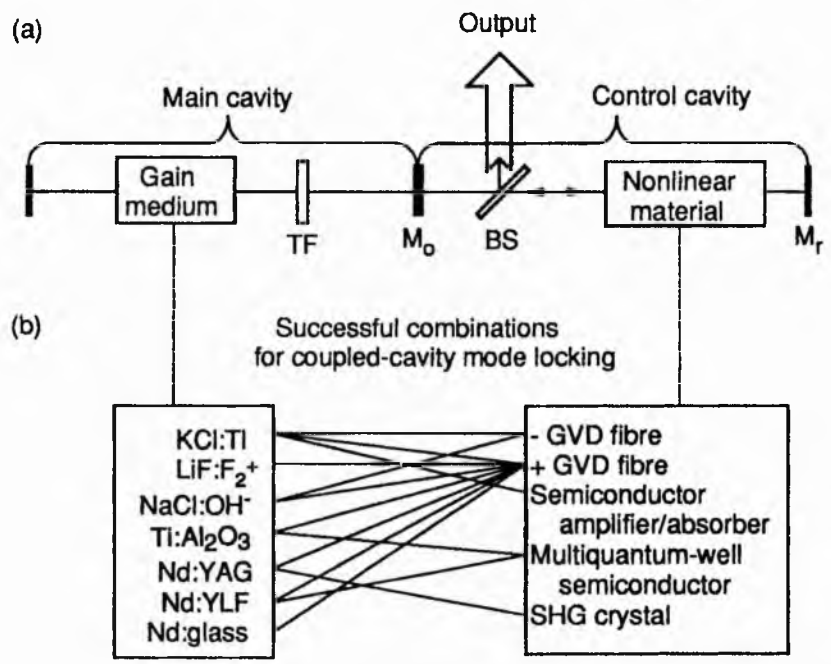

Fig. 6.1. (a) Schematic of coupled-cavity mode-locked (CCM) laser configuration (TF - tuning filter; BS - beamsplitter). (b) Possible combinations of gain medium and the nonlinear elements for constructing a coupled-cavity mode-locked laser. The lines between the corresponding elements show the combinations that have led to successful CCM operation.

Normally, for a CCM laser, provided that its nonlinear element in the control cavity has been appropriately selected, when the two cavity periods are properly matched, and a suitable optical intensity ratio is established, ultrashort pulses having durations in the range of several picoseconds to sub-100 femtosecond can be reliably produced. This can

be achieved either by a completely self-starting mechanism, (i .e. the main cavity laser along is under no external or internal modulation), or through a process of mode-locking enhancement, depending on the characteristics of the nonlinearity and the gain medium involved. In the operation of mode-locking enhancement, where the main cavity laser is either actively, synchronously or passively mode-locked (e. g. see the corresponding papers by Pinto *et al* 1987, Kean *et al* 1988 and Johnston *et al* 1989), the involvement of the control cavity leads to significantly improved pulse shaping/shortening effects.

6.1.2 Three typical forms of the CCM laser configuration

Although in Fig. 6.1(a), the nonlinear element has been located in front of the beamsplitter so that the transmitted beam is incident on it, such an arrangement serves merely as a simple illustration. For most of the practical CCM laser systems, due to the consideration of the convenience in alignment, it is often the reflected beam that is coupled into the nonlinear element [see Fig. 6.2(a)].

In a system of the type shown in Fig. 6.2(a), suppose an optical pulse (or a burst of light flux) travelling inside the main cavity is incident on the output coupler, then part of it will be reflected back to the gain medium and part of the transmitted beam will be directed into the nonlinear medium. After one cavity roundtrip time these two components, one having travelled in the main cavity where it experienced amplification, and one propagated in the control cavity having had nonlinear phase/amplitude modulation, will meet each other and interfere. A similar event can occur with the system shown in Fig. 6.2(b), where one of the two interfering pulses passes the gain and the nonlinear medium twice within every cavity roundtrip, whereas the other only passes the gain medium during the same time period. In fact, the system in Fig. 6.2(a) can be regarded as a laser with a nonlinear Fabry-Perot (NFP) interferometer as its output coupler where for system in Fig. 6.2(b) the output coupler is a nonlinear Michelson (NM) interferometer. Therefore, in terms of interference, the NFP-type coupled-cavity mode-locked laser involves multiple beam interference, whereas the NM-type coupled-cavity laser relates solely to two beam interference. In practice, it has been frequently observed

that under similar pumping and bandwidth control conditions the NFP-type coupled-cavity mode-locked laser has the capability of producing shorter pulses than those obtained from the NM-type CCM laser. The difference between these two systems in terms of interference could be used to account for such observations. On the other hand, with regards to stability it has been found that the NM-type arrangement is superior to the NFP-type CCM laser. This may be explained by the fact that for a NM-type arrangement the gain medium is within the path of both cavities and so any variations, e. g. thermal drift, of the gain medium would not cause cavity-length mismatches. By contrast, in the NFP-type CCM laser, any fading of the gain after continuous operation for a certain time would make it necessary to readjust the laser cavity lengths.

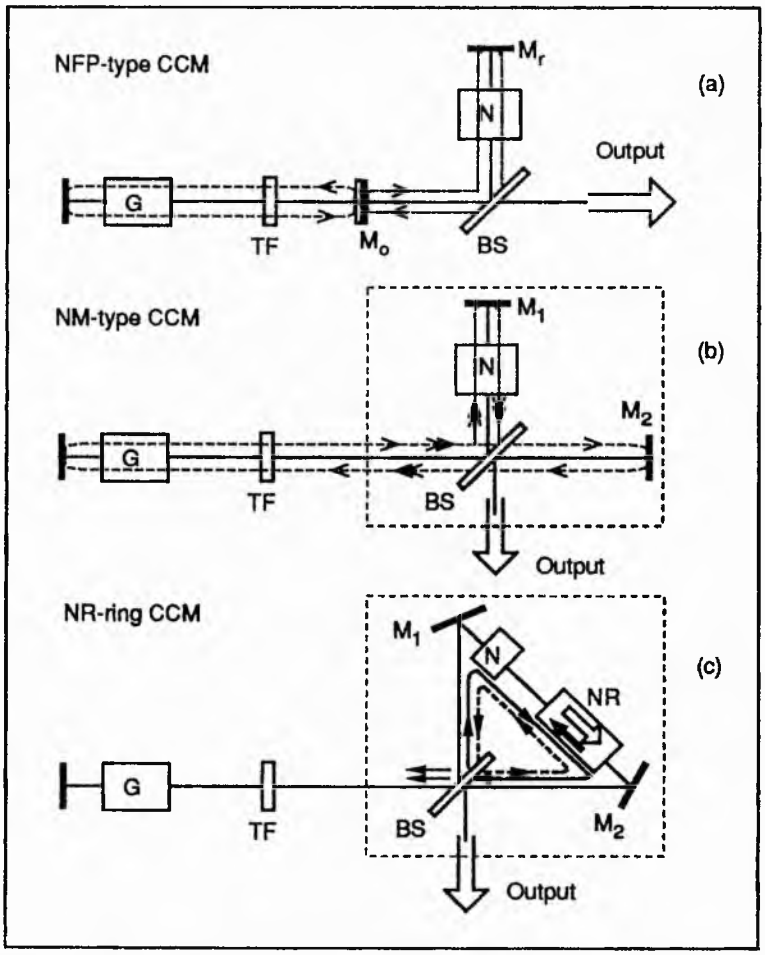

Fig. 6.2. Three types of coupled-cavity mode locking arrangements (a)with a nonlinear Fabry-Perot (NFP) interferometer (b) with a nonlinear Michelson (NM) interferometer (c) with a nonreciprocal antiresonant ring (NR-ring) as the respective output couplers. (G: gain medium; N: nonlinear elements; TF: tuning filter; BS: beamsplitter; NR: nonreciprocal device).

A common feature of the NFP-type and the NM-type coupled-cavity mode-locking arrangements is that they need a PZT-servo system to maintain the two cavity lengths properly matched during the mode-locking operation. This not only increases the complexity of the overall system but also becomes a fundamental source of the system noise at low frequencies. A special coupled-cavity arrangement where the cavity length mismatch control is not necessary is a laser with an antiresonant ring as its output coupler [see Fig. 6.2(c)]. In this case the ring includes a nonreciprocal device so that the beam propagates in one direction (say clockwise) experiences nonlinear modulation whereas the beam travels in another direction does not. Interference occurs between the two beams travelling through different directions when they have propagated through the ring. This antiresonant ring arrangement is actually a variation of the NM-type of CCM laser [If the two end mirrors, M_1, M_2 of the NM interferometer [see Fig. 6.2(b)] are properly rotated a ring structure will then be formed]. Therefore, as for the NM-type CCM configuration, the two cavities within an antiresonant ring system (one related to the clockwise ring and the other to the anti-clockwise) share a common arm that includes the gain medium. One distinguishing feature for the ring system is that the two coupled cavities are spatially overlapped.

6.1.3 Main features of a CCM KCl:Tl laser

It is instructive to consider the basic physical behaviour of a practical CCM laser such as the NFP-type coupled-cavity, mode-locked KCl:Tl laser illustrated in Fig. 6.3. In this case, the main cavity laser is synchronously pumped by a cw mode-locked Nd:YAG laser (Spectra-Physics, Series 3000) and the nonlinear medium incorporated in the control cavity is an optical fibre. Typical average power levels at several important locations within the laser are as indicated in Fig. 6.3. P_p is the pump power for the KCl:Tl colour-centre laser (CCL), which is controlled by a variable attenuator between the CCL and the pump laser, P_o is the output power of the CCL, P_{fi} is the incident power into the fibre, P_f the power exiting the fibre and P_m the power of the pulses fed back from the fibre. During an experiment, P_{fi}, and therefore P_f and P_m, is adjusted by rotating the variable

attenuator disc A2. When A2 is fixed, the maximum value of P_f can be obtained by optimizing the coupling at C1. P_m can be maximized in turn by optimizing the coupling at C2. A typical total coupling efficiency (i.e. P_f/P_{fi}) of 70% is readily obtained.

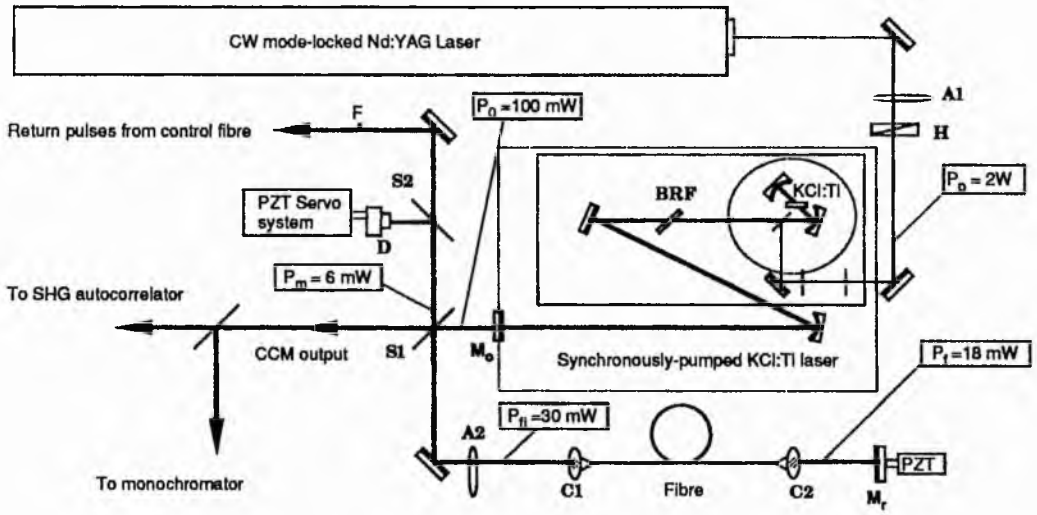

Fig. 6.3. Experimental arrangement for a coupled-cavity mode-locked KCl:Tl colour-centre laser. The output mirror of the colour-centre laser $\mathbf{M_0}$ and the end mirror $\mathbf{M_r}$ form the control cavity. **A1, A2** - variable attenuators; **H** - halfwave plate; **S1, S2** - beamsplitters; **D** - photodetector; **BRF** - birefringent filter. Point F is the position where the return signal from the control cavity can be monitored.

Normally, in the absence of the control cavity the output pulses from the main laser have durations of several tens of picoseconds and the corresponding SH signal out of the autocorrelator (see Ch. 4) is relatively low. However, when the control cavity is involved the coupled-cavity mode-locking process can lead to a dramatic decrease in the output pulse duration and a ~x100 increase in the SH signal level has been observed. Two representative examples of sequences of SH intensity autocorrelation traces are shown in Fig. 6.4(a), (b) for laser pulses produced with the control cavity blocked and unblocked respectively. [Vertical scale in Fig. 6.4(b) is 100 times greater than that in Fig. 6.4(a)].

A significant feature of the CCM KCl:Tl laser is that it has an essentially passive nature[1] in that whenever the coupled-cavity mode locking occurs the pulse repetition frequency for the main cavity laser is no longer necessarily locked to that of the pump laser. In consequence, a frequency beat can arise between the signals from the acousto-

[1] This passive nature actually determines that the coupled-cavity mode-locked KCl:Tl laser pulses are of good quality in terms of both low amplitude and phase noise features (Finch *et al* 1990).

optic modulator in the pump laser and that from the CCM laser output (see Fig. 6.5). (Normally, the beat frequency is in the few kHz range, depending on the setting of the main cavity length). Such a passive characteristic in fact represents a common behaviour of all the CCM lasers. As mentioned in the subsection 6.1.1, for many laser systems coupled-cavity mode locking can be achieved from a completely self-starting process. Therefore, in principle, mode locking of the main cavity laser is only necessary when the initial light fluctuations inside the laser cavity are not strong enough to exploit the nonlinearity included in the control cavity.

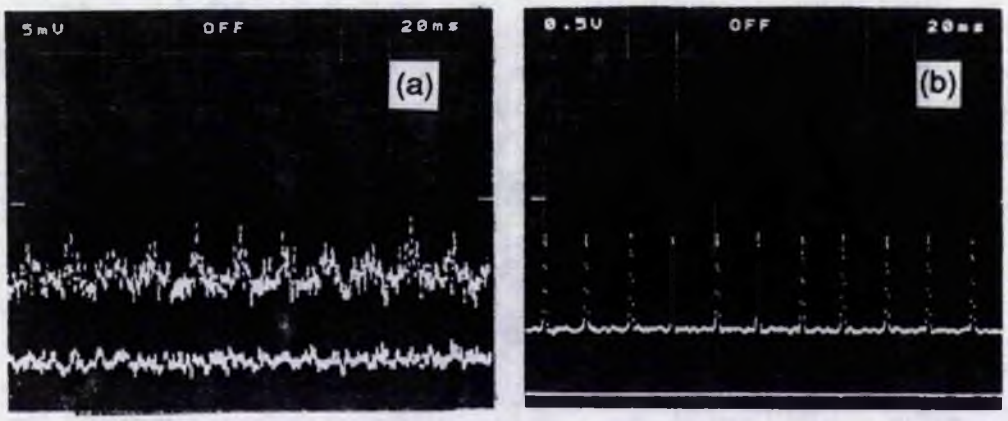

Fig. 6.4. Sequences of intensity autocorrelation traces for the pulses produced with the control cavity blocked (a) and unblocked (b). The bottom line in each oscillogram indicates the zero signal level.

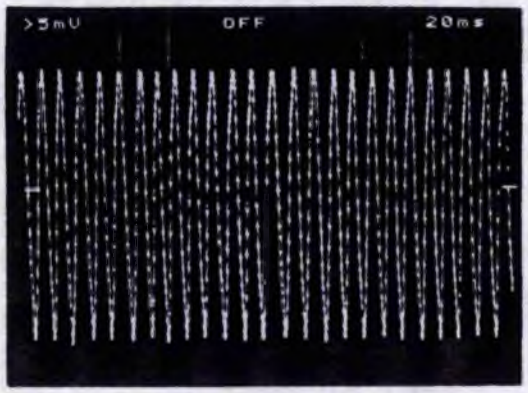

Fig. 6.5. Beat signal between the CCM KCl:Tl laser output and that derived from the acousto-optic oscillator for the mode-locker in the Nd:YAG pump laser.

To overcome the influence of the cavity length drifting during the CCM operation, a PZT-servo system is needed to automatically compensate for any cavity length mismatches that arise[2]. This is realized by using a photodiode (denoted as **D** in Fig. 6.3)

[2] Owing to the control-cavity length drift and the dependence of the overall reflectivity of the NFP

to detect a component of the signal intensity returned from the control cavity, and then an error signal derived from the difference of this average photodetector voltage and a preset reference voltage is amplified and applied to the piezo-electric transducer (PZT) to which the end mirror of the control cavity is connected (see Fig. 6.3). Because adjusting the reference voltage level means shifting the control cavity length particular positions for the end mirror can thus be selected, at which mode-locking enhancement is achieved.

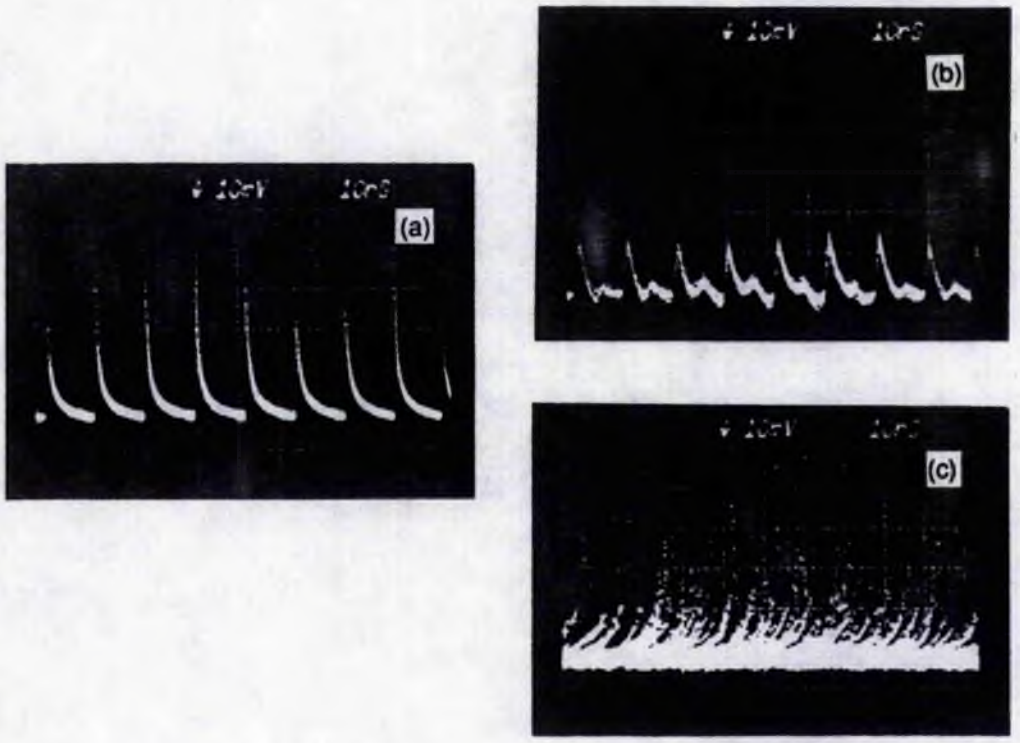

Fig. 6.6. Pulse train traces from the KCl:Tl laser without the control cavity (a), with the control cavity out-of-phase (b) and in-phase (c) locked, recorded with a sampling-oscillascope that has a triggering signal derived from the pump laser.

It is interesting to note that for the coupled-cavity arrangement shown in Fig. 6.3 in addition to the desired special 'in-phase' locking, which leads to the generation of shorter pulses with much extended spectra (e. g. see Fig. 8.3), a state of 'out-of-phase' locking of the two cavity lengths is also observable by adjusting the reference voltage of the PZT

---

interferometer on its end mirror separation, the involvement of the control cavity leads to a fluctuation of output power level of the CCM laser system. Since mode-locking enhancement occurs only at certain power levels within this fluctuation range, without using the PZT-servo system the coupled-cavity mode locking will not be sustained and will only operate in a state which flickers between "off" and "on".

servo system. In this 'out-of-phase' locking condition the spectrum of the laser output becomes narrower with the control cavity compared with that recorded for the CCL laser alone, and correspondingly the pulses are broadened rather than being compressed. This is evident in the data shown in Fig. 6.6, where the pulse train from the KCl:Tl laser without [Fig. 6.6(a)] and with [Fig. 6.6(b), (c)] the control cavity are measured using a sampling oscilloscope. From Fig. 6.6(b) it can be seen that the out-of-phase locking of the coupled cavities led to broadened output pulses. This is in a complete contrast to the cases where the in-phase locking is achieved [Fig. 6.6(c)]. In the latter, shorter pulses are generated but because the laser output is no longer synchronized with the pumping pulses they can not be properly sampled by using the triggering signal derived from the pump laser.

Finally, as far as the control of the laser operation is concerned, the amount of optical power coupled into the control cavity has a major influence on the CCM process. A power that is too low will simply not lead to any mode-locking enhancement whereas an excessive power may introduce other undesired nonlinear effects which often give rise to instability. In addition, other system parameters such as the effective lasing bandwidth, pumping power level, central lasing wavelength also have an important impact on the performance of the CCM laser. A range of experimental results together with related discussions on these aspects will be presented in Ch.8.

6.2 Review of the development of CCM lasers

The start of the development of coupled-cavity mode locking can be dated back to the invention of the first soliton laser[3] (Mollenauer and Stolen 1984). Two years later Piche *et al* (1986) performed a mode locking experiment on a CO_2 laser with a nonlinear-Michelson interferometer as the output coupler. (However, at that time no one had realized that there was a close connection between the above two laser systems).

[3] Here the term soliton laser is specified for a NFP-type coupled-cavity KCl:Tl laser with a single-mode optical fibre that supports bright optical solitons in the control cavity. Note that, in a more general sense, a soliton laser may not necessarily have two cavities, such as that for a fibre Raman amplification soliton laser (Islam *et al* 1986). Nevertheless, this single-cavity type of soliton lasers is not discussed in this present context.

Breakthroughs were achieved when the St. Andrews research group led by Professor Sibbett, and the British Telcom research lab (Blow, Nelson) independently observed significant mode-locking enhancement for a NFP-type coupled-cavity KCl:Tl laser incorporating a non-soliton control fibre in 1988 (Sibbett 1988, Kean *et al* 1988, Blow and Nelson 1988). Meanwhile, theoretical analyses by Blow and Wood also showed that coupled-cavity mode locking could be achieved with either a nonlinear amplifier or absorber (Blow and Wood 1988). Such achievements stimulated further studies that immediately led to the recognition that mode-locking with a coupled-cavity arrangement is a very general mode-locking scheme. Because of the differences in highlighting the more distinct features of this new type of mode locking it has been named as *coupled-cavity mode locking* (Miller and Sibbett 1988, Zhu *et al* 1989a), *additive pulse mode locking* (Mark *at al* 1989) and *interferometric mode locking* (Piche *et al* 1989). In this section both experimental achievements and theoretical advances in the study of coupled-cavity mode locking will be summarized.

6.2.1 Experimental achievements

A summary of some of the experimental results regarding coupled-cavity mode locking in various laser types is presented in Table 6.1. Other results which are mainly related to the studies on the further features of this type of mode-locked laser are given in Table 6.2.

It is worth mentioning that mode locking with a linear external cavity has also been reported for a synchronously pumped dye laser (Beaud *et al* 1990) and a cw pumped Ti:Al_2O_3 laser (French *et al* 1990). For the former, the pulse duration was increased from the 450 fs to 660 fs as a result of the involvement of control cavity, but on the other hand the mode locking quality was improved because the broader pulses are close to the bandwidth limit. The results for the mode locking in a Ti:Al_2O_3 laser using a linear cavity could be confusing because it obviously contradicts all the other reports on coupled-cavity mode locking where the nonlinear element in the control cavity is critically important. Nevertheless, if it is noted that a Ti:Al_2O_3 laser can be self-mode locked (Spence *et al* 1991) then the question on the necessity of nonlinearity in the control cavity

may be abolished. It is quite possible that in the experiment of French and colleagues it may be the involvement of the linear external cavity that helps to achieve a suitable power level in the main cavity such that the self-mode locking can be started.

As far as the uses of coupled-cavity mode-locked lasers are concerned, it is noted that a CCM, NaCl:OH^- laser (Yakymyshyn and Pollock 1989) and a CCM, Ti:Al_2O_3 laser (Curley and Ferguson 1991) have been exploited to obtain tunable femtosecond pulses in the near-infrared and blue wavelength region respectively through a process of frequency doubling. Applications of a CCM, KCl:Tl laser in the study of fast dynamics in a semiconductor material (Downey *et al* 1986) dispersive features and nonlinearities in optical fibres (Zhu and Sibbett 1990d, 1991, also see Ch. 10) have also been performed.

Table 6.1 Some of the experimental results for various CCM lasers

1984 *Soliton laser* Mollenauer and Stolen, gain medium: KCl:Tl (synchronously pumped), nonlinear element: - GVD fibre (D = 15 ps/nm/km @ 1.5 μm). Typical results: (a) L_f = 60 cm, Δt = 210 fs; (b) L_f =22 cm, Δt = 130 fs.
1986 *Passive mode-locking with a nonlinear Michelson interferometer* Ouellette and Piche, [nonlinear Michelson type], gain medium: CO_2, nonlinear element: Ge crystal. Typical results: L_n = 4 cm, Δt = 8.5 ~ 3 ns.
1987 *Soliton laser* Mitschke and Mollenauer, gain medium: KCl:Tl (synchronously pumped), nonlinear element: - GVD and dispersion-flatened fibre (D = 2.2 ps/nm/km @ 1.5 μm). Typical results: (a) L_f = 40 cm, Δt = 60 fs.
1988 *CCM lasers* • Kean *et al*, gain medium: KCl:Tl (synchronously pumped), nonlinear element: + GVD fibre/InGaAsP semiconductor diode amplifier. Typical results: for the fibre, L_f = 2 m, Δt =1ps; L_f = 24 cm, Δt = 260 fs. for InGaAsP, L_n = 250 μm, $I_{current}$ =20 mA, Δt = 1.4 ps. • Blow and Nelson, gain medium: KCl:Tl (synchronously pumped), nonlinear element: + GVD fibre (|D| = 10 ps/nm/km @ 1.5 μm). Typical results: L_f = 2.4 m, Δt = 3 ps.

1989 *CCM lasers*

- Yakymyshyn *et al*, gain medium: NaCl:OH^- (synchronously pumped), nonlinear element: + GVD fibre (|D| = 5 ps/nm/km @ 1.51 μm).

  Typical results: L_f = 60 cm, Δt = 75 fs.

- French *et al*, gain medium: Ti:Al_2O_3 (actively mode-locked), nonlinear element: + GVD fibre.

  Typical results: L_f = 63 cm, Δt = 770 fs.

- Barr and Hughes, gain medium: Nd:YAG (long-pulse pumped), nonlinear element: KTP SHG crystal.

  Typical results: L_n = 5 mm, Δt = 30 - 50 ps.

1990 *CCM lasers*

- Spielmann *et al*, gain medium: Nd:glass (cw pumped), nonlinear element: + GVD fibre.

  Typical results: L_f = 90 cm, Δt =380 fs.

- Liu and Chee, gain medium: Nd:YlF (cw pumped), nonlinear element: + GVD fibre.

  Typical results: L_f = 90 cm, Δt =3.7 ps.

- Goodberlet *et al*, gain medium: cw diode-pumped Nd:YlF, Nd:YAG, nonlinear element: + GVD fibre.

  Typical results: for Nd:YAG, L_f = 83 cm, Δt =1.7 ps.

  for Nd:YlF, L_f = 155 cm, Δt =2.0 ps.

- Carruthers and Duling III, (Nonreciprocal antiresonant ring arrangement) gain medium: Nd:YAG (cw pumped), nonlinear element: KTP crystal.

  Typical results: L_n = 5 mm, Δt =11 ps.

- Huxley *et al*, gain medium: Nd:YAG (high power, λ = 1.06, 1.32 μm, cw pumped), nonlinear element: +GVD fibre.

  Typical results: L_f = 30 cm, Δt =9 ps.

1991 *CCM lasers*

- Fermann *et al*, Using a nonlinear amplifying loop mirror*, gain medium: Nd-doped fibre (cw pumped; with acousto-optic modulator for starting), nonlinear element: + GVD fibre.

  Typical results: L_f(passive fibre) = 150 cm, L_f(gain fibre) = 20 cm, Δt =125 fs.

* This laser has an arrangement similar to that shown in Fig. 6.2(c) but the ring structure in this case is composed of a fibre loop and within this loop the gain medium is included. In addition, a fibre-grating compressor is located in the common arm. The authors have named this mode locking as "*Additive-pulse-compression mode locking*".

Table 6.2 Further experimental results of CCM lasers

1987 • Finto *et al*, gain medium: KCl:Tl (actively mode-locked), nonlinear element: - GVD fibre. Typical results: L_f = 1.88 m, Δt = 380 fs.
1989 • Sibbett, Zhu *et al*, gain medium: KCl:Tl (synchronously pumped), nonlinear element: - GVD fibre. Typical results: L_f = 2.8 m, Δt = 4ps ~ 330 fs. Observation of the involvement of modulational instabilty in the control fibre. • Mark *et al*, Liu *et al*, gain medium: KCl:Tl (synchronously pumped), nonlinear element: + GVD fibre (|D| = 2 ps/nm/km @ 1.5 μm). Typical results: L_f = 40 cm, Δt = 127 fs. [Pulse addition model proposed (see next subsection)] • Zhu *et al*, gain medium: KCl:Tl (synchronously pumped), nonlinear element: (+ GVD) Er-doped fibre (|D| ≤ 3.5 ps/nm/km @ 1.51 μm). Typical results: L_f = 21 cm, Δt =75 fs. Observation of the involvement of self-Raman effect in the control fibre. • Goodberlet *et al*, gain medium: Ti:Al_2O_3 (cw pumped)*, nonlinear element: + GVD fibre. Typical results: L_f = 5 ~ 50 cm, Δt = 1.4 ps. * This is the first demonstration of self-starting of coupled-cavity mode locking.
1990 • Zhu *et al*, gain medium: KCl:Tl (synchronously pumped), nonlinear element: Er-doped fibre. Typical results: Intra- and extracavity frequency-chirp compensation both leading to the pulses having durations under 100 fs. • Krausz *et al*, gain medium: Nd:glass (actively pumped), nonlinear element: + GVD fibre. Typical results: L_f = 85 cm, Δt =650 fs. • Zhu *et al*, gain medium: KCl:Tl (synchronously pumped), nonlinear element: Er-doped fibre. Typical results: Pulse-shaping effects caused by cavity length mismatch revealed. • Keller *et al*, gain medium: Ti:Al_2O_3 (cw pumped), nonlinear element: GaAs/GaAlAs quantum well structure. Typical results: L_n ~ 1.0 μm, Δt =2 ps.
1991 • Keller *et al*, gain medium: Nd:YLF (cw pumped), nonlinear element: InGaAs/GaAs quantum well structure. Typical results: L_n ~ 1.0 μm, Δt =4 ps. • Kong *et al*, gain medium: Nd:YLF (cw pumped), nonlinear element: + GVD fibre. Typical results: with an asymmetric cavity (length) arrangement, up to a sixfold increase over the fundamental main cavity repetition rate is achieved. Δt = 4 ~ 11 ps. • Sibbett, Grant *et al*, gain medium: KCl:Tl, NaCl:OH^- (cw pumped), nonlinear element: InGaAsP semiconductor amplifier. Typical results: for KCl:Tl, L_n ~ 250 μm, Δt =280 fs. for NaCl:OH^-, L_n ~ 250 μm, Δt =850 fs.

6.2.2 Theoretical interpretations

The basic principle of the soliton laser proposed by Mollenauer is that, through the formation of optical solitons (or solitonic pulses) in the control cavity, within every cavity

roundtrip period a shorter pulse is reinjected back to the main cavity from the control fibre. This returned pulse which has a larger spectral extension drives the main laser to oscillate with more modes coupled together and so shorter pulses are thereby produced. Associated with this picture, Belanger (1988) has analysed the soliton laser as an injection mode-locking scheme. He has successfully demonstrated that the laser action can be essentially controlled by a small seeding signal from the external nonlinear cavity. Nevertheless, the question that may be raised for this model, as well as the other soliton laser theories, is that temporal pulse compression by the control fibre is regarded as a vital factor in making the coupled-cavity laser system work effectively[4].

The correctness of the soliton laser picture was first challenged by Blow and Wood (1988). Through simulating the dynamic process of a homogeneously broadened laser system coupled to a control cavity where either a nonlinear absorber or a saturable amplifier was incorporated Blow and Wood have shown that mode locking could be improved in both cases. They therefore correctly indicated that the formation of solitons in the external cavity is not essential for coupled-cavity mode locking. Regardless as to whether the pulses returned from the control cavity are broadened or compressed, provided the other operational conditions such as the phase matching, power levels etc. are appropriately satisfied then a mode-locking enhancement can be obtained. The real importance of the nonlinearity in the external cavity is not to temporally compress the incident pulses but to induce mode coupling for the main cavity laser. As having been verified by experiments it is now clear that these two actions do not necessarily mean the same thing.

Based on the idea that when the two coherent pulses are added together the resultant pulse may have a duration shorter than either of the two additive ones, Mark *et al* (1989) have proposed a pulse addition model (which is where the term additive-pulse mode

---

[4] Theoretical investigations on soliton lasers have been unanimously based on the single group of results by Mollenauer and his co-workers. This in some way limits the scope of the associated theories. In particular, many of the analyses or simulations in these studies (e. g. Haus and Islam 1985, If, *et al* 1986, Blow and Wood 1986) have been concentrated on the topic of which order of solitons can be produced and stabilized and which can not. Nowadays it is clear that these are in fact not the critically important aspects for coupled-cavity mode locking.

locking comes from) to explain the mechanism for the mode locking involving the coupled cavities. This model[5] attributes the mode locking enhancement to the interferometric addition between the pulse returned from the control cavity and the pulse circulating in the main cavity rather than the pulse compression in the control cavity. In other words, if the whole control cavity is taken as a termination, because of the interferometric pulse addition effect such a termination will always return a pulse shorter than the one incident upon it as long as an appropriate phase shift between the two additive pulses is maintained, and no matter whether the pulse in the control cavity is temporally compressed or broadened. Therefore, the experimental results for coupled-cavity mode locking achieved with either positive GVD or negative GVD fibres, or any other nonlinear devices can all be explained. Ippen *et al* (1990) have further expanded this model by including the effect of dispersion and the function of gain.

More comprehensive analyses and simulations of the coupled-cavity mode locking process have been performed by Piche and his coworkers (Oullette and Piche 1988, Morin and Piche 1989, Morin *et al* 1990). In their work, instead of merely focusing on pulse addition at one side of the output coupler, more attentions has been given to the interactions of the entire two cavity system, especially, the influence of the main cavity status on the pulse evolution process has been appropriately addressed. This enables them to show that distinct operational regimes exist for particular selections of the parameters in the coupled cavities. Such results, in contrast to the other modelling approaches which are mainly qualitative explanations, are more consistent to the experimental observations.

In addition to the major theoretical studies mentioned above numerical simulations of the influence of an empty external cavity on a mode locked laser has also been carried out by Kelly (1989). As expected, Kelly did not predict any mode-locking enhancement from his calculations for the absence of nonlinearity in the control cavity. Nevertheless, Kelly's modelling illustrated that the impact of the control cavity on the mode-locked main cavity laser is dependent on three main factors. These are the phase matching condition, the

---

5 It actually has the same principle as that used by Ouellette and Piche in the analyses of modelocking a CO_2 laser with a nonlinear-Michelson interferometer,

coupling strength and the upper-laser-level lifetime of the gain medium. Such a statement is in fact also true for the coupled-cavities where a nonlinear medium is incorporated.

It is interesting to note that Bulushev *et al* (1990) has proposed a laser configuration where the entire control cavity is formed by a fibre loop. Their theoretical simulation indicates that self-starting passive mode locking can also be realized for this special coupled-cavity system.

Finally, it should be pointed out that as the growth of experimental achievements regarding to coupled-cavity mode locking in various laser systems with very versatile arrangements takes place more extensive theoretical investigations towards a better understanding of the physical mechanisms are still required. On the whole, it is now clear that coupled-cavity mode locking is a very powerful and reliable means for generating picosecond-femtosecond laser pulses. It has some passive features but unlike the conventional saturable absorbers it does not have the shortcoming of being limited to a limited range of working wavelengths or power levels that are associated with particular absorbers. In a more general sense, the revolutionary aspect of this new type of mode locking lies in that it represents a successful exploitation of nonlinear effect in respect of the control of the phase coupling of longitudinal modes. It can therefore be regarded as a milestone that signifies the entry of mode locking techniques into a truely new era.

Chapter 7

Relevant Features of a KCl:Tl Colour-Centre Laser

To have a proper control and better understanding of the operation of coupled-cavity mode locking, it is important to have some essential knowledge of the basic features of the main cavity laser involved in such a scheme. In this chapter a general description is presented for the KCl:Tl colour-centre laser, which in this case represents the main-cavity laser. A detailed analysis is then given for the characteristics of birefringent filters. These filters play significant roles in the laser operation in terms of pulse train stability, pulse duration and wavelength tunability. The chapter is completed with some experimental results relating to the spectral tuning features of the laser.

7.1 The KCl:Tl colour-centre laser

An analogy between colour centres in crystals and the doped ions in more traditional gain media (e. g. Nd:YAG or Nd:glass) in terms of the details of the atomic energy level structure serves to illustrate that appropriate colour-centre crystals can be implemented as laser-active media. Since the demonstration of the first colour-centre laser operation by Fritz and Menke (1965), there are more than 15 different useful colour centre crystals, most of which are alkali-halides, which provide a total spectral range of 0.8 - 4.0 μm. To date, colour-centre lasers have become important coherent light sources in the near- and mid-infrared spectral regions which are of particular importance in the study of optical fibres and molecular spectroscopy. [Detailed introductions to colour-centre lasers and the associated techniques can be found in the paper by Mollenauer (1987)].

7.1.1 General introduction to colour centres

Colour centres in optical crystals are known to be related to some special types of microscopic defects in the material lattice (Javan 1967). Such defects typically appear as anion vacancies or vacancies in which one or more electrons are trapped. Normally, because of the interaction of the trapped electrons, or the doped atoms with their

surrounding crystal ions, the atomic energy level structure of the associated particles at the centres is deformed and so it selectively absorbs visible light. This gives rise to crystal colouration due to so-called F-centre defects ['F' from fabre, German word for colour]. Colour centres can be deliberately created by two main methods. One is called *additive colouration* which involves bringing a heated crystal into an equilibrium with a bath of metal vapour and the other is the *radiation damage*. (The radiation source can be ultraviolet light, X-rays, γ-rays or electron beams, depending on the particular crystal hosts). According to structural details of the centres, such as the number of vacancies, the number of foreign alkali-metal ions, or the configuration of relaxed states after excitation etc., colour centres are categoried into various classes. For example, a F_2^+ centre means that there are two associated anion vacancies in each centre where one electron is trapped and shared such that the centre has a positive charge[1].

Various F centres (anion vacancies which trapped electrons) such as F_A(II) centres, F_B(II) centres and F_2^+ centres (Gellermann *et al* 1982), still dominate the category of laser-active colour centres. There are also other types of centres like Tl^0(1) (Gellerman *et al* 1981), H_3 (Rand and DeShazer 1985) and N_2 (Pollock *et a*l 1989) centres, which serve as useful laser gain media. Note that for the same two host crystals, if their centre types are different from one another these two colour centre media will produce laser emission at different wavelengths. Another factor that influences the lasing wavelength is the doped element ions. For instance, a sodium-doped KCl colour centre crystal lases from 1.62 - 1.91 μm while for a lithium-doped KCl crystal which has exactly the same centre type with the previous one, a lasing range of 2.00 - 2.50 μm is observed. If the crystal has both Na and Li dopants the lasing wavelength ranges from 1.67 - 2.46 μm (Schneider and Moss 1983).

As gain media, colour-centre crystals have large emission cross-sections ($\sigma \geq 10^{-16}/cm^2$) and are described as homogeneously broadened, four-level systems. Their

[1] As a further example, a F_A(II) centre means that the centre has one foreign alkali-metal ion in the surroundings of the centre and at the ground state only one potential valley exists while at the relaxed excited state (following excitation) it is changed to have two potential valleys.

bandwidths are normally very broad ($\Delta\lambda/\lambda > 10\%$), leading to an excellent frequency-tunability and sources of ultrashort pulses (Mollenauer *et al* 1982, Reekie *et al* 1983). The major disadvantage for colour centre lasers is that in order to prevent the degradation of the centres caused by heating effects the crystals must generally be kept at a low temperature (~77K) during operation, and so a cryogenic vessel has to be used (German 1979; also the operator manuals for the colour-centre lasers manufactured by Burleigh Inc.).

7.1.2 KCl:Tl colour centre lasers

The designation, $Tl^0(1)$ colour centre, denotes a centre which is formed by one neutral Tl atom in the vicinity of one anion vacancy (see Fig. 7.1). The energy level change of these Tl atoms caused by the perturbation of the field of the adjacent anion vacancy makes it possible for the centres to become laser-active (Mollenauer *et al* 1983). In practice, to obtain a KCl:$Tl^0(1)$ colour centre crystal having useful laser performance, the KCl crystal with 0.2 mol% Tl^+ dopants is first produced and is then exposed to an electron beam to create the $Tl^0(1)$ centres (Mollenauer *et al* 1982). The importance of KCl:$Tl^0(1)$ colour centre laser lies not only in that it is one of the most stable colour centre lasers but also that, rather more significantly, its tuning range (1.4 ~ 1.6 μm) peaks near the prepared 1.5 μm optical communication band. Some basic parameters relating to the essential properties of a KCl:Tl colour centre crystal [the simplified notation for the Tl centre is used in the following text so that Tl replaces $Tl^0(1)$] are listed in Table 7.1.

Table 7.1 Basic parameters for a KCl:Tl colour-centre crystal

Absorption band ($\Delta\lambda_a$):	650 cm^{-1}
Absorption peak (λ_{ao}):	1.04 μm
Gain cross-section (σ):	1.3×10^{-17} cm^2
Tuning range ($\Delta\lambda$):	1.4 - 1.6 μm
Peak wavelength (λ_o):	1.51 μm
Upper-laser-level lifetime (τ):	1.6 μs

Under the excitation of a cw mode-locked Nd:YAG laser beam the recorded fluorescence spectrum for the KCl:Tl crystal is shown in Fig. 7.2, where an approximate

absorption band [after the data given by Gellermann *et al* (1982)] is also included. The set-up for the KCl:Tl colour-centre laser which was used throughout the work reported in this thesis is illustrated in Fig. 7.3. The laser is essentially a modified Burleigh F-centre laser (FCL) system. The cryogenic crystal chamber has a vacuum of ~10^{-6} Torr and a copper cold finger in contact with the crystal at one end is cooled by liquid N_2 contained in a Dewar located above the chamber. The original tuning arm is replaced by an extended zig-zag cavity on the optical table where such an arrangement facilitates the alignment. Mirror M2 has a curvature of 1 m so that the agstimatic structure of the cavity can be remained (Kean 1989), The output coupler is flat and has a transmission ~20%.

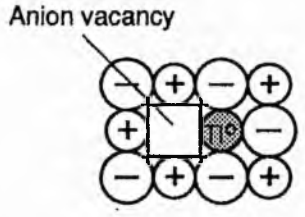

Fig. 7.1. $Tl^0(1)$ colour centre.

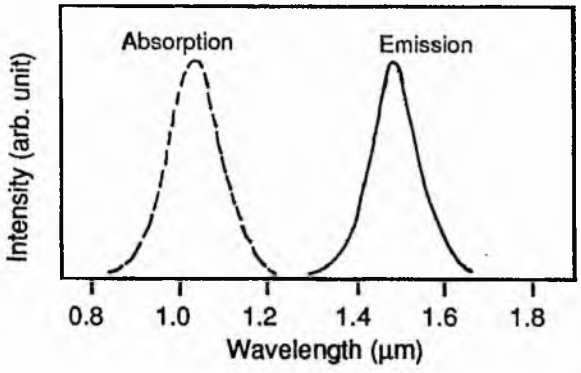

Fig. 7.2. Fluoresence spectrum of a KCl:Tl colour-centre crystal. (The dashed line shows the associated absorption band).

Under the synchronous mode-locking scheme, the typical slope efficiency and tuning features of the laser (with 1-mm-thick birefringent filter) are shown in Fig. 7.4a, 7.4b repectively. It should be pointed out that throughout the operation of the laser, the average pump power from a cw mode-locked Nd:YAG laser is maintained at a level not larger than 2W. This is mainly for the convenience of the practical operating and monitoring conditions of the laser, as well as the objective of extending the actual lifetime of the colour-centre crystal as a gain medium. It is possible, however, to operate the laser under a chopped-pumping scheme so that a higher pump power level (say 6 W) can be

achieved. This can lead to a slope efficiency as high as ~20% and a tuning range covering 1.4-1.6 μm (Mollenauer 1982). All of these features are naturally dependent upon the quality of the laser crystal purchased.

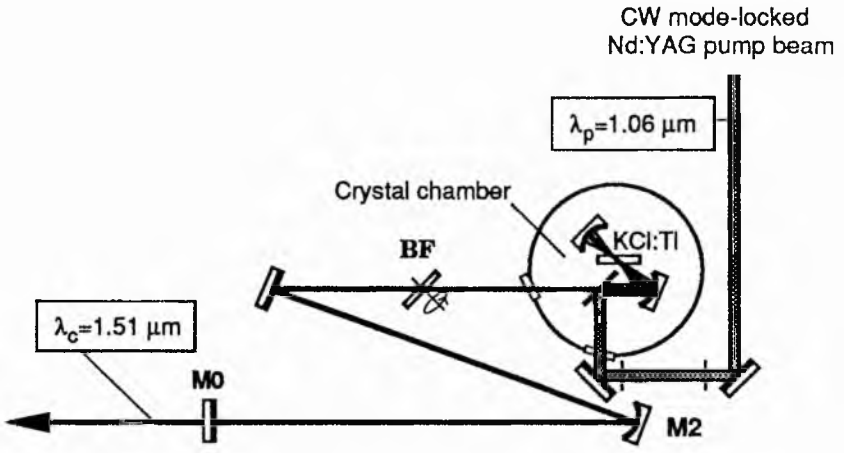

Fig. 7.3. Experimental arrangement for the KCl:Tl colour-centre laser used in our work.

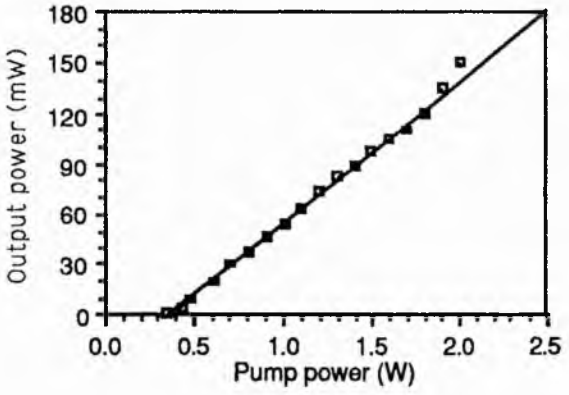

Fig. 7.4a. Output power of the synchronously mode-locked KCl:Tl colour-centre laser as a function of pump power.

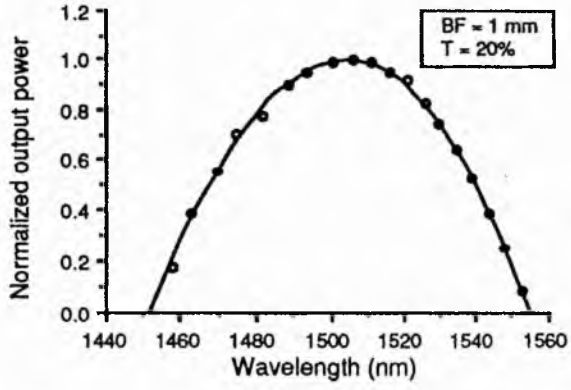

Fig. 7.4b. Typical wavelength tuning curve for the KCl:Tl colour-centre laser.

It is worth mentioning that because the upper laser level of the KCl:Tl crystal has a fairly long lifetime, the pulse evolution kinetics in the synchronously mode-locked KCl:Tl laser are expected to be distinctively different from those in dye lasers under a similar pumping scheme. For most of the laser dyes the upper laser level lifetime is only a few nanoseconds (usually less than the associated cavity-roundtrip period) and so the formation of the dye laser pulse after the first pulsed pumping action is almost instant. In contrast, for a KCl:Tl laser, after the excitation of the initial pumping pulses the gain lasts for a much longer time (~1 μs), which means that the laser will operate in a quasicontinuous manner and no short-bursts of radiation are formed immediately inside the cavity. It is the gain modulation formed by the consecutive synchronous pumping cycles that is responsible for constraining the KCl:Tl laser to progressively produce shorter pulses. It thus takes a relatively long time for the synchronously pumped KCl:Tl laser to establish the steady-state mode-locked condition.

In a more general sense, it is useful to appreciate that the gain saturation in gain media having long lasing-relaxation-times, (e. g. KCl:Tl crystal), is mainly an energy effect rather than intensity, and so an energy accumulation process is necessary to induce gain saturation. For the same reason, stronger pumping of the KCl:Tl crystal, which leads to a more rapid increase of the energy of each pulse, will enhance the energy saturation and accelerate the progress of mode-locking process and ultimately leads to the production of shorter pulses (Mollenauer 1982).

By using an fast electro-optical switch (Pockels cell) to quickly switch on the pumping pulses and at the same time monitoring the rise time of the second harmonic signal generated by the laser output (see Ch. 10) the time scale of the pulse evolution process in the synchronously pumped KCl:Tl laser can be conveniently determined. An example of the rate of rise of the SH signal recorded after the pumping to the KCl:Tl laser is switched on is reproduced in Fig. 7.5. From this trace, where some slight over shooting effect is evident, it can be deduced that the kinetic process for establishing the steady-state mode-locked pulses takes about 20 μs to fulfil, which corresponds to approximately 1600 cavity roundtrips.

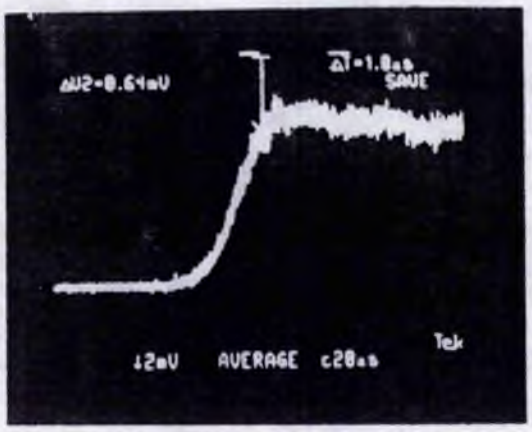

Fig. 7.5. Rise time features of the second harmonic signal generated by the KCl:Tl laser output recorded after the pumping to the laser has been suddenly switched on.

Typical autocorrelation traces for the output pulses from the synchronously pumped KCl:Tl laser can be found in Figs. 9.19, 9.20 in Ch. 9. Generally speaking, these results are very much affected by the alignment of the laser system. In particular, the amount of cavity-length mismatch and the thickness of the intracavity birefringent filter are especially critical for the mode-locked laser. A group of autocorrelation traces under the conditions of varying amounts of cavity-length mismatches are reproduced in Figs. 7.6(a)-(d). The zero mismatch position is determined through observing the maximum value of the autocorrelation intensity. The exponential-like profile of the autocorrelation trace measured at this position [Fig. 7.6(a)] is most likely due to the fluctuation of pulse durations (see Footnote 5 in Ch.4). The trace associated with the negative mismatch [the laser cavity is shorter than that of pump laser; Fig. 7.6(c)] has a smooth and discrete shape, but has a tendency to collapes during laser operation, and this therefore represents an unstable operational regime. For slight positive mismatch [Fig. 7.6(b)], the autocorrelation trace has the typical feature relating to noise bursts, which indicates an incomplete mode-locking process although the overall laser output is relatively stable. For more positive mismatch [Fig. 7.6(d)], the pulse quality further degrades and becomes more like a white noise burst (see Section 4.3 in Ch. 4), implying that few of lasing modes are actually phase-locked.

In the course of this work the observations indicated that the cavity-length mismatch effects implied that a relatively larger tolerance existed for the positive mismatch than

that for the negative mismatch[2]. Spectral measurements also showed that at slight, positive mismatch, the laser spectrum is broader than that recorded at matched position. This is consistent with the data from the temporal measurements. [The narrow spike on the autocorrelation trace shown in Fig. 7.6(b) for the pulses produced at a positive mismatch is a clear indication of the existence of a relatively large bandwidth, which does not occur for the trace relating the matched cavities shown in Fig. 7.6(a)].

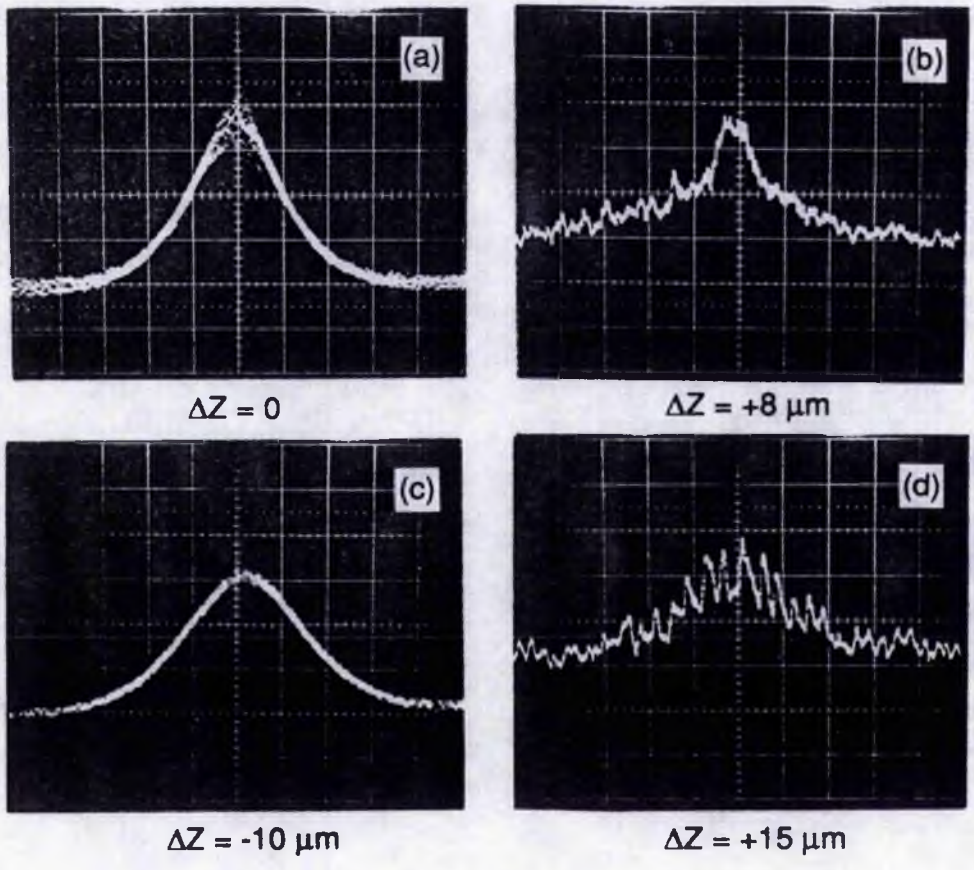

Fig. 7.6. Intensity autocorrelation traces for the pulses from the synchronously mode-locked KCl:Tl laser where the cavity-length mismatch conditions are as indicated. (7ps/div.; with 1mm-thick birefringent plate].

---

[2] Such a phenomenon, which is also evident in many synchronously pumped dye lasers (Ausschnitt *et al* 1979), is a common feature for various types of synchronously mode-locked lasers. This is because in negative mismatch condition the circulating pulse returns to the gain medium before the subsequent pump pulse is present and so it will experience substantially less or no gain. For positive mismatch, the laser pulse reaches the gain medium later than the pump pulse but the finite upper laser level lifetime of the gain medium can enable the gain to be sustained so that despite the belated arrival of the laser pulse it can still see a proper amount of gain. Because of this, the positive mismatch is better tolerated by gain media, like the KCl:Tl colour centre crystals, which have relatively long upper laser state lifetimes.

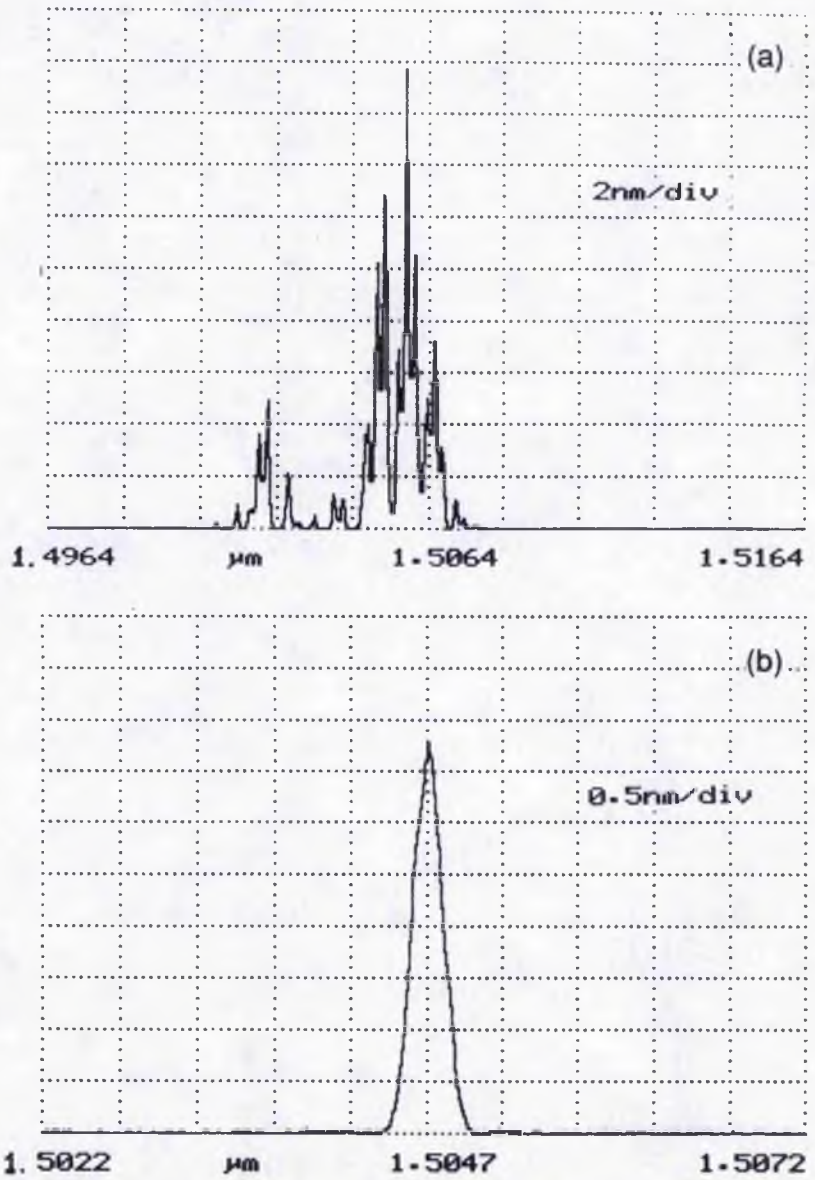

Fig. 7.7. Spectra for the synchronously mode-locked KCl:Tl laser: (a) without birefringent filters (b) with a 1 mm thick birefringent filter. (These results were obtained using an optical spectral analyser having a resolution of 0.1 nm).

Whenever the cavity length is properly selected, the quality of the output pulses will be almost solely determined by the characteristics of the birefringent tuning filters. For thin filters, or in the absence of a filter, there is a greater access to oscillating unlocked modes in the laser spectrum and hence the pulses have larger duration and exhibit poor coherence quality [see Fig. 3.5(b)]. The striking difference in the structure of the laser output spectra with and without the bandwidth restriction by birefringent filters can be examined by using a high resolution optical spectral analyser. With such an instrument,

the measured spectra are as shown in Fig. 7.7. It can be readily seen that without birefringent filters the laser spectrum [Fig. 7.7(a)] has a broader bandwidth and considerable substructure within the profile whereas the spectrum obtained with a 1-mm-thick intracavity birefringent filter has a single discrete character with a narrow bandwidth.

7.2 Characteristics of birefringent filters

Birefringent plates (BP) as phase retardation devices have been widely used inside or outside laser cavities to change the polarization status of the laser beams (Yariv and Yen 1982). In 1973, Yarborough first suggested that a tilted BP inserted in a laser cavity could be used as a tuning device to select the lasing wavelength. This is the so-called birefringent filter (BRF). Simplicity of control, low insertion loss and ability to handle high intensities are the main advantages of this type of optical filter.

Theoretical analyses of the eigenvalue of a resonator with a birefringent filter have been presented by Bloom (1974) using the Jones matrix, and by Holtom and Teschke (1974) with an approach of Stokes four-by-four matrices. Further discussion on suppressing the secondary peaks was reported by Hodgkinson and Vukusic (1978). An explicit Jones transformation matrix for a tilted BP, the optic axis of which was in the plate surface, was first derived by Preuss and Gole (1980). The tolerances on the filter plate thickness and the effect of the manufacturing inaccuracies on the properties of a BRF were analysed by Kachanov (1982). A more general derivation and analysis of computational formula for the transmissivity coefficient of an arbitrary birefringent selector was given by Bonarev and Kobtsev (1986).

For the work mentioned above the context was mainly considered for tunable single frequency CW lasers, where several birefringent plates are generally combined to form a birefringent filter. The thinnest plate is used to determine the tuning range whereas the thickest determines the limiting bandwidth. (In many cases, Fabry-Perot etalons are used to further narrow the bandwidth). The selection of the optimum ratio of the plate thicknesses to achieve spectra that are characterised by a narrow linewidth with all the

secondary peaks effectively suppressed and a large, smooth tuning range is a primary consideration for single mode laser systems[3].

Another important use of the BRF is the limitation of the excess bandwidth of mode-locked lasers (Mollenauer 1985). In these circumstances, because of the inverse relation between bandwidth and pulse duration, narrow bandwidths are not desired. In general, therefore, one birefringent plate (at most two) with a properly chosen thickness will be enough to provide the required bandwidth and tuning parameters. In the following section, a comprehensive analysis of the characteristics of a BRF that is compatible with mode-locked lasers is given. Some detailed derivations and relevant basic knowledge of the Jones matrix are included as Appendix C.

7.2.1 Jones transformation matrix for a tilted birefringent plate

In many applications in order to avoid the surface reflection the birefringent plate(s) is (are) tilted at an angle θ with respect to the incident light beam (as shown in Fig. 7.8a). In this case the Jones transformation matrix given by Eq. (C.6) in Appendix C has to be modified because it is valid only for $\theta = \frac{\pi}{2}$. Assuming that the birefringent splitting of the emerging light rays is small such that it can be ignored, Preuss and Gole (1980) derived that,

$$M_b = (n_o^2 - \cos^2\phi\cos^2\theta)^{-1}$$

$$\begin{bmatrix} (n_o^2 - \cos^2\theta)\cos^2\phi e^{i\delta_e} + n_o^2\sin^2\phi e^{i\delta_o} & n_o(n_o^2 - \cos^2\theta)^{1/2}\sin\phi\cos\phi(e^{i\delta_e} - e^{i\delta_o}) \\ n_o(n_o^2 - \cos^2\theta)^{1/2}\sin\phi\cos\phi(e^{i\delta_e} - e^{i\delta_o}) & n_o^2\sin^2\phi e^{i\delta_e} + (n_o^2 - \cos^2\theta)\cos^2\phi e^{i\delta_o} \end{bmatrix} \tag{7.1}$$

where,

$$\delta_e(\theta, \phi) = \frac{2\pi}{\lambda} n_e L \left[\frac{1 + \frac{\cos^2\theta\cos^2\phi}{n_e^2} - \frac{\cos^2\theta\cos^2\phi}{n_o^2}}{\sqrt{1 - \frac{\cos^2\theta\sin^2\phi}{n_e^2} - \frac{\cos^2\theta\cos^2\phi}{n_o^2}}} \right] \tag{7.2}$$

---

[3] Suggestions on the alignment of a BRF assembly which normally consists of three birefringent plates have been given in several articles (Preuss and Gole 1980, Mudare and O'Shea 1983, Dunn 1982). By comparing a large number of different numerical results, Bonarev and Kobtsev (1986) found that the optimum ratios of plate thicknesses were 1:3:11 or 1:4:13 rather than the commonly used 1:4:16 and 1:2:15 ratios.

$$\delta_o(\theta, \phi) = \frac{2\pi}{\lambda} n_o \ell \left[1 - \frac{\cos^2\theta}{n_o^2} \right]^{-1/2} \tag{7.3}$$

ℓ is the thickness of the birefringent plate. Eq. (7.1) is the commonly used Jones matrix for a tilted BP (Preuss and Gole 1980) and obviously, for $\theta = \pi/2$, it reduces to Eq. (C.6).

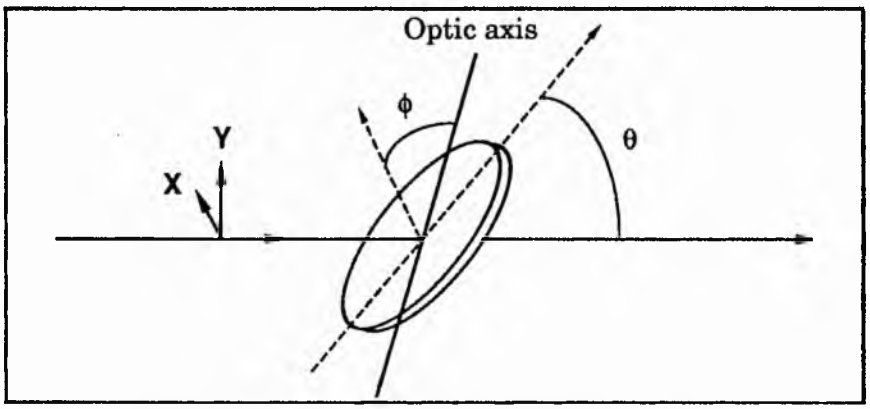

Fig. 7.8a. A tilted birefringent plate with tilting angle θ.

However, as shown later, the optical path difference between the ordinary and extraordinary beams contributed by birefringent splitting is in fact comparable to that arising from the refractive index difference in the two polarizations. For this reason, the approximation which is made for obtaining Eq. (7.1) is not valid[4]. A more accurate formulation must be established where

$$M_b = \left(1 - \frac{\cos^2\phi\cos^2\theta}{q n_e^2} \right)^{-1}$$

$$\begin{bmatrix} \left[1 - \frac{\cos^2\theta}{q n_e^2} \right] \cos^2\phi\, e^{i\delta_e} + \sin^2\phi\, e^{i\delta_o} & \sqrt{1 - \frac{\cos^2\theta}{q n_e^2}}\, \sin\phi\cos\phi (e^{i\delta_e} - e^{i\delta_o}) \\ \sqrt{1 - \frac{\cos^2\theta}{q n_e^2}}\, \sin\phi\cos\phi (e^{i\delta_e} - e^{i\delta_o}) & \sin^2\phi\, e^{i\delta_e} + \left[1 - \frac{\cos^2\theta}{q n_e^2} \right] \cos^2\phi\, e^{i\delta_o} \end{bmatrix} \tag{7.4a}$$

Here,

$$q = 1 - \left[\frac{1}{n_o^2} - \frac{1}{n_e^2} \right] \cos^2\theta \cos^2\phi \tag{7.4b}$$

---

[4] For the purposes of qualititive analyses Eq. (7.1) could still be useful, but for the selection of a specific filter an accurate formula must be used to determine the relevant practical parameters.

$$\delta_e = \frac{2\pi}{\lambda}\left[n_e\sqrt{1 - \frac{\cos^2\theta\sin^2\phi}{n_e^2} - \frac{\cos^2\theta\cos^2\phi}{n_o^2}} - n_o\sqrt{1 - \frac{\cos^2\theta}{n_o^2}} - \frac{n_o}{\sqrt{1 - \frac{\cos^2\theta}{n_o^2}}}\right]\ell \qquad (7.5)$$

$$\delta_o = \frac{2\pi}{\lambda}\frac{n_o\ell}{\sqrt{1 - \frac{\cos^2\theta}{n_o^2}}} \qquad (7.6)$$

[Derivation of the above formulae is included in Appendix C].

7.2.2 Transmissivity of a BP located between polarizers

For a general polarization system several polarization devices may be included. In these cases a overall transformation matrix can be introduced, which is simply a product of individual matrices in a certain sequence. That is

$$M = M_n M_{n-1}\cdots M_1 \qquad (7.7)$$

where M_n is the matrix for the n_{th} device encountered by the incident beam. It can be readily shown that the system matrix M retains the form given by Eq. (C.2), i. e.

$$M = \begin{bmatrix} m_{11} & m_{12} \\ m_{21} & m_{22} \end{bmatrix}$$

and thus the transmissivity of the system is given by

$$T \equiv \frac{|E_{xo}|^2 + |E_{yo}|^2}{|E_{xi}|^2 + |E_{yi}|^2}$$

$$= \frac{(|m_{11}|^2 + |m_{21}|^2)|E_{xi}|^2 + (|m_{12}|^2 + |m_{22}|^2)|E_{yi}|^2 + Y}{|E_{xi}|^2 + |E_{yi}|^2} \qquad (7.8)$$

where $Y = 2\mathrm{Re}[(m_{11}m_{12}^* + m_{21}m_{22}^*)E_{xi}E_{yi}^*]$.

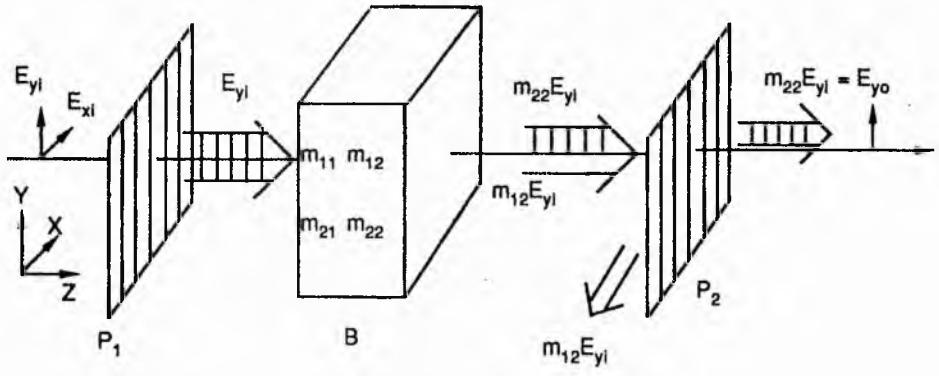

Fig. 7.8b. A birefringent plate located between two parallel polarizers.

Now consider a tilted birefringent plate placed between two parallel polarizers (see Fig. 7.8b). Provided that the incident wave is linearly polarized ($E_{xi} = 0$) and in the same direction with that of the two polarizers, the total transmissivity for the system will be[5]

$$T = |m_{22}|^2 \tag{7.9}$$

where m_{22} is the matrix element for the BP. From Eq. (7.4a), we obtain

$$m_{22} = \left[1 - \frac{\cos^2\phi\cos^2\theta}{qn_e^2}\right]^{-1}\left\{\sin^2\phi\, e^{i\delta_e} + \left[1 - \frac{\cos^2\theta}{qn_e^2}\right]\cos^2\phi\, e^{i\delta_o}\right\} \tag{7.10}$$

Substituting Eq. (7.10) into Eq. (7.9) leads to

$$T = 1 - A\sin^2\frac{\delta}{2} \tag{7.11}$$

where A is a middle variable, given by

$$A = A(\theta, \phi, n_e, n_o) = \frac{q^2n_e^4 - qn_e^2\cos^2\theta}{(qn_e^2 - \cos^2\phi\cos^2\theta)^2}\sin^2 2\phi \tag{7.12}$$

$\delta = \delta_e - \delta_o$, is the difference of phase shift for the two polarizations. From Eqs. (7.2) and (7.3), it can be deduced that

$$\delta = \frac{2\pi}{\lambda}\left[n_e \frac{1 + \dfrac{\cos^2\theta\cos^2\phi}{n_e^2} - \dfrac{\cos^2\theta\cos^2\phi}{n_o^2}}{\sqrt{1 - \dfrac{\cos^2\theta\sin^2\phi}{n_e^2} - \dfrac{\cos^2\theta\cos^2\phi}{n_o^2}}} - n_o\frac{1}{\sqrt{1 - \dfrac{\cos^2\theta}{n_o^2}}}\right]t \tag{7.13a}$$

If the effect caused by the birefringent splitting is not ignored, δ should be derived from Eqs. (7.5) and (7.6), that is,

$$\delta = \frac{2\pi}{\lambda}\left[n_e\sqrt{1 - \frac{\cos^2\theta\sin^2\phi}{n_e^2} - \frac{\cos^2\theta\cos^2\phi}{n_o^2}} - n_o\sqrt{1 - \frac{\cos^2\theta}{n_o^2}}\right]t \tag{7.13b}$$

It can be seen from Eq. (7.11) that $T_{max} = 1$ and $T_{min} = 1 - A$. A represents the transmissivity contrast and may be defined as the *extinction coefficient* of the system. Note that A is a function of the adjustable variable ϕ. When ϕ is changed by rotating the BP, A is also changed. The relation between A and ϕ based on Eq. (7.12) is shown in Fig.

[5] If $E_{xi} \neq 0$, $T = |m_{22}|^2 |E_{yi}|^2/[|E_{xi}|^2 + |E_{yi}|^2]$. For $E_{xi} = E_{yi}$, $T = |m_{22}|^2/2$.

7.9. An optimum rotation angle of ϕ can be introduced, at which A has a maximum value. From Fig. 7.9, it can be found that $\phi_{opt} = 40^o$. (This corresponds to the value of ϕ deduced from Eq. (7.12) where $A = 1$)[6].

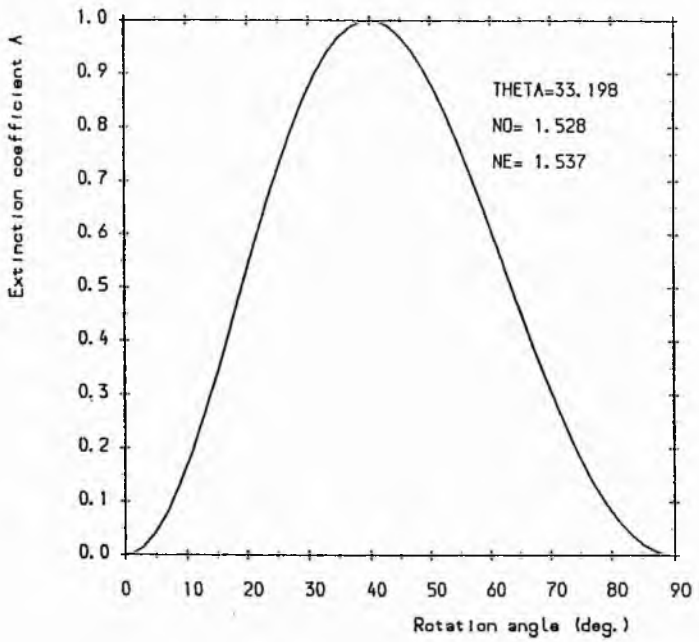

Fig. 7.9. Extinction coefficient defined from Eqs. (7.11) and (7.12) for a system of a birefingent filter lacated between polarizersl.

δ is a function of wavelength and so a curve of T versus λ can be drawn on the basis of Eq. (7.11) for a given rotation angle ϕ (see Fig. 7.10). The associated FWHM bandwidth for the transmissivity peak can be shown to be

$$\delta\lambda = \delta\lambda(n_e, n_o, \theta, \phi, \lambda, \ell) = \frac{2}{\pi}\frac{\lambda^2}{\ell\Delta}\sin^{-1}\left[\sqrt{\frac{1}{2A}}\right] \qquad (7.14a)$$

where, $\Delta = (\lambda/2\pi\ell)\delta$ is the effective refractive index difference between the extraordinary and the ordinary waves. Δ is given by

$$\Delta = \left[n_e\sqrt{1 - \frac{\cos^2\theta\sin^2\phi}{n_e^2} - \frac{\cos^2\theta\cos^2\phi}{n_o^2}} - n_o\sqrt{1 - \frac{\cos^2\theta}{n_o^2}}\right] \qquad (7.14b)$$

The free-spectral range (FSR) $\Delta\lambda$ is

---

6 Although high transmissivity is always required for a filter used in cw single frequency lasers, this may not be the case in mode-locked lasers because high extinction or good contrast of transmissivity often implies a narrower bandwidth [see Eq. (7.14a)].

$$\Delta\lambda = \frac{\lambda^2}{\ell\Delta} \tag{7.15}$$

Note that $\Delta\lambda$ is also a function of n_o, n_e, θ, ϕ, λ, and ℓ.

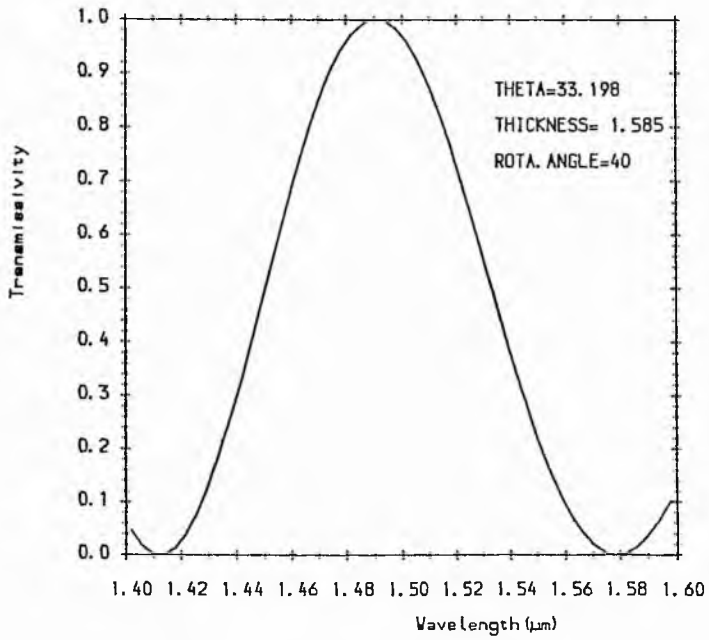

Fig. 7.10. Transmissivity as a function of wavelength.

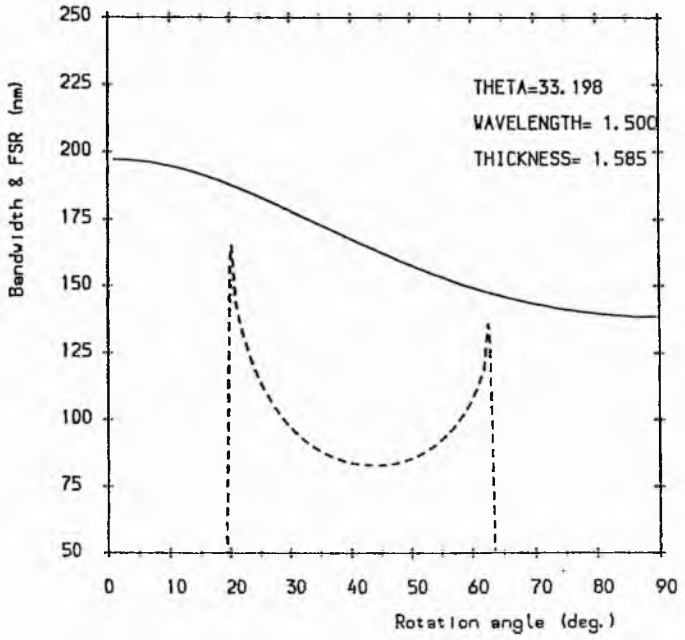

Fig.7.11. Variation of bandwidth (dashed line) and FSR (solid line) as a function of rotation angle ϕ.

Eq. (7.14a) only applies under the condition of $1/(2A) < 1$, (i. e. $A > 1/2$), otherwise $\delta\lambda > \Delta\lambda$ exists and the definition of $\delta\lambda$ will be no longer meaningful. The curves of $\delta\lambda$ and $\Delta\lambda$ versus the rotation angle ϕ are shown in Fig. 7.11. As expected, at the angle at which the extinction coefficient A reaches the maximum the bandwidth approaches the minimum. Using Eq. (7.14a), a simplified formula for evaluating the bandwidth of a BP with a given thickness can be obtained, as outlined in Example I.

Example I. An approximate formula for calculating the bandwidth of a BP

Suppose: $\lambda = 1.5\ \mu m$, $A \approx 1$, $\theta = \frac{\pi}{2} - \theta_b = 33.198^o$, $\phi = 40^o$, $n_o = 1.5283$, $n_e = 1.5369$ (for sapphire)

Substituting these values into the expression of the refractive index difference results in

$$\Delta = 8.518 \times 10^{-3}$$

With this value of Δ, Eq. (7.14a) reduces to

$$\delta\lambda \approx \frac{130}{\ell}\ (nm) \qquad (7.16)$$

where ℓ has the unit of mm. Eq. (7.16) has been utilized in the selection of the thickness of a BP used for filtering the spectral components for the pulses feedback from the control fibre in our coupled cavity mode-locked KCl:Tl laser (see Sec. 8.1)

For a BP located between two partial polarizers, it can be derived that (see Appen. C)

$$T = 1 - A' \sin^2\frac{\delta}{2} \qquad (7.17)$$

where the extinction coefficient A' satisfies

$$A' = (1 - t_s^2)A \qquad (7.18)$$

Obviously, $A' < A$, which means, compared with perfect polarizers, with partial polarizers the contrast of the transmissivity of the system is reduced, i.e. a high background $T_{min} = (1-A) + At_s^2$ exists in the curve of T versus δ. Similar to Eq. (7.14a), the transmission bandwidth of the system is given by

$$\delta\lambda = \frac{2}{\pi}\frac{\lambda^2}{\ell\Delta}\sin^{-1}\left[\sqrt{\frac{1}{2A'}}\right] \qquad (7.19)$$

In this case, it can be seen that the bandwidth is larger than that given by Eq. (7.14a) owing to $A' < A$. Eq. (7.19) implies that the filtering feature of a BP is strongly dependent

upon the polarization status of the beams involved. Poor polarization thus leads to a compromised performance.

7.2.3 Selection of the thickness of a BP

Suppose the phase difference $\delta = \delta_e - \delta_o = 2m\pi$ (m is an integer), it can be shown that the matrix given by Eq. (7.4a) will reduce into a unit matrix multiplied by a complex constant

$$M_b = e^{i\delta_e}\begin{bmatrix} 1 & 0 \\ 0 & 1 \end{bmatrix} \tag{7.20}$$

This implies that under these particular conditions the birefringent medium would have no influence on the incident beam (no losses introduced and also no energy transfer between the two polarizations). Therefore $\delta = 2m\pi$ represents the *transparent condition* of a BP. Since δ is a function of both wavelength and thickness, then for a selected wavelength appropriate thicknesses of the BP can be found to enable $\delta = 2m\pi$ to hold. This is the principle of selecting the correct thickness of a BP in the cases where the other parameters such as the incident angle θ and the rotation angle ϕ are fixed. Substituting $\delta = 2m\pi$ into Eq. (7.13b) gives the expression for the plate thicknesses:

$$L_m = \frac{m\lambda}{n_e\sqrt{1 - \frac{\cos^2\theta\sin^2\phi}{n_e^2} - \frac{\cos^2\theta\cos^2\phi}{n_o^2}} - n_o\sqrt{1 - \frac{\cos^2\theta}{n_o^2}}} \tag{7.21}$$

Similarly, if the effect of birefringent splitting is neglected then from Eq. (7.13a)

$$L'_m = \frac{m\lambda}{n_e\dfrac{1 + \dfrac{\cos^2\theta\cos^2\phi}{n_e^2} - \dfrac{\cos^2\theta\cos^2\phi}{n_o^2}}{\sqrt{1 - \dfrac{\cos^2\theta\sin^2\phi}{n_e^2} - \dfrac{\cos^2\theta\cos^2\phi}{n_o^2}}} - n_o\dfrac{1}{\sqrt{1 - \dfrac{\cos^2\theta}{n_o^2}}}} \tag{7.22}$$

If the beam double-passes a BP, as in a standing-wave cavity for one roundtrip of propagation, the transparent condition will be $\delta = m\pi$ instead of $\delta = 2m\pi$. Therefore, from Eqs. (7.21) and (7.22) this gives

$$L_{ms} = \frac{L_m}{2} \tag{7.23}$$

$$L'_{ms} = \frac{L'_m}{2} \tag{7.24}$$

Example II. Selection of the thickness of a BP

Suppose: $\lambda = 1.50\,\mu m$, $\theta = \frac{\pi}{2} - \theta_b = 33.198^\circ$, $\phi = 41^\circ$, $n_o = 1.5283$, $n_e = 1.5369$,

Substituting these values into Eqs. (7.26) – (7.29) respectively gives thickness values:

$$\ell_m = m\lambda/(8.5181 \times 10^{-3}) = 0.1761m \text{ (mm)} \quad (7.25)$$

$$\ell_m = m\lambda/(4.8953 \times 10^{-3}) = 0.3064m \text{ (mm)} \quad (7.26)$$

$$\ell_{ms} = m\lambda/(2 \times 8.5181 \times 10^{-3}) = 0.0881m \text{ (mm)} \quad (7.27)$$

$$\ell_{ms} = m\lambda/(2 \times 4.8953 \times 10^{-3}) = 0.1532m \text{ (mm)} \quad (7.28)$$

The results calculated from Eqs. (7.25) to (7.28) with different values of m are listed in Table 7.1. A large difference can be found between the values obtained from the approximate Eqs. (7.26), (7.28) and those from the accurate Eqs. (7.25), (7.27). The results included in Table 7.2 are taken from the accurate Eqs. (7.25) and (7.27), but for different central wavelengths. (sapphire plate assumed).

7.2.4 Tuning characteristics of a birefringent plate

When a birefringent plate is used for the purpose of wavelength tuning, it is normally tilted at the Brewster angle (i.e. $\theta = \frac{\pi}{2} - \theta_b = \frac{\pi}{2} - \tan^{-1} n_o$), and can be rotated around the direction normal to its surface. From Eq. (7.21) it can be seen that once the thickness of the BP has been chosen, the only controllable variable is the rotation angle ϕ. At a certain maximum transformation order a change in ϕ will result in a corresponding change in λ in order to make the equality of Eq. (7.21) hold. In this situation, Eq. (7.21) can be rewritten as

$$\lambda_m(\phi) = \frac{\ell_o}{m} \Delta(\phi) \quad (7.29)$$

ℓ_o is the chosen thickness of the BP, m is the the order for the maximum transformation and $\Delta(\phi)$ is given by Eq. (7.14b)[7]. Eq. (7.29) governs the wavelength tuning characteristics and from this equation various tuning curves can be obtained for different integral values of m (see Fig. 7.12). From Eq. (7.29), it is also obvious that the larger the

[7] From Eqs. (7.29) and (7.14b), the reason for tilting a BP at an angle θ can be readily established. On letting $\theta = \pi/2$, we have $\lambda = (\ell/m)(n_e - n_o)$. This is the formula corresponding to an ordinary phase retarder, where no controllable variables exist for tuning the wavelength. Thus, a birefringent filter is actually based on a similar basic principle to a Pockels cell (Junghans *et al* 1974) or a Solc filter (Yariv and Yen 1982). the only difference being that for the Pockels cell and the Solc filter the controllable physical parameter is the voltage applied to the device, i. e. $\Delta = \Delta(v)$, rather than of $\Delta = \Delta(\phi)$ given in Eq. (7.14b). Because of this similarity, some of discussions on the characteristics of the Pockels cell or Solc filters, such as transmission bandwidth, the effect of non-perfect polarizers can also apply.

Table 7.1 Optimum thickness for a birefringent plate

($\lambda = 1.50\ \mu m$ $\theta = 33.198^\circ$ $\phi = 41^\circ$ $n_o = 1.5283$ $n_e = 1.5369$)

Max.Trans	L_m (accurate formulae) (mm)		L'_m (approx. formulae) (mm)	
order m	ring cavity	standing-wave cavity	ring cavity	standing-wave cavity
1	0.1761	0.0881	0.3064	0.1532
2	0.3522	0.1761	0.6128	0.3064
3	0.5283	0.2642	0.9192	0.4596
4	0.7044	0.3522	1.2256	0.6128
5	0.8805	0.4403	1.5320	0.7660
6	1.0566	0.5283	0.8384	0.9192
7	1.2327	0.6163	2.1448	1.0724
8	1.4088	0.7044	2.4512	1.2256
9	1.5849	0.7925	2.7576	1.3788
10	1.7610	0.8805	3.0640	1.5320
11	1.9371	0.9686	3.3704	1.6852
12	2.1132	1.0566	3.6768	1.8384
13	2.2893	1.1447	3.9832	1.9916
14	2.4654	1.2327	4.2896	2.1448
15	2.6415	1.3208	4.5960	2.2980
16	2.8167	1.4088	4.9024	2.4512
17	2.9937	1.4969	5.2088	2.6044
18	3.1698	1.5849	5.5152	2.7576
19	3.3459	1.6730	5.8216	2.9108
20	3.5220	1.7610	6.1280	3.0640

Table 7.2 Optimum thickness for a birefringent plate (mm)

($\phi = 41^\circ$ for different central wavelengths)

Max. Trans	$\lambda = 1.5$ (mm)[a]		$\lambda = 0.91$ (mm)[b]		$\lambda = 0.5$ (mm)[c]	
order m	r	s	r	s	r	s
1	0.1761	0.0881	0.1044	0.0522	0.0605	0.0303
2	0.3522	0.1761	0.2088	0.1044	0.1211	0.0605
3	0.5282	0.2641	0.3132	0.1566	0.3132	0.1566
4	0.7044	0.3522	0.4176	0.2088	0.2423	0.1211
5	0.8805	0.4402	0.5220	0.2610	0.3028	0.1514
6	1.0565	0.5283	0.6264	0.3132	0.3633	0.1817
7	1.2326	0.6163	0.7308	0.3654	0.4239	0.2120
8	1.4088	0.7044	0.8353	0.4176	0.4845	0.2423
9	1.5849	0.7924	0.9397	0.4698	0.5450	0.2725
10	1.7610	0.8805	1.0441	0.5220	0.6056	0.3028
11	1.9370	0.9685	1.1485	0.5742	0.6662	0.3331
12	2.1131	1.0566	1.2529	0.2065	0.7268	0.3634
13	2.2892	1.1446	1.3573	0.6787	0.7873	0.3936
14	2.4653	1.2326	1.4617	0.7308	0.8479	0.4239
15	2.6414	1.3207	1.5662	0.7831	0.9084	0.4542
16	2.8175	1.4087	1.6706	0.5383	0.9690	0.4845
17	2.9936	1.4968	1.7750	0.8875	1.0296	0.5148
18	3.1697	1.5848	1.8794	0.9397	1.0901	0.5450
19	3.3458	1.6729	1.9838	0.9919	1.1507	0.5753
20	3.5219	1.7609	2.0882	1.0441	1.2112	0.6056

r: ring cavity, s: standing-wave cavity

a: $n_o = 1.5283$, $n_e = 1.5369$

b: $n_o = 1.5365$, $n_e = 1.5453$

c: $n_o = 1.5459$, $n_e = 1.5551$

value of m, the shorter the central wavelength of a tuning curve will be, and vice versa. Although theoretically m can take any integral number, in practice because the gain spectrum always has a limited range, it will limits the actual values of m (see Example III).

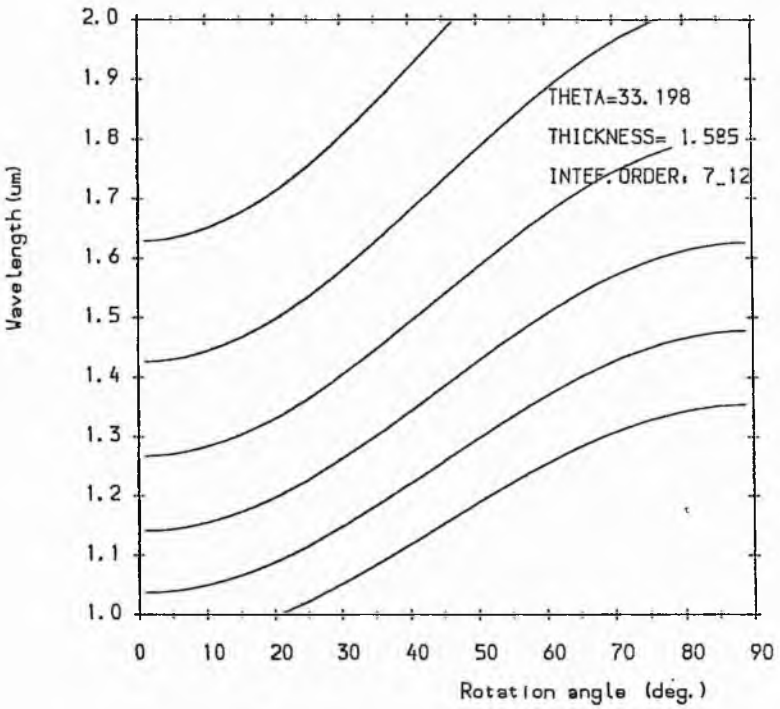

Fig. 7.12. Wavelength tuning curve for a birefringent plate.

Example III. Determination of practical maximum transformation order

Suppose the potential gain bandwidth is

$$\Delta\lambda = 1.45 \sim 1.55 \ \mu m$$

The minimum and maximum values of m can be estimated by

$$m_{min} = \text{Trunc.}\left[\frac{t_0}{1.55}\Delta_{min}\right] \tag{7.30}$$

$$m_{max} = \text{Trunc.}\left[\frac{t_0}{1.45}\Delta_{max}\right] + 1 \tag{7.31}$$

where Trunc. stands for the truncation function for getting an integral value of m, Δ_{min}, Δ_{max} represent the minimum and maximum values of the effective refractive index difference Δ respectively. Through numerical calculation, the range of Δ is plotted against the rotation angle in Fig. 7.13, from which it can be deduced that

$$\Delta_{min} = 0.720 \times 10^{-2} \tag{7.32}$$

$$\Delta_{max} = 1.026 \times 10^{-2} \tag{7.33}$$

Substituting Eq. (7.32) into Eq. (7.30), and Eq. (7.33) into Eq. (7.31) yields

$$m_{min} = \text{Trunc.}\,[t_0 \times 4.64\,] \tag{7.34a}$$

$$m_{max} = \text{Trunc.}\,[t_0 \times 7.07] + 1 \tag{7.34b}$$

where ℓ_0 has a unit of mm. For $\ell_0 = 1.58$ mm, then

$$m_{min} = 7$$

$$m_{max} = 12$$

The m values associated with the curves shown in Fig. 7.12 are determined in this way. From Fig. 7.12, it can be seen that the $m = 7$ and $m = 12$ curves (the highest and the lowest respectively) do not permit tuning in the 1.45 - 1.55 μm wavelength range of interest. This is due to the fact that excess tolerance is given in the truncation action performed by Eqs. (7.30) and (7.31).

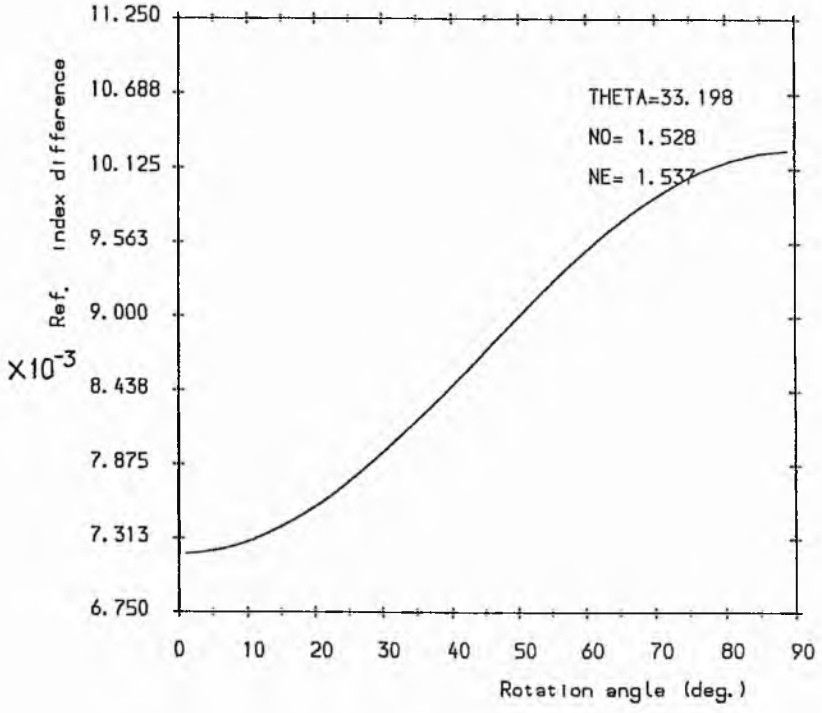

Fig. 7.13. Variation of the effective refractive index difference with rotation angle.

Eq. (7.29) also indicates that within a given rotation range, more maximum transformation order exist for larger ℓ_0, which simply means less accurate tuning can be obtained for thicker BP. This is also clearly shown in the experimental results given in the next section. Further examination of the tuning characteristics of a BF can be attained by looking at the differential of wavelength against the rotation angle ϕ. That is, from Eq. (7.29),

$$\frac{d\lambda}{d\phi} = \frac{\ell}{m}\left[\frac{n_e\cos^2\theta\,\sin 2\phi\left[\frac{1}{n_o^2} - \frac{1}{n_e^2}\right]}{2\sqrt{1 - \frac{\cos^2\theta\,\sin^2\phi}{n_e^2} - \frac{\cos^2\theta\,\cos^2\phi}{n_o^2}}}\right] \tag{7.35}$$

With Eq. (7.35), the required rotational range of ϕ for achieving the desired wavelength tuning can be estimated by $\Delta\lambda \approx \frac{d\lambda}{d\phi}\Delta\phi$. This is highlighted in example IV.

Example IV. Estimate of the required rotational range for a birefringent filter

Suppose: $m = 10$, $\theta = \frac{\pi}{2} - \theta_b = 33.198$, $\phi = 40^o$, $n_o = 1.5283$, $n_e = 1.5369$, $\ell = 1.86$ mm,

From Eq. (7.35)

$$\frac{d\lambda}{d\phi} \approx 20 \text{ (nm/ deg)} \tag{7.36}$$

If the gain bandwidth is given by $\Delta\lambda_g = 100$ nm, the required rotational range is

$$\Delta\phi \approx \Delta\lambda\left[\frac{d\lambda}{d\phi}\right]^{-1} = 5^o \tag{7.37}$$

From the above two equations it is clear that in practice a rotation stage that is used to accommodate a BRF needs only to have a small rotation range but a high precision.

7.2.5 Multipass effect

In all the previous discussions we have mainly concentrated on the features of a BF for the situations where only single, or at most double passes have been considered. However, when a BP is used in a laser cavity, many passes are involved. Normally, in these cases, a ratio about 10 -10^2 exists between the bandwidth derived from Eq. (7.16) and the actual lasing bandwidth, i. e.

$$\delta\lambda \approx (10 - 10^2)\delta\lambda_g \tag{7.38}$$

where $\delta\lambda_g$ is the bandwidth of laser output. The explanation of Eq. (7.38) is the existence of the multipass effect combined with the action of the gain. It is known that the actual lasing bandwidth is identical to the bandwidth of the net gain which is the product of the loss profile and the gain profile. The shape of gain profile depends on the pumping intensity and the characteristics of the gain medium whereas the loss profile is mainly dictated by the BRF inserted in the cavity.

The effect of multipass on the bandwidth can be investigated by determining the multipass transformation matrix, which is given by

$$M_{multi} = (M_s)^m \tag{7.39}$$

where M_s is the transformation matrix for a single pass, n is the number of multipass. For the case of a BP located between two perfect polarizers, the matrix for n passes is

$$M_{multi} = \begin{bmatrix} 0 & 0 \\ 0 & m_{22} \end{bmatrix}^n = \begin{bmatrix} 0 & 0 \\ 0 & (m_{22})^n \end{bmatrix} \tag{7.40}$$

From Eq. (7.8), the overall transmissivity of the system is given by

$$T = |(m_{22})^n|^2 = (1 - A\sin^2\frac{\delta}{2})^n \tag{7.41}$$

where A, δ are determined by Eq. (7.12) and (7.13b) respectively. A simple derivation gives the relation between bandwidth and the multipass number, which is

$$\delta\lambda = \frac{2}{\pi}\frac{\lambda^2}{\ell\Delta}\sin^{-1}\left[\sqrt{\frac{2[1-(0.5)^{1/n}]}{2A}}\right] \tag{7.42}$$

Obviously, if $n \to \infty$, $\delta\lambda \to 0$; for $n = 1$, Eq. (7.42) reduces to Eq. (7.14a). A numerical result from Eq. (7.42) is shown in Fig. 7.14. It can be seen that as n increases $\delta\lambda$ decreases. When n is above 30, the decreasing rate of $\delta\lambda$ becomes small.

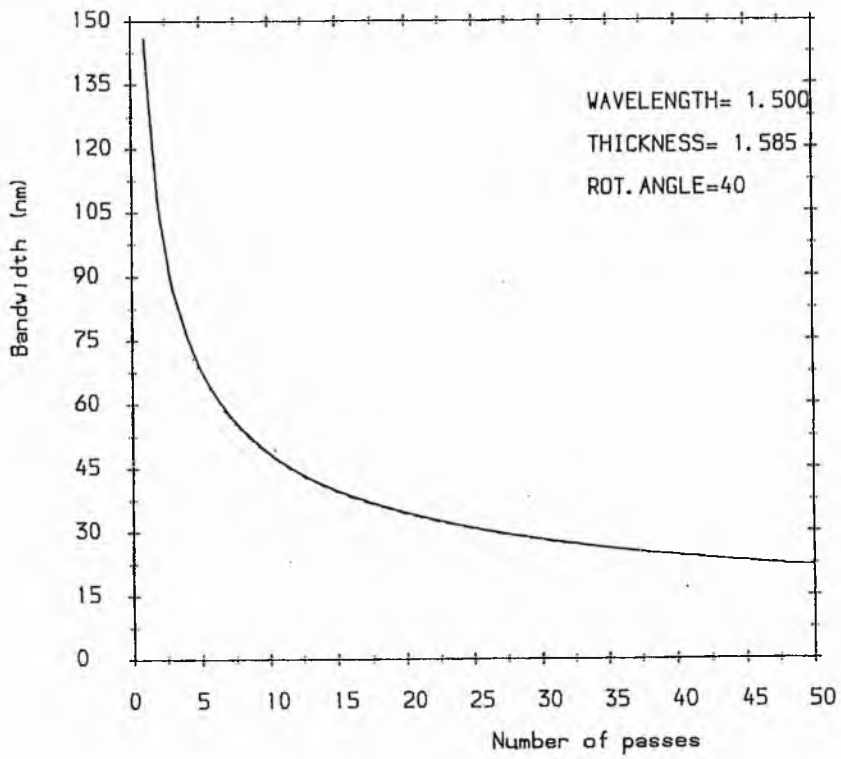

Fig. 7.14. Dependence of the transmission bandwidth of a birefringent filter on the number of passes.

As for the case of a BP between two partial polarisers, considering Eq. (C.34) in Appendix C, the multipass matrix is given by

$$M'_{multi} = \begin{bmatrix} t_s^2 m_{11} & t_p t_s m_{12} \\ t_p t_s m_{21} & t_p^2 m_{22} \end{bmatrix}^n \tag{7.43}$$

Unlike the case described by Eq. (7.40), for this situation the beam will change its polarization after each pass. Only numerical results of the relation between the bandwidth and the pass number can be obtained. It is expected that as n increases towards infinity the polarization status tends to reach a stable state and the transmission bandwidth would vary in a way similar to that shown in Fig. 7.14.

7.2.6 Eigenvalues for a resonator containing a birefringent filter

Referring to the laser cavity shown in Fig. 7.15, when the laser has an established stable polarization status, the self-consistent condition exists, i.e.

$$\mathbf{M}\mathbf{E}_i = d\mathbf{E}_i \tag{7.44}$$

where M is the Jones transformation matrix for one roundtrip, d is a constant matrix, the values of which determined by $|M - dI| = 0$ are called the eigenvalues of M. Normally two different eigenvalues, say d_1 and d_2, exist. The transmissivity of the resonator is given by

$$T = |d_i|^2 \tag{7.45}$$

where $|d_i|$ takes the value of the larger of $|d_1|$, $|d_2|$.

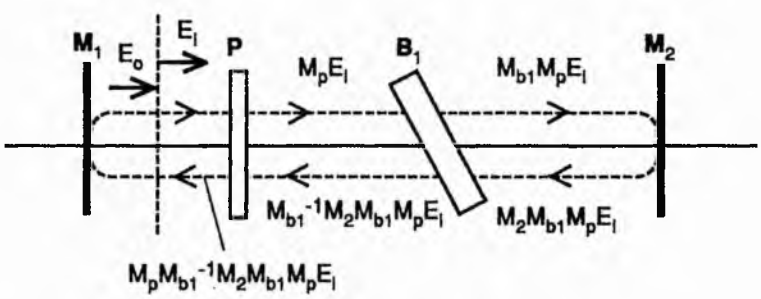

Fig. 7.15. A simplified resonator comprising typical polarization devices. B_1 is the birefringent plate, P is an equivalent partial polariser that represents the effect contributed by all the Brewster-angled surfaces in the cavity except those of the birefringent plate.

The roundtrip matrix M for the standing-wave cavity shown in Fig. 7.15 can be written as

$$M = M_2 M_p M_{b1}^{-1} M_1 M_{b1} M_p \tag{7.46}$$

where M_1, M_2 are the Jones matrices for the two end mirrors, M_p, M_b for the equivalent polarisers and birefringent plates respectively. These matrices are given by

$$M_1 = M_2 = \begin{bmatrix} -1 & 0 \\ 0 & 1 \end{bmatrix} \tag{7.47}$$

$$M_p = M_p(\nu_b) = \begin{bmatrix} (t_s)^{\nu_b} & 0 \\ 0 & 1 \end{bmatrix} \tag{7.48}$$

$$M_{b1} = \begin{bmatrix} t_s^2 m_{11} & t_s m_{12} \\ t_s m_{21} & m_{22} \end{bmatrix} \tag{7.49}$$

$$M_{b1}^{-1} = \begin{bmatrix} t_s^2 m_{11} & -t_s m_{12} \\ -t_s m_{21} & m_{22} \end{bmatrix} \tag{7.50}$$

Note that ν_b is the number of the Brewster-angled surfaces in the cavity excluding those of BPs, m_{ij} (i, j = 1, 2) is determined by Eq. (7.4a) and t_s is equal to $2n/(1+n^2)$. Substituting Eqs. (7.47) - (7.50) into Eq. (7.46) yields

$$M = \begin{bmatrix} t_s^{2(\nu_b+1)}(t_s^2 m_{11}^2 + m_{12}^2) & t_s^{(\nu_b+1)} m_{12}(t_s^2 m_{11} + m_{22}) \\ t_s^{(\nu_b+1)} m_{21}(t_s^2 m_{11} + m_{22}) & t_s^2 m_{12}^2 + m_{22}^2 \end{bmatrix} \tag{7.51}$$

If the matrix for the BP is written in a form of the product of three matrices, namely

$$M_{b1} = M_{t1} M_b M_{t1}$$

where the two M_{t1}'s describe the Brewster-angled surfaces of the BP, Eq. (7.46) can be re-expressed as

$$M = M_2 M_p(\nu_b+1) M_b^{-1} M_{t1} M_1 M_{t1} M_{b1} M_p(\nu_b+1) \tag{7.52}$$

where $M_p(\nu_b+1) = M_p(\nu_b) M_{t1}$. From Eq. (7.52), it can be seen that the transformation process in one roundtrip inside the cavity can be dealt with as equivalent to a beam passing twice through a BP located between two different partial polarisers.

Suppose the effect of one of the BP Brewster-angled surfaces, that adjacent to M_2, can be neglected, then the roundtrip matrix given in Eq. (7.52) will reduce to

$$M = M_2 M_p(\nu_b+1) M_b^{-1} M_1 M_b M_p(\nu_b+1) \tag{7.53}$$

This is equivalent to the situation of one BP of double thickness sited between two partial polarisers characterized by $M_p(\nu_b+1)$, i. e.

$$M = M_p(\nu_b+1) M_b(2l) M_p(\nu_b+1) \tag{7.54}$$

Eq. (7.54), or (7.53), shows the main difference between a BP inserted in a standing-wave cavity or travelling-wave cavity. Passing the BP twice in one roundtrip doubles the effective thickness of the BP.

For the case where more than one BP, say two BPs, are used in a linear cavity, the transformation matrix for one roundtrip is

$$M = M_1 M_p M_{b2}^{-1} M_{b1}^{-1} M_2 M_{b1} M_{b2} M_p \qquad (7.55)$$

In this situation, if the effect of Brewster-angled surfaces between two BPs is neglected[8], the two BPs with thickness ℓ_1 and ℓ_2 respectively will be equivalent to one BP with a thickness of $\ell_1 + \ell_2$.

7.3 Experimental tuning curves for the synchronously-pumped KCl:Tl colour-centre laser

On the basis of the theoretical work presented in section 7.2 relating to the tuning characteristics of birefringent filters, the tuning features of the synchronously-pumped KCl:Tl colour-centre laser could be studied in quantitative terms. Because the laser crystal, the dichroic beam splitter, the chamber window and the birefringent plate are all placed at a Brewster-angle the laser output beam has a high degree of linear polarization. This ensures that the wavelength tuning function of the birefringent filters can be fully exploited within the laser cavity. The BRF placed at the location as shown in Fig. 7.3, is mounted on a special rotation stage supplied by the manufactures (Burleigh Inc.). Through a transformation of straight-line movement to rotation, this stage provides a precise rotation of the mounted birefringent plate around the direction of its normal (with an angular resolution ≤ 0.1 degree). Unfortunately, the stage does not have any scale definition. (The amount of the rotation movement in measurements was counted in terms of the number of "turns" of a rotating knob). Thus, to obtain any actual values about the rotation angles of the BRF, a calibration must be carried out. The result of such calibration is shown in Fig. 7.16(a). The corresponding angular degree for one turn was

8 In practice, appropriate index matching liquid can be added between two birefringent plates to combine them into one plate with the sum thickness.

determined by the property of $\pi/2$ periodicity of the tuning curve according to Eq. (7.29), such that, 1 turn ≈ 0.8 deg. could be deduced.

For the mount provided the available maximum rotation range was only ~ 35° and so to achieve the whole curve shown in Fig. 7.16(a) the filter had to be taken out when the stage reached its end, and then the stage was rotated back to the starting position and the filter put back again several times. Each time the BRF was taken out, a particular lasing wavelength was noted and when the BRF was put back into the mount it was ensured that the laser operated at the same wavelength. This would guarantee that the BRF was put back at exactly the same rotation angle, ϕ, as it was before being taken out.

7.3.1 KCl:Tl laser with 1 mm BRF

In addition to the calibration of the actual rotation angle, the data in Fig. 7.16(a), also illustrate other important features involved in the tuning of the laser. For instance, when the rotation angle, ϕ, is equal to 0° or 90°, i. e. the optical axis of the birefringent plate is either parallel or perpendicular to the polarization direction of the incident beam, the filter no longer has any filtering effect, and thus the laser simply operates at the central gain wavelength, which was, for the KCl:Tl crystal used, λ_c = 1510 nm. This is consistent with the predictions from Eqs. (7.11) and (7.12), where if $\phi = 0, 90°, 180°$, then $A = 0$, T = 1.

Another interesting aspect is that Fig. 7.16(a) shows that for the 1 mm thick birefringent filter only one full-range tuning curve exists within the 90° rotation range and on each side of this curve a "dead tuning region" exists. This latter feature can be utilized to identify this full-range tuning curve and so is helpful in locating the filter at the correct rotation angle in practice.

In Fig. 7.16(b) the associated change in output power as the laser was tuned is illustrated. As expected, the laser output power decreased when the laser was tuned away from its central wavelength of the gain bandwidth and peaked again whenever the lasing wavelength was close to λ_c. (The two small dips that appeared on each side of the peak around the 90° angle are not properly understood as yet).

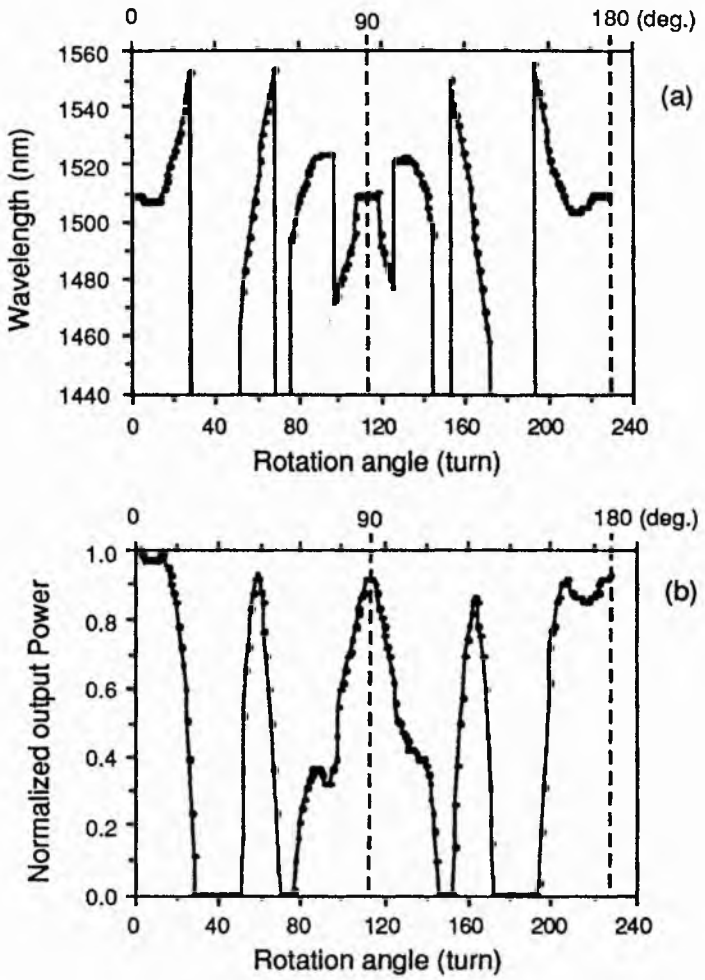

Fig. 7.16. Frequency-tuning characteristics (a) and the associated power change (b) for the KCl:Tl laser. (1 mm thick birefringent filter was used as the tuning device. The rotation angle is the angle between the optical axis of the birefringent plate and the plane of incidence).

7.3.2 KCl:Tl laser with 2 mm or 4 mm BRF

With a 2-mm-thick birefringent filter incorporated inside the laser cavity, the corresponding laser tuning feature is represented in Fig. 7.17(a). It can be seen that there are about 6 curves within the 90° rotation range, associated with 6 orders. A pair of narrow but still detectable "dead tuning regions" exist beside the central full-range tuning curve. When the 2-mm filter was replaced by one having a 4-mm-thickness, no such dead regions were observed [see Fig. 7.17(b)]. The tuning curves (10 different orders), are all closely interconnected. As the BRF was rotated the laser output power decreased and increased alternatively but laser oscillation was maintained. (The associated measurement indicated that the maximum change of the optical power was about 50% as

the result of tuning). The reason why less tuning range is availabe with the 4-mm-thick filter compared with that from the 2-mm one may be attributed to the fact that for the thicker filter the associated FRS becomes smaller (see Eq. 7.15) and so the wavelength difference between the m_{th}-order longest wavelength and the $(m+1)_{th}$-order shortest wavelength is decreased.

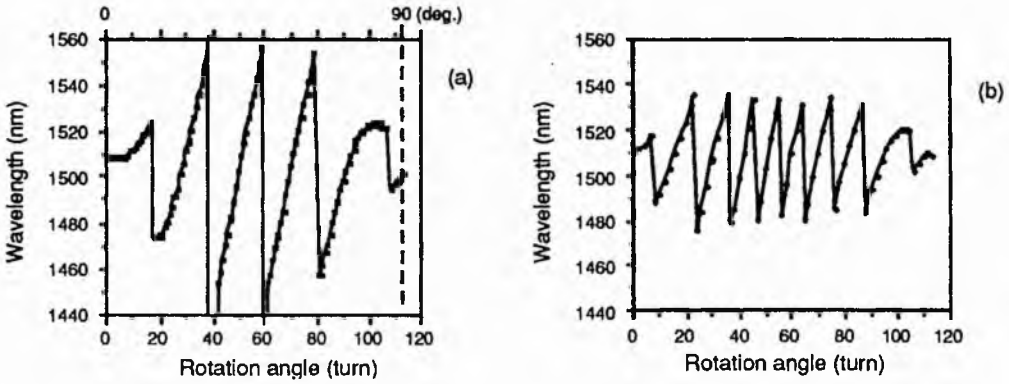

Fig. 7.17. Tuning curves of the synchronously-pumped KCl:Tl laser, obtained with (a) 2-mm- and (b) 4-mm-thickness birefrigent plates.

In the situations where several tuning curves are available for use, two questions could be raised. One is that what would happen if the BRF is just rotated to the angle at which the two neighbouring tuning curves are connected together. Such a query has been carefully examined in experiments. It was found that the laser often operated at two wavelengths simultaneously, with one spectral component substantially stronger than another. Further experimental data showed that there were actully three possible lasing wavelengths under this particular circumstance. These wavelengths are the central lasing wavelength determined by the gain medium (~1510 nm), the longest wavelength achievable from one tuning curve (~1555 nm) and the shortest wavelength from the other tuning curve (~1455 nm). It is obvious that in any cirumstances in order to achieve reliable operations the laser should not be tuned to these especially sensitive points. On the other hand, the bistable or tristable features related to this type of frequency tuning status represents an interesting aspect which is worthy of further study. (Note that this peculiar phenomenon only occurs for relatively thick birefringent filters).

Another question relating to the existence of several tuning curves is how to decide which curve should be used when the effective lasing bandwidth is of primary concern. From Eq. (7.29), it is known that for the same central lasing wavelength, a higher order tuning curve relates to a smaller effective refractive index difference and so according to Eq. (7.14a) a narrower bandwidth exists. Therefore, to minimize the bandwidth restriction, the laser should be operated under the lower order tuning curves. In other words, the tuning curves which are obtained with relatively smaller rotation angles are generally preferred.

7.3.3 KCl:Tl laser with 0.5 mm or 0.3 mm BRF

The tuning features of the KCl:Tl laser obtained with 0.5 or 0.3 mm filters are shown in Fig. 7.18(a), (b) respectively. The corresponding changes in laser output power in the two cases are also included. It can be seen that the tuning curves for the 0.5 mm BF are related to three maximum transformation orders and for the 0.3 mm filter only two orders exist[9]. This is in agreement with the prediction from Eq. (7.29) and also confirms that a less compulsary requirement on the angular resolution of the rotation stage can be accepted when thin birefringent plates are used. [From Eq. (7.35), it is known that $\frac{d\lambda}{d\phi}$ is proportional to the thickness of birefringent plates and so for thin filters the tuning is less sensitive as expected].

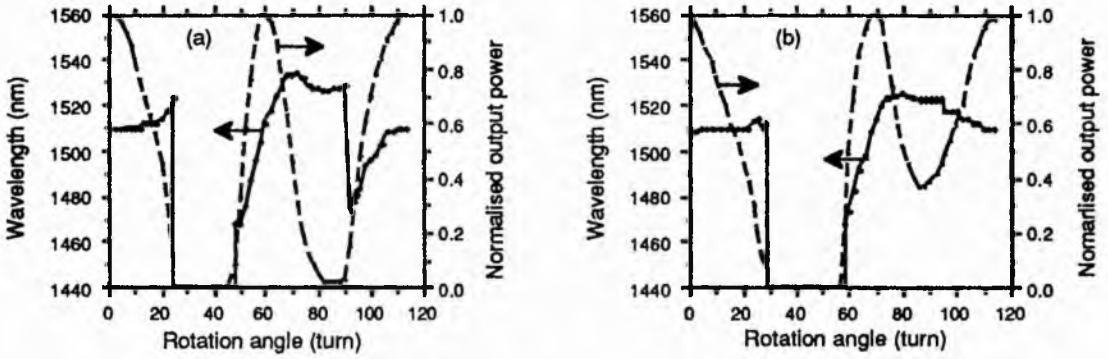

Fig. 7.18. (a) Tuning curves and the associated change in laser output power obtained with 0.5 mm thick birefringent filter. (b) as for (a) but with 0.3 mm BRF.

---

9 Because of the small thickness of the filter, a large effective refractive index difference and so a large rotation range is needed in order to form a $\pi/2$ change of the beam polarization at a given wavelength. This can account for the existence of the fairy large "dead region" between the tuning regions.

In comparison with the result for a 1-mm-thick BRF [Fig. 7.16(a)] the tuning range obtained with these two thinner filters are much smaller (Especially for the 0.3 mm one only a range of 1470-1530 nm is covered). The overall tuning quality of the tuning curves in terms of linearity is also very poor in these two circumstances. This is most likely caused by the incorrect thickness of the filters. Once the filter becomes very thin, only a few maximum transformation orders can exist, and so the thickness of the filter must be very accurate to permit a tuning curve centred at the peak of the gain and extending across the entire wavelength range of the gain medium. For the same reason any defects in thinner filters would have a much severer influence on the laser tuning characteristics compared with thicker filters. Finally, it may be worth mentioning that the concept of the thick or thin filters is really of primary relevance to the working wavelengths of the laser.

7.4 Conclusions

With its advantages of good tunability, reasonably large output power and acceptable stability, the KCl:Tl colour-centre laser is a very useful near-infrared laser source. When such a laser is synchronously mode-locked the intracavity birefringent filter (BRF) will have the function not only of wavelength tuning (as for single frequency lasers) but also and more importantly for the practical bandwidth restriction of the laser pulses. To select a birefringent plate with the correct thickness, the use of the approximate Jones transformation matrix for a tilted filter derived by Preuss and Gole can lead to severe errors and thus the accurate Jones transformation matrix given in this work - Eq. (7.4a), which takes into account the beam splitting effect should be employed.

In general, a thicker BRF gives rise to a more pronounced bandwidth restriction and provides a larger number of wavelength tuning curves within a given rotation range for the angle between the optical axis and the incident plane. The smaller free spectral ranges associated with the thicker filters will also reduce the actual achievable wavelength tuning range. For thinner filters the opposite is true.

In the cases where a thicker intracavity BRF is incorporated the tuning of the laser to the edges of any two neighbouring tuning curves should be avoided because these joint

positions represent a very unstable operational regime where the actual lasing wavelength can easily jump from one value defined by one tuning curve to another defined by a neighbouring tuning curve. Where use is made of thin filters it is worth paying particular attention to the large "dead tuning regions" that exist (see Sec. 7.3). Under these conditions if the thickness of a thin filter is not correctly selected so that the dead region is close to or even just overlapped with the centre of the gain then no appropriate wavelength tuning can be achieved. It follows therefore that the applicability of intracavity birefringent filters must be carefully considered for the tuning/bandwidth requirements of a mode-locked laser.

Chapter 8

Performance of the CCM KCl:Tl Colour-Centre Laser - I

As already mentioned in chapter 6, soon after the recognition that the coupled-cavity mode locking is in fact a very general scheme for producing ultrashort laser pulses, there have been a great many efforts to apply this method in various laser types[1]. In parallel with such work we have directed our studies towards obtaining a more complete knowledge of the operating characteristics and thus a better understanding of the physics involved for this mode locking scheme. To achieve this purpose and avoid the unnecessary confusion that may arise in dealing with comparisons of different laser systems regarding the features of coupled-cavity mode locking just one laser type - the KCl:Tl colour-centre laser is described here. Extensive experimental studies on the various aspects of the performance of this coupled-cavity mode-locked KCl:Tl colour-centre laser under different operational conditions have been conducted.

In this chapter, the first group of results relate to the performance of the coupled-cavity arrangements where a AT & T fibre and subsequently an erbium-doped counterpart were used (Sec. 8.1). Complementary investigations of the dependence of laser behaviour on system parameters, fibre types, and the influence of non-SPM nonlinearities are reported in the sections 8.2-8.4.

8.1 CCM, KCl:Tl laser with AT & T fibre or Er-doped fibre

8.1.1 Spectral and temporal characterisation of the CCM KCl:Tl laser with the AT & T fibre

The study of coupled-cavity mode locking started with an effort to reexamine the performance of a soliton laser, i. e., the coupled-cavity mode-locked laser that has a specific control fibre supporting optical solitons. To make the results comparable with

[1] This active trend did however show a lack of comprehensive studies of the operating characteristics of this type of mode locking during the past 2-3 years. In particular, the dependence of the CCM laser behaviour on the general system parameters has not been adequately addressed until the work reported in this and subsequent chapters was undertaken.

those reported by Mollenauer and Stolen (1984) the same type of anomalously dispersive single-mode fibre as that employed in the first soliton laser was used in the control cavity of our laser. This particular fibre[2], provided by Mollenauer (AT & T Bell Lab.), has the properties of dispersion parameter |D| = 15 ps/km/nm, Kerr coefficient $n_{2I} = 3.2 \times 10^{-16}$ cm^2/W and core diameter of 8.6 μm. In our experiments (the fibre was cut to 2.8 m), it was found that instead of having only one or several discrete critical intrafibre power levels at which the mode locking is enhanced, appropriate coupled-cavity mode locking could be achieved for a continuous range of intrafibre power levels. Associated with this power range a variety of spectral characteristics could be observed for the CCM laser system.

The variation of the CCM laser spectrum with the power coupled into the control fibre is shown in Fig. 8.1. It was observed that for stable operation the average power in the fibre (P_f) should exceed some "threshold" power level (P_{th}), which was believed to be determined by the Kerr coefficient n_{2I} and the effective cross-sectional area of the fibre core but not necessarily equal to the N=1 soliton power level. From Fig. 8.1, it can be seen that under our experimental conditions P_{th} was ~15mW and when P_f is larger than P_{th}, three distinct operating regimes can be identified. Firstly, in the average power range of 15 - 21 mW, the spectrum of the CCM laser is continuously and symmetrically broadened [see Fig. 8.1(a, b)] and the pulse duration reduces correspondingly. Secondly, for powers from 22 mW to 25 mW, the spectra become more unstable and noisy and additional relatively narrow 'peak' spectral features occur. Meanwhile, fluctuations appear in the wings of the recorded autocorrelation traces. Thirdly, above powers of 25 mW or thereabouts, these peak spectral features rapidly increase in intensity and the broader spectral features become noticeably less noisy. The corresponding autocorrelation traces confirm better stability again and the pulse durations increase slightly as indicated in Fig. 8.2. [This "triple-phase" behaviour is very similar to that described by Tai *et al* (1986) for

---

[2] For brevity it is simply referred to here as the "AT & T fibre". We stress that such a fibre does not represent the only fibre type that can sustain bright optical solitons although it is sometimes also called "soliton fibre".

their first observation of modulational instability in optical fibres. Further discussions on this will be included in Sec. 8.4].

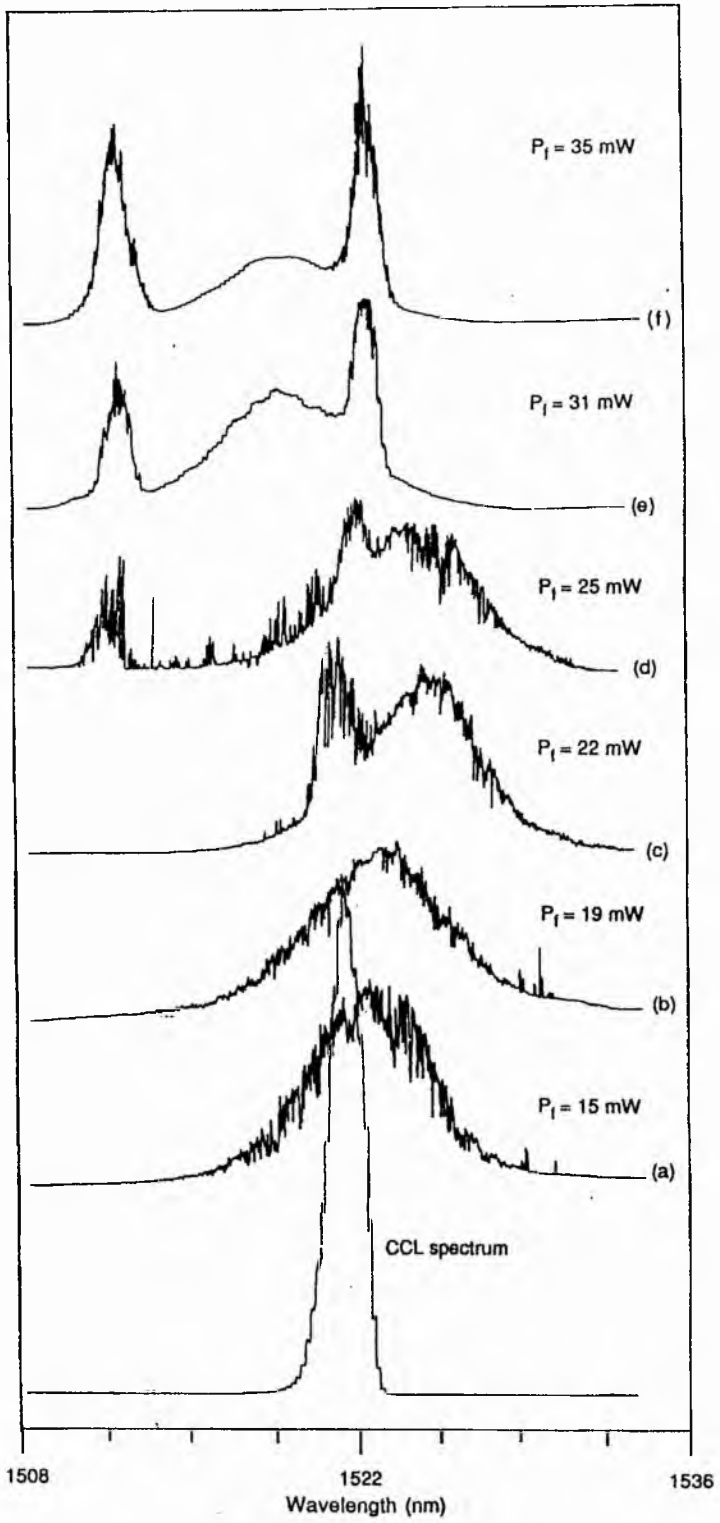

Fig. 8.1. Spectra of CCM laser pulses measured for different power levels in the fibre.

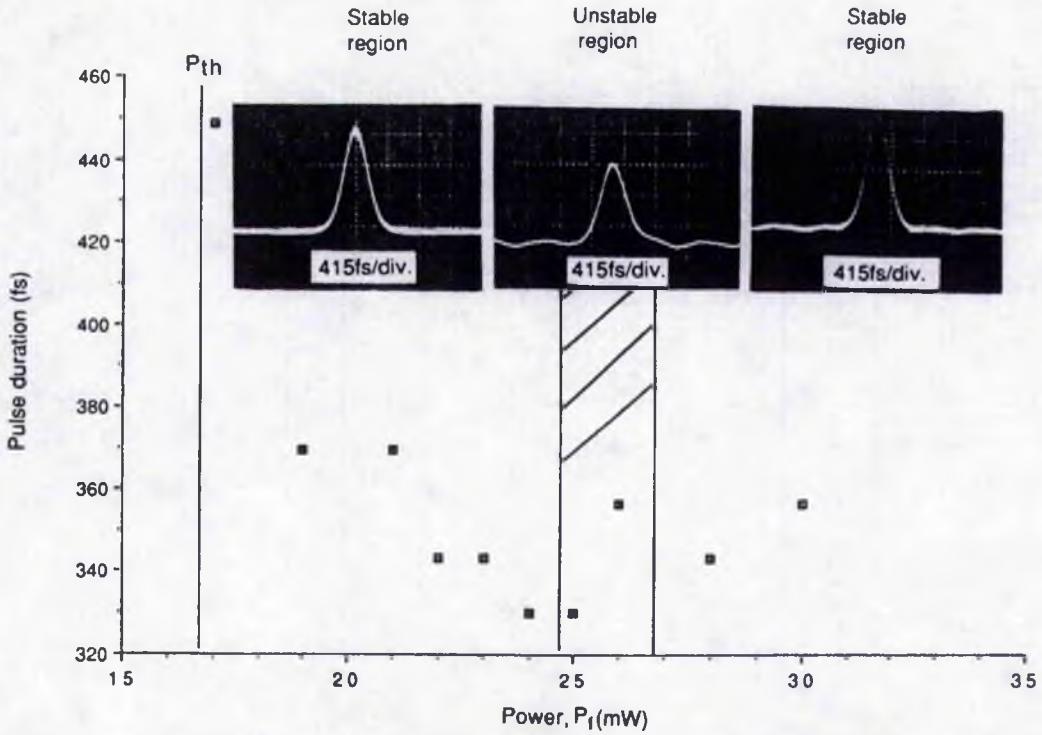

Fig. 8.2. Variation of pulse duration with the average optical power in the 2.8-m-long soliton laser control fibre [These data indicate the influence of modulational instability (see discussion in Sec. 8.4)].

When the average power after the fibre (P_f) is about 19 mW and the main and control cavity lengths are properly matched an optimum performance can be observed in terms of the most stable pulse generation accompanied by symmetrical spectral characteristics (see Fig. 8.3). Under the same conditions, the spectrum of the pulses fed back to the main cavity and the corresponding real-time SHG autocorrelation traces are reproduced in Fig. 8.4. It can be seen that in this stable regime the durations of the pulses out of the fibre are about 180 fs, which is significantly shorter than that of the pulses into the fibre (360 fs). This is consistent with a solitonic temporal narrowing effect as described by Mitschke and Mollenauer (1986).

During these experiments it was also observed that the spectral characteristics of the CCM laser not only depended on the power level in the fibre but was also strongly related to any cavity-length mismatch. In particular, the SPM-induced spectral broadening was sometimes towards the longer wavelengths and sometimes to the shorter wavelengths (see Fig. 8.1). It has been observed that the direction of the spectral broadening is mainly determined by the extent of the cavity length mismatch as indicated in Fig. 8.5. It can be

seen that the induced spectral broadening shifts to the longer wavelengths [traces (d)- (g)] when the mismatch of cavity length is positive (i.e. the length of control cavity is longer than that of main cavity) and vice versa for traces (a)-(c).

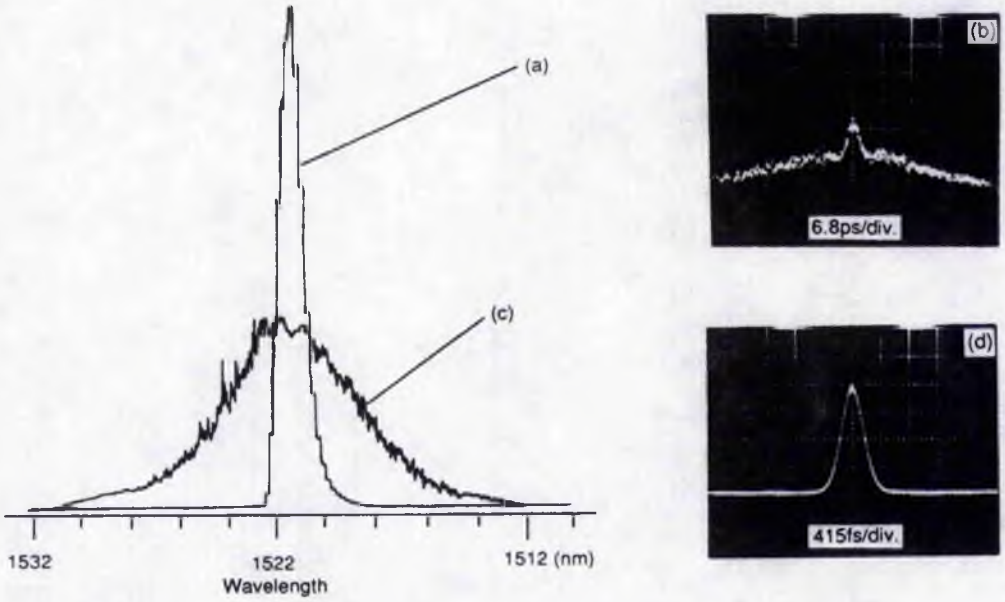

Fig. 8.3. Spectral and temporal (intensity autocorrelation) characteristics for a synchronously pumped (a, b) and CCM (c, d) KCl:Tl colour-centre laser respectively.

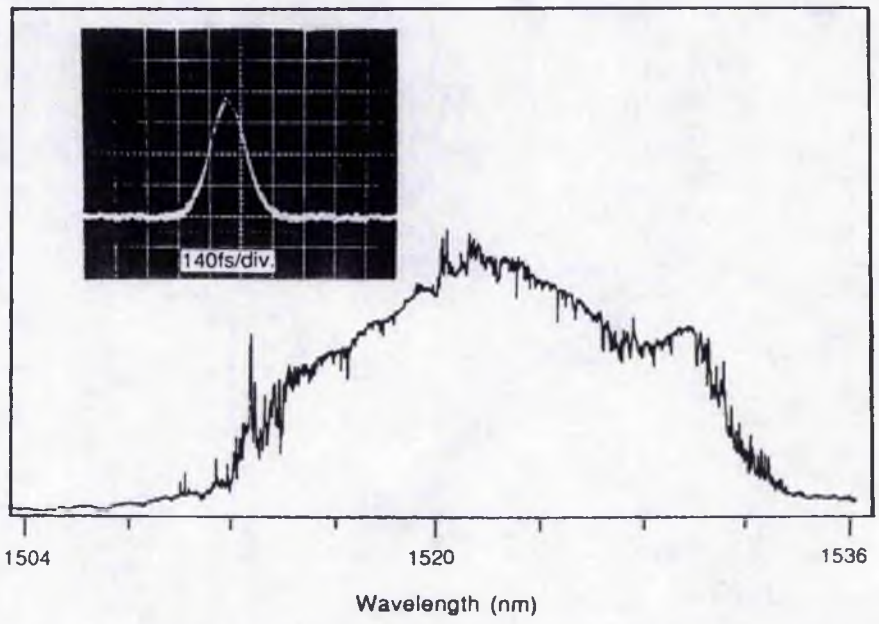

Fig. 8.4. Spectrum of the pulses returned from the control fibre to the main cavity obtained under the same optimised operating conditions of Fig. 8.3.

The basis for these observations can be understood by considering the frequency chirp that is induced in the fibre within the control cavity. It is expected that due to the SPM effect the propagating pulse will be up-chirped. If the anomalous dispersion in the fibre does not fully compensate this frequency chirp then the leading and trailing portions of the pulses fed back to the main cavity will contain different spectral components: longer wavelengths in the front and shorter wavelengths on the rear. Therefore, when the cavity lengths are mismatched, say the control cavity is longer than the main cavity (i.e. positive mismatch) only the leading edge of the return pulse overlaps with the pulse circulating within the main cavity. An interferometric interaction therefore takes place between the fedback self-phase-modulated pulse and the main cavity pulse such that laser oscillation will be established preferentially at longer wavelengths. A negative cavity mismatch condition will correspondingly favour laser oscillation

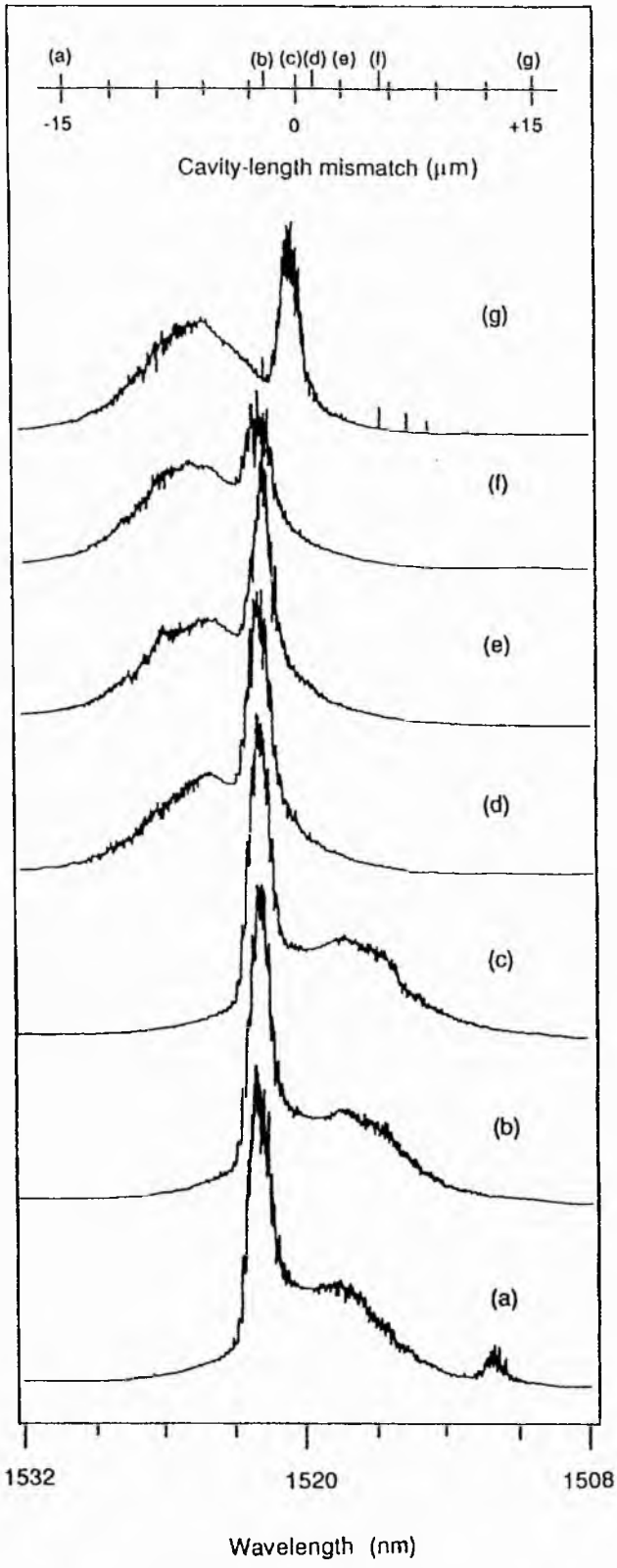

Fig. 8.5. CCM laser spectra (a-g) recorded at various cavity-length mismatches.

growth at the shorter wavelengths. The main spectral peak in Fig. 8.5 is very close to the injected CCL spectral centre. The existence of this peak would indicate an distorted spectral broadening process that occurs in the control cavity during the CCM operation.

When P_f was about 24 mW and the cavity lengths were closely matched, an interesting bistable phenomenon was observed, where two quite distinct autocorrelation profiles could be recorded (see Fig. 8.6). One corresponds to spectral broadening to the shorter wavelengths and the other to longer wavelengths relative to the spectrum of the colour-centre laser. Under an external perturbation, such as repeated knocking on the optical table, the two states switch sequentially from one to the other. In this case a symmetrically vibrating spectrum as illustrated by Fig. 8.7 could be observed. This type of bistability has already been analyzed to some extent by Ouellette and Piché (1986) and reference has also been made to an observation of a similar effect in the soliton laser (Mollenauer 1985) but no experimental data were presented there.

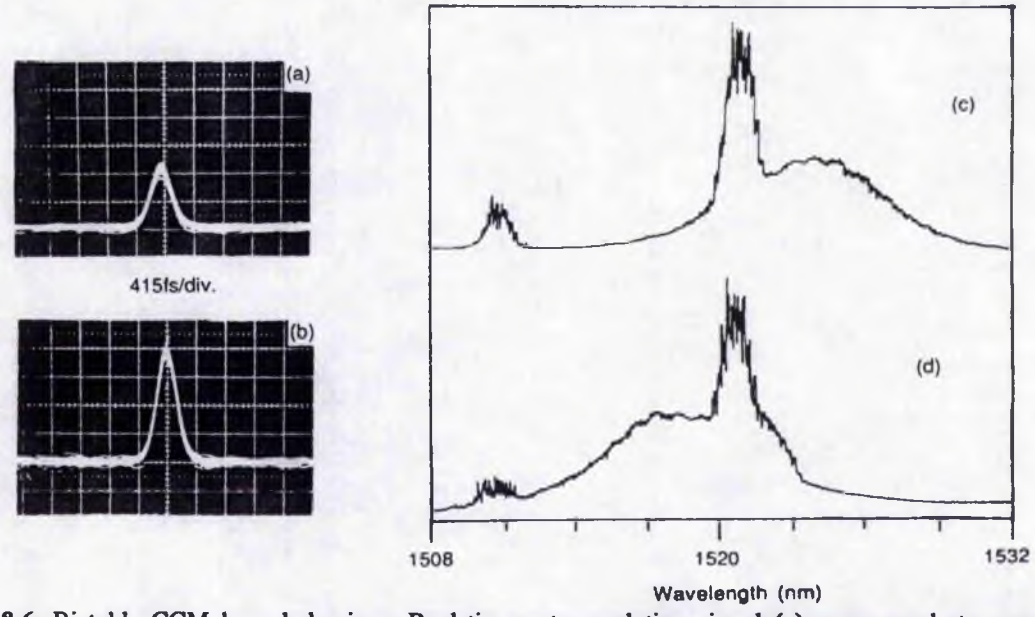

Fig. 8.6. Bistable CCM laser behaviour. Real-time autocorrelation signal (a) corresponds to spectral broadening to longer wavelengths (c), and enhanced real-time autocorrelation signal (b) corresponds to spectral broadening to shorter wavelengths (d).

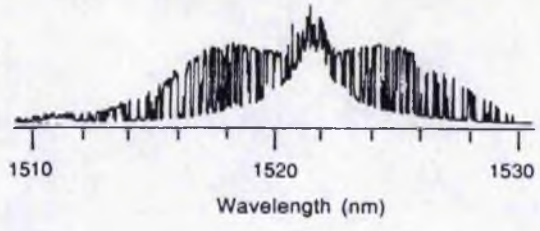

Fig. 8.7. Spectrum of the CCM laser under bistable conditions. In this case the spectral peak of the CCL was set at 1522nm, which almost overlaps the spectral centre of the CCM laser spectrum illustrated.

8.1.2. Coupled-cavity mode locking using an erbium-doped fibre

With the AT & T fibre it was difficult to obtain the pulses having durations less than 200 fs from our coupled-cavity mode-locked system (Kean *et al* 1989). In subsequent studies it was decided to use erbium-doped fibres as the nonlinear medium in the control cavity. The first erbium-doped fibre (Type-I in Table 8.1 in Page 195) used had a dopant concentration = 6×10^{18} cm^{-3}, NA = 0.24, λ_{cutoff} = 1.3 μm, core diameter = 4.6 μm and an estimated zero dispersion wavelength around 1.44 μm. [Single-pass propagation studies have indicated that this erbium-doped fibre exibits a substantially greater amount of spectral broadening than that for its erbium-free counterparts (see Ch. 10)].

By optically pumping the Er-fibre (using a Kr^+ laser, 647, 676 nm lines) the presence of gain nonlinearity can contribute to the kinetics of the CCM process. Discernible levels of exploitable optical nonlinearity could be observed at average powers ~3 mW in 'pumped' fibres as compared to power ~5 mW in the unpumped fibre samples having lengths of 2.5 m in both cases. These power levels are more than three times lower than those which apply to the previously used AT & T fibre. Although one of the initial aims in employing the Er-doped fibre was to use it as a nonlinear amplifier, the experimentally recorded low P_{th} value for the CCM operation with unpumped doped fibre redirected the emphasis of the research towards the passive nonlinearities of the fibre. (i. e. the fibre was unpumped for the remainder of results produced here).

The spectra of the synchronously-pumped colour-centre laser and the CCM laser system having a 30-cm-long Er-doped fibre are shown in Fig. 8.8(a), (b) respectively. It can be seen that the spectrum of the CCM laser is symmetrically broadened by a factor of approximately x12. The inset of Fig. 8.8 is the corresponding SHG intensity autocorrelation trace for the CCM laser output where the bandwidth (19 nm) and pulse duration (140 fs) product of 0.355 implies that the CCM laser pulses have $sech^2$-like intensity profiles. These data, which should be compared to those in Fig. 8.3 with much larger spectral bandwidth and shorter pulse duration, were recorded when a 0.3-mm-thick birefringent filter was included in the main cavity and the average power in the fibre, P_f, was 18 mW.

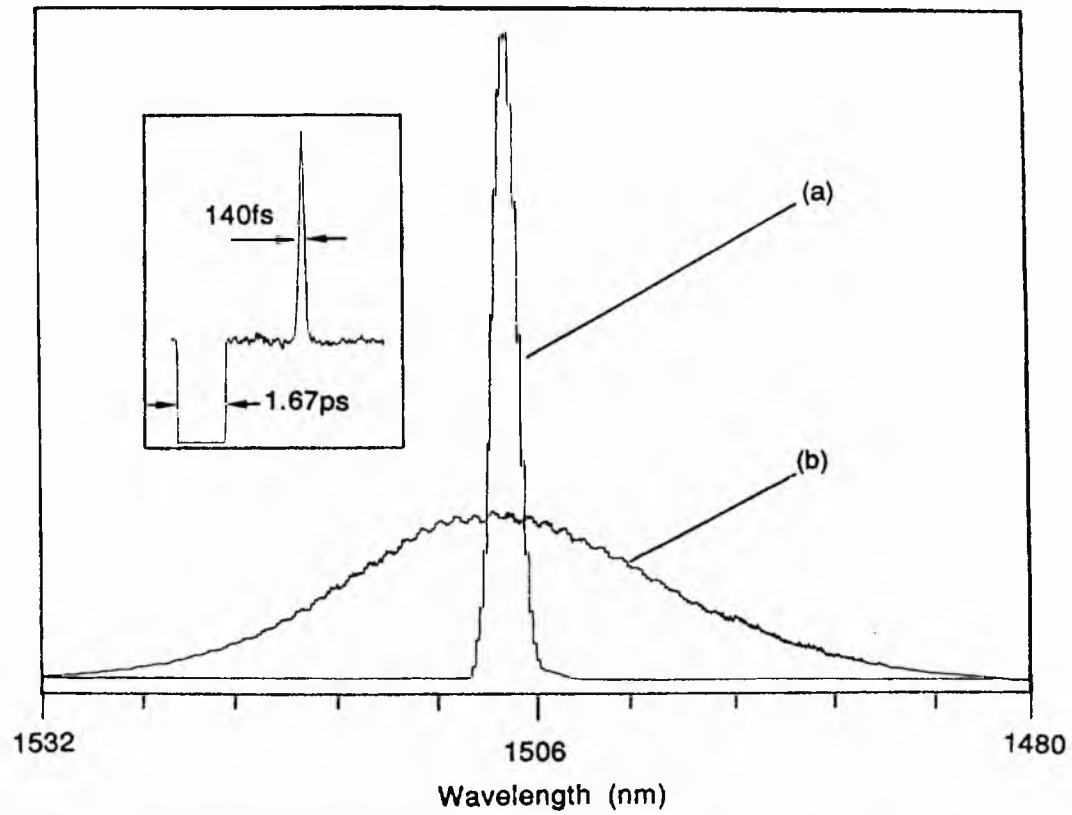

Fig. 8.8. Spectra for (a) synchronously-pumped KCl:Tl colour-centre laser, (b) CCM laser with a 30-cm-long erbium-doped control fibre. The inset is the SHG intensity autocorrelation trace which corresponds to the spectral trace (b).

As P_f increases, an unstable operational regime accompanied by a pulse splitting phenomenon was observed. This has been attributed to the influence of a selectively strong self-Raman effect (for details see Sec. 8.4). The Raman conversion can be avoided either by reducing the pulse power in the fibre or alternatively by using a shorter length of fibre. This was achieved by cutting back the fibre length to 21 cm, for which the interferometric and intensity and autocorrelation profiles of the CCM laser pulses have been included as Fig. 8.9(a), (b) (average power in fibre of 17 mW). In this case the pulses had durations as short as ~75 fs ($sech^2$-pulseshape assumed). The measurements from the associated interferometric autocorrelation trace indicates that within the FWHM of the pulse intensity profile there are only 15 optical cycles. It is emphasised here that these stable sub-100 fs CCM laser pulses have been produced at quite low intrapower levels in the erbium-doped fibre, and it is clear that the features of very low dispersion, relatively small core diameter and somewhat higher n_{2I} value of this fibre are all responsible for this achievement (see Ch.9).

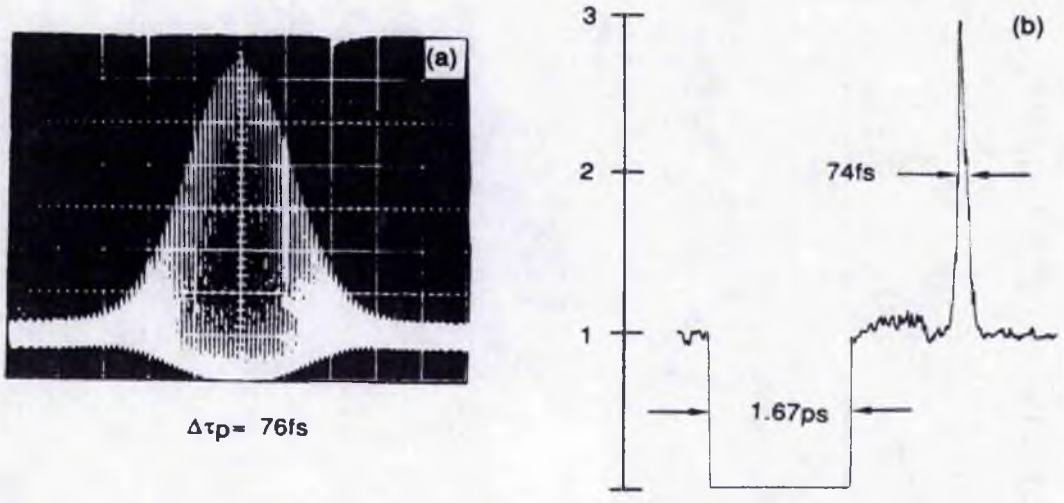

Fig. 8.9. Interferometric (a) and intensity (b) autocorrelation traces of 75 fs pulses from the CCM laser for a 21-cm-long erbium-doped control fibre.

In an attempt to make the pulse durations yet shorter the 0.3 mm thickness birefringent filter was either removed from the main cavity or its optical axis set parallel to the polarization direction of the laser beam so that the available lasing bandwidth would not be restricted. However, the measurements taken under these conditions showed that, rather than becoming shorter, the pulse durations from the CCM laser actually increased to ~130 fs. Observations of the pulses returned to the main cavity indicated that the feedback pulse durations were ~180 fs. A selection of typical temporal and spectral data thus obtained are presented in Fig. 8.10(a)-(d). It can be seen that the spectrum corresponding to the pulses returning from the control fibre had two principal peaks: one 'blue' and one 'red' with respect to the injected CCM spectrum [Fig. 8.10(a)]. One of these features was preferentially selected using an extracavity birefringent filter and polarizer combination. By carefully rotating the birefringent filter (setting its optical axis at an appropriate angle), either the blue or the red spectral peak could be selected with a relatively good discrimination as illustrated by Fig. 8.10(e), 8.10(g). It should be noted that the pulse duration associated with the red peak is approximately half of that of the CCM laser pulses (the shortest durations recorded were ~60 fs) whereas the pulses relating to the blue spectral peak are slightly broader than the CCM laser pulses. The generation of these spectral peaks are typical results of the action of self-phase-

modulation (Stolen and Lin 1978). The lack of symmetry in the spectrum evident in Fig. 8.10(c) most probably arises from the self-Raman effect. For this short length of fibre the overall Raman gain is not sufficiently large to dominate the SPM process as noted in Fig. 8.27 in Sec. 8.4.

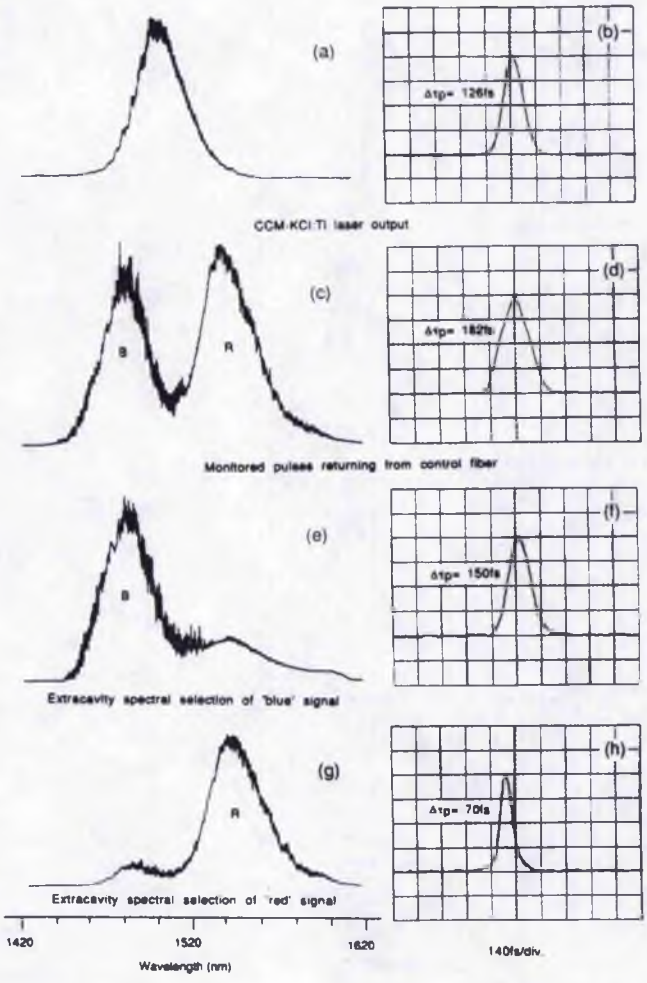

Fig. 8.10. Spectra and temporal characteristics of: (a), (b) — CCM KCl:Tl laser without intracavity birefringent filter; (c), (d) — pulses returning from fibre in the control cavity; (e), (f) — spectrally selected 'blue' component of return pulses; (g), (h) — spectrally selected 'red' component of return pulses.

The reason why the CCM laser can not produce shorter pulses when the birefringent filter is removed from the main cavity may be understood in the following terms. Firstly, in the later stages of pulse evolution in the CCM laser the presence of high peak-power pulses in the doped fibre gives rise to a large degree of SPM-induced frequency chirp.

The related interferometric interactions with the pulses circulating in the main cavity means that some portions of these interacting pulses could lose phase coherence and the mode-locking enhancement process is thus frustrated. This would also explain why the spectrally-broadened returning pulse [Fig. 8.10(c)] does not produce further spectral broadening in the CCM laser output. Secondly, the large value of 0.56 of the bandwidth (32 nm)-duration (126 fs) product for the CCM laser pulses [Fig. 8.10(a), (b)] implies that there is a large amount of frequency chirp on these pulses. Therefore, in this case chirp compensation elements would be needed in either of these two cavities for the purpose of ensuring that optimally short pulses are produced. The inclusion of a birefringent filter of suitable thickness would be expected to be very important because it serves to provide not only adequate bandwidth restriction but also offers a possibility of choosing the favored intracavity dispersion. Consequently, optimum interferometric interaction between the circulating and the return pulses is more readily established so that near-bandwidth-limited much shorter pulses can be obtained from the CCM laser. Methods of frequency chirp compensation, involving glass rods for example, have been used either inside or outside the composite cavity to successfully compress such pulses (Zhu *et al* 1990a, also see Ch.9)

8.2 Dependence on system parameters

For the coupled-cavity laser as shown in Fig. 6.3, many parameters or variables of the system can affect the laser performance. In addition to the fibre type used in the control cavity that can be selected according to requirement, the relative pulse intensities in the main and control cavities, the central lasing wavelength, the effective gain bandwidth, the cavity period mismatch and fibre length are all accessible variables. Obviously, the manner in which the changes in each of these parameters influences the performance of the laser and how these parameters are interlinked in respect of coupled-cavity mode locking are of fundamental importance.

In order to achieve acceptably good operation of the coupled-cavity mode-locked laser, it was observed that whenever the other system parameters had been preselected the

intrafibre power (P_f) must be within a specific latitude $P_{th} < P_f < P_M$. When P_f was less than a minimum of threshold power P_{th} the CCM laser did not exhibit a substantial enhancement of mode-locking and when P_f exceeded a maximum value P_M the laser did not operate in a suitably stable manner. Normally, within this latitude a range of output pulse durations could be obtained. If any of the system parameters was altered this latitude of operation would be changed (either shifted or reduced/enlarged). Therefore, his specific optical power range in the control-cavity fibre could be designated as an "operational-window". Investigations of how this window would be affected by the variation of the system parameters are described in the following subsections. (All the results presented have been obtained for the same type of Er-doped fibre as mentioned in the previous section).

8.2.1 Fibre length

Distinctive features in the plot of pulse duration versus P_f for three different lengths of fibre used in the control cavity can be seen in Fig. 8.11(a). For the 2-m-long fibre the CCM operation starts at a relatively low value of P_f (~ 4 mW) and the associated pulse duration is about 450 fs. As P_f is increased the pulse duration initially decreases to a minimum value of 320 fs and subsequently increases. When P_f = 12 mW the CCM process becomes ineffective because of system instability. A similar feature may be found for the 0.7-m-long fibre although the minimum pulse duration appears just before the laser operation becomes unstable. Within the operational latitude for the set-up having a 0.3-m-long fibre, however, this type of behaviour was not observed because the pulse durations decreased monotonically as P_f was increased.

The minimum optical power P_{th} required to achieve the coupled-cavity mode locking for various lengths of fibres is shown in Fig. 8.11(b). It can be seen that as the fibre length, L, increases P_{th} decreases accordingly, and it can be deduced that the products of $P_{th}L$ for higher P_{th} (associated with shorter fibre lengths) are always smaller than those that apply to lower P_{th} and longer L values. Such a characteristic shows a discrepancy of the SPM-induced nonlinear phase shift from the ordinary expression $\Delta\phi \sim IL$. This

deviation may be attributed to two effects. One is the possible involvement of the higher-order terms of the intensity-related nonlinearity in the cases of higher power levels. Another is the effect of the group velocity dispersion which under our experimental conditions leads to a reduction of the effective pulse intensity in the longer fibre lengths. On the whole, on the basis of the data shown in Fig. 8.11(a), (b), it may be concluded that CCM operation will generally be established under the conditions where the combination of either lower powers P_f and longer fibres give rise to the generation of broader pulses or higher values of P_f and shorter fibres lead to reduced pulse durations.

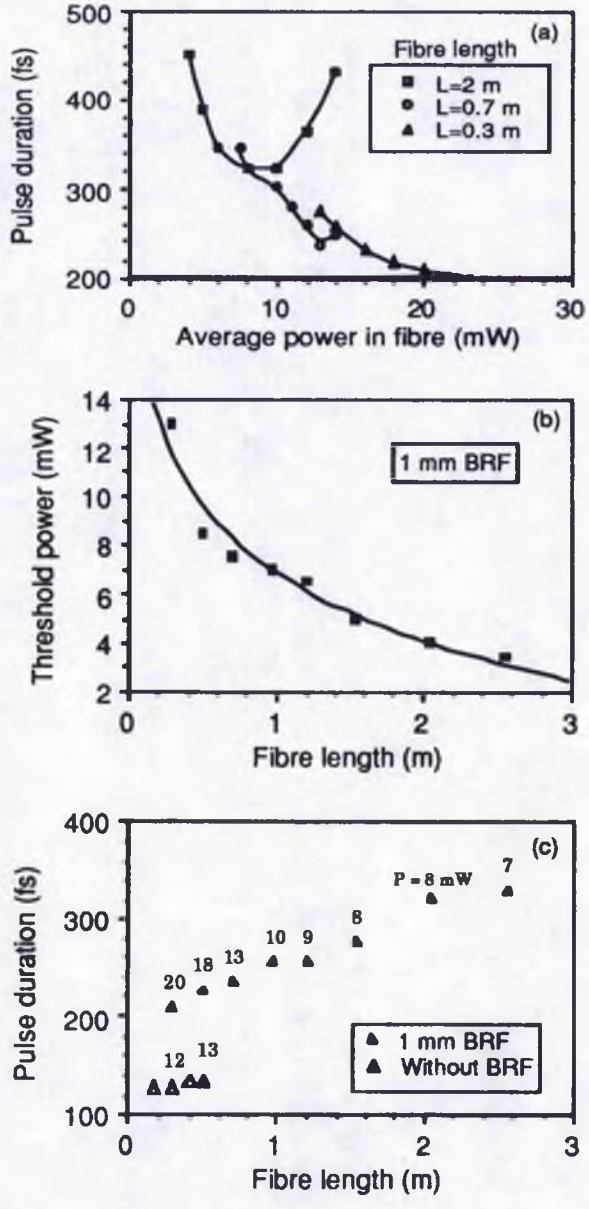

Fig. 8.11. (a) Operational windows of the CCM KCl:Tl laser with a 1-mm-thickness birefringent filter (BRF) for three different lengths of Er-doped control fibres. (b) Threshold power for achieving CCM operation as a function of fibre length. (c) Variation of CCM laser pulse duration with fibre length.

In Fig. 8.11(c) the variation of CCM laser pulse duration with the fibre length is indicated. From Fig. 8.11(a) it follows that for a given length of fibre the CCM laser pulses may have a range of durations, and so the points included in Fig. 8.11(c) represent data that have been taken from within operational ranges at each fibre length. The numbers associated with each datum in Fig. 8.11(c) are the average powers P_f at which the measurements were recorded. Basically these samples are the "working points" around the centre of the operational windows where the laser stability was a maximum. It should be pointed out that such a relation between the pulse duration and fibre length can be strongly influenced by the thickness of birefringent filter, which determines the permitted spectral gain bandwidth in the main cavity. This forms the subject matter of the next subsection.

8.2.2 Thickness of birefringent filter

It was found that thicker birefringent filters were required to ensure stable CCM operation when longer fibre samples were used in the control cavity. With short fibre lengths there is more tolerance on the thickness of birefringent plate but naturally the thicker plates restrict the bandwidth to the extent that this limits the duration of CCM laser pulses that can be established. As shown in Fig. 8.11(c), for the fibres shorter than 0.6 m, pulses obtained when the birefringent filter was removed from the main cavity are significantly shorter than those generated when a 1-mm-thick birefringent plate was used.

A particularly noteworthy feature is that when the birefringent filter was absent the appropriate optical power P_f was significantly reduced although the average output power from the main cavity remained unchanged. This latter observation can be understood in terms of the bandwidth considerations in the CCM process. Because thinner birefringent filters (or in the limit when the birefringent filter is removed) lead to a main cavity pulse with a larger $\Delta\nu\Delta t$ value (i. e. extended spectral spread and larger pulse duration) and correspondingly the amount of spectral broadening in the control fibre is relatively small, the ratio of the spectral intensity of the return pulse to that of the pulse circulating in the main cavity will be much higher than that when thicker filters are used. Thus to achieve

an appropriate spectral intensity ratio which is needed to initiate the coupled-cavity mode-locking process the optical power in control fibre must be reduced in the cases where less bandwidth limitation has been imposed on the main cavity. For the same reason it would be understandable that when thicker birefringent filters are used the main cavity pulses (with smaller $\Delta\nu\Delta t$ value this time) will have relatively high spectral intensities and so the threshold power P_{th} for the CCM process will increase. Consistent results can be also found from the data shown in Fig. 8.12(a) where the operating power ranges are indicated for a fixed length of optical fibre (28.5 cm) for three distinct regimes of spectral control. It should be pointed out that such an influence on the establishment of the CCM pulses has not been addressed by any of the current theories (Ippen *et al* 1989, Morin and M. Piché, 1989) which merely focus on the pulse shaping effect as a result of temporal addition of the return pulse to the main cavity pulse. From our experimental observations, however, it is justified to state that in the discussions of the physical mechanism for a CCM laser system the ratio of the return pulse to main cavity pulse should be considered in terms that include the pulse spectral intensity rather than simply the temporal profile.

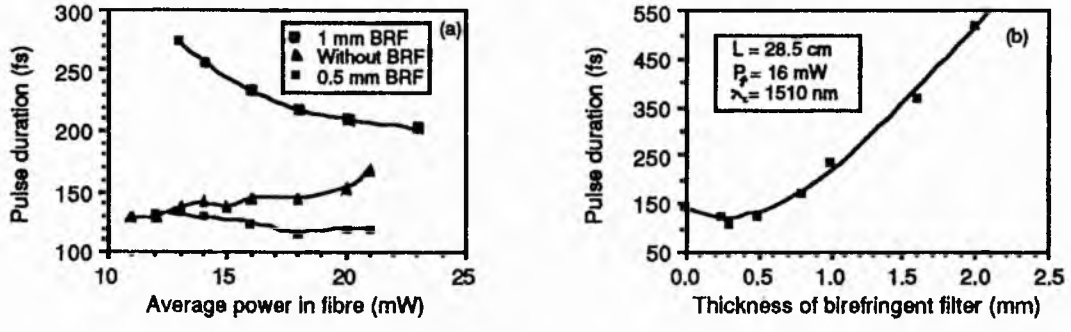

Fig. 8.12. (a) Operational windows of the CCM KCl:Tl laser for a 28.5-cm-long control fibre but with different thicknesses of birefringent filters used in the main cavity. (b) CCM laser pulse durations as a function of the thickness of birefringent filter.

From Fig. 8.12(a) it can be seen that for the laser having the 0.5-mm-thick birefringent filter the pulse durations are significantly less than those associated with the 1-mm-thick counterpart. When the birefringent filter was removed, however, the pulse durations did not become shorter but rather increased with higher values of power, P_f.

This is clearly illustrated by the plot of pulse duration versus filter thickness for a fixed P_f (~16 mW) given in Fig. 8.12(b). The output pulses from the CCM laser became shorter as the thickness of the birefringent filter was reduced to a value of 0.3 mm after which the pulse duration was seen to increase despite the fact that the maximum spectral bandwidth was obtained when no filter was used. These observations again indicated that without proper control of the CCM laser bandwidth the pulses tended to be so strongly chirped that the duration of the pulses could not be optimally compressed (see discussions in subsection 8.1.2). The data in Fig. 8.12(a) actually represent three possible operational states that are determined principally by the bandwidth limitation device in a CCM laser. These states may be described as (i) restricted bandwidth (1 mm BRF), (ii) excess available bandwidth (without BRF) and (iii) proper control of lasing bandwidth (0.5 mm BRF). At a power level, $P_f = 18$ mW the measured bandwidth-pulse duration products for these three cases were 0.32, 0.61 and 0.4 respectively.

8.2.3 Operating wavelength

During this experimental work it was also found that the operational window could be moved up and down by tuning the laser across its available gain bandwidth. Examples of the operational ranges for three selected central wavelengths are shown in Fig. 8.13(a). For the recording of these data a 1-mm-thick birefringent filter was used as the tuning element and the control fibre length was 28.5 cm. At a particular power [e.g. 16 mW in Fig. 8.13(a)] a plot of pulse duration as a function of wavelength can be obtained as shown in Fig. 8.13(b). This wavelength-dependent feature of the CCM operation could be attributed to two factors: one is the dependence of the transmission bandwidth of a birefringent filter on the corresponding operating wavelength (see Ch. 7); the other is the dispersive feature of the control fibre. With the other system parameters fixed, it is possible that an optimal operating wavelength exists at which the interplay between nonlinearity and the dispersion in the control cavity favours the efficient phase coupling between the return pulses and the main cavity pulses, and so shorter pulses can be generated.

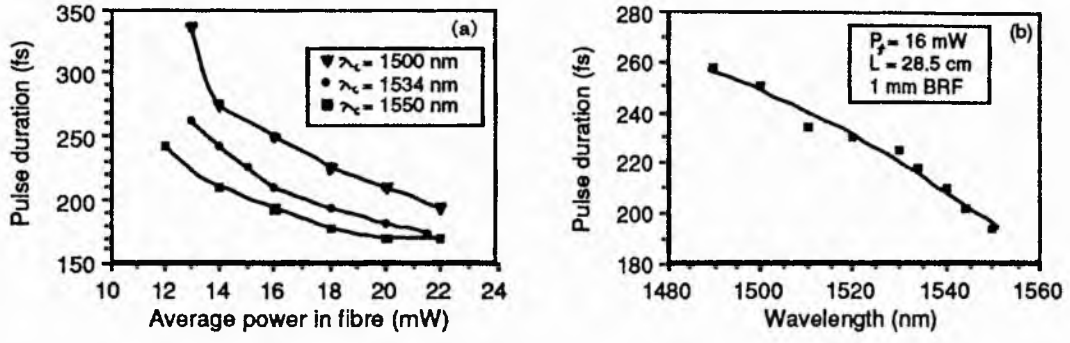

Fig. 8.13. (a) CCM laser operational windows when the laser was tuned to three different central wavelengths. (b) Dependence of CCM laser pulse durations on the operating wavelength.

8.2.4 Main cavity power

In Fig. 8.14 the relationship between the main cavity output power and the operational window of the CCM laser (16.5 cm long Er-doped fibre in the control cavity) is illustrated for the condition where there was no birefringent filter in the main cavity. The data in Fig. 8.14(a) were obtained under the condition where the pump power to the KCl:Tl crystal was continuously increased while the main cavity output power levels, P_o and the associated changes in the threshold power in the fibre, P_{th}, were simultaneously measured. It is clearly evident that as the main cavity power was increased the threshold power level P_{th} for achieving the CCM operation increased accordingly. Such a tendency further confirms that the required minimum nonlinear phase shift in terms of mode-locking threshold and steady-state stability experienced by the pulses propagating in the control cavity is directly related to the main cavity parameters. In other words, different ranges of pulse intensity, the effective gain bandwidth or the operating wavelength in the main cavity place particular demands on the control cavity parameters. This view is to be contrasted to that taken in the early studies of a soliton laser (Mollenauer and Stolen 1984), where the "absolute" power level in the control fibre was considered to be the only necessary prerequisite condition to ensure that second-order optical solitons would be generated.

The variation of pulse durations from the CCM laser as a function of the main cavity output power shown in Fig. 8.14(b) implies that an optimum average power level range ~70-80 mW can be deduced. It should be noted that in this case the power level in the

fibre, P_f, was fixed at 20 mW (except for the point as indicated) and thus the abscissae in Fig. 8.14(b) can be directly related to the spectral-intensity ratio of the return pulse to the main cavity pulse. Therefore this plot indicates that in order to generate the shortest CCM laser pulses an optimum ratio of the return pulse to the main cavity pulse intensities must be established.

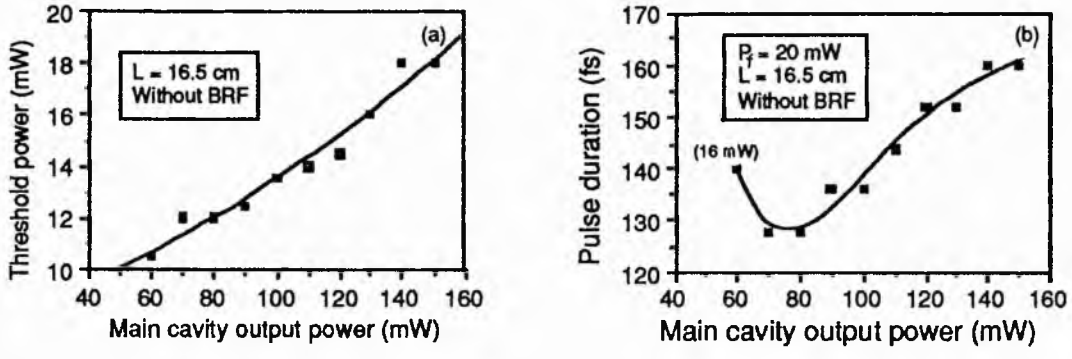

Fig. 8.14. CCM threshold power (a) and pulse duration (b) as a function of the main cavity output power.

8.1.5 Cavity length mismatch

The synchronization between the pulses returning from the control cavity and the main cavity pulses requires that the cavity lengths should be properly matched during the CCM operation. In practice this is observable as the existence of a small tolerence on the variation of any of the two cavity lengths. In this work it was revealed that within this tolerance range slight mismatches between the control cavity and the main cavity led to the generation of asymmetrical pulses and consequent asymmetrical spectral extensions in the control fibre (for detailed discussions on this see Ch. 9).

The variation of pulse duration with cavity length mismatch under the conditions of P_o = 70 mW, P_f = 16 mW and with a 1-mm-thick birefringent filter is included as Fig. 8.15. It is interesting to note that within the ± 30 μm cavity length mismatch the associated changes of the repetition frequency of CCM laser pulse train were only ± 20 Hz, which is much less than that associated with the cavity period mismatch. This could be caused by some self-compensation mechanism for the effective optical path length of the control cavity related to the large pulse shaping effect. (Note that the cavity length

mismatch reported throughout this thesis was achieved by adjusting the position of the retroreflecting mirror of control cavity). The actual pulse repetition frequency of the CCM laser is determined predominantly by the main cavity length although the existence of the control cavity gives the coupled-cavity laser its passive characteristics.

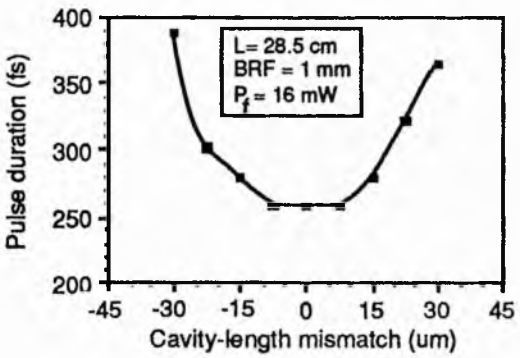

Fig. 8.15. Variation of CCM laser pulse duration as a function of cavity-length mismatch.

8.3 Influence of different control fibres

In the previous section we have concentrated on the effects of the various system parameters on the performance of our CCM colour-centre laser where a particular Er-doped optical fibre was incorporated. More generally, the influence of different control fibres on such a laser system have also been examined. For doing this each of seven distinct types of optical fibres have been used in the nonlinear external cavity. These fibre types were: three erbium related [two Er-doped with medium and low dopant concentrations and one Er-host (essentially Er-free) fibre], one Nd-doped, one dispersion-flattened, one dispersion-shifted and one standard commercial fibres. These samples are specified by a range of characteristics in terms of the group velocity dispersion and exploitable nonlinearity. The relevant parameters for these fibres are given in Table 8.1.

When a new control fibre was used the other system parameters, such as pump power, fibre length etc. were all kept as constant as practically possible so that a meaningful comparative assessment of the fibre behaviour could be made. The output of the main cavity laser was maintained at a fixed power level of 70 mW and no intracavity bandwidth limiting device was used during these experiments. (The optical power, P_f,

injected into the fibre could be varied from zero to an available maximum ~20 mW by rotating the variable attenuator included in the external cavity).

As mentioned previously, for a given control fibre, only a certain range of intrafibre power enables the coupled-cavity mode locking process to be initiated and sustained. At each power level within this permitted operational latitude the CCM laser normally produces pulses having a particular duration. When different types of fibre were incorporated into the control cavity, the variation of the output pulse duration with the effective intrafibre optical power would be expected to vary distinctively.

Table 8.1. Properties of the six fibre types*

Fibre type	Dopant conc.(cm^{-3})	$\Delta n \times 10^3$	Core diameter (μm)	λ_o (μm)	D(at 1.5μm, ps/km/nm)
Er-doped (I)	6×10^{18}	20	4.6	(1.45)	(2.6)**
Er-doped (II)	1.6×10^{17}	16	4.6	(1.43)	(4.1)
Er-free	—	20	4.6	1.66	-5.4
Nd-doped	$\geq 5\times10^{18}$	10	5.6	< 1.5	Unknown
D-shifted	—	9	~6	1.56	-4.1
D-flattened	—	—	~7	1.44†	1
Standard	—	—	8	~ 1.3	~15

* The parameters for the first five fibre types were provided by STC Technology Ltd and that for the dispersion-flattened fibre is from Philips International BV. The data in brackets represent predicted values.

** The sign of the group velocity dispersion predicted for this fibre is inconsistent with observed experimental data because no temporal compression has been recorded at the wavelength of 1.5 μm. We therefore refer to this Er-doped fibre in the text as of normally-dispersive type.

† This fibre has two zero dispersion wavelengths at 1.44 μm and 1.62 μm.

8.3.1 Typical experimental results

Of the seven fibres (all having lengths ~ 30 cm) it was found that while the standard fibre is used in the control cavity no coupled-cavity mode locking can be achieved within the available intrafibre power range. For the other six fibres the dependences of the CCM laser pulse duration on the average injected optical power level are shown in Fig. 8.16, where Fig. 8.16(a) for three normally-dispersive fibres and Fig. 8.16(b) for three anomalously-dispersive fibres. It can be seen that with the group of normal-dispersion fibres reliable CCM operation was obtained over a relatively large range of optical

powers. This is in contrast to those fibre samples having anomalous dispersion around the operating wavelength, for which a much more limited working range was observed.

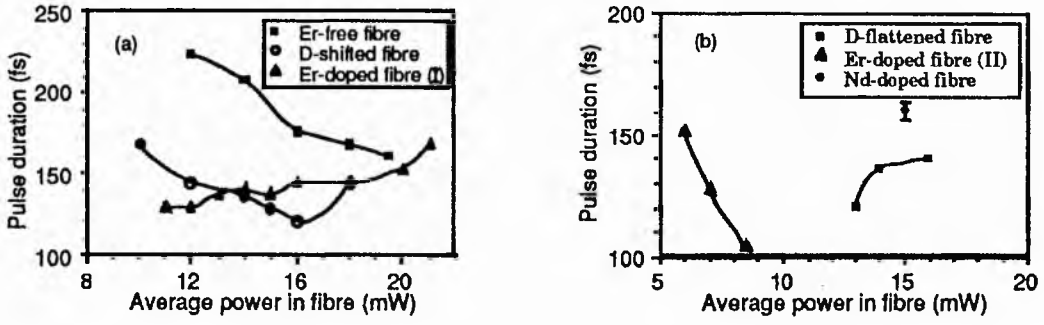

Fig. 8.16. Variations of the CCM laser pulse duration as a function of average power in normally-dispersive (a) and anomalously-dispersive (b) fibres involved.

Another distinct operational feature arising for these two groups of fibres is that the pulse durations increased during propagation in the normally-dispersive control fibres whereas temporal compression of the pulses occurred in the anomalously-dispersive counterparts. Representative temporal measurements which confirmed the pulse broadening in the normal-dispersion Er-doped fibre (I) and pulse compression in the dispersion-flattened fibre are reproduced in Fig. 8.17(a), (c) and Fig. 8.18(a), (c) respectively. The distinct shapes of the interferometric autocorrelation traces, particularly for the pulses returning from the control cavity, can be related to the difference in phase modulation (or frequency chirp) to which the pulses are subjected in these two fibre types (extensive study of the feature relating to the pulses coupled into and returned from the Er-doped control fibre is included in Ch. 10). Pulse durations can be readily deduced from the intensity autocorrelation traces such as those shown by the single bright line in Fig. 8.17(a), (c). The corresponding spectra for the CCM laser pulses and the feedback pulses from the control cavity are shown respectively in Fig. 8.17(b), 8.18(b). It is evident from these data that the self-phase-modulation induced spectral broadening occurs in both fibres but the pulses are temporally broadened from 128 fs to 172 fs in the Er-doped fibre and compressed from 140 fs to 116 fs in the dispersion-flattened fibre.

By referring to the data of Fig. 8.17(b), 8.18(b) it can be seen that the spectral broadening process appears to be more efficient in the Er-doped fibre than for the dispersion-flattened fibre. The bandwidth of 29 nm for the CCM laser pulse spectrum ($\Delta\nu\Delta t = 0.49$) more than triples during propagation in the Er-fibre (I) [(see Fig. 8.17(b)]. Interestingly, the broader CCM laser bandwidth (46 nm) produced when the dispersion-flattened fibre is employed ($\Delta\nu\Delta t = 0.86$) is less than doubled during transit in the control fibre. Also the large steady-state bandwidth that is available for this CCM operation with the dispersion-flattened fibre offers the possibility of achieving extremely short durations if transform-limited pulses can be generated. (This is consistent with the results reported by Mitschke and Mollenauer (1987) who obtained pulse durations as short as 60 fs with a similar type of fibre in their soliton laser). From our spectral measurements the bandwidths have been seen to be as large as 50 nm and so if appropriate chirp compensation can be achieved through using prisms (Fork 1986) or glass rods (Zhu *et al* 1989c) in the cavities then pulses having durations of less than 50 fs could be produced.

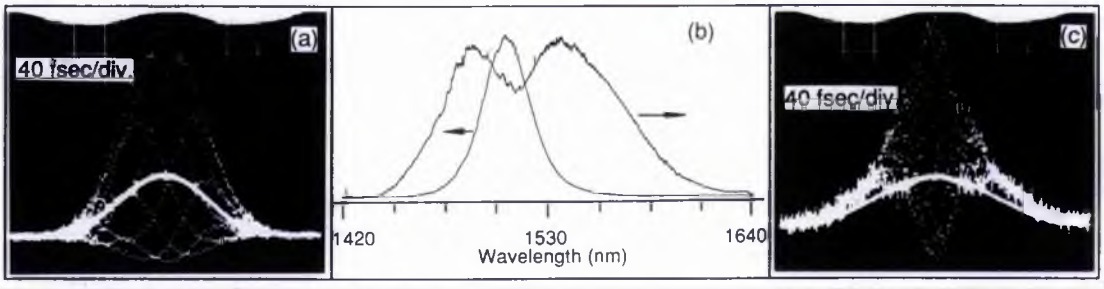

Fig. 8.17. Autocorrelation traces for the (a) CCM laser pulses, (c) pulses returned from the control cavity and (b) corresponding spectra. (These results are obtained at an optical power level of P_f=12 mW in the Er-doped fibre (I). The single bright lines in (a) and (c) relate to the intensity autocorrelation traces).

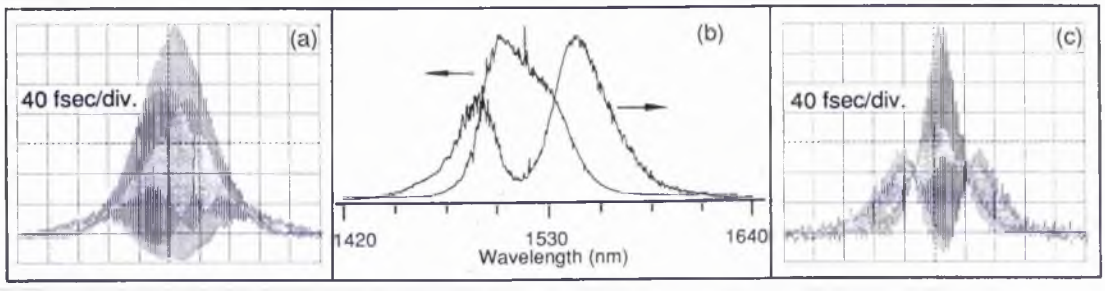

Fig. 8.18. As for Fig. 8.17 except for the dispersion-flattened fibre with P_f = 16 mW.

Of the six fibres that lead to the CCM operation the fibre sample having a relatively low doping concentration of erbium [Er-fibre (II)] was found to require the lowest level of injected power to initiate and sustain reliable CCM operation [see Fig. 8.16(b)]. It was observed that above 9 mW any increase of the intrafibre power, P_f, led to an unstable but quite distinct operational regime, in which a narrow and enhanced peak was evident in the recorded spectra. This spectral peak with a linewidth ~ 2 nm, on top of a broader spectral profile, could be progressively shifted towards shorter wavelengths by increasing the control cavity length and vice versa (see Fig. 8.19). The intensity of this peak feature could be minimized by adjusting the reference level in PZT servo-control system but it could not be removed unless the process of mode-locking enhancement was stopped. Associated with the appearance of this spectral peak the autocorrelation traces for the laser pulses showed obvious fluctuations with nearly regular ripples. The pulsewidths relating to the spectra shown in Fig. 8.19(a)-(c) are 104 fs, 108 fs and 104 fs respectively. It is also noteworthy that similar spectral and temporal behaviour has also been observed for the dispersion-flattened fibre where the critical power to reach this unstable operational status was ~ 16 mW.

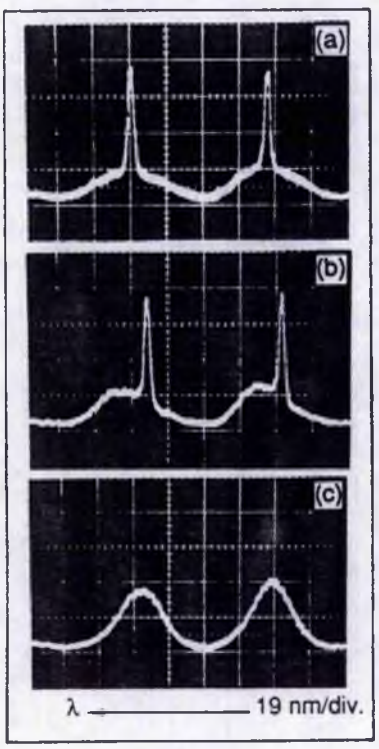

Fig. 8.19. CCM laser spectra for the Er-doped fibre (II) obtained from a scanning Fabry-Perot interferometer. (a) P_f = 12 mW, (b) as for (a) but the control cavity length is increased by 7 μm, (c) P_f = 8.5 mW.

Incorporation of the Nd-doped fibre in the control cavity gave rise to a stable CCM laser operation at essentially one specific power level, which renders this kind of fibre a rather unpromising candidate for the CCM scheme. Despite this, however, it is worth mentioning that for the 150 fs CCM laser pulses the feedback pulses from the control cavity had durations of only 96 fs. This represents the largest observed compression ratio of the three anomalously dispersive fibre types that were studied here. Spectral and temporal data relating to the pulses into and out of the Nd-doped fibre obtained at the "single working point" are shown in Fig. 8.20. It can be seen that the spectrum broadened in the fibre from 18.5 nm to 25 nm, which when combined with the associated pulse durations implies bandwidth-pulse duration products of 0.39 and 0.33 for the CCM laser pulses and for the feedback pulses respectively. This decrease in bandwidth-pulse duration product for the return pulses has not previously been reported for any other type of control fibre.

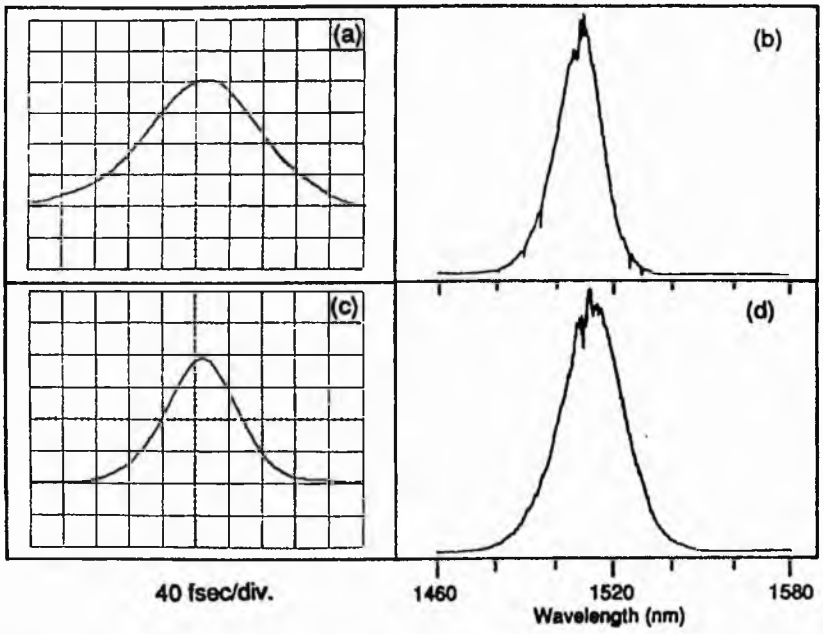

Fig. 8.20. Intensity autocorrelation traces and the corresponding spectra for the CCM laser pulses (a,b) and the associated pulses returned from the Nd-doped control fibre (c, d) .

The Er-doped fibre (II) in the normal-dispersion fibre group [Fig. 8.16(a)] provided the largest operational latitude in terms of an intrafibre power range. Extensive studies of the use of this type of fibre in a CCM laser have been partly described in Sec. 8.1 and more comprehensively in Sec. 8.2. The increase in pulse duration as the power, P_f, is

raised [see Fig. 8.16(a)] is symptomatic of the lack of adequate spectral bandwidth control during the overall CCM process. This gives rise to the presence of excess frequency chirp which serves to frustrate the degree of enhanced mode locking (see Sec. 8.1, where it has been shown that by inserting a birefringent filter of 0.3 mm thickness in the main cavity, stable CCM laser pulses having durations ~75 fs have been obtained).

The data obtained for the Er-free fibre and that for dispersion-shifted fibre in Fig. 8.16(a) indicate that the pulse durations decreased as the coupled powers increased except that, for the latter, when $P_f > 16$ mW the pulse duration increased. The Er-free fibre is the host medium that is prepared for accepting the erbium dopant and the performance of the CCM laser incorporating this fibre is quite different from that for the two Er-doped fibres. Typical spectra for the CCM laser pulses (a) and the pulses returned from the Er-free fibre (b) are as shown in Fig. 8.21 for which the associated pulse durations were measured to be 208 fs, 288 fs respectively. It can be seen that for this fibre sample the degree of spectral broadening experienced by the pulses in the control cavity is obviously smaller than that relating to Er-doped and dispersion-flattened fibres (Fig. 8.17, 8.18). Nevertheless, because of the much broader temporal duration of the pulses the value of $\Delta\nu\Delta t$ products under this circumstance is still high and from the data of Fig. 8.21 and the pulse durations given above the bandwidth-pulse duration products of 0.73 for the CCM laser pulses and 1.96 for the feedback pulses can be deduced.

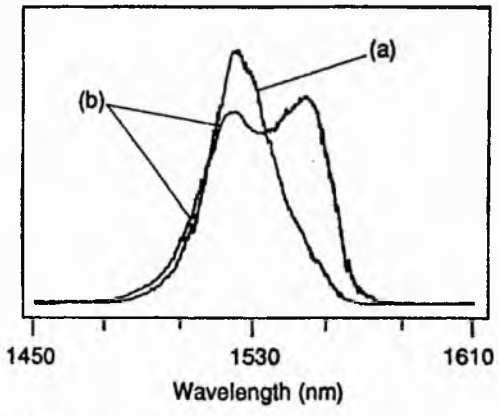

Fig. 8.21. Spectra for the (a) CCM laser pulses and (b) pulses returned from the control cavity for the Er-free fibre with $P_f = 13$ mW.

8.3.2 Discussions

From the experimental data presented above, it can be seen that the laser behaviour is strongly influenced by the choice of fibre. Proper coupled-cavity mode-locking operation

relating to the fibres having negative group velocity dispersion generally has a rather strict requirement on the optical power coupled into the fibre, and in these cases the laser system is much more sensitive to the amount of cavity length mismatch as well. The reason for this may be attributed to the difficulties of achieving an appropriate phase match in a laser system into which an anomalously-dispersive fibre has been incorporated. It is now well established (Zhu *et al* 1989, Ippen *et al* 1989) that a suitable phase match must exist between the radiation in the main cavity and that returning from the nonlinear external cavity if optimum coupled-cavity mode-locking is to be achieved. For anomalously-dispersive fibres the solitonic effect can exert a relatively large and complicated phase modulation on the return pulses. Consequently, to obtain a suitable phase match with the main cavity both the linear and nonlinear relative phase shifts (determined by cavity length mismatch and the coupling power respectively) must be within an appropriate range. Such a mechanism may also be invoked to account for the fact that although temporal compression arises in all three anomalously-dispersive fibres the associated CCM laser pulses are not necessarily shorter than those obtained using normal-dispersion control fibres.

It has already been observed that there is a required minimum intrafibre power level (or threshold power P_{th}) to initiate the CCM operation and for a fixed fibre type this threshold, P_{th}, depends upon the main cavity parameters (see Sec. 8.1). From Fig. 8.16 it can be seen that when the parameters of the main cavity are fixed, quite different values of P_{th} apply to the various fibre samples. This may be understood by regarding all the fibres as pure SPM media and assuming that each fibre type exhibits a characteristic amount of exploitable nonlinearity. Unfortunately this is not the case in practice, because the presence of different types of dispersion will make a major difference to the actual nonlinear phase shift. For fibres having the same core cross-section, same n_{2I} value and same absolute dispersion parameter $|D|$, it is expected that a negatively dispersive fibre will lead to lower P_{th} because of the pulse compression due to soliton effect which causes an increase in effective peak intensity. It is, therefore, justified to conclude that the

difference in the CCM laser performance for different control fibres is connected with the distinct features of these fibres in the aspects of both dispersion and nonlinearity.

The occurrence of the sharp spectral peak shown in Fig. 8.19 most likely results from an excessively large nonlinear phase shift imposed on the feedback pulses during each transit in the control fibre. It implies that for a proper CCM operation, in addition to the required minimum nonlinear phase shift, an upper limit of the value of Φ_{NL} for the return pulses also exists even under the condition that no other nonlinear effects except SPM are involved. This can be expressed as $(\Phi_{NL})_{min}<\Phi_{NL}<(\Phi_{NL})_{max}$, where $(\Phi_{NL})_{min}$ is associated with the threshold power condition and $(\Phi_{NL})_{max}$ is the tolerated maximum value of Φ_{NL}. In the steady state Φ_{NL} can be derived from the degree of spectral extension observed in spectral measurements such as those shown in Fig. 8.17(b), 8.18(b). Normally, as P_f increases the spectral extension is correspondingly enlarged. But when P_f increases to a certain level this spectral expansion no longer occurs and the laser operation becomes unstable. This is likely to be the case where Φ_{NL} is sufficiently close to $(\Phi_{NL})_{max}$ and an estimate of $(\Phi_{NL})_{max}$ can thus be made. From our spectral data it can be estimated that $(\Phi_{NL})_{max} < 2\pi$.

It is believed that during the processes involved in establishing coupled-cavity mode locking the nonlinear phase shift experienced by the pulses injected into the fibre would increase with successive roundtrips until a steady state has been reached. But, if the magnitude of Φ_{NL} has already increased to 2π before a steady state is found, the coupled-cavity mode locking would not become stable. Such a situation would be more likely to occur for the CCM system incorporating an anomalously-dispersive fibre since larger nonlinear phase shifts may be promoted by the temporal compression due to solitonic influences. This is borne out in these experiments where the CCM laser operation associated with the three normally-dispersive fibres does not become unstable within the available optical power range, because the temporal broadening effects may sufficiently reduce the effective optical peak intensity such that the nonlinear phase shift, Φ_{NL}, is always less than 2π.

It is known that the extent of pulse broadening in the normally-dispersive fibre is related to the magnitude of group velocity dispersion (GVD). Large values of GVD means strong temporal broadening of the propagating pulses and the associated reduction in the peak intensity implies smaller nonlinear phase shifts. For a CCM laser, this means that the total nonlinear effect can be frustrated by a larger group velocity dispersion, such that the CCM laser pulses produced under these circumstances will be broader.

8.4 Involvement of other optical nonlinearities

When the optical power coupled into the control cavity is sufficiently high or the length of the control fibre is sufficiently large other types of optical nonlinearity, such as modulational instability, self-Raman effect etc. may also be involved in the coupled-cavity mode locking process. The appearance of these non-SPM nonlinearies in the control fibre while the short pulses evolve distorts the regular spectral broadening induced by self-phase modulation. As a consequence this can influence the generation of shorter pulses in that the phase coupling of the longitudinal modes in the composite-cavity arrangements can be seriously compromised.

8.4.1. Influence of modulational instability

It has been briefly mentioned that a close similarity exists between the observed CCM laser behaviour illustrated by Fig. 8.1 and those reported by Tai *et al* (1986) on the modulational instability (MIS) recorded for the pulses propagating through an anomalously dispersive fibre. The observed fluctuations evident in the autocorrelation trace at $P_f \sim 25$ mW in Fig. 8.1 are believed to be the signature of the involvement of MIS in the coupled-cavity mode-locking process. When P_f is larger than this power level, the spectral peak caused by MIS in the fibre experience an exponential growth.

From Eq. (5.76b) in Ch. 5, a relationship between the sideband separation caused by modulational instability and the intrafibre power can be derived. In substituting experimental parameters into Eq. (5.76) and using an effective area $A_{eff} \approx 10^{-6}$ cm^2, we obtain

$$\Delta\lambda = 0.45\sqrt{P_p[W]} \ \text{[nm]} \tag{8.1}$$

For an average power of P_f = 22mW and a pulse duration of 360 fs (Fig. 8.3), the associated peak power is about 700 W. Substitution of this value into Eq. (8.1) gives $\Delta\lambda$ = 12 nm. This result is fairly consistent with the experimental observations shown by Fig. 8.1(e), (f), where $\Delta\lambda$ is 10.5 nm. Fig. 8.22 shows the modulation sideband shift $\Delta\lambda$ as a function of the peak power in the fibre where both experimental and theoretical [Eq. (8.1)] data are included. It can be seen that over the power range shown in Fig. 8.22 the observed modulation sideband shifts are almost constant, which is to be contrasted to the theoretical prediction. It is worth noting that a similar observation has been reported by Tai *et al* (1986) for their single pass experiments, but in our case the deviation is distinctly larger. The reason for this could be that as the power in the fibre increases a more marked depletion of the injected CCL carrier signal arises through both MIS and SPM effects, which leads to a deviation from the theoretical formula Eq. (5.73a) for which source-power depletion has been neglected.

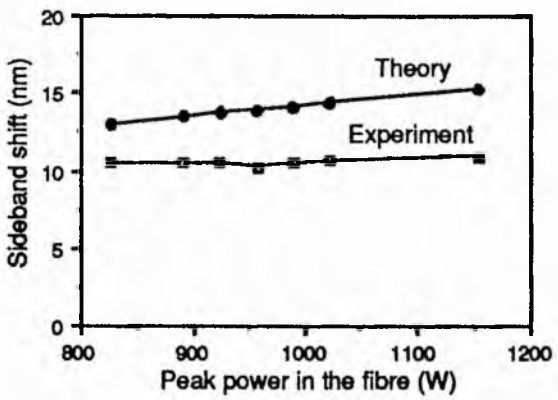

Fig. 8.22. MIS-induced sideband shift plotted as a function of the peak power in the fibre.

Another means of inferring the existence, or otherwise, of the MIS effect is to check whether the modulation signal can experience a threshold gain in the control cavity fibre during the CCM laser operation. Subsituting P = 700 W and a fibre round-trip length (2L) of 5.6 m into Eq. (5.78) yields

$$\alpha 2L = 2.9 \qquad (8.2)$$

This gain factor is about six times lower than that normally specified as the threshold criteria for other nonlinear effects such as stimulated Brillouin scattering and stimulated

Raman scattering (Stolen 1980). However, in our case we need not expect this value to satisfy a defined exp(21) or exp(16) gain threshold, because in the CCM laser system the fibre is within a resonator and so a multiple-pass influence is likely to be present. It is reasonable to assume a minimum effective round-trip number of 10, such that from Eq. (8.2) the estimated gain of exp(29) would significantly exceed the threshold requirement.

A further example of a CCM laser spectrum with peak features arising through the influence of MIS has been reproduced as Fig. 8.23(d). For the sake of comparison, the corresponding spectrum of the CCL itself (obtained by blocking the control cavity) is recorded in this plot [Fig. 8.23(c)] with the same wavelength and intensity scales. It can be seen that the longer wavelength spectral peak has substantially overlapped with the CCL spectrum, which may be regarded as a central carrier signal band. The shorter wavelength peak is the sideband induced by MIS. The reason why only one sideband exists instead of one on either side of the central frequency as observed by Tai *et al* (1986) is attributable to the wavelength transmission characteristics of the birefringent filter in our main cavity. This filtering effect can also be recognized by the spectra shown in Fig. 8.24, where the spectrum of the CCM laser 8.24(a), the spectrum of pulses out of fibre 8.24(b), as well as the spectrum of the CCL laser alone 8.24(c) were recorded on the same wavelength scale. It can be seen that compared with the spectrum out of the fibre the short wavelength sideband peak which emerges from the main cavity is significantly attenuated. Moreover, to obtain access to a wide bandwidth the birefringent filter was tuned to enable the colour-centre laser to operate at longer wavelengths around 1520 nm (~12 nm from the gain center) and as a consequence the MIS-induced signal was regularly observed at shorter wavelengths. Alternatively, by tuning the colour-centre laser to a shorter wavelength around 1490 nm the MIS-related spectral features were recorded at wavelengths exceeding that of the CCL.

The kinetics of pulse evolution for these conditions in the CCM laser system may be briefly reviewed in the following way. When the CCL pulses are injected into the fibre in the control cavity, SPM gives rise to coherent spectral broadening and this becomes an accumulative process in the coupled-cavity configuration. As mentioned previously, the

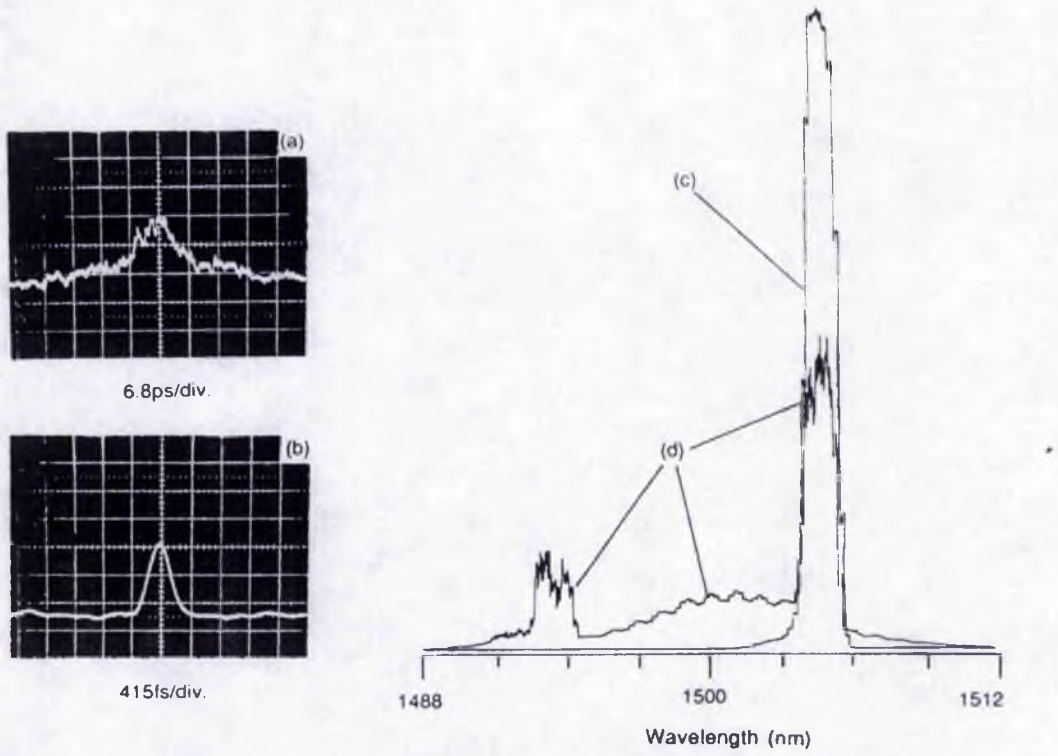

Fig. 8.23. SHG intensity autocorrelation traces for (a) KCl:Tl laser alone, (b) CCM laser and the corresponding spectra (c), (d) respectively.

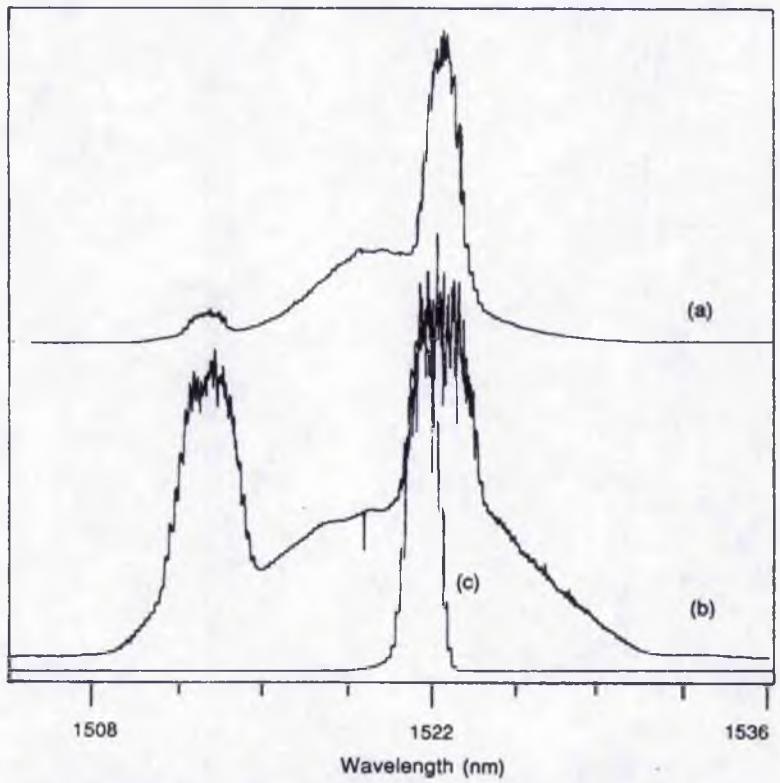

Fig. 8.24. Spectral bandwidth limitation imposed upon the CCM laser by the intracavity birefringent filter.

interplay in the gain medium between the spectrally-broadened control-cavity pulse and the pulse circulating in the main cavity leads to an enhanced phase-locked spectral bandwidth. This process continues until a bandwidth limitation (which could exist in either cavity) is reached and steady-state spectral characteristics are thus established. We believe that the central broad spectral feature seen in Fig. 8.23(d) (oscillating ripples result from a beamsplitter interference effect) is associated with the steady-state phase which leads to the overall character of the recorded autocorrelation trace [Fig. 8.23(b)].

When MIS is present other effects must be considered because for optical powers above the MIS threshold, part of the energy at the carrier frequency would be transferred to the signal at the sideband frequency as deduced from Eq. (8.1). Competition may therefore exist between the SPM and the MIS spectral broadening or shifting effects which ultimately influence the efficiency of the mode-locking enhancement process for the CCM system. It is expected that, in general, the modes at the sideband frequency [Fig. 8.23(d)] would not be correlated with the other portion of the broadened spectrum. Thus this peak spectral feature induced by MIS could have a perturbative effect on the CCM laser, which would account for the ripples which appear on the wings of the autocorrelation traces [see Fig. 8.23(b)]. It is noteworthy, however, that although these MIS-induced spectral features exist, the broad spectral component contributed by SPM still dominates and consequently the modulation depth on the corresponding autocorrelation traces is quite small, in contrast to the data from the single-pass experiments described by Tai *et al* (1986). In our work, for the sideband shift of 11 nm, the corresponding modulation period in the time domain is given by

$$T = \frac{\lambda^2}{\Delta\lambda c} \approx 0.7 \text{ ps} \tag{8.3}$$

which is comparable to the pulse duration. Consequently an intensity modulation is more readly observable on the wings rather than the peak of the autocorrelation profile.

In order to avoid the detrimental effect caused by MIS and thereby achieve optimized stability from the CCM laser over an extended range of powers into the control fibre, two effective measures have been demonstrated in our work. One is to impose a bandwidth

restriction in the main cavity by using a thicker birefringent filter. Another is to improve the selectivity of the PZT-servo system to respond to an error signal which more precisely represents the phase match requirement of the SPM signal rather than that relating to MIS.

The implementation of the first method is quite straightforward. When a 1-mm-thick birefringent filter was used the spectral peaks caused by the MIS effect were always observed when P_f satisfied the threshold power requirement. Substitution of this filter by one of 4 mm thickness gave results as illustrated in Fig. 8.25 where it can be seen that over the power range available the dependence of pulse duration t_p on the power P_f is quite different from that shown in Fig. 8.2, and no peak features were recorded in the corresponding spectra. An inevitable limitation of this method is that as a result of bandwidth restriction in the main cavity the overall pulse durations from the CCM laser are increased.

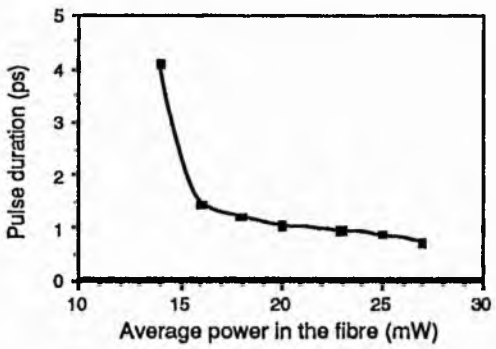

Fig. 8.25. Pulsewidth variation with power P_f for the CCM laser, having a 4 -mm-thick birefringent filter.

The second method is based on the understanding that the signal which is associated with SPM-induced spectral broadening will have different phase matching requirements from those associated with the MIS sidebands. Therefore, instead of taking the error signal for adjusting the control cavity length directly from beamsplitter S2 (see Fig. 6.3, note that this signal is an averaged combination of both SPM-broadened spectrum and MIS-induced spectral peaks), the signal was taken via the monochromator. By this means, the component of the error signal contributed by MIS could be filtered out and consequently, an error signal which relates more specifically to the phase match between

the remaining pulse in the main cavity and the SPM return pulse is obtained. With this selection of error signal, we have been able to stabilize the CCM laser system at the power levels of P_f from 22 mW to 25 mW and obtained pulses with symmetrical spectra that were free from peak features, and autocorrelation traces having no evidence of fluctuations. This indicates convincingly that the MIS-induced spectral peaks have been effectively suppressed.

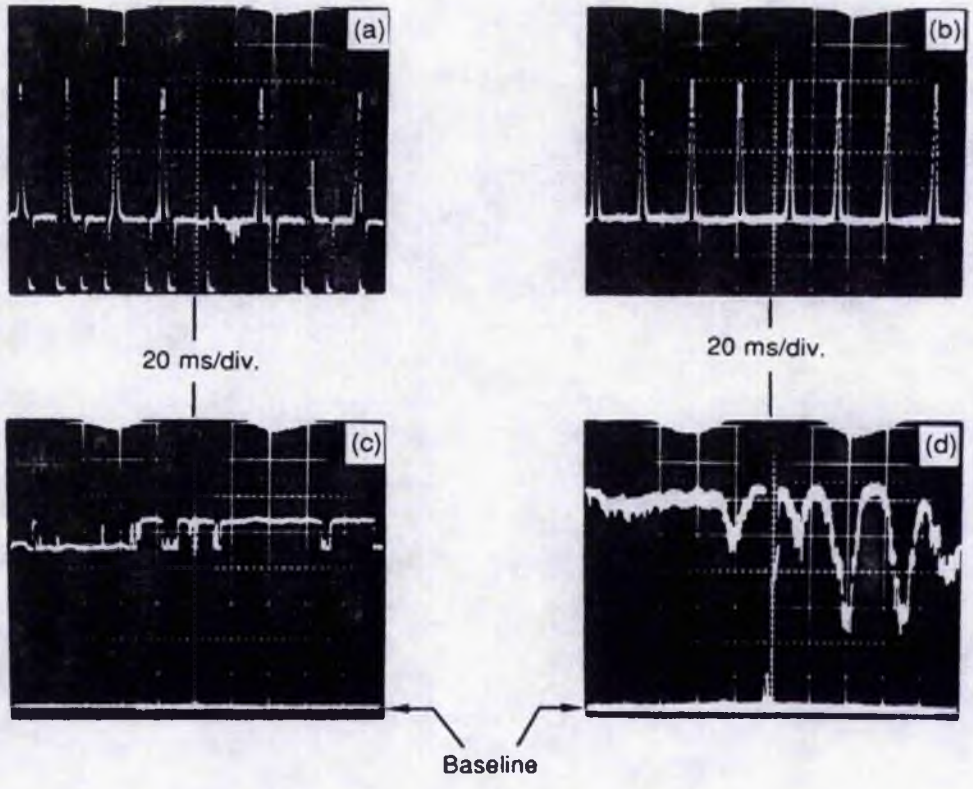

Fig. 8.26. Sequence of SHG autocorrelation profiles for the CCM laser obtained when the cavity length control servo system received the error signal from (a) beamsplitter S_2 and (b) via the monochromator. The corresponding error signals are given in (c) and (d) with baseline as indicated.

Fig. 8.26(a), (b) represent a comparison between the SHG autocorrelation traces from the CCM laser recorded with the two different error signals. Error signals derived from the beamsplitter, S2 directly [Fig. 8.26(c)] and via the monochromator [Fig. 8.26(d)] were respectively used for the cavity-length servo adjustments [note that when Fig. 8.26(a), (b) were produced all the other experimental conditions were unchanged]. It can be seen that the error signal involving the monochromator displays higher fluctuations and also a

higher temporal resolution, which probably allows the servo system to respond promptly and precisely, driving the control cavity into a proper matched condition.

8.4.2 Influence of self-Raman effect

It has been mentioned (subsection 8.1.2) that as the coupling power into the control cavity (30 cm, Er-fibre) was further increased from the status where the data Fig. 8.8 were obtained the laser output gradually became unstable. In these cases the shape of the autocorrelation trace was seen to change noticeably, which implied some variations in pulseshape. Under these higher-power conditions (P_f = 24 mW) a slight alteration in the reference level of the cavity-length-servo system led to the intensity autocorrelation profile and corresponding spectral characteristics shown in Fig. 8.27(a), (b) respectively. The two spectral peaks in Fig. 8.27(b) are separated by 24 nm which is substantially smaller than the value that can be attributed to the peak gain characteristics of Raman scattering in the silica fibre (Stolen 1980) at 1.5 μm. However, this may be explained in terms of the self-Raman effect (see Sec. 5.2) by which the soliton self-frequency shift has been interpreted (Gordon 1986).

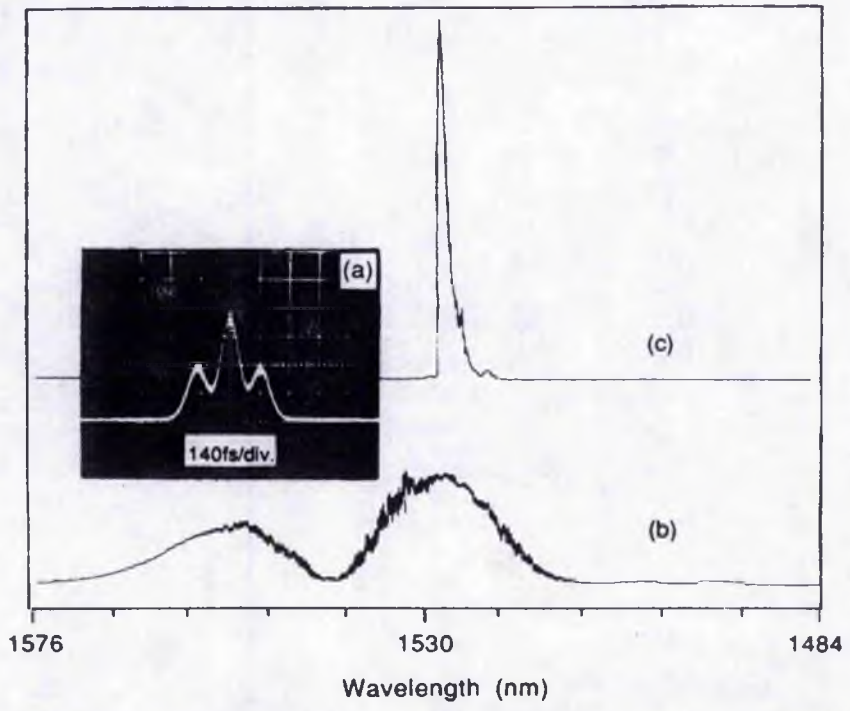

Fig. 8.27. Self-frequency shift phenomenon observed from the CCM laser. The real-time autocorrelation trace (a) corresponds to the CCM laser spectrum (b). The spectrum for the KCl:Tl synchronously-pumped colour-centre laser is included as (c).

It should be noted that the spectral peak in the shorter wavelength band in Fig. 8.27(b) is centred closer to the wavelength of the injected colour-centre laser spectrum [Fig. 8.27(c)]. Therefore, compared to the spectrum shown in Fig. 8.8, we believe that in the early stages of the CCM operation, it is this spectral peak that initially evolves and progressively expands. The coherent addition of this spectrally broadened radiation (due to SPM) to that corresponding to that of the pulse circulating in the main cavity contributes to the process of coupled-cavity mode-locking whereby the duration of pulses out of the main cavity become significantly shorter and the optical peak power in the fibre increases accordingly. This pulse-narrowing process takes place over many roundtrips until the peak power in the fibre reaches a level at which the pulse spectral intensity can provide sufficient Raman gain so that the longer wavelength components are "self-amplified". This process thus leads to an effective energy transfer that accentuates the spectral growth towards longer wavelengths. Ultimately, the spectral peak at the longer wavelengths [Fig. 8.27(b)] is generated and because of dispersive effects in the fibre, a satellite pulse would be produced. This is consistent with the observed autocorrelation trace in Fig. 8.27(a) where the recorded triple peak feature corresponds to a double-pulse temporal profile[3].

Further evidence of the involvement of the self-Raman effect in the coupled-cavity mode locking process can also be found in the spectra for the pulses returned from the control cavity as shown in Fig. 8.28. These data were obtained for a slightly shorter fibre length (L_f=21 cm) under the similar contidition to those when the results in Fig. 8.10 were taken, but the differences for this latter situation are that no birefringent filter was used and only fluctuations (not separated pulses) were observed in the time domain. The noise spike at the centre of the trace (d) [also traces (f) and (g)] roughly indicates the

---

[3] It is interesting that in spite of the existence of such a self-frequency shift the CCM laser can still be stabilized to certain extent, which at least provides the possibility to record the result shown in Fig. 8.27. It is expected that when the two pulses exist the requirement on the phase match in such a two-cavity system must be more critical or restricted than that for a single pulse. Moreover, because of the dispersion in the fibre, each time the double pulses pass through the control cavity the two components would be further separated. Therefore, there must be some dispersion compensation effect in the gain medium, which pulls the stretched pulses back to the original separation. Without such a dynamical balance it would have been impossible to observe the three-peak autocorrelation trace from the CCM laser under these experimental conditions.

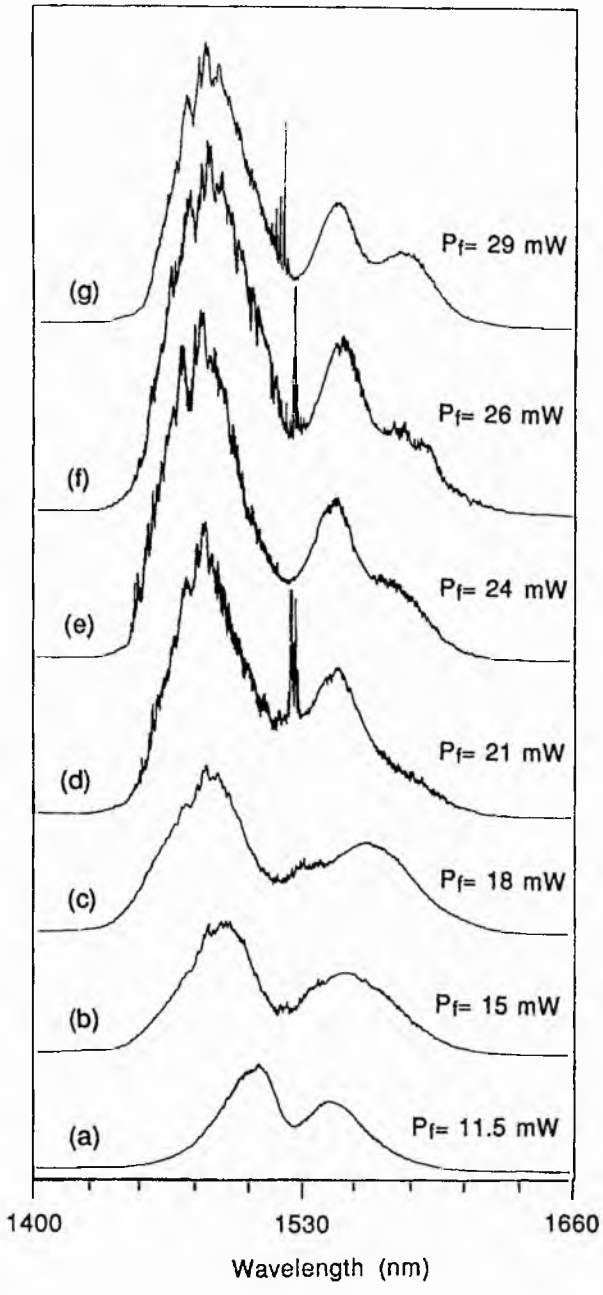

Fig. 8.28. Variation of the spectra as a function of intrafibre power measured for the pulses returned from the control cavity during the coupled-cavity mode locking operation.

spectral position of the KCl:Tl colour-centre laser (the peak gain is at 1510 nm). It can be seen that at lower power levels [Fig. 8.28(a)-(c)] as P_f increases the spectrum becomes broader and the two features on both shorter and longer wavelengths separated further. When P_f is above 21 mW the overall spectral broadening process becomes more and more asymmetric [Fig. 8.28(d)-(g)]. Starting from trace (d) depletion can be seen on the longer wavelength features and meanwhile a new spectral peak at even longer wavelength gradually emerges, which becomes rather distinct at the power lever $P_f = 29$ mW [Fig.

8.28(g)]. These results provide a good demonstration of how the self-Raman effect can begin to influence the coupled-cavity mode locking process as the power coupled into the fibre is increased. It can thus be expected that once the self-Raman signal occurs further increases of coupling power would no longer induce the CCM laser to produce pulses having yet shorter durations. The interferometric autocorrelation trace for the return pulses that consist of the self-Raman component can be found in Sec. 10.2.

8.5 Conclusions

The coupled-cavity mode locking is a very general mode-locking scheme. Even with the AT & T fibre sophisticated performances can arise, which is unlike the original picture associated with the first soliton laser, where only the power level coupled into the control fibre was considered to be important. Stable sub-100 fs pulses (the shortest ~ 75 fs) can be achieved by replacing the AT & T fibre with an Er-doped fibre although the latter slightly broadens the incident pulses because of its normal dispersion characteristics around 1.5 μm.

To describe how the CCM laser behaviour is influenced by some of the principal system parameters the concept of an "operational window" which refers to the specific power range in the control fibre demanded for coupled-cavity mode locking has been introduced. According to the different combinations of the relevant system parameters within such a window three distinct operational features have been observed. These are that as the optical power in the fibre increases (i) pulse durations decrease [e.g. the lowest curve in Fig. 8.11(a)], (ii) pulse durations increase [e.g. the middle curve in Fig. 8.12(a)] and (iii) the pulse durations first decrease and then increase [e.g. the upper curve in Fig. 8.11(a)].

Each parameter combination defines particular operational states of CCM laser and provides a base from which other adjustments can be readily implemented. For instance, if an operational window "(i)" is observed it probably means that less bandwidth restriction (i.e. use of a thinner birefringent filter) would make the pulse duration decrease while operational windows "(ii)", "(iii)" usually indicate that an excess of nonlinear phase

shift has been imposed on the return pulses such that either shorter fibre lengths or thicker birefringent filters ought to be employed. Also, in the cases where insufficient power is available to couple into the control cavity an alternative to using a longer fibre with a lower group velocity dispersion is to replace the birefringent filter with a thinner one (or remove it) to ensure that proper CCM operation can be established and maintained.

Given all the other system parameters it has been shown that for achieving a proper coupled-cavity mode locking in terms of both pulse duration and system stability normally-dispersive fibres having a relatively low group velocity dispersion [e. g. the Er-doped fibre (I)] are preferred media for the control cavity. The horizontal location of the starting point of Δt-P_f curve, i. e. the value of the threshold power P_{th} (see Fig. 8.16) can normally be taken as an indication of the amount of exploitable nonlinearity in the fibre involved. For laser arrangements where only limited amounts of intrafibre power are available fibre samples which exhibit relatively large exploitable nonlinearity [e.g. Er-fibre (II)] should be selected for the purpose of coupled-cavity mode locking. The ordinates of the Δt-P_f curve for a CCM laser are more related to the magnitude of the group velocity dispersion in the fibre samples employed. For normally dispersive fibres broader CCM laser pulses will definitely imply a higher GVD value. In the experiments described here the Er-free fibre appears to exhibit the largest GVD among the three normally-dispersive fibres.

When the CCM laser is operated at high intrafibre power levels the other nonlinear effects such as modulational instability and the self-Raman effect are likely to take place in the control fibre. For relatively long (e. g. 2.8 m in our case), anomalously dispersive control fibres modulational instability is more likely to occur whereas for small fibre lengths (say 30 cm) with any type of dispersion, once the pulse duration becomes very short, the self-Raman effect may become quite severe. In general, all of these non-SPM nonlinearities have a deleterious influence on the coupled-cavity mode locking and so particular measures must be taken to avoid them. In another respect, however, the observation of the MIS, self-Raman effects in the CCM system also suggest that the coupled-cavity mode-locking arrangement may not only be an important technique for the

generation of femtosecond pulses but it also constitutes a useful test-bed for the quantitative study of optical nonlinearities.

In general, these experimental results illustrate that the coupled-cavity mode-locked laser is clearly a multi-parameter system. Therefore, to achieve an optimized CCM laser operation, fibre types, fibre lengths and main-cavity parameters must be considered in a collective manner. By so doing, the performance of the CCM, KCl:Tl laser in particular has been shown to be especially impressive for the femtosecond regime.

Chapter 9

Performance of the CCM KCl:Tl Colour-Centre Laser - II

The work described in this chapter includes the studies of frequency-chirp compensation, pulse shaping effects and pulse evolution kinetics in the coupled-cavity mode-locked KCl:Tl colour-centre laser. The results for the first two topics relating to the characterization and control of the pulses generated from the laser are believed to have substantial significance and relevance to the development and exploitation of this type of mode-locked laser systems. A knowledge of the dynamical process of the CCM KCl:Tl laser should be seen in a more theoretical context where it can contribute towards a better understanding of the relevant physical mechanisms involved in the coupled-cavity mode locking prodedures.

9.1 Frequency-chirp compensation

By examining the interferometric autocorrelations of the CCM colour-centre laser pulses it was observed that the pulses were often highly chirped as a direct result of insufficient spectral bandwidth restriction within the laser. The origin of these chirps from the SPM effect implies that they are dominated by a positive sign (up chirp). Therefore, two ways of using ordinary glass rods that have negative GVD at 1.5 μm for compensating for these frequency chirps could be successfully employed, and this led to the generation of sub-100 fs bandwidth-limited pulses.

9.1.1 Extracavity chirp compensation

As indicated in Fig. 8.12(b) in Ch. 8, when the tuning filter was removed from the main cavity the output pulses of the CCM laser did not become as short as expected, although the associated lasing bandwidth did become much broader. The reason for this is that the pulses were actually heavily frequency-chirped. In the cases where a 21 cm length of erbium-doped fibre (with a dopant concentration of 6×10^{18} cm^{-3}) was incorporated in the control cavity, a typical autocorrelation and spectral data for the CCM laser output pulses

are as shown in Fig. 9.1. The high degree of frequency chirp within the pulses may be evidenced by the elevated wings of the interferometric autocorrelation trace in Fig. 9.1(a), the large bandwidth-duration product ($\Delta t \Delta \nu$ = 0.75 compared to 0.315 for a $sech^2$ intensity pulse profile) and the disparity between deconvolved FWHM durations obtained from the interferometric and intensity autocorrelations[1].

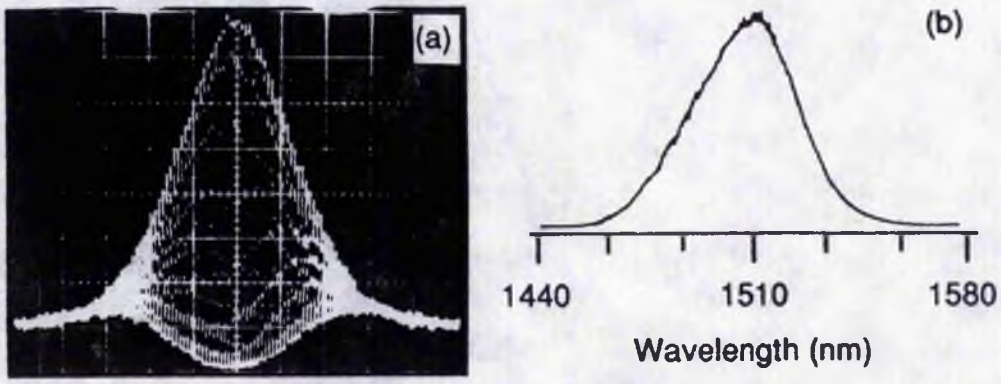

Fig. 9.1. (a) Interferometric autocorrelation and (b) spectrum of a 140 fs pulses generated by the CCM KCl:Tl laser operated with no bandwidth-limiting elements in the main cavity. The elevated wings of the autocorrelation indicate the presence of substantial frequency chirp.

To determine the nature of the chirp implied by Fig. 9.1 the frequency-chirped laser pulses were passed through various lengths of glass rod (Heraeus: Suprasil I, D =13.8 ps/nm/km @ 1.5 μm). The dependence of the resultant compression factor (input pulse duration divided by output duration) as a function of glass rod length is illustrated in Fig. 9.2. The theoretical trace shown on Fig. 9.2 has been calculated according to the reciprocal of Eq. (5.13a) and by assuming a linear chirp within the input pulse that has a Guassian pulseshape. It can be seen that the measured data do not exactly correlate with those predicted by theory but this is not unexpected because the incident chirped pulse do not have Gaussian profile and the chirp (originating from the Kerr effect) is only linear across its central peak intensity region. The general trend which implies the existence of the maximum compression ratio is clearly substantiated by the theory. At wavelengths around 1.5 μm glass is anomalously dispersive and thus the temporal compression exhibited by the CCM pulses and the chirp compensation are indicative of the presence of

[1] This latter point is quite important in that interferometric autocorrelations do not give definitive pulse duration measurements if frequency chirp is present (see the relevant discussions given in Ch. 4).

a positive frequency chirp through the pulse centre. This chirp which results from self-phase-modulation arises primarily through the pulse propagation in the erbium-doped fibre within the control cavity.

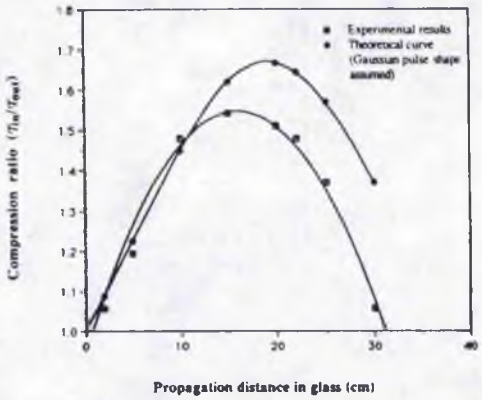

Fig. 9.2. Compression ratio (input pulse duration divided by output pulse duration) as a function of propagation distance through glass. The dotted curve relates to a theoretical estimate assuming a Gaussian intensity profile and linear frequency chirp across the pulse.

For the optimum length of the glass rod the pulses were temporally compressed to a minimum duration of 89 fs. The corresponding interferometric autocorrelation trace for these compressed pulses is shown in Fig. 9.3(a). It can be clearly seen that the traces no longer have elevated wings as in Fig. 9.2(a). This confirms that most of the frequency chirp of the pulses has been removed after passing through the glass rod. A comparison of the intensity autocorrelations of the pulses before and after propagation through the glass rod is given in Fig. 9.3(b). A pulse duration of 140 fs can be deduced from the outer trace, which was recorded without compression and is the corresponding intensity autocorrelation to the interferometric trace of Fig. 9.1(a). The result of pulse compression shown by Fig. 9.3 vividly illustrates the effectiveness of using glass as a comparatively simple chirp compensation element.

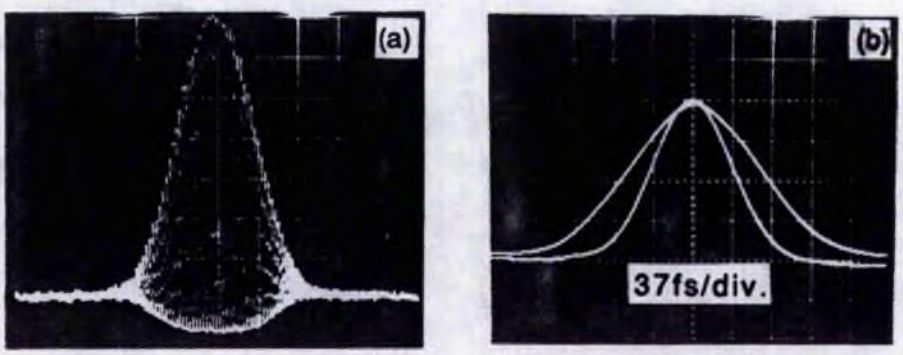

Fig. 9.3. Interferometric autocorrelation of 89 fs obtained by passing the CCM laser output pulses through 20 cm of glass. (b) Comparaison of intensity autocorrelations before (top trace) and after (bottom trace) chirp compensation.

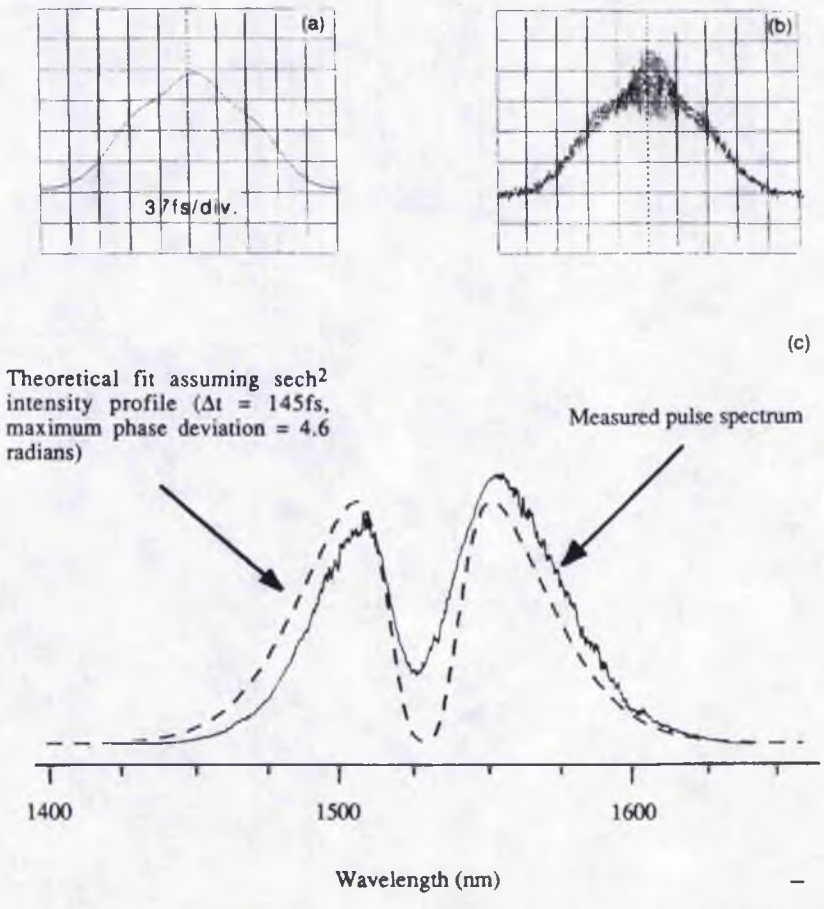

Fig. 9.4. (a) Intensity autocorrelation, (b) interferometric autocorrelation, and (c) spectrum of pulses leaving erbium-doped fibre in control cavity. In (c) a theoretical spectrum has been computed for an input pulse of 145 fs duration, an average power of 14 mW, and an initial self-phase-modulation frequency chirp of peak phase deviation $\theta_0 = 2$ rad.

The spectral and temporal characteristics of the pulses leaving the control cavity have also been analysed and the data of Fig. 9.4(a)-(c) correspond to the intensity, interferometric autocorrelation traces and spectrum of the return pulse respectively. These pulses are so excessively chirped by experiencing the SPM in the fibre that there is a complete loss of coherence between the leading and trailing portions of the pulse. As a consequence the wings of the interferometric autocorrelation show an averaged unmodulated trace and appreciable fringe visibility only appears at small relative delays in the autocorrelator. (This is analogous to white light fringes in the Michelson interferometer.) At zero delay we would still expect to see 100% modulation of the

second harmonic. The recorded higher background level could be explained in terms of either polarization rotation in the fibre (thereby compromising the phase matching in the autocorrelator frequency-doubling crystal) or alternatively this effect may be due to temporal scrambling of oppositely chirped regions of the pulses due to GVD. The associated spectral data Fig. 9.4(c) are consistent with the presence of substantial SPM. Shown together with these data is a calculated spectrum for the pulses returning from a 21 cm long fibre, the associated incident pulses are assumed to have a duration of 145 fs and an average coupled fibre power of 10 mW.

In this analysis the fibre is treated as a pure SPM device and the optical pulse out of the control fibre was modelled by

$$V(t) = A(t)e^{-i[\omega_o t + \Delta\phi(I,t)]} \qquad (9.1)$$

A(t) is the electric-field envelope for the pulses coupled into the fibre, ω_o is the carrier frequency of the pulse. The time dependent phase term in the above equation is given by

$$\Delta\phi(I, t) \approx -\frac{\omega_o n_{2I} I_o 2L_f}{c} I(t)$$

where n_{2I} is the nonlinear refractive index of the medium, L_f is the fibre length, I_o the optical peak intensity and I(t) the normalised pulse intensity profile (taken as $sech^2$). Since the input pulse to the fibre was also chirped this was accommodated by assuming an initial self-phase modulated pulse of a given peak phase deviation, ϕ_o, so that the emergent pulse from the fibre has a field function described by

$$V(t) = A(t)e^{-i[\omega_o t - \phi_o I(t) + \Delta\phi(I,t)]} \qquad (9.2)$$

The initial peak phase deviation of the pulse was taken to be ~2 radians [estimated from numerical interferometric autocorrelation fits to Fig. 9.1(a)] and the good agreement of this simulation to the measured data shows that the optical Kerr effect is the predominant nonlinear process in the fibre. The asymmetry of the measured spectrum (slightly higher intensity and broader bandwidth for the longer wavelength feature) is most readily attributed to a slight temporal asymmetry in the profile of the CCM pulses or possibly the onset of a self-frequency shift due to Raman scattering (see subsection 5.2.3).

The data of Fig. 9.5 for the return pulses from the control cavity were taken following their propagation through 20 cm of glass. Note that the pulse duration has been reduced from 170 fs to 60 fs at FWHM, although the existence of a relatively large pedestal in the pulses can be inferred.

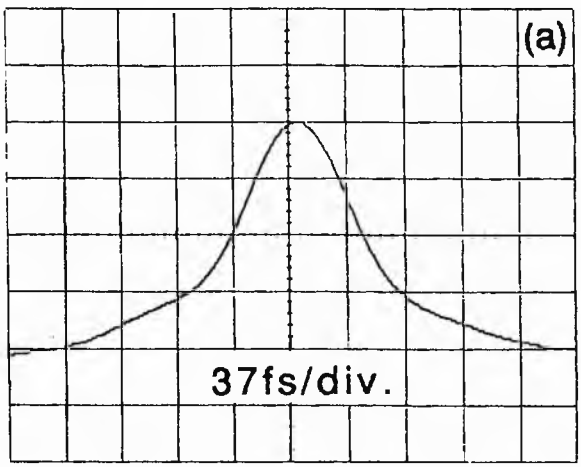

Fig. 9.5. Intensity autocorrelation of control-cavity pulses following propagation through an extracavity 20 cm-length of glass.

9.1.2 Intracavity chirp compensation

A natural progression from the above experimentation was to attempt to compensate the pulse frequency-chirp inside the CCM laser cavity itself. Because the SPM arises in the optical fibre, the compensating glass elements were introduced into the coupled nonlinear cavity. Both CCM and control cavity pulses were monitored for a series of inserted lengths of glass and the variation of pulse durations with propagated glass path length is indicated by Fig. 9.6. It is noteworthy that the ratio of CCM to control-cavity pulse durations could be altered by the insertion of appropriate lengths of glass rods. In other words, by adjusting the lengths of glass the pulses can be either temporally compressed or broadened in a control cavity incorporating a particular optical fibre. Such observations can be properly understood by the fact that the overall GVD feature in the control cavity has been changed through adding different lengths of glass rods. (As a longer glass rod is incorporated into the control cavity, more negative dispersion is present, and so eventually this leads to the change of the effective dispersive status of the control cavity from normal to the anomalous type in particular wavelength regions).

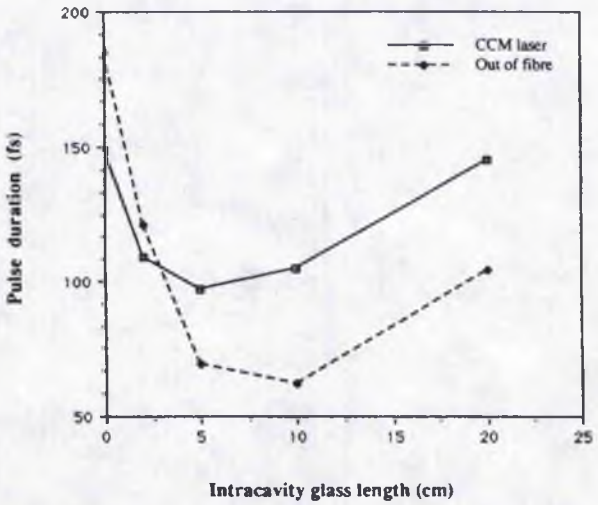

Fig. 9.6. Plot of pulse duration obtained from CCM main cavity and control cavity as a function of glass-rod length inside control cavity.

The autocorrelation data of Fig. 9.7(a), (b) were recorded for CCM laser pulses where a 10 cm length of glass was inserted into the control cavity. This interferometric autocorrelation trace indicates that the pulse is essentialy chirp-free and the deconvolved FWHM of 90 fs compares favourably with to 96±2 fs measured from the intensity autocorrelation results. The bandwidth-duration product in this instance was measured to be 0.36.

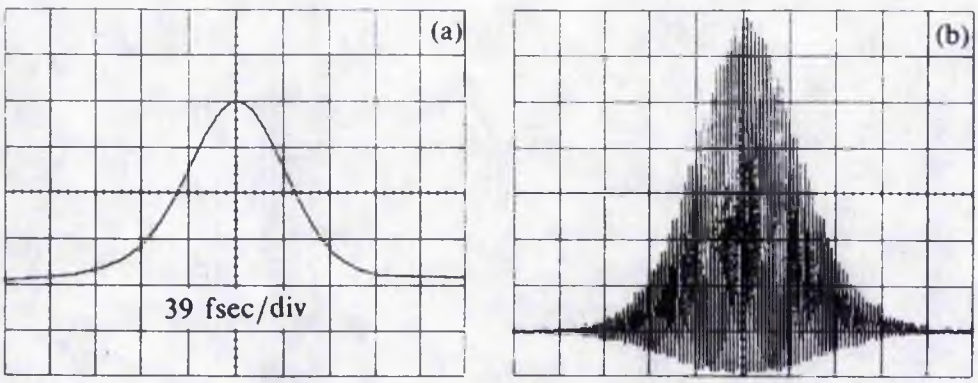

Fig. 9.7. (a) Intensity and (b) interferometric autocorrelation of 96 fs duration pulses obtained from a CCM laser with 5 cm of glass in the control cavity.

From the data in Fig. 9.6, it can be seen that when the glass rod incorporated in the control cavity is 10 cm long the return pulses have the shortest duration which is just above 60 fs. However, it by no means represents the shortest duration that can ultimately be obtained for these return pulses. If the optical power couped into the fibre increases pulses with even shorter durations can be produced. One example of these records is shown in Fig. 9.8(a). From the very limited number of fringes existing across this

recorded SHG autocorrelation trace, which is a mixture of both intensity and interferometric types, it is clear that the associated return pulses must have a temporal duration shorter than any other pulses we have recorded and reported so far. The spectrum for these pulses is shown in Fig. 9.8(b), where it is interesting to see that, unlike the ordinary SPM-induced spectral extension, very different features exist on each side of the spectrum. This is possibly a result of the presence of different types of dispersion across the recorded wavelength range: negative dispersion at the longer wavelengths, where larger negative GVD available from the glass rod, and normal dispersion at the shorter wavelengths ($\lambda \leq 1520$ nm), where the negative GVD of the glass rod is not so large that the normal dispersion in the control fibre has not been cancelled out completely. Such a mixture of dispersive features experienced by return pulses may be also used to account for the fact that it is often found difficult to stabilize the laser while it is operated under this regime.

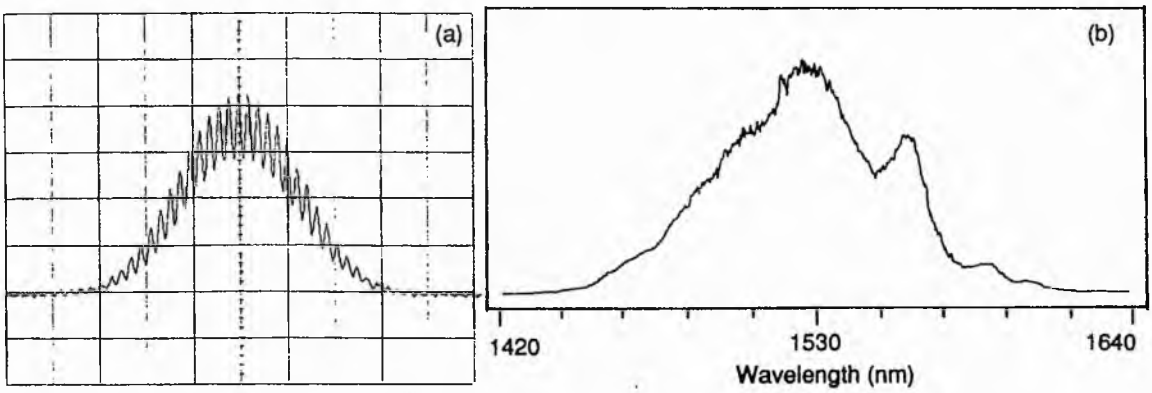

Fig. 9.8. Autocorrelation trace (a) and spectrum (b) for extremely short pulses returned from the control cavity where a 10-cm-long glass rod is incorporated in addition to a 21-cm-length of erbium-doped fibre with medium dopant concentration.

9.2 Pulse shaping effects

As already mentioned in Ch. 8, cavity length mismatches in a coupled-cavity mode-locked laser can introduce shaping effects on the laser pulses. Specifically, a negative mismatch (i. e., control cavity shorter than the main cavity) leads to the CCM laser pulses having a faster leading edge and slower trailing edge whereas positive mismatches give rise to slower leading edges and faster trailing edges.

It is known that for asymmetrical pulses propagating in optical fibers spectral broadening resulting from self-phase-modulation (SPM) will also be asymmetrical (Lin and Stolen 1978). Thus, if the incident pulses have sharper leading edges the exiting spectra will be more extended towards the longer wavelengths. It therefore follows from this that the shape of the CCM laser pulses, which corresponds also to those pulses injected into the control fibre, can be identified by monitoring the pulse spectra emerging from the control cavity.

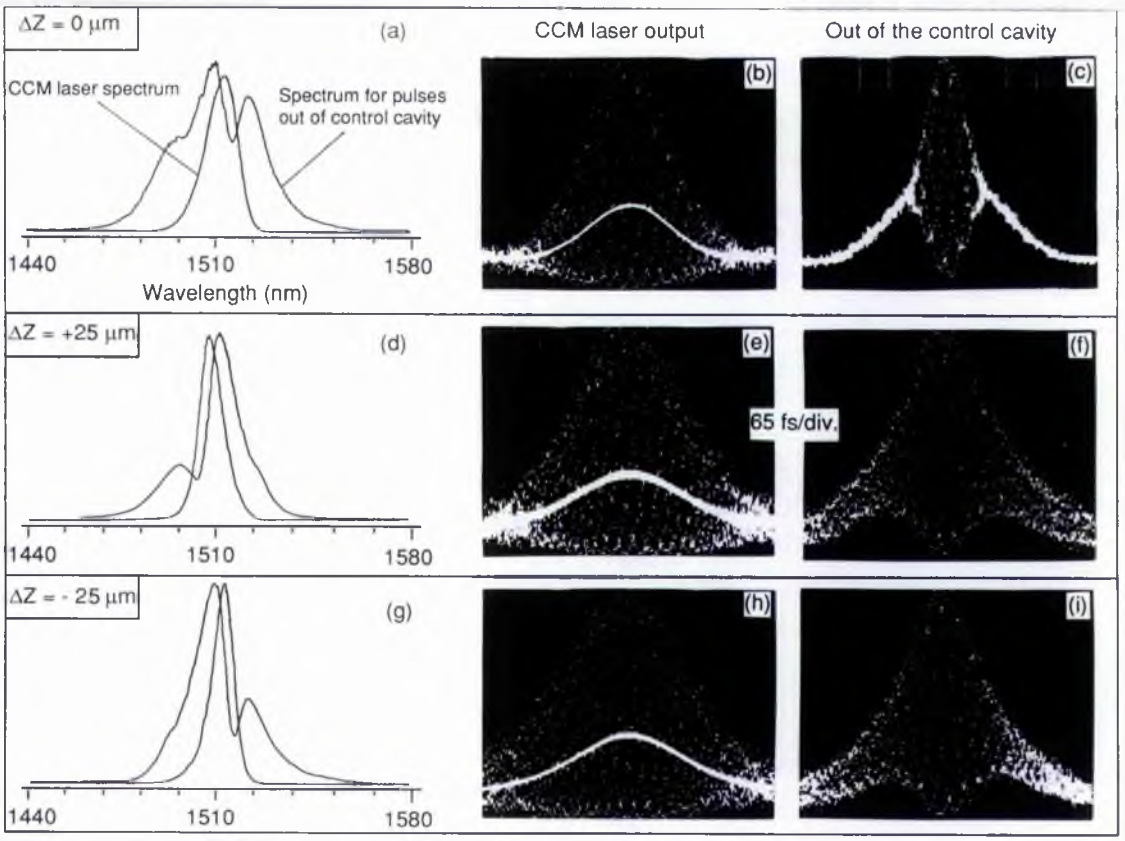

Fig. 9.9. Spectral and temporal characteristics for the CCM laser output and the feedback pulses from the control cavity. (a-c) relate to matched cavities; (d-f) and (g-i) for 25 μm positive and negative cavity-length mismatches respectively.

One group of spectral and temporal data for the CCM laser pulses and the pulses returning from the control cavity are shown in Fig. 9.9, where traces (a)-(c) relate to the condition where the two cavity lengths are approximately matched and traces (d)-(f), (g)-(i) relate to 25 μm positive and negative cavity mismatches respectively. The narrower spectra in Fig. 9.9(a), (d), (g) are the CCM laser output spectra which correspond

respectively with the SHG autocorrelation traces in Fig. 9.9(b), (e), (h) where both intensity (the bright line) and the interferometric (fringe resolved) detail have been recorded together. The three broader spectral traces are the feedback pulse spectra from the control cavity. Their temporal counterparts are described by the autocorrelation traces shown in Fig. 9.9(c), (f), (i). The approximately equal degree of spectral broadening to longer and shorter wavelengths at the matched position [Fig. 9.9(a)] and obviously unequal spectral expansions at mismatched positions [Fig. 9.9(d), (g)] can be clearly seen. For the positive mismatch [Fig. 9.9(d)] the spectrum for the pulses from the fibre has a relatively low-intensity shorter wavelength ('blue") feature and a higher-intensity longer wavelength ("red") feature. These measurements indicate that the "blue" feature has a greater spectral displacement from the injected CCM laser peak. Such characteristics imply that the incident CCM laser pulses must have a slower leading edge and faster trailing edge. Consistent analysis also applies to the data for the negative mismatch [Fig. 9.9(g)], where the generation of asymmetrical CCM laser pulses having sharper leading edges and slower trailing edges is observed.

The origin of these characteristics is readily understandable. For the positive (or negative) mismatch, most of the energy in the pulse returning from the control cavity overlaps with the trailing (or leading) portion of the main cavity pulse such that a sharpening of the main cavity pulse due to the coherent addition of the two pulses will occur mainly in the trailing (or leading) edge. Expanded scans of the measured spectra clearly indicate that once the pulse shaping caused by cavity length mismatch occurs the CCM laser spectrum will become asymmetrical as well. This agrees closely with the theoretical predictions presented by Finch (1989), where spectra have been deduced for specific examples of chirped and asymmetrical pulses. Careful examination of the spectra for the CCM laser output in Fig. 9.9(d) and (g) reveals some degree of asymmetry where for positive mismatch [Fig. 9.9(d)] there is an extended tail to longer wavelengths and for negative mismatch the shorter wavelength components are more prevalent. [Slight asymmetry is also evident in the CCM laser spectrum at the "matched" position represented by the data of Fig. 9.9(a). This implies that this arbitrarily determined zero

mismatch is probably somewhat inexact in that a minor amount of negative mismatch still remains].

It is noticeable that compared with the pulse duration of 230 fs at the matched position [Fig. 9.9(b)], the CCM laser pulse duration at the mismatched positions [Fig. 9.9(e), (h)] were ~260 fs. Corresponding spectral bandwidths were measured to be 12 nm for the matched [Fig. 9.9(a)] and 9 nm, 8.5 nm for the two unmatched cases [Fig. 9.9(d), (g)]. Thus the deduced pulse duration-bandwidth products are 0.37, 0.31 and 0.29 respectively. The reduced values of these duration-bandwidth products for the unmatched conditions further confirm the existence of asymmetrical pulse shapes. [In general, for unchirped pulses the more asymmetrical the pulse intensity profile, the smaller will be the associated bandwidth-duration products (Finch 1989; Table 7.1)]. The maximum mismatch tolerated in the CCM operation was about ± 30 μm relative to the arbitrarily determined matched position [Fig. 9.9(a-c)]. When the cavity length mismatch ΔZ was altered from zero to ± 25 μm [see Fig. 9.9(d-f), (g-i)] continuous spectral changes from symmetrical to increased asymmetry and temporal broadening were observed in the pulses. When |ΔZ| was close to the maximum mismatch value the CCM laser became unstable and frequent operational drop-outs were observed.

In addition to the pulseshape-related spectral profiles mentioned above, the pulse shaping effects can also be deduced from the character of the interferometric autocorrelation traces shown in Fig. 9.9(c), (f), (i). For the approximately symmetrical pulses [Fig. 9.9(b)], because of the combined effects of self-phase-modulation (SPM) and group velocity dispersion (GVD), the pulses after passing through the fibre (one round trip) are so strongly chirped that the visibility of the fringes in the wings of the interferometric autocorrelation trace was degraded [see Fig. 9.9(c)]. However, for the asymmetrical pulses [Fig. 9.9(e), (h)] after experiencing the phase modulation in the fibre better fringe visibility is still retained in the wings of the autocorrelation traces [Fig. 9.9(f), (i)]. This is due to two effects. The asymmetrical pulse has an extended leading or trailing edge which effectively increases the interference latitude for the autocorrelation. Also, the difference in the rate of change of intensity of the front and back edges of the

pulse causes an asymmetrical chirp distribution and a reduced relative frequency shift between the front and rear regions such that a more pronounced interferometric interaction occurs in the wings of the autocorrelation profile. Interestingly, a careful inspection of Fig. 9.9(f), (i) indicates that the two wings in each trace are slightly asymmetrical. [For Fig. 9.9(f), the right hand side wing has relatively longer fringes along the vertical direction than the left hand wing whereas for Fig. 9.9(i) it is just the opposite]. Such asymmetries are not due to any alignment problems in the autocorrelator, but, arise from the unbalanced dispersion in the two arms of the Michelson interferometer. When no compensation plate is included then the beam from one arm experiences twice pathlength in the glass substrate of the beam splitter[2] (see Sec. 4.3).

It was observed that the pulses out of the control cavity had durations that were always exceeded those of the CCM laser pulses. For the traces shown in Fig. 9.9(c), (f), (i), the intensity autocorrelation measurements give pulse durations of 260, 300 and 300 fs respectively. These results imply that the Er-doped fibre used in these experiments had a normal group velocity dispersion at 1510 nm, which is inconsistent with the calculated value given in Table 8.1.

Finally, it should be mentioned that regardless of the sign of GVD in the control fibre this pulse shaping influence arising from cavity length mismatches has also been evident in the other types of fibers such as a dispersion-flattened fibre, where pulse compression exists under almost the same operating conditions as those that apply to the Er-doped fibre. Since the dispersion-flattened fibre (provided by Philips Company) has a very small value of group velocity dispersion ($|D| < 2$ ps/nm/km in the 1400-1620 nm range) it can be approximated to a nearly ideal optical Kerr element. Therefore, a simulation of the observed temporal and spectral characteristics of the shaped pulses can be readily undertaken by assuming an asymmetrical pulse shape with a certain amount of "Kerr-type" chirp across it and then numerically computing its interferometric autocorrelation and corresponding spectrum. The example of recorded and calculated interferometric autocorrelation traces and spectra shown

---

[2] In such a situation, the autocorrelator behaves as a cross-correlator, especially for very short pulses, and so the asymmetry in the pulses to be measured can be detected.

in Fig. 9.10 are seen to be in reasonable agreement. It was found that for an optimal fit some positive linear chirp was required to be present in the pulse and the degree of self-phase-modulation (SPM) was larger than expected for the length of fibre actually used. This additional frequency chirp can readily arise in the input main cavity pulse and is due to both residual SPM transferred to the circulating pulse from the control cavity and other frequency-chirping processes such as gain saturation in the laser crystal. For the measured spectrum [Fig. 9.10(c)], the enhancement of the longer wavelength feature and the presence of a weak signal component at the extreme 'red' end may be attributed to self-Raman effects.

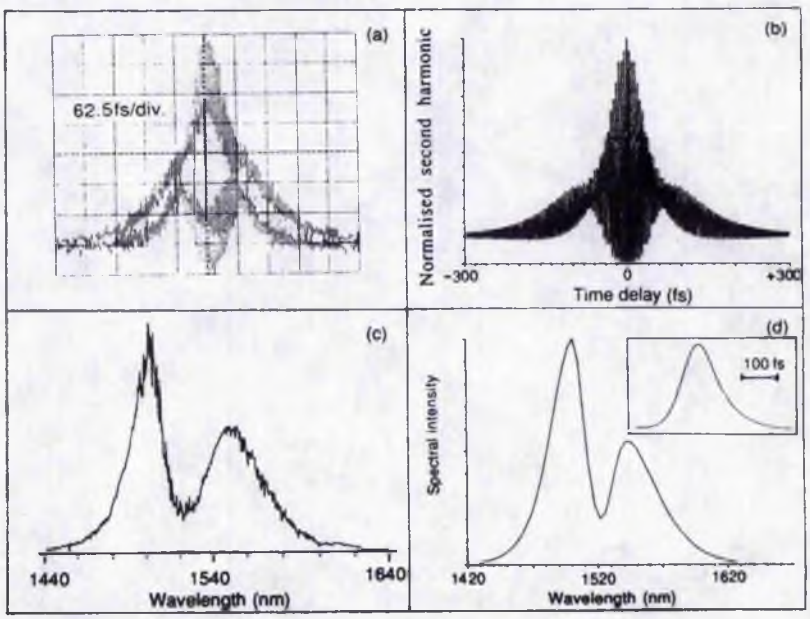

Fig. 9.10. Comparision of experimental measurements [Fig. 9.10 (a) (c)] with the theoretical predictions [Fig. 9.10 (b) (d)] of the interferometric autocorrelation trace and the associated spectrum for asymmetrical chirped pulses. The measured pulses having a duration of 120 fsec are the pulses out of the control cavity which incorporated a 28 cm dispersion-flattened fibre. The calculated pulses with sharper leading edges [see inset of Fig. 9.10(d)] have been described by an amplitude function:

$$A(t) = \frac{\exp[i(\omega_0 t + \Phi_{max} I(t) + bt^2)]}{\exp(-rt) + \exp(t)}$$

where b = 0.04 THz/fsec, Φ_{max} = - 2.8 radians, r = 2.6 and $I(t) = |A(t)|^2/I_o$.

9.3 Pulse evolution kinetics

Although some experimental investigations of the pulse evolution in a coupled-cavity laser have now been reported (Zhu *et al* 1990e) most previous information on this topic had been derived from numerical simulation studies (If *et al* 1986, Blow and Wood

1988). In this section details and discussions of the experimental data on the pulse evolution process in a coupled cavity mode-locked KCl:Tl laser will be presented.

9.3.1. Control-cavity switching

The measurements of pulse build-up time were made initially by switching "off" and "on" the voltage applied to a Pockels cell incorporated within the control cavity and simultaneously monitoring the change of the second harmonic intensity produced by the laser pulses [see Fig. 9.11(a)]. It is known that when the control cavity is at a state of "off" the output pulses from the main laser have durations of several tens of picoseconds and the corresponding SH signal is relatively low. However, when the control cavity is switched to the "on" state the coupled-cavity mode-locking process starts and leads to a dramatic decrease in the output pulse duration and a ~ x100 increase in the SH signal level was observable (see Ch. 6). Because the average power of the pulse train incident on the frequency-doubling crystal is essentially unchanged whenever the control cavity is blocked or unblocked, the increase of second harmonic intensity in the latter case can thus be taken as a clear indication of a reduction in laser pulse duration. Therefore, the time scale of the short pulse build up in the coupled-cavity mode-locked laser can be related to the time during which the SH signal increases from the initial lower intensity level to the final steady-state higher level [see Fig. 6.4(a), (b)].

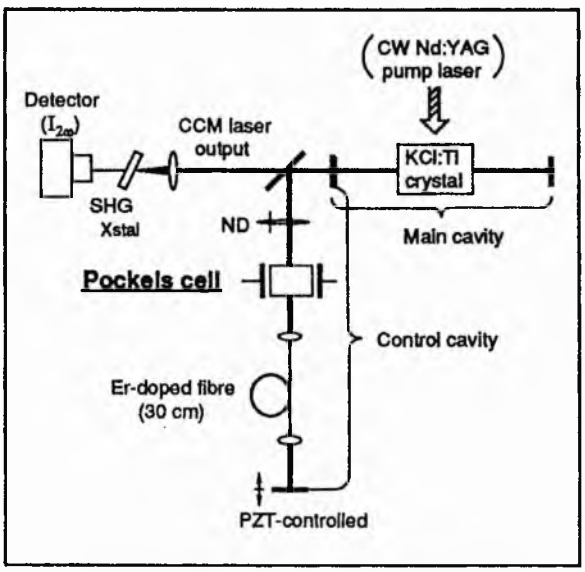

Fig. 9.11(a). Experimental layout for pulse evolution study of a coupled-cavity mode-locked KCl:Tl laser with control-cavity switching.

In practice, the switching of the control cavity from "off" to "on" was implemented by removing the quarter-wave voltage from the Pockels cell. The exact value of the voltage was adjusted such that after one roundtrip propagation in the fibre and the Pockels cell the polarization of the beam was rotated by 90 degrees, and so the overall return signal out of the control cavity had a polarization direction which was orthogonal to that determined by the Brewster-angle tilted elements in the main cavity. Therefore, most of the return signal was rejected by the main cavity before it reached the gain medium. This was equivalent to a "off" state of the control cavity and thus no mode-locking enhancement could be achieved under these conditions.

One example which shows the rapid increase in SH signal after the Pockels cell voltage was turned "off" is reproduced in Fig. 9.11(b). The Pockels cell switching time was less than the 12 ns laser roundtrip time and the result was taken with one arm of the autocorrelator blocked. This represents an average of several recordings taken using a Tektronix 2221 digital storage oscilloscope. It can be seen that the risetime was ~4.5 μs in this particular case, which indicates that it took about 360 cavity roundtrips for the steady-state CCM operation to be established. The overall time resolution of the entire detection system was estimated to be ~100 ns.

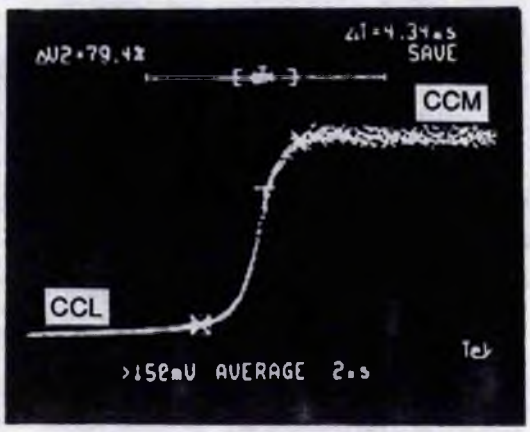

Fig. 9.11(b). Build up of SHG intensity as the CCM laser pulses evolve (CCL denotes Colour-Centre Laser alone).

One of the interesting phenomena observed in the experiments was that following the switching action of the Pockels cell there was generally a variation in the time delay before the SH signal started to increase and also the risetimes were seen to vary substantially. Such an observation confirms that the degree of phase match at the initial

stage of pulse evolution plays a crucial role in determining the actual pulse build-up time. If the cavity phases are matched when the control cavity is switched "on" the CCM process will start immediately and the SH intensity will thus have a rapid rise. In contrast, if the initial phases are not properly matched when the control cavity is switched to "on" the CCM process would not start until some adjustment of the cavity periods occurs to produce a suitable phase relationship.

Two representative single-shot measurements, which illustrate the random delay of the starting time for the short pulse to build up, are shown in Fig. 9.12(a), (b). The fiducial lines on the left side of the photographs indicate the time when the switching action on the Pockels cell was taking place and these were used as the trigger references. The time interval between the trigger reference and the rise of the SH trace in each figure indicates a time delay of 96 μs [Fig. 9.12(a)] and 39 μs [Fig. 9.12(b)] respectively. For the many single-shot recordings the shortest delay was seen to be about 10 μs and there were also instances when the build up of shorter pulses did not occur. (Such a non-appearance may be attributed to the failure to satisfy the phase-matching condition for the cavities during the observational period.) The variation of these time intervals and the occasional non-appearance of shortened pulses implies that the phase setting at the time when the external cavity is opened is critically important for pulse evolution. This obervation signifies a fundamental feature of the kinetics involved in a CCM laser. The uncertainty of the phase matching at the beginning of the pulse evolution process can be regarded as direct evidence of the essential passive nature of this type of mode locking. The initial phase condition in the control cavity will actually determine the onset-time and most likely influences the rate of the pulse shortening process. It has been found that a small range in the phase setting is tolerated by the laser for achieving noticeable pulse compression. This acceptable phase range has been experimentally determined to be $\Delta\phi \approx 2\pi/5$. In general, $\Delta\phi$ varies when the system parameters such as the coupling power, the offset of the control cavity length etc. are adjusted.

Because of the random time delay which was observed to be in the 10-100 μs range it was concluded that it was not essential to incorporate a fast switch to observe the pulse

build-up process in the coupled-cavity laser. Therefore, instead of using the fast electro-optical switch to turn "off" and "on" the nonlinear-cavity feedback an approach of "phase-switching" have also been employed. In this case the phase of the returned pulse was altered with respect to the main cavity pulse by translating the end mirror. This was implemented by applying a ramp voltage to the piezo-electric-translation (PZT) stage upon which the end mirror of the control cavity was mounted. This ramp voltage and the corresponding induced variations in the SH signal are reproduced in Fig. 9.13(a). [The trace in Fig. 9.13(b) is a magnified portion of the rising edge of SH intensity trace shown in Fig. 9.13(a)]. We can see that the trace has a similar risetime to those recorded using the intracavity-Pockels cell scheme [see Figs. 9.12(a), (b)]. It should be pointed out that in order to make this comparison the recorded traces for the SH signal in Fig. 9.13 were taken while the unbiased Pockels cell was retained within the control cavity.

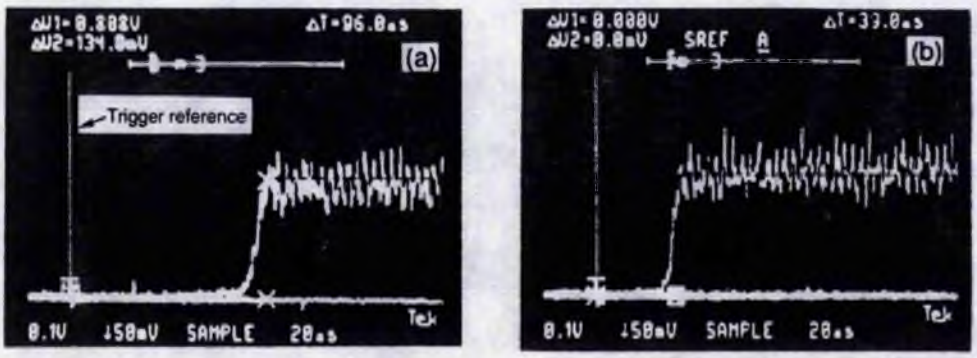

Fig. 9.12. Variation in time delay for the initiation of the coupled-cavity mode-locking process after the control cavity was switched from "off" to "on" (see text).

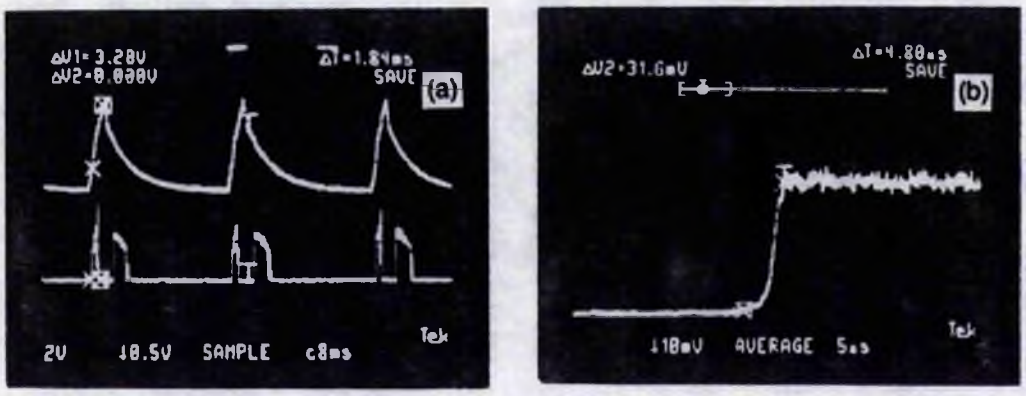

Fig. 9.13. Results of phase-switching achieved by altering the voltage applied to the PZT stage which translates the control-cavity end mirror.

9.3.2 Pump-beam switching

As shown in Fig. 9.14, instead of inserting the Pockels cell in the control cavity, an alternative approach for studying the pulse build-up process involved the switching of the pump beam intensity. In the operation of pump-beam switching the control cavity was coupled from the outset of the lasing process and thus differed from the control-cavity switching where the control cavity was switched to "open" after the main cavity pulse had already been established.

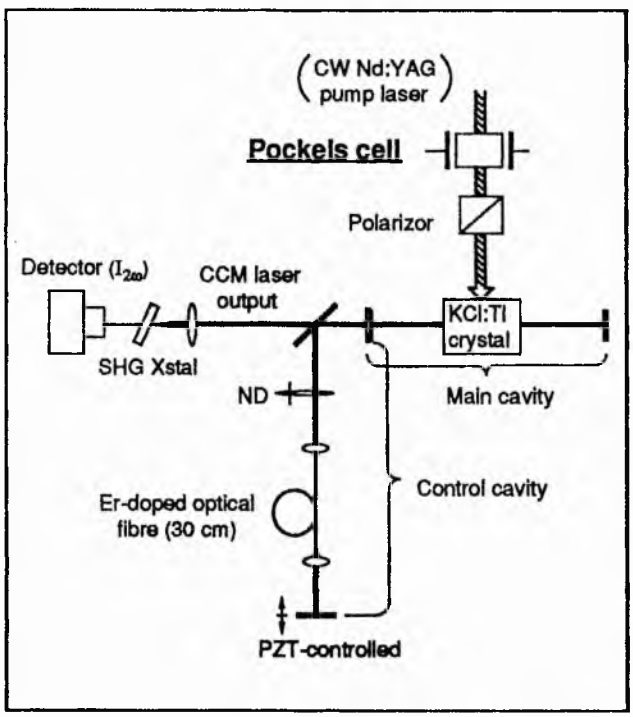

Fig. 9.14. Schematic of pump-beam switching configuration.

A representative single-shot record is shown in Fig. 9.15 where it can be seen that the pulse build-up time is 1μs, which is equivalent to approximately 80 cavity periods. The observed strong oscillation could be attributed to the gain relaxation kinetics of the KCl:Tl crystal, which has an upper laser state lifetime ~1.6 μs (see Ch. 7). The large reduction of the pulse build-up time, indicated in Fig. 9.15, is not due to the method of switching but can be attributed to the increase of the optical power fed back to the main cavity when the insertion loss of the Pockels-cell switch was removed. The estimated maximum intensity ratio of the return pulse to the main cavity pulse (inside the main

cavity) was 1:2000 when the Pockels cell was in the control cavity whereas on its removal the intensity ratio increased to 3:2000 (see data of Fig. 9.15). A relationship between the pulse risetime and the intrafibre power obtained in our experiments is shown in Fig. 9.16. Within the intrafibre power range involved, it was evident that, as the coupling power into the fibre increased, the CCM laser pulses built up more rapidly. In recording the data shown in Fig. 9.16 the average output power from the main cavity laser, P_o, was maintained at 70 mW. When P_o was increased to 85 mW the highest available intrafibre power was 26 mW and the observed shortest SH signal risetime was only 200 ns.

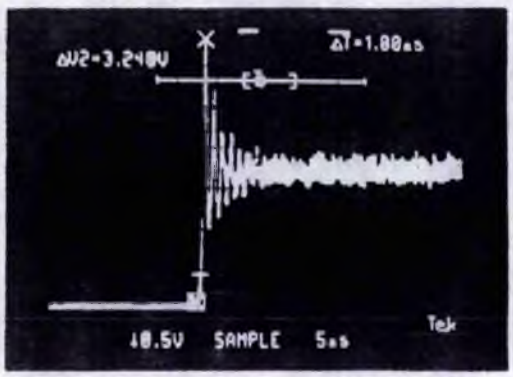

Fig. 9.15. SHG signal characteristic associated with the rapid evolution of the CCM laser pulses.

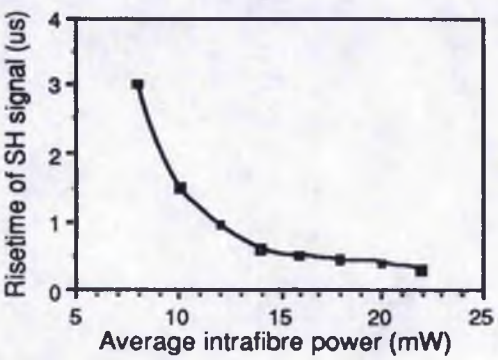

Fig. 9.16. Build-up time of SHG signal as a function of average intrafibre power.

As for the control-cavity switching, it was observed that after each pump-beam switching action the starting time for the SH signal build-up was also random. A distinct feature in the latter case was that the laser system seemed to be initially oblivious to the existence of the control cavity such that the pulses were established first in the main cavity, reaching the steady state for the synchronous-pumping condition, and then the

subsequent effect of the control cavity led to a sharp rise in the SH intensity level. This is evident in the two superimposed oscillograms shown in Fig. 9.17, where these single-shot data were recorded at different sensitivities and with one trace inverted. The inverted trace which was recorded at a high sensitivity scale (10mV/div.) shows that the SH signal level starts to increase rather slowly before the subsequent rapid increase is observed. This slow rise is related to the initial period of pulse build-up process which occurs mainly in the main cavity. During this stage, the relatively slow increase of pulse peak power results in a SH intensity that is consistent with the steady-state operation of KCl:Tl colour-centre laser without the control cavity. (This SH intensity level is indicated by the bottom line shown in Fig. 9.17.) A dramatic enhancement of mode locking in the coupled cavities then takes place if the phase matching of the return pulse with the main cavity pulse is appropriate. This observation indicates that a required optical peak power must be injected into the control cavity to ensure that a sufficient nonlinear phase shift is produced to achieve the coupled-cavity mode locking. Therefore, as far as the pulse evolution kinetics are concerned, the two switching methods (control-cavity switching and pump-beam switching) do not have any essential difference except that with pump-beam switching, in addition to monitoring the process of mode-locking enhancement, we have also observed the early period of pulse build-up in the main cavity.

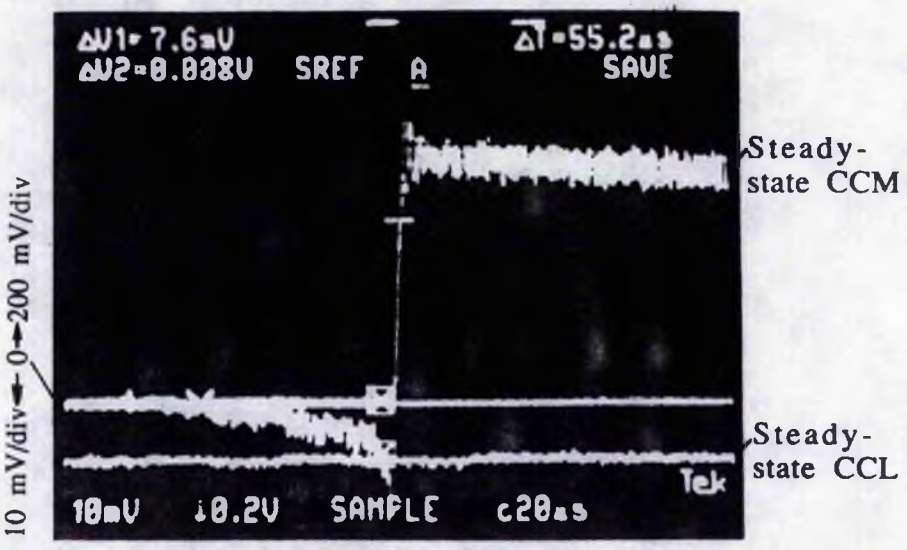

Fig. 9.17. Characteristics of the SHG signal build-up measured at two oscilloscope sensitivities during pump-beam switching. The bottom line, which represents the signal level obtained when the control cavity was blocked, and the trace immediately above it are inverted and at a magnified scale (10 mV/div.).

The traces shown in Fig. 9.18, with quite different risetimes, are two representative examples taken from successive single-shot measurements. These data were recorded under similar experimental conditions with the exception that the phase shifts of the return pulse to the main cavity pulse at the time when the mode-locking enhancement started could not be exactly the same because of uncontrolled cavity-length drift.

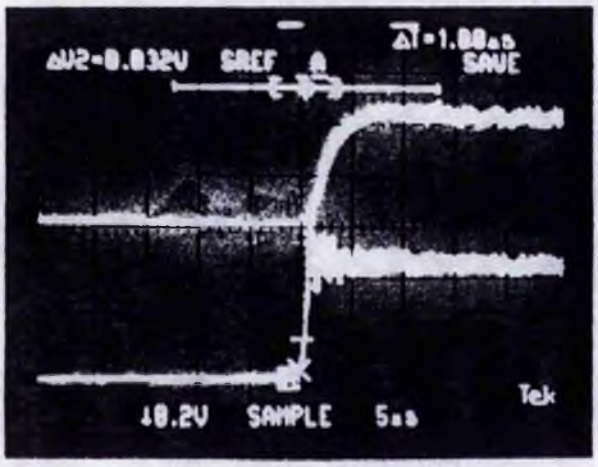

Fig. 9.18. Variation in build-up times for two individual single-shot measurements.

9.3.3 Effect of initial pulse characteristics

In addition to the observations mentioned above, we have also examined the influence of initial pulse characteristics on the pulse evolution process. (Here, "initial" relates to the time when the coupled-cavity mode locking starts). It is known that the characteristics of the initial pulse out of the main cavity can be readily controlled by the intracavity tuning element (see Ch. 8). For instance, if a thicker birefringent filter which has narrower transmission bandwidth is used in the main cavity the laser bandwidth will be more restricted and thus the initial pulse for the CCM process will have a relatively clean shape and a smaller pulse bandwidth-duration product. If a thin filter, or no filter, is included in the main cavity the laser output will have a large amount of excess non-mode-locked frequencies, which leads to a noise burst.

The two SHG autocorrelation traces shown on the left sides of Figs. 9.19(a), 9.20(a) are the two typical examples of the colour-centre laser pulses produced under the extreme conditions of either restricted bandwidth or an absence of bandwidth limitation. It can be seen that in the former case where a 1-mm-thick birefringent plate was inserted in the main cavity the autocorrelation trace has a smooth shape with a peak-to-background ratio

of 3:1, while in the latter case with no birefringent plate in the main cavity, the trace [Fig. 9.20(a)] more closely resembles the characteristic 3:2:1 profile associated with the autocorrelation for a noise burst (see Ch. 4). The corresponding spectra for these two typical cases are reproduced in Fig. 9.19(b) and Fig. 9.20(b) respectively. From these groups of temporal and spectral data the bandwidth-duration products can be deduced to be 3.1 for the relatively clean pulses and 9.3 for the noise bursts.

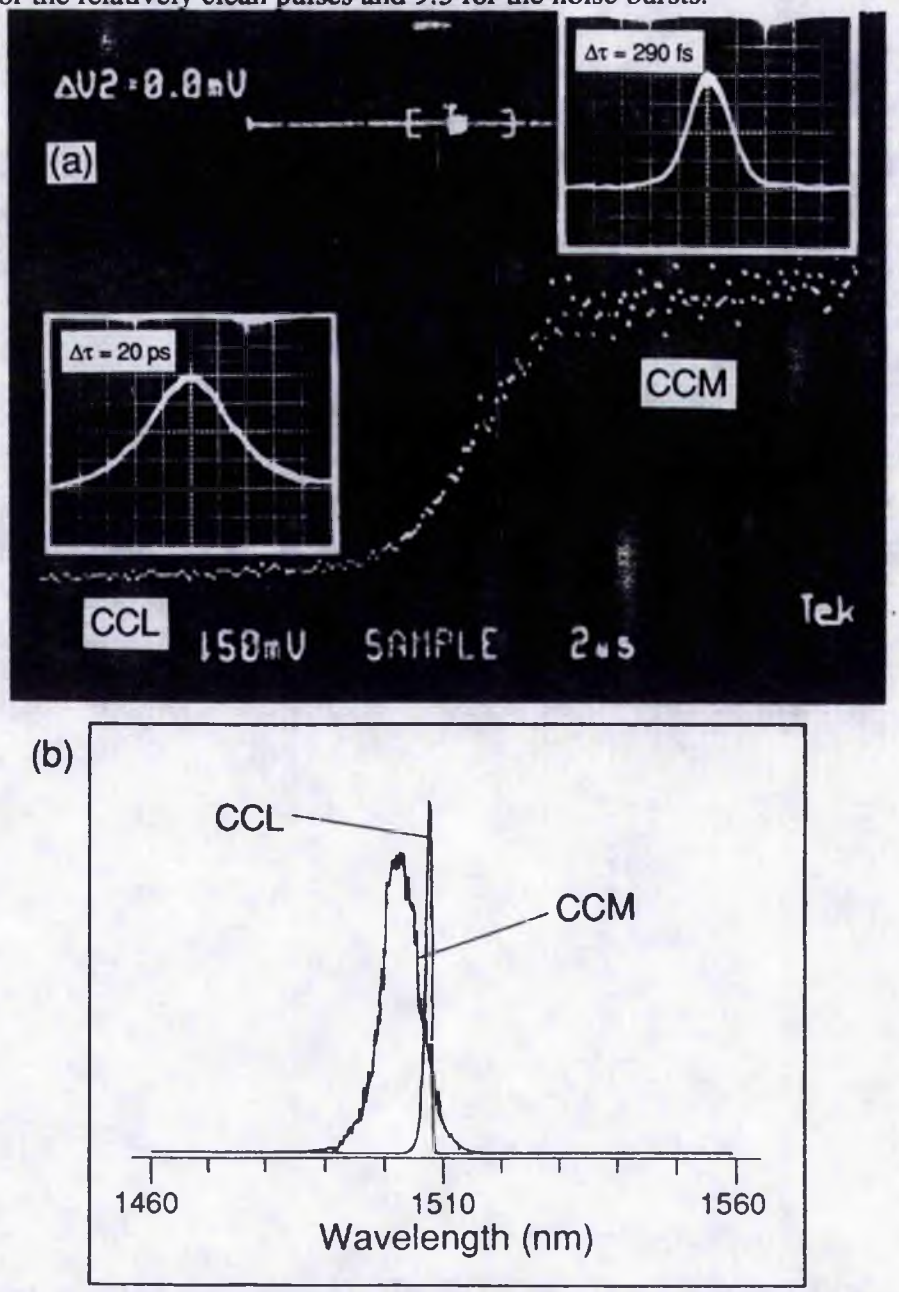

Fig. 9.19. (a) Increase of SH signal in the case where the initial "clean" pulse with $\Delta\tau = 20$ ps evolved into the bandwidth-limited 290 fs pulse. (b) Corresponding spectra for the pulses before (CCL) and after (CCM) coupling of the control cavity. (In recording the CCL spectrum the signal was attenuated by x 5 with respect to that used in measuring the CCM spectrum).

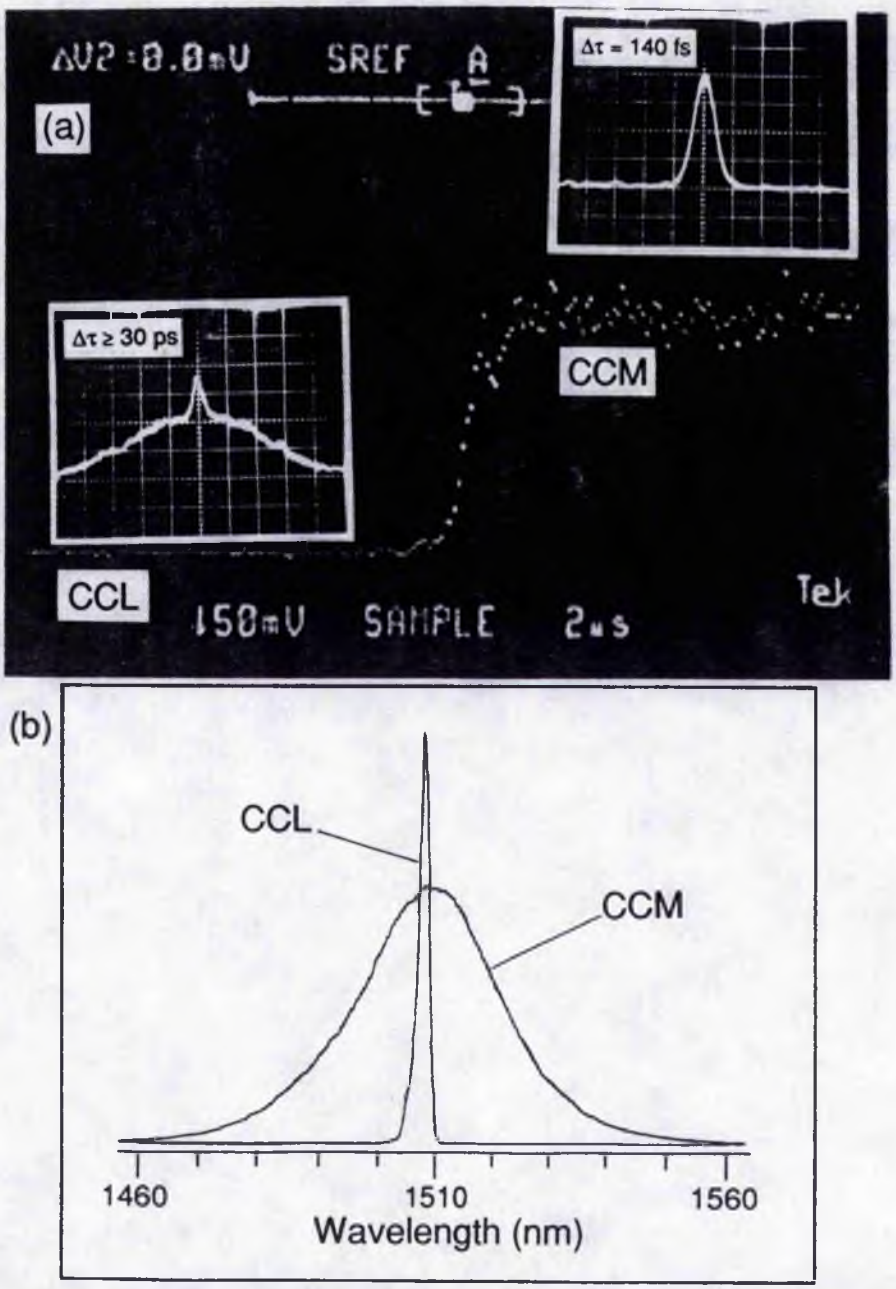

Fig. 9.20. As for Fig. 9.19, except that the initial pulse was a noise burst ($\Delta\tau \geq 30$ ps) and the associated steady-state CCM laser pulse was shorter ($\Delta\tau = 140$ fs) and not bandwidth-limited. (10 times attenuation in measuring the CCL spectrum).

The build up of the SH intensity as the coupled-cavity mode-locking process evolves for these two particular initial circumstances are also shown in Fig. 9.19(a) and Fig. 9.20(a), where the related autocorrelation traces for the final steady-state CCM operation are presented at the top-right of each figure. The spectra for the CCM laser pulses are also included in Fig. 9.19(b) and Fig. 9.20(b). It is interesting to see that for the clean initial pulses which had a duration of 20 ps [Fig. 9.19(a)] it took about 5 μs to reach the steady-

state CCM operation at which stage the pulse duration was reduced to 290 fs and the $\Delta\upsilon\Delta\tau$ value was 0.27. At the same intrafibre power level, for the initial noise burst which had a duration in excess of 30 ps the CCM kinetic process reached the steady state in approximately 1 μs and led to a pulse duration of 140 fs with an associated $\Delta\upsilon\Delta\tau$ value of 0.53. Finally, it should be seen that, similar to Fig. 9.18, even at the same intrafibre power level for different single-shot measurements there is a variation of the SH signal risetime, due to the differences in the initial phase-matching condition. Therefore, to make a proper comparison of the results in Fig. 9.19 and Fig. 9.20 the SH signal traces in these two figures represent a selection of the fastest profiles for the many single-shot observations made for each situation.

9.4. Conclusions

According to the experimental results and the relevant discussions given above the following three conclusions can be drawn:

(i) Operating the coupled-cavity mode-locked colour-centre laser without any bandwidth limiting elements in the main cavity leads to the production of frequency-chirped pulses with large bandwidth-duration products. Such frequency chirps originating from the SPM process in the control cavity can be compensated in either an extracavity or intracavity configurations involving suitable lengths of glass rod. In both cases sub-100 fs, essentially chirp-free, optical pulses can be readily obtained.

(ii) Mismatching of the control cavity length with respect to that of main cavity leads to the variation of the intensity profile of CCM laser pulses. The changes of the temporal features can be conveniently deduced from the shape of the corresponding spectra and the interferometric autocorrelation traces associated with pulses exiting from the control cavity. In general, a positive mismatch leads to the CCM laser pulses having slower leading edges and faster trailing edges, and vice versa for a negative mismatch.

(iii) In a CCM KCl:Tl laser the timescale of the pulse evolution process can vary dramatically, depending on the status of phase matching and power coupling between the control and the main cavity pulses. In the situations where the dynamic process develops

very fast (less than 100 cavity roundtrip periods) overshooting occurs in the associated SHG signal level, which possibly means the instant existence of extremely short pulses during the establishment of the coupled-cavity mode locking.

The observed phenomenon of a random delay in the starting time for pulse evolution represents a very significant characteristic involved in this type of mode-locked lasers. Although the record of the most rapid pulse build-up result ($\leq$ 20 cavity roundtrips) is faster than those predicted in existing theories, the dependences of actual risetimes on the intensity ratio of the feedback pulse to the main cavity pulse and their initial state of phase relation are as expected. The observations of a discrete initial pulse leading to a slower pulse evolution to the CCM steady state compared with that from a noise burst further indicate the important influence of bandwidth limitation during the coupled-cavity mode-locking operation.

Chapter 10

Applications of the CCM KCl:Tl Colour-Centre Laser

In addition to its use in the evaluation of the time resolution of various measurement devices such as ultra-fast photodiodes and electron-optical streak cameras, our coupled-cavity mode-locked KCl:Tl colour-centre laser has also proved to be a powerful tool in the study of pulse propagation in optical fibres in femtosecond regime. In particular, it was used as an ultrashort pulse laser source for carrying out single-pass experiments in various fibres outside the laser cavity, and as an "integrated" test-site when it was directly exploited for the characterization of optical fibre which was incorporated within the control cavity. The experimental data that relate to the research work in these two aspects will be presented in this chapter.

In section 10.1 the characterization of the dispersive behaviour of an erbium-doped fibre incorporated in the control cavity is reported. These results were achieved by tuning the central lasing wavelength around the primary absorption band of the fibre. Also in the first section a series of spectral and temporal recordings for the pulses coupled into and returned from the same type of control fibre but with a shorter length are presented. Such data give a clear picture of how the CCM laser pulses are frequency-chirped due to the transit in the control fibre and thus the dispersive and nonlinear features of the fibre can be examined. In section 10.2, the experimental results and associated analyses relating to femtosecond pulse propagation in five different fibre types outside the laser cavity are described. These five monomode fibre types included two erbium-doped (with medium and lower dopant concentrations respectively), one erbium-free, one standard and one soliton-laser samples[1]. During these single-pass experiments, besides the recording of ordinary spectral extension for the Er-free and one of the Er-doped fibre samples, the novel phenomenon of spectral narrowing in the soliton-laser fibre, the standard fibre, and an extreme spectral extension with a distinctive antiStokes signal at 1.35 μm for the

[1] This soliton (laser) fibre, also called AT & T fibre, is the same one as that described in Ch.8.

second eribum-doped fibre (the one with relatively lower dopant concentration) have also been observed. This latter observation has been attibuted to a special type of nonlinear process - self-phase-modulation mediated four-wave mixing.

10.1 Intracavity characterisation of the control fibre

10.1.1 Absorption feature of the Er-doped fibre

Referring to the CCM laser arrangement shown in Fig. 6.3, the single-pass transmissivity of the Er-doped fibre incorporated in the control cavity can be determined by measuring the average power before objective C1 (P_{fi}) and that after objective C2 (P_f). The result of such a measurment relating to different incident wavelength is shown in Fig. 10.1(a), where the absorption feature of the fibre can be clearly seen. The minimum value of transmissivity at 1534 nm is associated with the absorption center of the erbium-dopant (Mears *et al* 1987). (Note that during this measurement the tuning of the laser wavelength was achieved by rotating a 1-mm-thick birefringent filter and to avoid the effect of absorption saturation, P_f was maintained at ~ 0.5 mW).

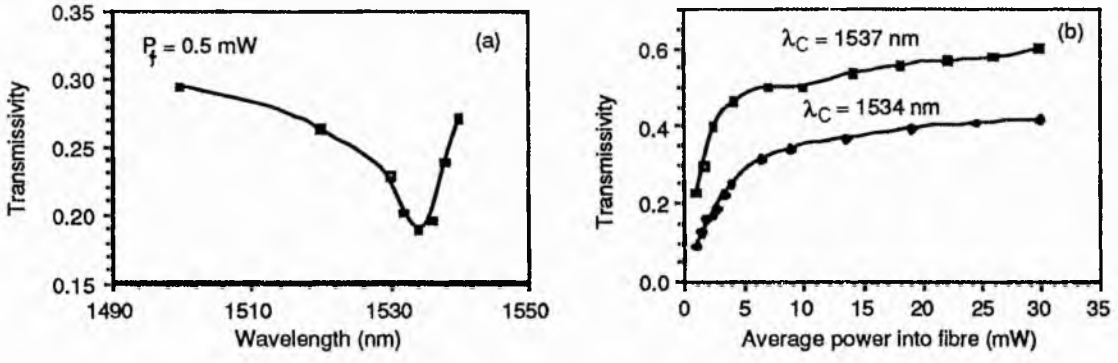

Fig. 10.1. (a) Transmissivity of a 2.56 m long erbium-doped monomode optical fibre as a function of wavelength (see text); (b) Absorption saturation behavior of the same fibre at 1534 nm and 1537 nm.

The measured saturation behavior of the absorption in the erbium-doped fibre is included as Fig. 10.1(b), where the incident colour-centre laser beam was tuned either to the absorption center (1534 nm) or somewhat away from the peak absorption at 1537 nm. The saturation power in both cases was deduced to be ~2mW (for P_{fi}). It follows, therefore, that the nonlinearity associated with absorption will only be significant at

incident average power levels up to around 2 mW. Because the minimum power in the fibre required for mode-locking enhancement in our experiments was 4 mW it may be contended that the absorption-related nonlinearity was unlikely to have contributed significantly to the CCM process.

10.1.2 Dispersion effect around the resonant region

To examine the influence of dispersive feature of the fibre on the performance of the CCM laser, particular attention has been paid to the variations in the CCM laser output when the central wavelength was deliberately tuned across the absorption center of the erbium-dopant in the control fibre. In this case, for the sake of easy operation and the better stability the fibre was cut back from 256 cm to 30 cm. Intensity autocorrelation profiles were recorded both for the CCM laser pulses and for the feedback pulses from the fibre whenever the laser wavelength (λ_c) was centered at 1508 nm, 1534 nm and 1540 nm respectively [see Fig. 10.2, noise signal on traces (b), (d), (f) is associated with the recording of feedback pulses at reduced intensity levels]. For the reason already mentioned, the optical nonlinearity due to the absorption in the fibre can effectively be ignored but it must be recognized that related changes in the dispersion which arise near the absorption centre (Siegman 1986; chapter 9) are likely to significantly affect the propagation behavior of the pulses. It can be seen from the experimental data in Fig. 10.2 that tuning the laser to different wavelength regions (λ_c) leads to quite distinct temporal characteristics in the exiting pulses. When λ_c = 1508 nm, the return pulses from the fibre [Fig. 10.2(b)] are noticeably broader than the corresponding CCM laser pulses [Fig. 10.2(a)]. When λ_c = 1540 nm, pulse compression takes place in the fibre and so the return pulses [Fig. 10.2(f)] are shorter than the injected CCM laser pulses [Fig. 10.2(e)]. At the absorption center (λ_c = 1534 nm), however, a hybrid-state of group velocity dispersion (GVD) was evident where the autocorrelation traces associated with the return pulses were observed to have profiles such as those in Fig. 10.2(d) or 10.2(f) and sometimes a broader trace like Fig. 10.2(b) was recorded with some substructure features at higher power levels. In other words, the trace shown in Fig. 10.2(d), which indicates a feedback-

pulse duration similar to that of the CCM laser pulses [Fig. 10.2(c)] is but one of three possible modes of this "absorption-resonance" fibre behavior.

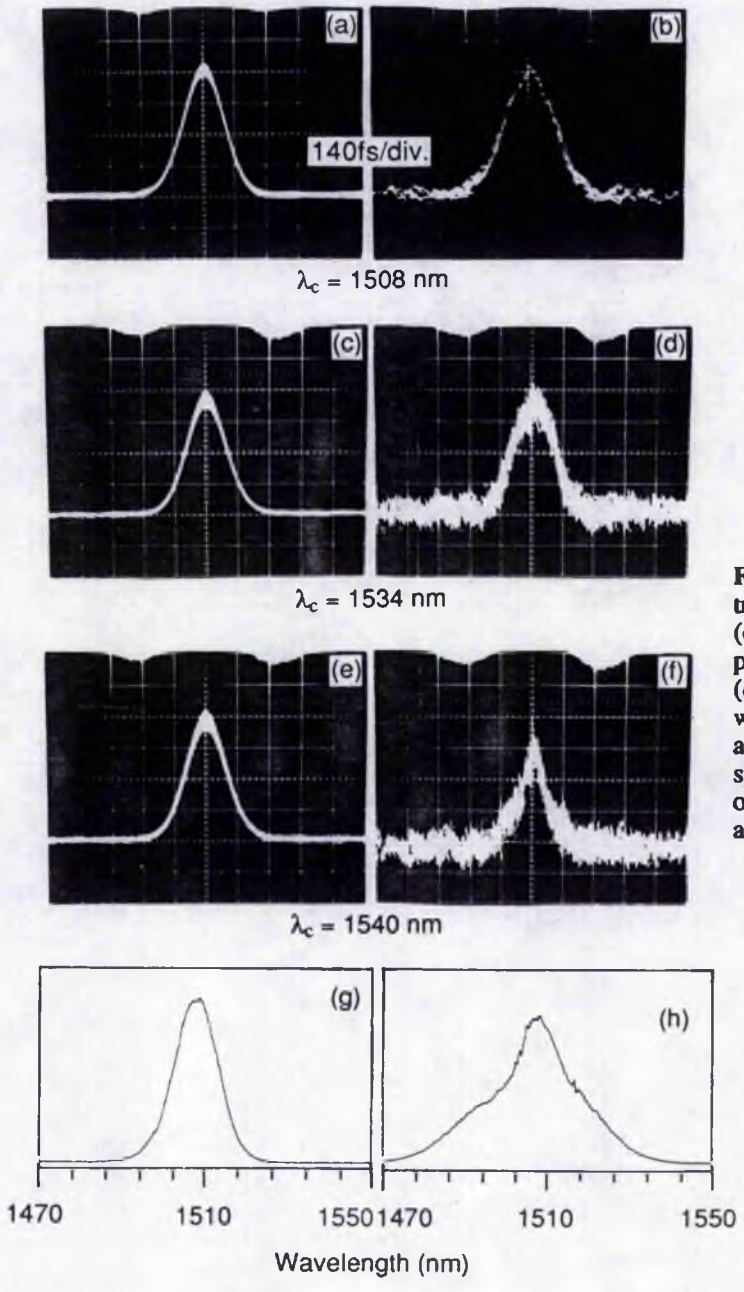

Fig. 10.2. Intensity autocorrelation traces for CCM laser output ((a), (c), (e)) and the corresponding pulses out of the control cavity ((b), (d), (f)) recorded when the laser was tuned to 1508 nm, 1534 nm, and 1540 nm respectively. The spectra associated with the pulses of (a) and (b) are included as (g) and (h).

The range of temporal characteristics included in Fig. 10.2(a, b, e, f) indicate an off-resonance dominant fibre group velocity dispersion that can be described as of the normal [giving temporal broadening Fig. 10.2(b)] or anomalous [giving temporal compression Fig. 10.2(f)] type. Near the absorption-centre for the erbium dopant, the dispersive

character of the fibre can be an admixture of both n-GVD and a-GVD contributions which in some instances may balance [e. g. Fig. 10.2(d)]. More generally, of course, there can be some imbalance that leads to a predominance of either normal or anomalous dispersion and, as stated earlier, all three cases have been observed in practice. (It is interesting that this overall dispersion which results from the combination of material and waveguide contributions can be described as normal up to wavelengths around 1520 nm in the erbium-doped fibre, whereas an erbium-free fibre counterpart has normal dispersion extending to 1660 nm according to the data provided by STC company).

For the CCM laser pulse durations (~240 fsec) involved in these studies, the average power in the fibre was 24 mW and the spectral bandwidths were typically 13 nm. Two examples of spectral measurements corresponding to the results in Fig. 10.2(a), (b) are shown in Fig. 10.2(g), (h) respectively. The spectral broadening due to the self-phase-modulation (SPM) in the Er-fibre which can be clearly seen for λ_c = 1508 nm was typical of that observed at λ_c = 1534 nm and λ_c = 1540 nm. From the spectral and temporal results reproduced in Fig. 10.2 it could thus be considered that some complex pulse shaping kinetics may arise through the interplay of the competing temporal broadening and shortening mechanisms that exist when spectrally-broad femtosecond pulses propagate in doped fibres. The role of the erbium dopant is therefore of fundamental importance in the determination of the GVD characteristics of the fibre.

10.1.3 Spectral and temporal features for the pulses coupled into and returned from the control fibre

From the results presented in the previous two chapters it has been clear that the CCM KCl:Tl laser can be controlled to produce ultrashort pulses at 1.5 μm wavelength region with a variety of features in terms of both temporal duration and spectral bandwidth, and also that at the steady-state both pulses coupled into and returned from the control cavity can be conveniently monitored and thus compared. Such a property has been utilized in an extensive study of the femtosecond propagation in the control fibre.

A group of eight sets of spectral and temporal data for the pulses coupled into and those corresponding ones returned from the control cavity are reproduced as Fig.

10.3 [1]-[8]. Both intensity and interferometric autocorrelation traces for the incident pulses, which are identical to the CCM laser output (see Fig. 6.3), are given on the left-hand side. The right-hand side traces are those for the corresponding return pulses. The spectra for both incident and return pulses are located in the middle column, where as indicated by the arrows the narrower ones with a single feature are the spectra for incident pulses. An exception to this is Fig. 10.3 [1], where the spectral extension in the control fibre is not that large and so it can only be identified by looking at the slightly more extended wings of the spectrum associated with the return pulses. (Interestingly, in terms of FWHM the returned spectrum in this particular situation is slightly narrower than the incident one). The timescale in Fig. 10.3 [1] is also different from the rest in that it is twice that of the others. For Fig. 10.3 [2]-[8] the scale is 40 fs/div. and the fringes in the interferometric autocorrelation traces, which correspond to the coherent additions of the measured pulses "walking" through each other in the autocorrelator, can be clearly seen.

Based on the data in Fig. 10.3, plots of the spectral bandwidth and temporal duration for the return pulses versus the associated incident values can be obtained as illustrated in Fig. 10.4(a), (b) respectively. From Fig. 10.4(a), it can be seen that only for the first three datum points the output bandwidth increases as the incident bandwidth is increased but the points associated with larger incident bandwidths are very scattered. This may be related to the fact that in only the first three cases the incident pulses are properly bandwidth limited, which ensures that a larger bandwidth is associated with a smaller pulse duration and thus a higher peak intensity, whereas the others are not (see the values given in Fig. 10.3). For the circumstances relating to [4] to [8] in Fig. 10.3 the incident pulses have increasing values of both temporal duration and spectral bandwidth, and the associated interferometric autocorrelation traces indicate an increasing amount of frequency chirp. The data in Fig. 10.4(b) show an overall increase in the output pulse duration as the incident pulses become broader (small fluctuations exist in the region where incident pulses are shorter, which could be a result of the involvement of a stronger SPM effect.

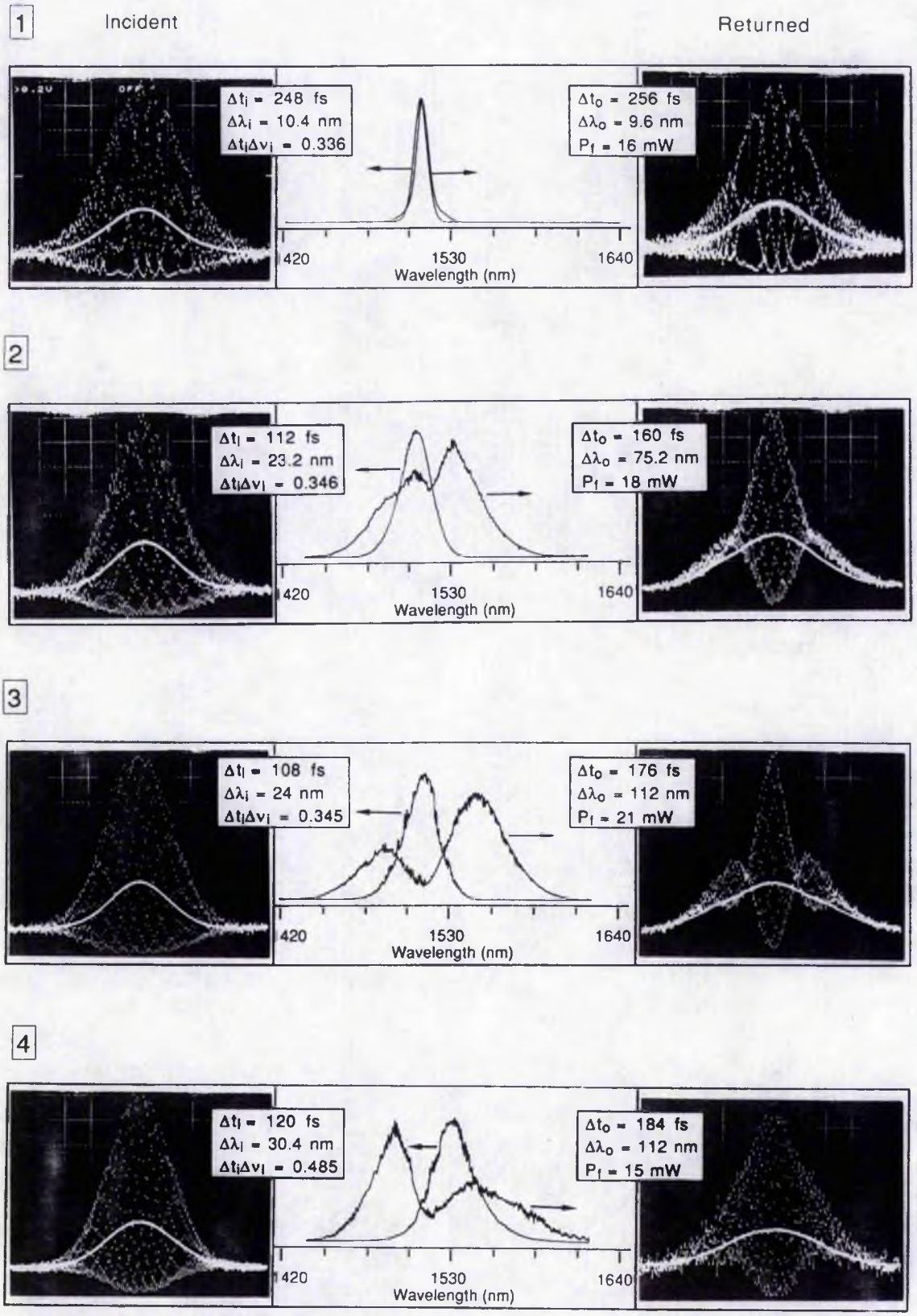

Fig. 10.3(1)-(8). Autocorrelation traces and spectra for the pulses coupled into and returned from the control cavity measured when the CCM KCl:Tl laser was operated under different steady-state conditions with a 28.5-m-long Er-doped control fibre.

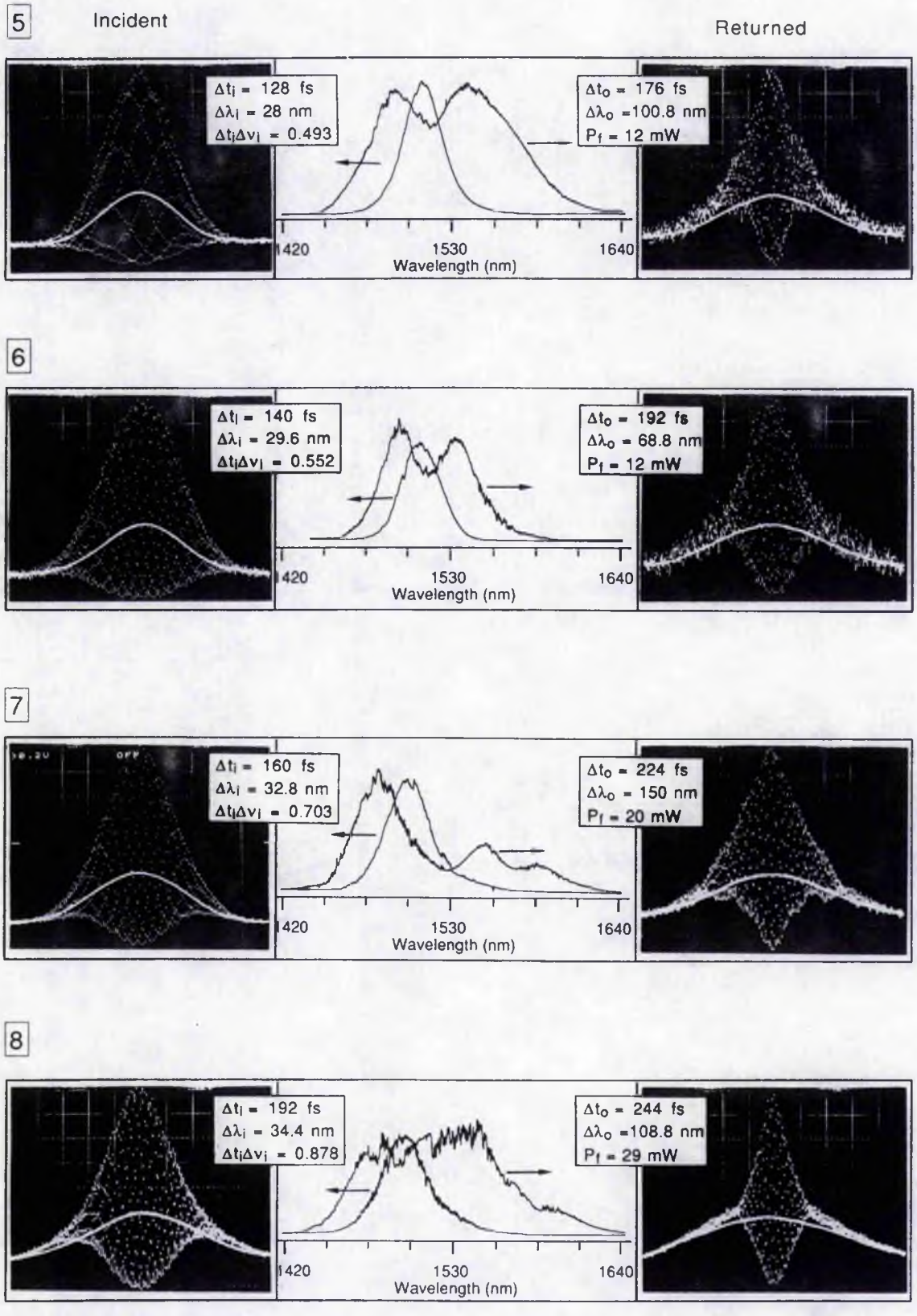

Fig. 10.3(1)-(8). Autocorrelation traces and spectra for the pulses coupled into and returned from the control cavity measured when the CCM KCl:Tl laser was operated under different steady-state conditions with a 28.5-m-long Er-doped control fibre.

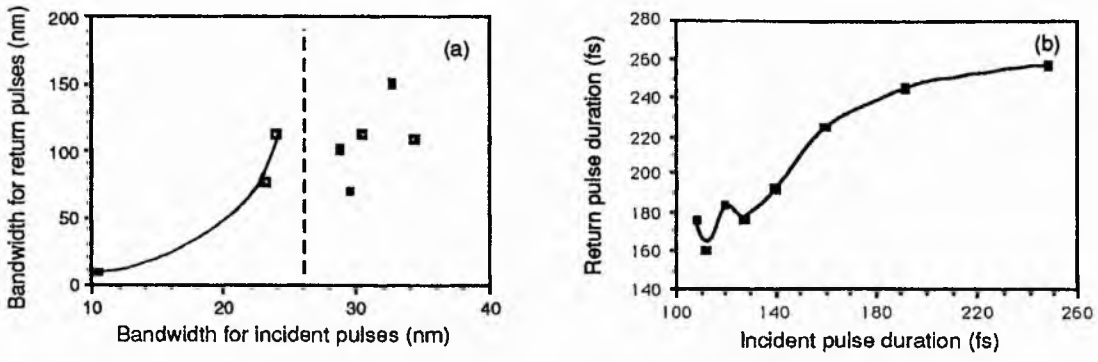

Fig. 10.4. Variation of the spectral bandwidths (a) and temporal durations (b) for the return pulses as a function of the corresponding input values. [These data are deduced from the recordings reproduced in Fig. 10.3(1)-(8)].

Using Eqs. (5.14b), (5.72a) and the parameters of incident pulses in Fig. 10.3, the values of the two important characteristic lengths - dispersion distance z_D and the spectral spread distance z_s can be determined for each situation. Substituting these z_D, z_s values into Eqs. (5.14a) and (5.72b) respectively gives rise to the values of relative temporal broadening for a pure GVD medium and the spectral extension based on a pure SPM medium under the given conditions. These are as shown in Fig. 10.5, 6, where the data of $\Delta t_o/\Delta t_i$, $\Delta\lambda_o/\Delta\lambda_i$ directly obtained from the measurements are also included. These two graphs provide a useful view of how the control fibre functions as a mixture of both dispersive and nonlinear (SPM) medium. The curves in Fig. 10.5 imply that the actual pulse broadening is larger than that expected for a pure dispersive medium, and the curves in Fig. 10.6 indicate that the measured spectral broadening is smaller than that precicted for a pure SPM medium. Both of these results are consistent with expectations. It is known that, in general, for a normally dispersive medium the presence of SPM stretches the spectrum of the pulses and as a result of this the dispersion effect will be enhanced. Alternatively, provided that the consideration is based on a pure SPM medium the appearance of any normal dispersion will cause the increase of pulse duration and so decrease of effective peak intensity, and hence the actual SPM-induced spectral extension will be reduced. Also from Figs. 10.5, 6, it can be seen that the extent of the relative spectral extension is several times larger than that of temporal broadening. Therefore, it may be concluded that the control fibre under these conditions plays a role dominated by

the SPM effect, (or to say it more presicely, the SPM effect in the fibre is stronger than its GVD counterpart). Such a feature is in fact also reflected by the relationship $z_S < z \leq z_D$ that exists in our experiments.

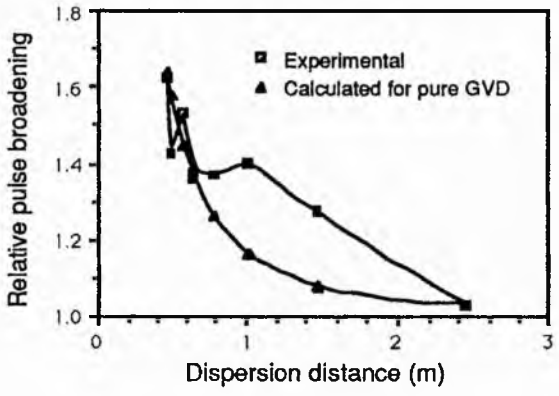

Fig. 10.5. Comparison of the measured pulse broadening with that predicted for a pure GVD medium as a function of dispersion distance, z_D. [The calculation is based on the formula $\Delta t_o/\Delta t_i = (1 + z/z_D)^{1/2}$ with $z = 0.6$ m, $z_D \sim (\Delta t_i)^2/D$, $D = 7.5$ ps/nm/km, Δt_i equal to the actual incident pulse durations given in Fig. 10.3].

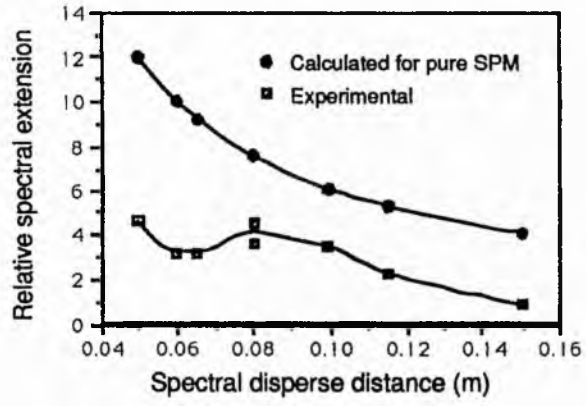

Fig. 10.6. Comparison of the measured spectral extension with that predicted for a pure SPM medium as a function of spectral spread distance, z_S. [The calculation is based on the formula $\Delta\lambda_o/\Delta\lambda_i = (1 + z/z_S)^{1/2}$ with $z = 0.6$ m, $z_S \sim \Delta t_i/n_{2I}P$, $n_{2I} = 3.2 \times 10^{-16}$ W/cm^2, Δt_i , P are taken as those shown in Fig. 10.3].

In addition to the above discussions, it is worth mentioning that the interferometric autocorrelation (IFA) traces in Fig. 10.3 for the return pulses provide a useful way to examine the characteristics of the linear and nonlinear phase shifts experienced by the pulses propagating through the control fibre. For instance, in situation [1], the IFA trace for the return pulses has almost the same profile as that for the associated incident pulses, which means that at this particular steady state the chirp in the pulses caused by the propagation in the control cavity is marginal. (This is associated with the observed relatively minor difference in the spectral features of the return and incident pulses). In situation [2], however, the visibility of the fringes in the wings of the IFA trace for the return pulses disappear, which indicates that the chirp in the return pulses is very

substantial. For the corresponding IFA trace in situation [3], the fringes lose visibility more rapidly away from the central position but they subsequently reappear before finally disappearing in the extreme wing regions. Such a modulated profile is a typical IFA shape that reflects the existence of even larger frequency chirp (Finch 1990, Ch7; The frequency chirp related to the phase shifts in the return pulses in our situations is expected to be close to the nonlinear type because of the existence of stronger SPM, therefore the relevant calculations and analyses by Finch for frequency chirps generated in a Kerr device can be applied). In the cases where the incident pulses become yet more frequency-chirped (situation [5] - [8]), it can be seen that the chirps within the return pulses have increased accordingly.

The interesting shape of the IFA trace in situation [7] can be viewed in conjunction with its associated spectrum that has one additional feature at the longer wavelengths. (In situation [8], the similar spectral feature is just about to occur). This new spectral component, most likely due to the self-Raman effect (Ch. 5), may develop into a new pulse if it experiences a sufficiently strong dispersion, as described in Ch.8. However, for situation [7] it seems that this self-Raman signal had not been fully separated from its "parent pulse". It is perhaps rather surprising to notice that the peak intensities in the fibre for situation [2] and [3] are actually higher than those in situation [7] and [8], but in the former two situations no self-Raman effect is observed. Such a result seems to imply that under the condition of similar peak intensities the chirped pulses favour the generation of self-Raman signal because in this case the spectra of the propagating pulses are more extended.

Finally, as far as the asymmetry of all the other return spectra except that in situation [7] is concerned, it may be attributed to the asymmetry of the incident pulses as discussed in Ch.9.

10.2 Femtosecond pulse propagation in optical fibres (single pass)

The experimental arrangement for the femtosecond pulse propagation in various optical fibres is shown in Fig. 10.7. The laser source, which was the coupled-cavity mode-

locked KCl:Tl color center laser, was controlled to have an output pulse duration of 120 fs ± 15 fs and a bandwidth-duration product of 0.36 ± 0.05. This was achieved by using a 21 cm long Er-doped monomode optical fibre in the control cavity and a 0.5-mm-thickness birefringent filter in the main cavity. Representative intensity and interferometric autocorrelation traces and corresponding spectra for the laser output pulses are reproduced in Fig. 10.8(a-c) respectively, where it can be deduced that the pulse duration Δt_i was 120 fs, the spectral bandwidth $\Delta\lambda_i$ was 21 nm and $\Delta t_i \Delta\nu_i$ was 0.34.

The beam from the CCM laser was directed via a beamsplitter S1, steering mirrors M_1, M_2, and subsequently focussed into the test fibre with a x20 microscope objective C1. The output beam from the fibre was then coupled into the scanning monochromator using the microscope objective C2 and mirrors M_3 and M_4. By rotating M_3 to direct the exit beam to the beamsplitter S2, the temporal characteristics of the pulses from the fibre could be monitored using a realtime autocorrelator. A unidirectional isolator inserted between the beamsplitter S1 and the CCM laser ensured that the feedback from the test-fibre could be avoided. For the incident pulses as shown in Fig. 10.2 and a pulse repetition period of 12.6 ns, the estimated average power range was 1-16 mW and the peak pulse power was 0.1-1.6 kW within the test fibre.

The propagation characteristics of the 120 fs-pulse sequence were monitored for five different types of fibres, among which the two erbium doped, one erbium-free and one standard fibres have the properties as listed in Table 8.1. (The properties of the AT & T fibre can be found in Section 8.1). Note that all these fibres are non-polarization preserving except the AT & T fibre. The three erbium related fibres have the same geometrical structure while the standard and the AT & T fibres have relatively large core diameters. From the relevant specifications of these fibres, it can be estimated that the typical peak intensity under our experimental conditions was ~5 GW/cm^2 (assuming a pulse peak power of 1 kW) for the erbium-related three fibre types and ~1 GW/cm^2 for the standard and AT & T fibres. For pulses of these peak intensities propagating in fibres having lengths ~ 0.2-3.7 m most of the nonlinear effects discussed in Subsection 5.2.3 would be expected to occur.

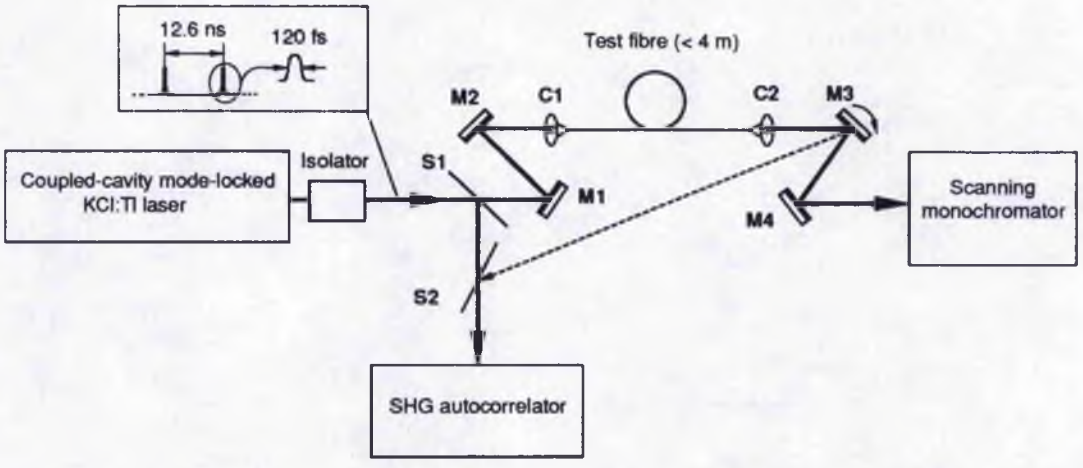

Fig. 10.7. Experimental arrangement for pulse propagation studies in monomode optical fibers. S1, S2 - beamsplitters; M1, M2, M3, M4 - steering mirrors; C1, C2 - microscope objectives. The mirror M3 can be rotated to direct the exiting beam to S2 for temporal measurements.

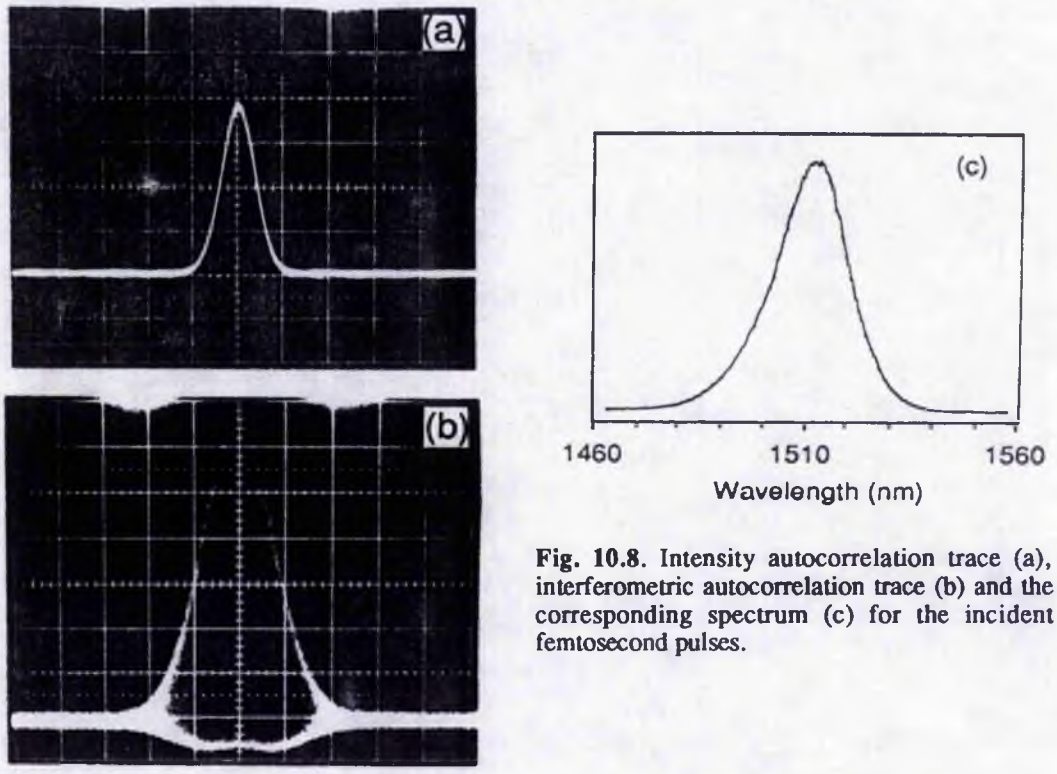

Fig. 10.8. Intensity autocorrelation trace (a), interferometric autocorrelation trace (b) and the corresponding spectrum (c) for the incident femtosecond pulses.

10.2.1 Spectral broadening in Er-free and the medium doped erbium fibres

A comparison of the spectral broadening behaviour of pulses propagating in approximately the same lengths of the erbium-doped fibre I (the one with a medium dopant concentration) and the Er-free counterpart (L = 2.58 m) is shown in Fig. 10.9. The average optical powers just inside the exiting end of the fibre were as indicated and these

values were deduced from those monitored by a power meter located between C2 and M3. From Fig. 10.9 it can be seen that the SPM-induced spectral broadening occurs in both fibres, but for the same power level a substantially greater amount of spectral extension is exhibited by the Er-doped fibre. At a power level $P_f = 12$ mW (see the two bottom traces in Fig. 10.9) the spectral extent for the erbium-doped sample is such that the second pair of spectral lobes caused by SPM were just being generated, which implies an associated nonlinear phase shift ~ 3π (Stolen and Lin 1978), whereas for the Er-free counterpart, the exiting spectral bandwidth of approximately twice that of the incident spectral width indicates a nonlinear phase shift of less than π.

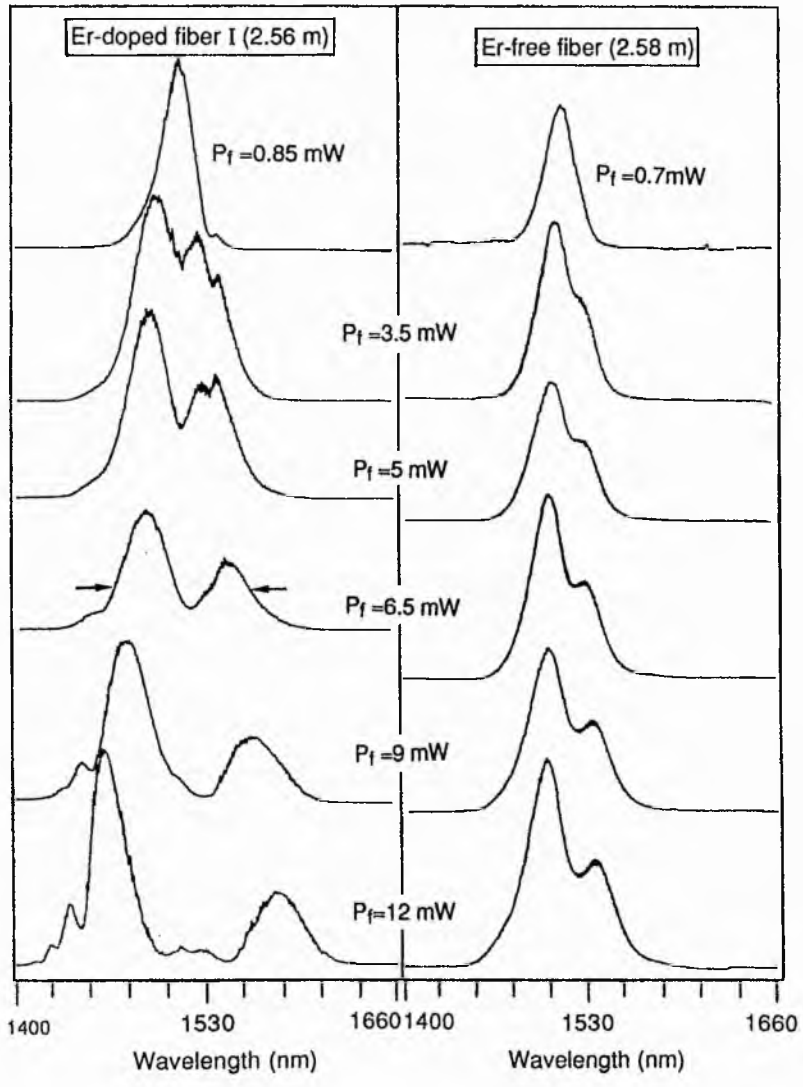

Fig. 10.9. Spectra of the pulses exiting the Er-doped and Er-free fibers as recorded for increasing power levels in the fibers.

A noticeable common feature of these two groups of spectra in Fig. 10.9 is the asymmetrical energy distribution where there are larger frequency shifts towards the "red" (i.e. longer) wavelengths and more energy is located at the "blue" wavelengths. The most likely origin for this is the temporal-profile asymmetry in the incident pulses, because it has been shown in the Ch. 9 that even slight mismatches in the cavity periods of a CCM laser can give rise to such an effect. The observable asymmetry in the spectrum shown in Fig. 10.8(c) could be evidence for the asymmetrical temporal profiles of incident pulses, which have sharper leading edges and slower trailing edges. [The reason for the small spectral peaks (~11 nm apart) among the short wavelength features of the erbium-doped fibre (see the three bottom traces in Fig. 10.9) have not yet been properly understood. One possibility is that it might be attributed to third-order dispersive effects (Bourkoff *et al* 1987)]. It will be shown by the experimental results described below that this type of erbium-doped fibre has a very small group velocity dispersion in this near-infrared spectral region and so the higher-order terms of GVD may play a significant role in determining the features of the propagating pulses.

Two examples of the autocorrelation traces for the exiting pulses are reproduced in Fig. 10.10(a), (b) respectively. It can be seen that for pulses exiting the Er-doped fibre, Fig. 10.10(a) provides evidence for strong pulseshape distortion (at a power level P_f=11 mW), whereas the pulses propagating through the Er-free fibre at a similar power level [P_f=10 mW, Fig. 10.10(b)] mainly experience a large amount of temporal broadening. For the latter case, if the fibre is assumed to behave as a purely dispersive medium, substitution of our experimental values Δt_i = 120 fs, Δt_o = 870 fs, z = 2.56 m into Eqs. (5.14a) and (5.14b) implies that $z_D \approx 0.36$ m and $|D| \approx 12$ ps/nm/km. Although this deduced value for the GVD is approximately twice that stated in Table 8.1 both results confirm that this Er-free fibre has normal dispersion in the 1.5 μm wavelength region. For the Er-doped fibre, however, the spectral spread caused by self-phase-modulation is so dominant that the interplay between the largely extended spectrum and the dispersion leads to obvious pulse distortion and so Eqs. (5.14) can not be used for an estimation of the GVD value. [Note that in our measurements the autocorrelator has a collinear

alignment such that an intensity autocorrelation trace with a peak-to-background ratio of 3:1 is expected for discrete pulses. (The base line is always set at the bottom grid line shown in the photographs). Any deviation of the measured traces from the 3:1 ratio would be an indication that the incident pulses have distorted shapes or that background energy is present].

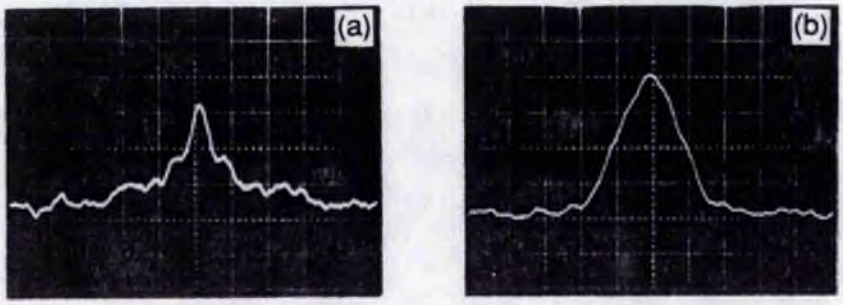

Fig. 10.10. Examples of SHG intensity autocorrelation traces for the exiting pulses from Er-doped fibre (a) and Er-free fibre (b), associated with power levels of 11 mW and 10 mW respectively.

From the recorded spectral traces of the type reproduced in Fig. 10.9 the dependence of spectral extent (or bandwidth), $\Delta\lambda_o$, on the optical power, P_f, can be deduced (see Fig. 10.11 where for the data relating to the erbium-doped fibre the full spectral latitude at half the maximum intensity of the weaker peak is taken). The top dashed line is a calculated result using Eq. (5.70b). In our calculations, the nonlinear refractive index (Kerr coefficient) n_{2I} is taken to be $\frac{5}{6} \times 3.2 \times 10^{-20}$ m^2/W, the fibre length L is 2.58 m and the incident central wavelength λ_c is 1510 nm. The peak optical intensity I_o was transformed into the experimentally measured average power P_f through the relationship $I_o = \frac{P_f T}{S\Delta t}$, where T = 12.6 ns is the pulse repetition period and $S = 1.1 S_{core}$ is the effective cross-section of the beam in the fibre. Substituting these parameters into Eq. (5.70b) and using the relationship $\Delta\lambda/\lambda = \Delta\omega/\omega$ gives an expression for spectral broadening:

$$\Delta\lambda_o \approx \Delta\lambda_i [1+1.6\, P_f(mW)] \qquad (10.1)$$

The theoretical data presented in Fig. 10.11 have been obtained using Eq. (10.1).

For the data presented in Fig. 10.11 it can be seen that both of the measured $\Delta\lambda_o$ versus P_f curves have reasonably good straight line fits (except with some deviations in

the lower power region) but their gradients are three times (for Er-doped fibre) and 12 times (for Er-free fibre) smaller than that of the pure SPM dependence. This may be explained by the fact that the length of these test fibres are all quite comparable to the dispersion length and so the group velocity dispersion becomes an important effect which opposes the spectral broadening induced by SPM. However, the precise reasons for the difference between the erbium-doped and erbium-free fibres in terms of the amount of nonlinear phase shift are not yet clear. Although the presence of the erbium ions may give rise to particular variations in the nonlinear refractive index value n_{2I}, the observed distinct dispersive features may also be responsible for the difference in the spectral extensions between these two fibres. As has already been understood, the differences in the group velocity dispersion may lead to the changes of the overall effective optical intensities present in the test fibres and therefore the intensity-dependent nonlinear phase shift will vary accordingly.

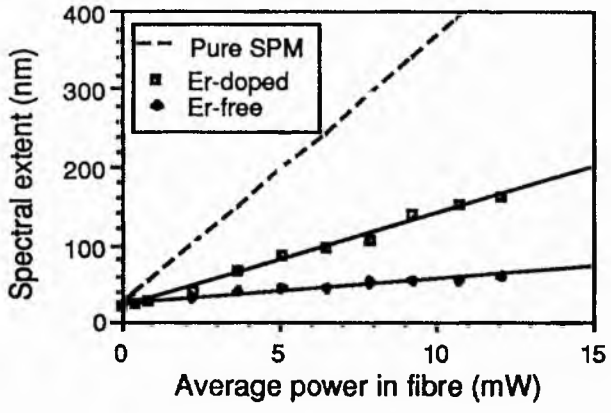

Fig. 10. 11. Spectral extensions as a function of optical power observed in the 2.56 m long Er-doped and the 2.58 m long Er-free fibers. The dashed line is a calculated result for the pure SPM effect when group velocity dispersion is ignored.

Similar spectral measurements for the same types of fibres but with shorter lengths led to the results shown in Fig. 10.12(a), where the solid lines are the best cubic fit to the data points. Such spectral extension appears to have a type of threshold behaviour, which implies that the linear relationship between $\Delta\lambda_o$ and P_f is no longer hold when the total nonlinear phase shift (proportional to the product of optical intensity and fibre length) is small. Such observations are consistent with the theoretical analyses given in Ch.5. regarding the appropriate expression of the SPM-induced spectral broadening. It has also

been pointed out in chapter 5 that when the nonlinear phase shift is small the spectral broadening should be described by Eq. (5.71c) rather than Eq. (5.70b) - the one that leads to the linear-relationship of Eq. (10.1).

By taking the point at a power P_f = 8 mW in Fig. 10.12(a), it can be inferred that in practice there is a threshold or critical value for the nonlinear phase shift, which, if denoted as $(\Delta\phi)_c$, is ~ 2.2 radians. This is consistent with the criterion defined in the paper by Stolen (1980), where an expression for a critical optical peak power has been deduced from a phase shift $(\Delta\phi)_c = 2.0$ radians.

To complement the spectra for the two regimes indicated in Fig. 10.12(a), temporal measurements taken by double exposures for both incident and exiting pulses for each fibre are shown in Fig. 10.12(b). It can be seen that the pulse duration is essentially unchanged after propagating through the Er-doped fibre [see Fig. 10.12(b)-A] but a relatively large pulse broadening effect is observable for the Er-free fibre [see Fig. 10.12(b)-B]. For the autocorrelation trace in Fig. 10.12(b)-A , the maximum difference in pulse durations that can be determined is ~15 fs and so by using Eqs. (5.14), the dispersion parameters of $z_D \geq 1.2$ m, $D \leq 3.5$ ps/nm/km can be estimated for this Er-doped fibre. Similarly, for the Er-free fibre, a temporal broadening of 182 fs can be measured from Fig. 10.12(b)-B and using the experimental value of 12 ps/nm/km for the dispersion parameter of this 0.44 m length of fibre then the predicted temporal broadening of 179 fs is in good agreement with that deduced from the autocorrelation data.

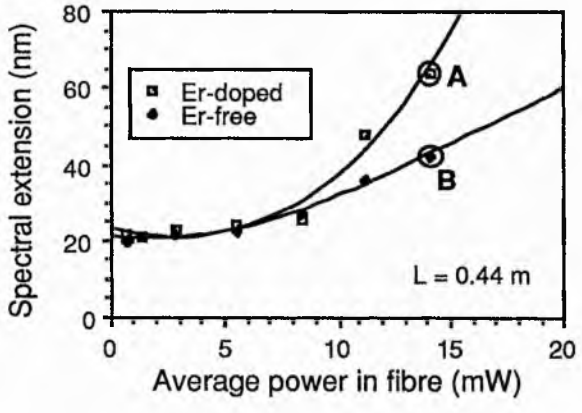

Fig. 10.12(a). As for Fig. 10. 11 except that the two types of fibres were cut back to a length of 0.44 m.

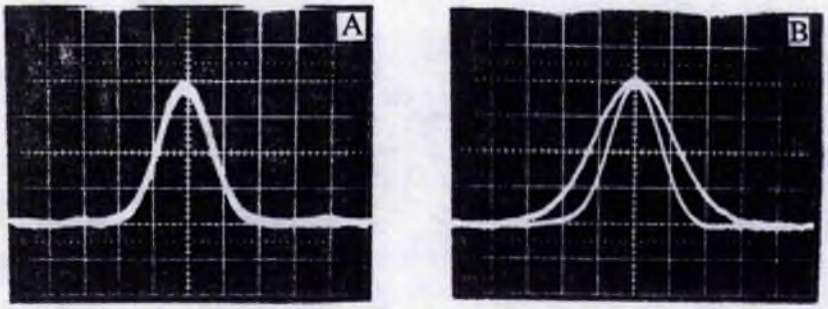

Fig. 10.12(b). Double exposures of the intensity autocorrelation traces for both incident and exiting pulses from the Er-doped (A) and Er-free (B) fibres associated with the two datum points indicated in Fig. 10. 12(a).

10.2.2 Spectral narrowing in the standard and AT & T fibres

In contrast to the spectral extension described above in either Er-doped fibre or its erbium-free counterpart, spectral narrowing of the propagating pulses has been observed in both soliton and standard fibre samples. As shown in Fig. 10.13, with an increasing coupling power into the 2.74-m-long AT & T fibre the spectrum of the exiting pulses becomes noticeably narrower. [Similar results were also recorded for the 2.61-m-long standard commercial monomode fibre (Newport Ltd.)]. Associated with these spectral narrowing recordings the temporal measurement shows the increase of pulse duration. For instance, at P_f = 5.5 mW the exiting pulses have a durataion of 490 fs, which is much longer than the incident pulses with a duration of 126 fs.

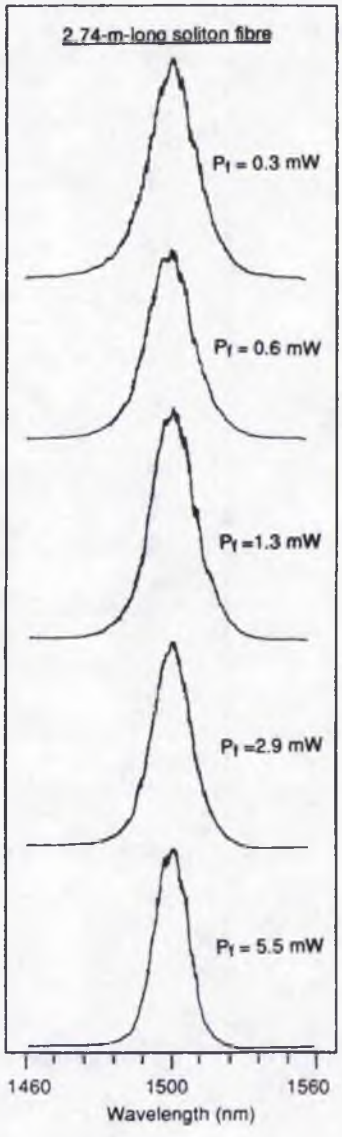

Fig. 10.13. Spectra of the pulses exiting from a AT & T fibre as recorded for an increasing average power level in the fibre.

A plot of the relationships between the spectral bandwidth of the exiting pulses and the average intrafibre power is given in Fig. 10.14 for the two indicated fibre samples. The spectral narrowing phenomenon evident in Fig. 10.14 seems quite unusual compared with many reported experimental results regarding the spectral features of propagating pulses, where spectral extension was almost unanimously recorded. Nevertheless, if we remember that the interplay between GVD and SPM in an anomalously dispersive medium may lead to the propagating pulses either temporally compressed or stretched depending on the power and the chirping feature of the incident pulses it will then be able to realize that the "spectral shrinking" can possibly exist due to the same solitonic effect.

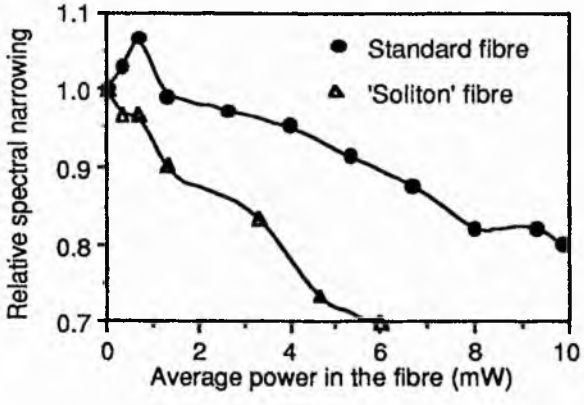

Fig. 10.14. Decreases of spectral bandwidth ($\Delta\lambda_0/\Delta\lambda_i$) with the increase of coupling power for the pulses exiting from a 2.61-m-long standard fibre (Newport Corp.) and the 2.71-m-long polarzation-preserving soliton fibre (AT & T fibre).

For the fibre where optical solitons can be sustained, the relationships between the spectral bandwidth of the propagating pulses and the distance along the fibre at different input power levels are as illustrated in Fig. 10.15, where P_1, P_2, P_n denote the power levels required for N = 1, 2, n solitons, L_0 is the soliton period. Three distinctive features about the spectral extension shown in this graph can be readily noticed. These are: (i) For $P < P_1$, $\Delta\lambda$ increases monotonically for an increasing propagation distance; (ii) For $P = P_1$, the N = 1 soliton is formed and so $\Delta\lambda$ remains constant throughout the propagation; (iii) For $P = P_n$ ($n > 1$), $\Delta\lambda$ increases and decreases periodically - each time when the propagation distance is equal to an integral multiple of L_0, $\Delta\lambda$ is restored to the initial value of the incident pulses.

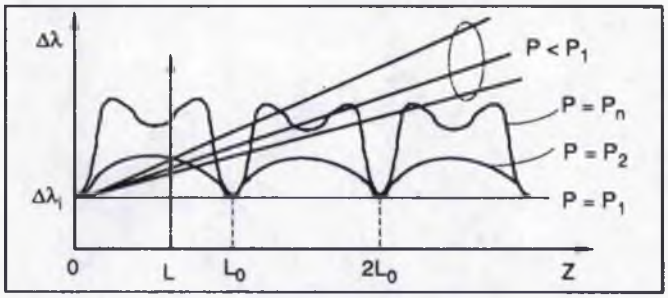

Fig. 10.15. Illustration of spectral extension in anomalously dispersive fibres: variation of the bandwidth for exiting pulses as a function of fibre length under different coupling powers; L_0- soliton period, P_i (i = 1, 2, n) - the optical powers corresponding to the soliton orders.

Utilizing the relationships indicated in Fig. 10.15, a dependence of spectral bandwidth for propagating pulses on optical coupling power can be established. This is as shown in Fig. 10.16, where for the sake of simplicity, the fibre length is selected to be equal to the soliton peorid. It can be seen that, as the power coupled into the fibre increases from zero to P_1, the spectral bandwidth first increases and then decreases. At $P = P_1$, the spectrum of the exiting pulses becomes identical to the incident spectrum (i. e. $\Delta\lambda = \Delta\lambda_i$) because in this case the pulses are actually N = 1 solitons. Above P_1 as the launching power continues to increase, $\Delta\lambda$ will increases sharply due to the pulse compression under the higher-order solitonic effect and subsequently decreases until $P = 2^2P_1$, at which the spectral bandwidth becomes equal to the initial value again (i. e. N = 2 solitons). Such a pattern of extension, shrinkage and restoration of the spectrum for the propagating pulses is retained for even higher power levels except that the rise and fell features are expected to be faster (see Fig. 10.16). (If $L \neq L_0$, the spectrum of the propagating pulses can only restore at $P = P_1$ and the overall spectral extension in these situations may have the feature like that shown by the dashed line).

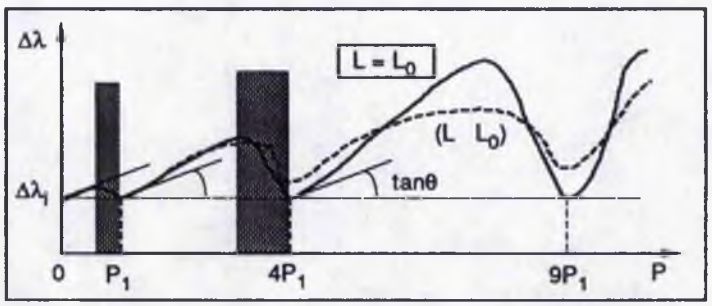

Fig. 10.16. Illustration of spectral extension in anomalously dispersive fibres: for the selected fibre lengths, the predicted changes of spectral bandwidth of propagating pulses versus coupling powers (solid line: L = L_0; dashed line: $L \neq L_0$). The shadowed area mark the regions where the increase in intrafibre power level leads to the decrease of spectral bandwidth. The slope characterised by tanθ is the assumed increase rate of spectral extension for a pure SPM medium.

At this point it has to be acknowledged that Fig. 10.15 and 10.16 represent only a qualitative description of spectral extension behaviour in anomolously dispersive fibres. (To determine the accurate form of the $\Delta\lambda$-P curve, which is dependent on the particular fibre length, numerical solutions to the nonlinear Schrodinger equation must be obtained). However, it can be appreciated from Fig. 10.15 and 10.16 that it clearly illustrates the existence of some specific power ranges, (shadowed portions in Fig. 10.16), within which an increase of optical power leads to a decrease in spectral bandwidth. Such a feature may just be used to give a good explanation to the spectral narrowing data recorded in Fig. 10.13, 14.

Through using the given fibre properties (D = 15 ps/nm/km, effective field area in the fibre core = 10^{-6} cm^2) and an input pulse duration of 140 fs, the N = 1 soliton intensity for these two fibres can be estimated to be 2 GW/cm^2. The actual maximum peak intensities associated with the data in Fig. 10.13, 14 are $\leq$ 1 GW/cm^2. Therefore, it is most likely that the spectral narrowing we observed is related to the optical power range just before the N = 1 solitons are formed (see Fig. 10.16). However, the remaining question about the data in Fig. 10.14 is that there is almost no increase of the spectral bandwidth even at the very low intrafibre power levels before the bandwidth actually starts to reduce, which are not consistent with that speculated from Fig. 10.16. One possible reason for this discrepancy could be that the test incident pulses are not properly bandwidth-limited, whereas the graph drawn in Fig. 10.16 is based on the assumption of transform-limited pulses.

10.2.3 Four-wave-mixing in the low doped erbium fibre

The detail of the spectral extension recorded for pulses exiting a 2.57-m-long sample of Er-doped fibre II is reproduced in Fig. 10.17. As indicated in Table 8.1, this particular fibre has a relatively low erbium-dopant concentration and a theoretically predicted zero first-order dispersion wavelength of 1430 nm. The vertical dashed-line in Fig. 10.17 indicates the central wavelength (~1510 nm) of the incident CCM laser pulse spectrum [see Fig. 10.8(c)].

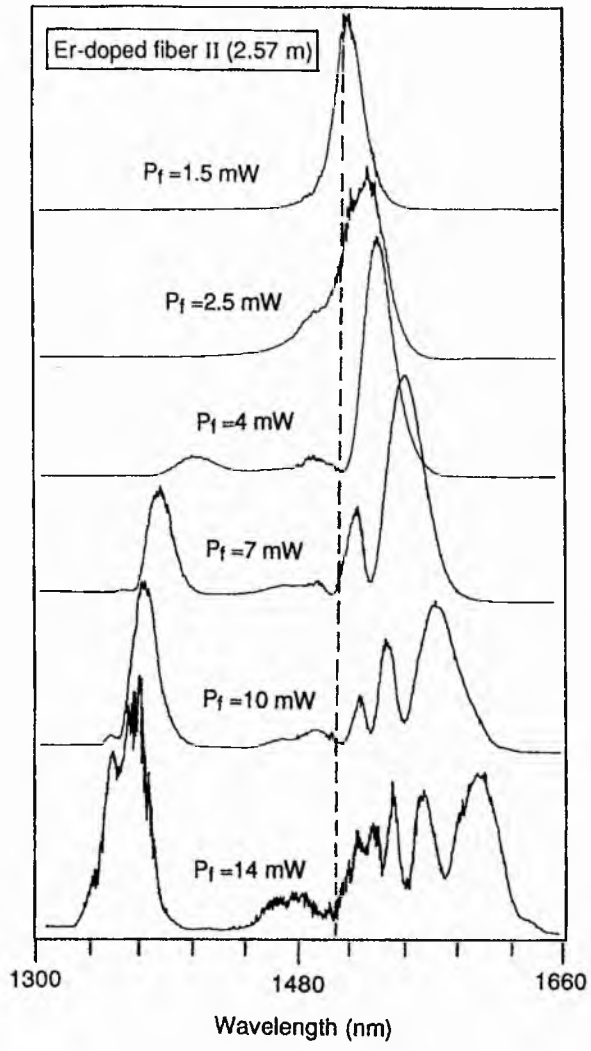

Fig. 10.17. Spectra for the pulses exiting the 2.57-m-long, Er-doped fiber II sample, measured for the power levels as indicated. The vertical dashed line denotes the central wavelength of the incident laser pulse spectrum.

It is interesting to note that the spectral broadening process in this fibre is dramatically different from that for the two samples discussed in the subsection 10.2.1. For this Er-doped fibre II, at lower power levels ($P_f < 2$ mW) the spectra extended symmetrically as would be expected for a dominant SPM process, but even at modest optical powers ($P_f \sim 2.5$ mW) some asymmetry in the recorded traces was already observable. Further increases of P_f led to the generation of a distinct anti-Stokes feature which was clearly displaced from the incident central wavelength. Significantly, the SPM features at shorter wavelengths were suppressed although their counterparts at longer wavelengths were clearly sustained (see the oscillatory features for the spectral profiles associated with powers $P_f \geq 4$ mW, at the wavelengths longer than 1510 nm in Fig.

10.17). As the power in the fibre was increased beyond 4 mW, the central wavelength of this anti-Stokes feature shifted further towards shorter wavelengths and had an increasing intensity and bandwidth. For instance, when the optical power P_f reached 14 mW, the strong anti-Stokes feature can be seen to have a central wavelength of 1358 nm and a bandwidth ~34 nm. Some subfeatures within this anti-Stokes peak may be caused by a self-induced phase-modulation.

Two examples of autocorrelation profiles recorded at powers $P_f = 4$ mW and $P_f = 10$ mW are presented in Fig. 10.18(a), (b). Pulse shaping [Fig. 10.18(a)] and pulse breakup [Fig. 10.18(b)] effects are clearly evident in these traces. At the lower power level the pulses have been compressed from 120 fs to about 85 fs during the propagation in the fibre as would be expected from a solitonic type of influence. Interpretation of the autocorrelation data for $P_f = 10$ mW is rather more difficult because the two subpulses [see Fig. 10.18(b)] could be associated respectively with the "blue" anti-Stokes and the "red" SPM-related components. As they propagate in the fibre, these two spectral "groups" will be subject to group velocity dispersion and the associated walk-off effects will be discussed below.

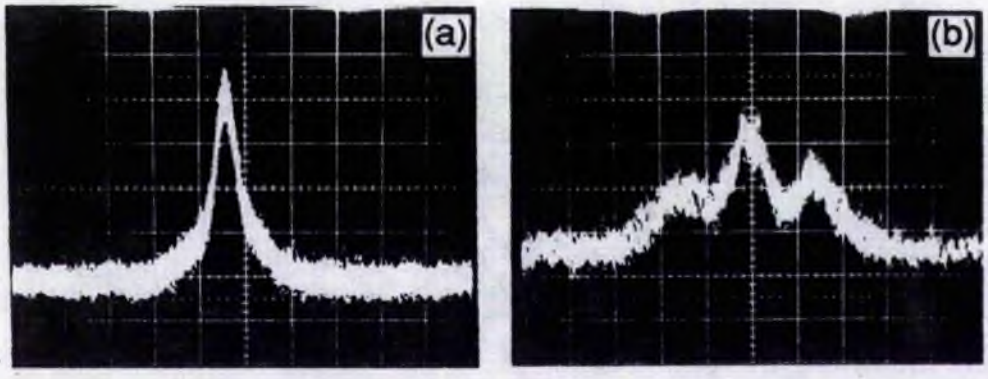

Fig. 10.18. Intensity autocorrelation profiles for the exiting pulses having the spectra shown in Fig. 10.17, at the power levels of 4 mW (a) and 10 mW (b) respectively.

Because the identification of precise pump and Stokes signal wavelengths is quite difficult from the spectra shown in Fig. 10.17, it was therefore necessary to make further measurements for different lengths of this type of doped fibre. The experimental data included as Fig. 10.19 show the spectral extensions (measured as for Fig. 10.9) plotted as

a function of average power, P_f, for three selected fibre lengths. For the 2.57 m long fibre, the rapid increase at 3 mW is associated with the appearance of a anti-Stokes signal (see Fig. 10.17). When the fibre was cut back to 0.44 m the spectra for the exiting pulses were characterized by a single feature, the bandwidths of which increased progressively with increasing incident optical power. When the power, P_f, reached the maximum available experimental value (~13 mW) the onset of a significant increase in spectral extension would imply that the anti-Stokes signal has begun to be generated. As expected, at this maximum power level, this feature did not appear for the 0.22 m long fibre. One conclusion that can be drawn from these spectral data of Fig. 10.19 is that a minimum nonlinear phase shift is required if the anti-Stokes signal is to be produced.

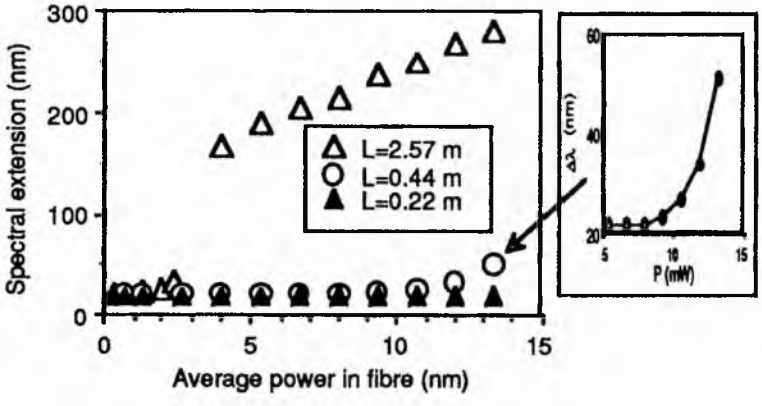

Fig.10.19. Variation of the spectral extensions with power P_f for the pulses propagating in three lengths of the Er-fiber II.

Given that the nonlinear phase shift is directly related to the SPM-induced spectral extension and that prerequisite conditions are imposed on the pump wavelength for four-wave-mixing to be sustained in a single mode optical fibre (Lin *et al* 1981, Garth and Park 1986, Sammut and Garth 1989), it follows that the observation of Fig. 10.17 could be described as a type of SPM-mediated four-wave-mixing process. In other words, although the injected laser pulses (λ_c~1510 nm) do not satisfy the phase-matching condition for realizing four-wave-mixing, SPM-related spectral extension provides appropriate new frequency components such that phase-matching is possible. These induced spectral components, which have wavelengths close to the actual zero-dispersion

regime of the fibre characteristics, constitute a suitable pump signal which leads to the generation of Stokes and anti-Stokes signals through the four-wave-mixing process.

Examples of spectral extension as observed for a 3.7 m long fibre (see Fig. 10.20) can be used to support this interpretation. An analysis of the trace shown in Fig. 10.20(a) can be undertaken as follows. Relative to the incident CCM laser central wavelength (λ_c as indicated), the assumed spectral peak (shown dashed) at λ_p is the expected feature on the shorter wavelength side of the SPM-broadened spectrum. If we assume that in practice this feature provides the pump signal (hence its depletion), a frequency shift of 389 cm^{-1} between the pump and the anti-Stokes signals would apply. Correspondingly, because of energy conservation ($\omega_{as} - \omega_p = \omega_p - \omega_s$) the relative spectral identity (or wavelength) of the Stokes signal would be as indicated in Fig. 10.20(a). At this deduced Stokes wavelength (λ_s = 1561 nm) some features which can be observed within the principal longer wavelength component of the spectral profile are consistent with this inference of a four-wave-mixing process.

The spectral identity of the pump, Stokes and anti-Stokes signals can also be established as indicated in Fig. 10.20(b), (c). It is especially noteworthy that as the optical power is increased there is an associated shift of the pump frequency towards shorter wavelengths, which is permitted through the enlarged SPM-induced spectrum. From the experimental data it was clear that this increase in effective pump frequency for the four-wave-mixing process gives rise to a larger difference between the pump and the Stokes (or anti-Stokes) frequencies. Such behaviour is compatible with the reported theoretical predictions by Garth and Park (1986). At the higher intensity levels that apply to the trace reproduced in Fig. 10.20(c), another pair of Stokes and anti-Stokes signals can be seen. These additional Stokes and anti-Stokes components are not expected to result from the higher-order four-wave-mixing process as reported by Sammut and Garth (1989). A more plausible explanation is that when the pulse power is sufficiently high, the nonlinear phase shift for the wings of pulses will become sufficiently large to generate the spectral components which meet the phase-matching conditions for four-wave-mixing.

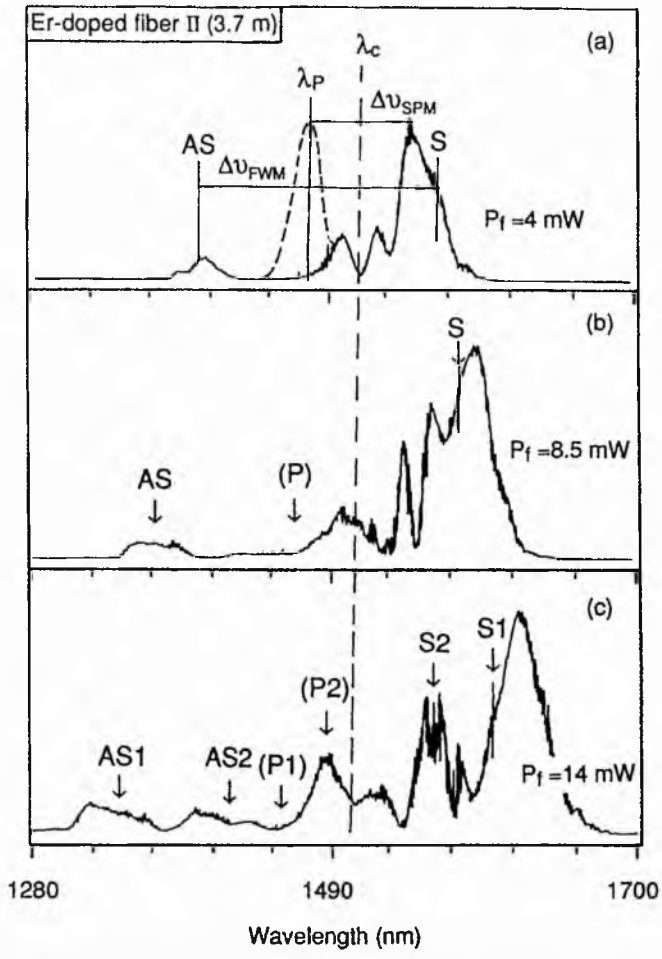

Fig. 10.20. Spectra of the pulses exiting a 3.7 m long Er-fiber II at the power levels as indicated, where the vertical dashed straight line marks the central frequency of the incident pulses. The dashed profile in Fig. 10.20(a) is the assumed SPM feature which should occur when no FWM process is involved (see text). AS - anti-Stokes; S-Stokes, P - pump.

10.2.4 Further analysis of the SPM-mediated four-wave-mixing

Detailed parameters for the Er-doped fibre II (precise refractive index profile, specific dispersion characteristics) have not been comprehensively determined so absolute calculations of the phase-matching conditions that relate to the above cannot yet be made. Nevertheless, some semiquantitive analyses can still be carried out.

As already described in Sec. 5.2 the phase-matching condition for the four-wave mixing process can be expressed as

$$\Delta\beta = \beta(\omega_{as}) + \beta(\omega_s) - 2\beta(\omega_p) = 0 \qquad (5.82)$$

To determine whether this condition is met in the present circumstances the experimentally measured values of the pump, Stokes and anti-Stokes frequencies can be

substituted into Eq. (5.89), which is a specific form of Eq. (5.82). For instance, if SiO_2 is assumed as the cladding material and a corresponding three-term Sellmeier equation (Fleming 1978) is used for calculating the refractive index at different frequencies, then from Eqs. (5.87), (5.84), it can be deduced for the data associated with the trace in Fig. 10.20(a) (λ_p=1472 nm, λ_{as}=1393 nm and λ_s=1561 nm) that the right-hand side of Eq. (5.89) is equal to 377 cm^{-1}. This can be compared to the measured value of 389 cm^{-1} for Ω and so Eq. (5.89) is essentially satisfied.

In general, the dependence of the FWM frequency shift on the incident optical intensity is involved in two related respects. One is the change of effective refractive index caused by optical Kerr-effect [Eq. (5.64)], and the other is the increase of effective pump frequency due to SPM-induced spectral extension which can be expressed as

$$\omega_I \approx \omega + \left(\frac{d(\Delta\phi)}{dt}\right)_{\text{trailing edge}} \tag{10.2}$$

In Eq. (10.2) ω_I denotes the pump frequency which is a function of intensity and $\Delta\phi$ is the nonlinear phase shift as given by Eq. (5.66).

In the usual four-wave-mixing process, such as that discussed for the parametric soliton laser (Suzuki *et al* 1989), the effect described by Eq. (10.2) was neglected ($\omega_I \equiv \omega$ assumed) and the influence of the intensity-dependent refractive index [Eq. (5.64)] on phase matching was incorporated by adding an additional term $\Delta\beta_{spm}$ in Eq. (5.86). However, we are dealing here with a SPM-mediated four-wave-mixing process such that Eq. (10.2) may have a comparable significance with Eq. (5.64). For a Gaussian pulse intensity profile an explicit expression of the intensity-dependent effective pump frequency that can be derived using Eq. (10.2) is:

$$\omega_I \approx \omega\,(1 + \alpha_1 I) \tag{10.3a}$$

$$\alpha_1 = a_1 2\sqrt{\frac{2\ln 2}{e}}\,\frac{n_{2I}L}{c\Delta t} \tag{10.3b}$$

In Eqs. (10.3) a_1 is a constant ($0 < a_1 \leq 1$) introduced to represent the influence of the four-wave-mixing process on the SPM-induced spectral growth where a_1=1 refers to the maximum possible increase of pump frequency due to SPM. It has been shown that an

approximately linear relationship exists between the FWM frequency shift and the effective pump frequency. [According to Garth and Park (1986), such a relationship is true for the pump frequencies that are not very close to the zero-dispersion region]. Similarly, the effect of Eq. (5.64) on phase matching also leads to a nearly linear dependence of FWM frequency shift on the incident optical intensity except when the intensity is very low (Suzuki *et al* 1989). Therefore, on the basis of these two characteristics, an overall linear relationship between the frequency shift of four-wave-mixing and the incident optical intensity would be expected for our experimental conditions. This can be expressed as:

$$\Omega_I \approx \Omega\,(1+\alpha_I I) = \Omega\,(1+\alpha_P P_f) \qquad (10.4)$$

where Ω_I denotes the intensity-dependent FWM frequency shift and α_I is a pulseshape-related factor. (The term $\alpha_I I$ may be related to an equivalent term involving the average power P_f in the fibre and another factor α_P. The values α_I, α_P can be readily determined experimentally). Fig. 10.21 shows the experimental data for the dependence of FWM frequency shift on the incident optical power, where the solid line is a fit using Eq. (10.4) with $\alpha_P = 0.1\ mW^{-1}$ (i. e. $\alpha_I = 1.7 \times 10^{-10}\ cm^2/W$).

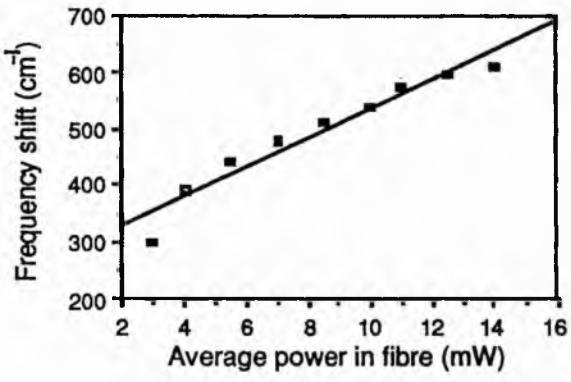

Fig. 10.21. Observed SPM-mediated four-wave-mixing frequency shift as a function of the average power in the fiber.

From Fig. 10.21 it can be seen that the linear relationship between Ω_I and P_f breaks down when the values of P_f are either too small or too large. The deviation at lower power levels would be expected by the approximation made in establishing Eq. (10.4). As for the discrepancy observed at the higher power levels, this is more likely to arise

through the involvement of a Raman scattering process where it should be noted that the observed FWM frequency shift is comparable to the ordinary Raman band ($\Delta\nu_R \sim 440$ cm^{-1}). Therefore, a competition between the stimulated Raman process and the parametric process may exist. It is known that when the pulse propagation distance in an optical fibre is longer than a "coherent length" l_c the four-wave mixing process will be perturbed by the generation of a Raman signal (Stolen and Bjorkholm 1982). Under these conditions the FWM phase-matching condition will no longer be met and so the conversion efficiency from the pump wave to Stokes and anti-Stokes waves drops accordingly (Chen and Snyder 1989, Chen 1989).

In the pump pulse regime, an evaluation of this coherent length can be made from the formula given by Stolen and Bjorkholm (1982) which may be adapted to the form

$$l_c = \frac{1}{2cD\Delta\lambda_p\Delta\nu_F} \tag{10.5}$$

where $\Delta\lambda_p$ is the spectral bandwidth of the pump wave and $\Delta\nu_F=\Omega/2\pi c$ is FWM frequency shift in cm^{-1}. If $\Delta\lambda_p$ is taken as the incident laser pulse bandwidth of 21 nm and a value of group velocity dispersion D =1 ps/nm/km is assumed for the effective pump wavelength, from Eq. (10.5) then l_c = 2.5 m. At first sight, this value looks slightly smaller than that expected by comparing the results in Fig. 10.17 and Fig. 10.20, which lead to 2.6 m < l_c <3.7 m. [It can be seen that for shorter fibre length (2.57 m) the observed four-wave mixing process has a higher conversion efficiency where the anti-Stokes is very distinctive and the pump signal is almost depleted and there is no obvious evidence of a Raman influence. With the 3.7 m length of fibre the recorded spectra had characteristics that could be attributed to a mixture of both FWM and Raman processes]. However, remembering that in this type of SPM-mediated four-wave mixing, the parametric processes do not occur until the incident pulses have propagated some distance then the value of l_c = 2.5 m is a realistic value.

The actual fibre length desired for achieving the SPM-mediated four-wave-mixing process would be the coherent length l_c given by Eq. (10.5) plus a "prerequisite distance", l_p. (l_p represents the propagation distance needed for the new frequencies which can meet

the phase matching condition to be generated through SPM-induced spectral broadening). It is understandable that this prerequisite distance is intensity-dependent where for a lower incident pulse intensity, a larger value of l_p would be required and vice versa. Corresponding to l_c a minimum SPM-induced nonlinear phase shift required for initiating four-wave mixing can be deduced. From the experimental data shown in Fig. 10.19 (for the 2.57 m long Er-doped fibre, associated with the minimum average power $P_f = 3.5$ mW) it can be deduced that $(\Delta\phi)_{min}$ is equal to 1.8π, for which the extended spectrum has two distinct features (Stolen and Lin 1978). As described above, one of these two features (on the shorter wavelength side) meets the phase-matching condition and thus enables the four-wave-mixing process to occur.

In Fig. 10.22 a group of intensity autocorrelation traces are shown for the pulses exiting the 3.7 m long Er-doped fibre II at various optical power levels. For the traces labelled (a) to (h) in Fig. 10.22 the corresponding optical average powers, P_f, are 2.8, 4.2, 5.6, 8.4, 11.2, 12.6, 12.6, and 16 mW. Traces (a) to (f) have the same time scale of 140 fs/div. while for trace (h), because of the relatively large temporal spread of the measured pulses, a time scale of 415 fs/div. has been used. [Trace (g) was recorded at the same power level as trace (f) but on a different time scale]. It can be seen that at lower power levels [traces (a - c)] the process of pulse shaping due to solitonic effects is evident. [With the dispersion parameter given in Table 8.1 (4.1 ps/nm/km), Kerr coefficient $n_{2I} = \frac{5}{6} \times 3.2 \times 10^{-16}$ cm^2/W, the peak intensity for N=1 soliton would be about 1 GW/cm^2 and the actual pulse intensity related to the trace shown in Fig. 10.22(a) is 1.7 GW/cm^2]. The exiting pulses corresponding to the trace reproduced in Fig. 10.22(b) had a large pedestal and a narrow central peak. This temporal peak had a duration of ~70 fs and when the power level was higher than 5.6 mW pulse breakup became a dominant feature and the time delay between the pulse subcomponents increased as the optical power was further increased. A plot of the relationship between the time delay, t_d, and the average power in the fibre, P_f, is shown in Fig. 10.23, where the solid line is a linear fit.

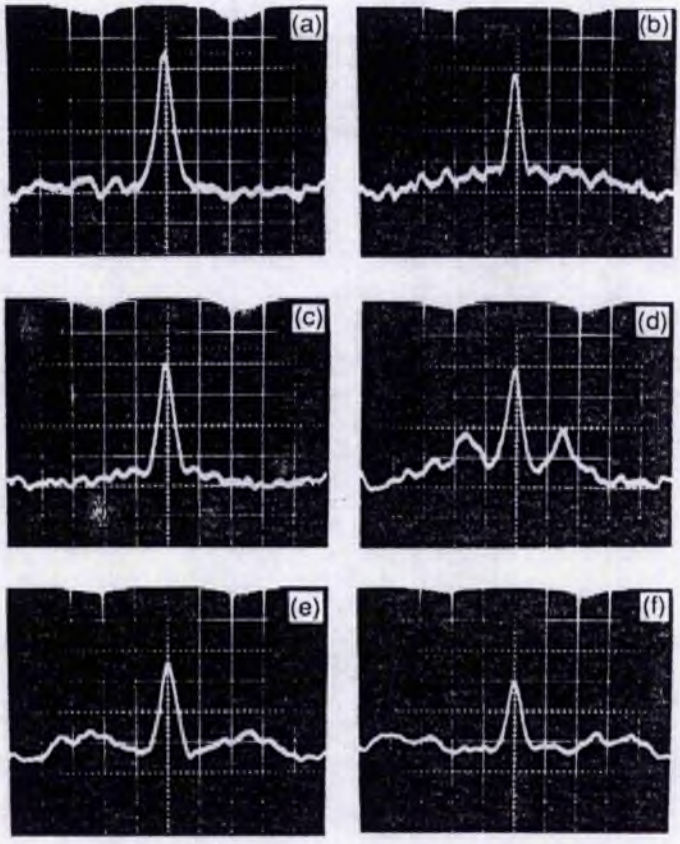

Fig. 10.22. Sequence of SHG autocorrelation profiles for the pulses exiting the 3.7-m-long Er-fibre II. The power levels, P_f that refer to Fig. 10.22(a-h) are: 2.8, 4.2, 5.6, 8.4, 11.2, 12.6, 12.6, 16 mW respectively. Traces (f) and (g) represent the same autocorrelation but in the two different time scales.

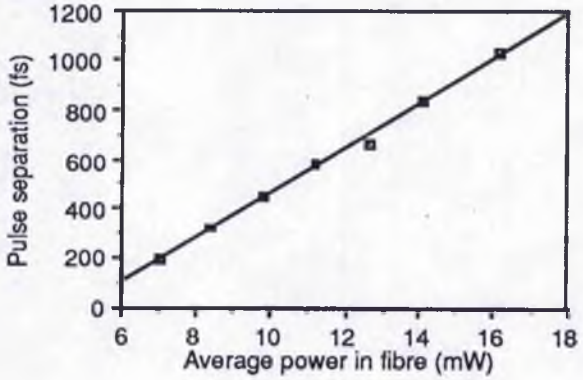

Fig. 10.23. Time delay between the dispersed pulse subcomponents as measured from the traces shown in Fig. 10.22 as a function of average power in the fibre.

Such behaviour is consistent with the onset of the four-wave-mixing process if it is considered that the observed time delay arises from group velocity dispersion between the anti-Stokes signal and the remaining group of spectral components having the longer wavelengths. It thus follows that the linear relationship between the time delay and the optical power can be explained with regard to the generation of the anti-Stokes signal at different local times (or at different spatial positions along the fibre) as determined by the propagating pulse powers. For instance, at higher incident power levels the parametric mixing occurs earlier and so the associated new frequency components have a longer propagation distance before exiting the fibre. Correspondingly, it would be expected that in this case an enlarged temporal separation would result. The experimental data presented in Fig. 10.23 only show the time delays for P_f larger than 6 mW because although FWM was observable at lower values of P_f, the small intensity and temporal-separation features were difficult to determine unambiguously.

It is worth mentioning that an important empirical formula which describes the overall spectral extension in the SPM-mediated four-wave-mixing process can be derived from the linear relationship revealed through the data of Fig. 10.23. Provided that $\Delta\lambda_d$ is the effective wavelength separation between the two groups of spectral components which experience different group velocity dispersions, then in the time-domain a delay between these two spectral features would be given by

$$t_d = \Delta\lambda_d D l \tag{10.6}$$

where the propagation distance, l, is the fibre length minus the prerequiste distance l_p,

$$\text{i. e.} \qquad l = L_o - l_p \tag{10.7}$$

For a given intensity the value of l_p can be simply determined by

$$I l_p = a_2 \tag{10.8a}$$

$$a_2 = \frac{(\Delta\phi)_{min}\lambda}{2\pi n_{2I}} \tag{10.8b}$$

Substituting Eqs. (10.7), (10.8a) into Eq. (10.6), we obtain

$$t_d = \Delta\lambda_d D \left(L_o - \frac{a_2}{I}\right) \tag{10.9}$$

Obviously, when $I = \frac{a_2}{L_o}$, $t_d = 0$. If we define $I_c \equiv \frac{a_2}{L_o}$ as a critical intensity above which the FWM process occurs in a fibre having a length equal to L_o, then Eq. (10.9) can be rewritten as

$$t_d = \Delta\lambda_d D L_o (1 - \frac{I_c}{I}) = \Delta\lambda_d D L_o (1 - \frac{P_c}{P_f}) \qquad (10.10)$$

where P_c is the critical average optical power corresponding to I_c. To maintain consistency between Eq. (10.10) and the experimentally observed dependence of $t_d \propto P_f$, indicated in Fig. 10.23, a relationship between $\Delta\lambda_d$ and the optical power given by

$$\Delta\lambda_d \propto \frac{P_f}{1 - \frac{P_c}{P_f}} \qquad (10.11)$$

has to be assumed. From Eq. (10.11) it can be seen that for $P_f << P_c$, $\Delta\lambda_d \propto \frac{P_f^2}{P_c}$, for $P_f >> P_c$, $\Delta\lambda_d \propto P_f$ and the specific case of $P_f = P_c$ marks the discontinuity of the spectral broadening process caused by the onset of the four-wave-mixing. Such a tendency is in a good agreement with the recorded spectral extension shown in Fig. 10.19. If two coefficients are introduced, Eq. (10.11) can be reexpressed as

$$\Delta\lambda_d \approx \begin{cases} \Delta\lambda_o(1+c_1 P_f^2/P_c) & (\text{for } P_f < P_c) \quad (10.12a) \\ \Delta\lambda_f(1+c_2 P_f) & (\text{for } P_f > P_c) \quad (10.12b) \end{cases}$$

where $\Delta\lambda_o$, $\Delta\lambda_f$ are the initial incident spectral bandwidth and the minimum spectral extension relating to FWM. The two constants c_1, c_2 in Eq. (10.12a, b) can be determined experimentally. For example, for the data of Fig. 10.19 which relate to the 2.57-m-length of doped optical fibre, c_1, c_2 can be deduced to be 0.3, 0.1 mW^{-1} respectively.

It is interesting to note that the two temporally-separated component features as shown in Fig. 10.22(f) - (h) have distinctly different profiles. This can be explained by the fact that the associated "spectral packets" for these two separated pulses lie in different dispersion regimes. The anti-Stokes wavelength is in the normal dispersion region and is subject to rapid temporal broadening whereas the longer wavelength complement (SPM, FWM and Raman contributions) in the anomalous dispersion region experiences a confining solitonic-type of pulse shaping influence. When the average power $P_f \geq 12$ mW substructure is noticeable in the recorded intensity autocorrelation traces [e.g. see Fig.

10.22(f)]. This could be attributed to the presence of the additional anti-Stokes signals. A time delay of ~260 fs between the first and the second anti-Stokes signals can be inferred from Fig. 10.22(f), and such a value indicates that [from Eqs. (10.6), (10.10), assuming P_c=3 mW] after the first anti-Stokes wave propagates a distance of 0.9 m in the fibre, the additional anti-Stokes wave is generated.

Finally, it should be pointed out that the exact intensity ratios of the two primary dispersed features are difficult to judge from the traces shown in Fig. 10.22 - especially those at the higher power levels. This is because the phase matching for the second harmonic generation in the autocorrelator has a limited bandwidth (Miller 1968), which, in our case, is ~ 200 nm. Therefore, some spectral filtering (or modification) will be imposed upon the recorded SHG autocorrelation traces. It is unlikely that this influence would be large enough to affect the essential characteristics as described above for the propagating pulses.

10.3 Conclusions

In summary, this work has shown some interesting characteristics of an Er-doped optical fibre when it is incorporated in an external cavity of a CCM KCl:Tl laser. When the lasing wavelength is tuned across the absorption centre of the erbium ion in the fibre both temporal broadening and compression features have been observed, which indicate the existence of dominant positive, or negative group velocity dispersion or a mixture of both in particular cases. In all three different situations of GVD in the fibre good performance of the CCM laser can be achieved, which once again proved that the coupled-cavity mode locking does not have any special requirement on the sign of group velocity dispersion in the control fibre. While the CCM laser is under different operational status, examination of both spectra and autocorrelation of the pulses coupled into and returned from the control cavity can provide a clear view of how the features of femtosecond pulses have been affected after one roundtrip of propagation in the control cavity. Accordingly, both nonlinear and dispersive functions played by the control cavity may be conveniently investigated. All of these demonstrate that the control cavity of a CCM laser offers a

useful "test-site" for the characterization of the nonlinearity and dispersion in optical fibres. It is to be expected that this technique could be more generally applied to a wide range of nonlinear elements within the various types of CCM lasers that either already exist or are undergoing development.

The propagation characteristics of femtosecond pulses in five different types of monomode optical fibres at wavelengths around 1510 nm has also been described in some detail. Of these five fibre types, in addition to the two Er-doped (with the dopant concentrations of $6x10^{18}$ and $1.6x10^{17}$ cm^{-3} respectively) and corresponding erbium-free fibres, a standard commercial fibre and a fibre of the same type used in the first soliton laser by Mollenauer were also tested. The differences of the spectral extensions and temporal variations for identical incident pulses propagating in these five types of fibres with various lengths have been comprehensively studied.

For the Er-free fibre which has a normal group velocity dispersion up to 1660 nm, the propagating pulses have a very limited spectral extension and thus experience predominant temporal broadening. In contrast, at the same power level and for the same fibre length, the results for the Er-fibre (type I having higher dopant concentration) show that significantly larger spectral broadening occurs, and the pulse broadening in the time domain is much smaller. For the standard and the soliton-laser fibres, however, as the coupling power increases spectral narrowing, rather than spectral extension, are distinctly observed. By making analyses of the spectral extension in anomalously dispersive fibres, such unusual results have been attributed to solitonic effects.

Pulse propagation in the Er-fibre having a lower dopant concentration (type II) exhibited an extremely large spectral extension which is characterised by a distinct anti-Stokes signal at enhanced shifts towards short wavelengths and a SPM-related residual complement at longer wavelengths. This novel behaviour has been shown to be a new type of FWM process, designated here as "SPM-mediated four-wave-mixing". Compared to the ordinary FWM process observed in a single mode optical fibre, in this parametric process the incident pulses do not directly generate the Stokes and anti-Stokes signal because the phase-matching condition is not satisfied. However, as a result of SPM-

induced spectral broadening, the frequencies which can intrinsically meet the phase matching condition are produced. In other words, the branch of the broadened spectral features associated with the trailing edge of the propagating pulse act as a pump to initiate the FWM process. Therefore, a typical characteristic of the SPM-mediated FWM is that a prerequisite propagation distance is needed in order to establish the necessary pump signal from the SPM effect.

Analyses of the need for this prerequisite propagation length, the coherent length, the relationship between the overall spectral extension and the optical intensity, as well as the observed results from temporal-domain measurements such as a pulse breakup phenomenon, have also been presented. All of these effects can be shown to be consistent with a SPM-mediated FWM process. Utilizing this new type of nonlinear process to develop an anti-Stokes amplifier or an up-converted parametric oscillator is proposed and will be the subject of future research studies.

Chapter 11

General Conclusions

11.1 General remarks

A review of the basic principles of characterization, generation, measurement and propagation of laser pulses having durations in the picosecond to femtosecond range are presented. New insight into, and some current interpretations of experimental data are also included. It is the author's hope that this part of work would not only be useful to those who may not yet be familiar with the background knowledge of this specific research area but also beneficial to those who are carrying ongoing research relating to ultrafast phenomena.

Experimental studies of mode locking in a KCl:Tl colour-centre laser where a nonlinear external cavity is involved show that this new type of mode locking is a practical and general means for generating ultrashort laser pulses. It can thus be regarded as a new member of the 'mode locking family' and named as *coupled-cavity mode locking (CCM)*, [or *additive mode locking (APM), or interferential mode locking (IMF)*]. This technique has the advantage of being of a passive nature, which means it has the capability of producing very short pulses by an intensity-driven process. It is free from main drawbacks of conventional passive mode locking techniques, such as being limited by the choice of available nonlinear absorber, or inability to handle high optical power and so on.

The practical configuration of a coupled-cavity mode-locked laser is very versatile. For instance, the auxiliary cavity can be a nonlinear Fabry-Perot cavity appended to the main laser cavity as in this work, or it can be a part of the main laser. For the latter, a nonlinear Michelson interferometer (or a nonlinear antiresonant ring structure) is used as the output coupler of a laser so that the two cavities are actually built within the single laser. Regardless as to how the two cavities are geometrically related, in each particular CCM laser system, a common feature is that the main cavity is responsible for the lasing

action whereas the auxiliary cavity that consists of an intensity-dependent nonlinear medium has the function of 'mode coupling control'.

Although in the last two to three years there has been an increasing number of investigations on coupled-cavity mode locking for various laser systems, it is a justifiable claim that none has established a plan as thorough as this work in respect of a comprehensive study of the various characteristics of a CCM laser. All the data relating to the features of coupled-cavity mode locking presented in this thesis have been obtained for a KCl:Tl laser, but it is believed that many of them are generally representative and may therefore apply to other coupled-cavity mode-locked laser systems.

11.2 Ultrashort laser pulses

Since the invention of the first laser in 1960 fast advances have been achieved in the area of ultrashort laser pulses. Although the record of the shortest pulses to date (6 fs: Fork *et al* 1987) was set up three years ago and many mode locking methods have been reported, extensive research towards developing new pulse generation techniques which can provide highly tunable, sufficiently intense picosecond-femtosecond pulses are still ongoing. This is because applications of the ultrashort laser pulses in both scientific research and industrial development have continued to place additional requirements on the laser pulses in respect of tunability, reliability, controllability, compactness etc rather than just a single interest in pulse duration.

Compared with the progress in and the variety of pulse generation techniques, pulse measurement have been mainly limited to using either electron-optical streak cameras in the picosecond regime or SHG autocorrelators in the femtosecond regime. For the latter, unfortunately, only the pulse duration can be estimated whereas the pulse shape cannot be unambiguously determined. Therefore, the development of alternative pulse measurement techniques are still required. In this work, two new measurement schemes have been proposed. These are based on two specific devices: one is *photon-optical streak camera* and the other the *first-order spectral autocorrelator*. Both of these belong to the linear measurement technique and should be able to provide the definite determination of pulse

intensity profiles.

For the photon-optical streak camera, neither electron-photon transformation nor other electronic systems are involved. The entire body of the device is an appropriately cut nonlinear material which has high optical Kerr coefficient. While the signal pulses to be measured are incident on the rear surface of the Kerr material a strong optical pulse beam illuminates the same area, causing a sufficiently rapid change of refractive index that different portions of the signal pulse are refracted at different angles, and so the transmitted pulse is spatially distributed[1]. Such a 'wholly optical' streak camera avoids problems arising from synchronization and therefore has the advantages of easy operation, low cost and improved subpicosecond time resolution.

The first-order spectral autocorrelator is designed to record the linear autocorrelation of the spectral field, i. e. $G(\Omega) \propto \int \upsilon(\omega)\upsilon^*(\omega - \Omega)d\omega$. Similar to the fact that Fourier transforming the first-order temporal autocorrelation gives rise to the spectral intensity, a Fourier transform of $G(\Omega)$ would yield the temporal intensity profile (see illustrations in Fig. 2.3).

As far as pulse propagation is concerned, a strong analogy between the impact of dispersion on the temporal features and that of self-phase modulation (SPM) on the spectrum of a propagating pulses is found. This leads to the recognition of a possible use of a SPM medium as a spectral compressor, provided that the incident pulses are suitably frequency-chirped. Corresponding to the dispersion parameter D, a spectral spread parameter F can be introduced, which, representing the spectral extension within a unit distance for a unit time duration, has been shown to be useful in the analyses of SPM-induced spectral extension.

Finally, at this stage, it is worth mentioning that throughout the contents of this thesis only the spectral and temporal features of optical pulses have been considered. In a more general and complete description the spatial and polarization characteristics for the pulses should also be included. In this sense, the optical pulses will be viewed as a packet of

[1] A similar idea can be used for making an optical switch. In this case the rear surface of the Kerr device is cut at an appropriate angle so that in the absence of the scan beam the signal beam is transmitted, whereas with the presence of the scan beam the signal will be totally reflected.

photons that propagate in space and interact with the medium.

11.3 Coupled-cavity mode-locked KCl:Tl colour-centre laser

This work has shown that the coupled-cavity mode-locked KCl:Tl colour-centre laser is a useful femtosecond laser source for the near-infrared spectral region. From this system, stable sub-100 fs pulses with controllable pulse shapes and a central wavelength around 1.5 μm can be readily produced. These results represent at least a 100 times reduction of pulse durations compared with the output from a synchronously pumped KCl:Tl laser.

Generally speaking, the laser performance can be significantly influenced by variation of the effective gain bandwidth, the type, the length of control fibre, and the coupling strength between the two cavities. The laser has also been shown to have an relatively large tolerance on the amount of cavity-length mismatch. Within this tolerance range (±25 μm typically) positive mismatch (the control cavity is longer than that of main cavity) leads to the generation of pulses having slower leading edges and faster trailing edges whereas the negative mismatch leads to the opposite result.

Normally, coupled-cavity mode locking can be achieved only for a specific range of optical power injected into the control cavity. If the coupling power is too low, no mode locking enhancement exists. If it is too high the laser output becomes unstable. This intrafibre power range, having been defined as the *operational window* of a CCM laser, can be shifted or narrowed/expanded by adjusting the main cavity parameters such as power level , effective gain bandwidth and central lasing wavelength.

It has also been found that incorporation of negative GVD fibre that supports bright optical solitons often leads to a smaller operational window than that when an equal length of positive GVD fibre was used. [Connected to such an observation is the interesting fact that it was usually more difficult to stabilize the laser for a control fibre that has anomalous (negative) GVD at the working wavelengths]. Another disadvantage of using negative GVD fibre is that when the fibre sample is relatively long another nonlinear effect, modulational instability, may occur, which will distort the process of mode locking enhancement. In our experiments the preferred control fibre that led to the

generation of most stable and shortest pulses was an Er-doped fibre. This fibre has a relatively small core area and was estimated to have very low positive GVD at 1.5 μm. In the cases where the peak intensity in the fibre was relatively high, continuous frequency shifts towards longer wavelengths caused by self-Raman effect have been observed. This can be an undesired effect which may however be avoided by either decreasing the coupling power or reducing the length of the control fibre.

To obtain the pulses having the desired durations from the CCM laser, in addition to adjusting the power level coupled into the control fibre an alternative and more effective way is to re-select a birefringent filter with a more appropriate thickness. Generally speaking, use of a thicker filter, which corresponds to a more strict bandwith control, leads to the generation of transform-limited pulses but with rather larger durations. On the other hand, if the filter(s) is removed from the main cavity, i. e. no extra bandwidth limitation is applied, the output pulses will become excessively frequency-chirped. Therefore an optimum bandwidth restriction exists, which can be experimentally determined from plotting a curve of pulse duration vs. thickness of birefringent filter.

For the situations where not enough bandwidth restriction exists the CCM laser pulses are up-chirped and so they can be compensated by using a negatively dispersive medium. Using a proper length of glass rod outside the cavities to directly compress the chirped CCM laser pulses has been successfully performed. After passing through a 20-cm-long glass rod the incident 150 fs pulses have been compressed down to ~90 fs. Another approach for chirp compensation is to place the glass rod in the control cavity, which also led to the generation of near transform-limited pulses under 100 fs.

The timescale of pulse evolution in our CCM, KCl:Tl laser has been determined to be in a range from just over 200 ns to several microseconds. The exact build-up time is not only dependent on the intrafibre power, the initial cavity mismatching condition but also the temporal and spectral features of the initial pulses. It was evident that for an initial pulse which was more like a noise burst having relatively large excess bandwidth, the pulse evolution was faster compared to the cases where the initial pulse had a clean profile, shorter duration and much smaller bandwidth-pulse duration product. Such an

observation has been explained in that the initial noise burst which although overall temporally broader has a bandwidth sufficient to support fluctuation features. This favours extension of the lasing spectrum, and so the mode coupling under the influence of nonlinear control cavity will be more effective.

It was also interesting to note that no significant difference was observed for the two situations where the fast electro-optic switch for observing the starting of pulse evolution was respectively placed in the control cavity and in the path of the pump beam. For pump-beam switching, pulses evolved in the main cavity first (the existence of control cavity seemed unimportant during this early stage). When the optical peak power in the main cavity reached a certain level such that the intensity-related nonlinearity in the control cavity became exploitable then the influence of control cavity took place.

Because different types of control fibre normally lead to distinct performance of a CCM laser, it follows that the coupled-cavity laser itself can also be utilized as a highly sensitive test site for characterizing the dispersive and nonlinear features of optical fibres. The spectral and temporal data for the pulses coupled into and returned from the control fibre recorded during the CCM operation provide very useful information of pulse propagation in the fibre involved, which are not readily to be obtained with other possible means.

With the femtosecond pulses obtained from our CCM, KCl:Tl laser, a group of single-pass experiments for different optical fibres have been conducted. Under the condition of almost constant input pulse duration (Δt_i = 120 fs) and fibre lengths less than 4 m, for two fibre samples the novel phenomenon of spectral compression was recorded whereas for one Er-doped fibre sample an unusual four-wave mixing process mediated by self-phase modulation was observed. This SPM-mediated four-wave mixing led to an extreme spectral extension covering a wavelength range of 1.3-1.7 μm. For the same Er-doped fibre but slightly shorter length (~2.5 m) the exiting pulses exhibited a distinct antiStokes signal at 1.35 μm. It is now planned that a loop configuration for this antiStokes signal can be exploited so that an up-converted fibre laser may be constructed.

11.4 Comments and suggested future studies

Because of time limitations, this work has been mainly concerned with the experimental studies of a coupled-cavity mode-locked KCl:Tl laser. Although the understanding of the mechanisms involved in coupled-cavity mode locking has been improved significantly in the past two or three years, it has to be said that compared with experimental achievements the theories that are currently available are not yet satisfactory[2].

It is noted that among the conclusions drawn by Blow and Wood (1988), it is claimed that incorporation of a saturable amplifier that leads to the pulses returned from the control cavity having broader temporal profiles and narrower spectra can still give rise to an improved mode locking. This has not actually been verified by experiments. Although many experimental results show mode locking enhancement regardless of any changes of pulseshape arising in the control cavity, there has not been any evidence indicating that the return pulse has a narrower spectrum than that of the main cavity pulse.

From the spectra recorded for the pulses with and without the nonlinear external cavity (e. g. Fig. 8.3) it is quite clear that there is not only a requirement for the control cavity to strengthen mode coupling but also, rather significantly, to induce more modes in the main cavity laser to lase. Without enlarging the effective lasing bandwidth it is obviously not possible to generate substantially shorter pulses. Therefore, it is believed that the spectral extension in the control cavity is especially important (Zhu *et al* 1989a).

---

[2] For example, several questions must be asked with regard to the pulse addition model. Firstly, when the interferometric addition of the two pulses is considered it is implicitly assumed that the two pulses have reasonably good coherence, whereas, in practice, this may not be so. It is evident that in many experiments the initial pulses during the process of mode locking enhancement are more like noise bursts (with large $\Delta\nu\Delta t$ values) rather than the clean pulses. Under these conditions, it is difficult to judge how the interferometric addition occurs between the two noise bursts. Secondly, because the amplitude of the return pulse is often much smaller than that of the main cavity pulse, if the coherent addition between the two pulses provides the only mechanism for pulse compression while all the other factors tend to broaden the pulses, it would take rather a long time for the pulse evolution process to be fulfilled in order to achieve a reduction of the pulse duration by two orders. By contrast, experimental data obtained in this work relating to the study of pulse evolution in a coupled-cavity mode-locked KCl:Tl laser (see Ch. 9) indicate that the timescale of pulse build up can be very fast - as little as 100 cavity roundtrips. Thirdly, pulse addition not only occurs for radiation on the internal side of the output coupler but also on the control-cavity side of the same mirror [see Fig. 6.2(a)]. It is thus unsatisfactory that in the pulse addition model only the addition on the inner side of the output coupler is accounted for whereas the effect relating to pulse addition on both sides of the output coupler should be included. Therefore, there is no convincing argument to justify that the control cavity termination should always return a shorter pulse back to the main cavity in order to achieve the mode locking enhancement.

Because of this spectral extension the entire control cavity will act as a non uniform spectral reflector - a reflector that favours the oscillation of the modes on both sides of the peak of the gain. A most important feature of this spectrally distributed reflectivity is that it is a function of peak intensity. The higher the peak optical intensity the larger will be the reflectivity at the wings of the spectrum. Thus, an 'avalanche' process of spectral extension and mode locking enhancement can occur during the process of pulse evolution. That is, as the pulse duration becomes shorter the spectral extension in the control cavity becomes larger and as the spectral extension for the return pulses becomes larger more modes in the main cavity are induced and phase-coupled together, such that yet shorter pulses can be produced. In the time-domain picture, the nonlinear external cavity should be taken as both an amplitude and a phase modulator. It is rather unfortunate that the pulse addition model only considers the amplitude effect whereas in practice both phase and amplitude modulation must be responsible for mode locking enhancement.

The idea of pulse addition leading to a shorter resultant pulse actually applies even to two identical pulses, which implies that pulse compression in the coupled cavities in principle may have little to do with nonlinearities in the control cavity. Although, it has been shown that the SPM-induced frequency chirp in the return pulse helps pulse shortening in a way that when it is added to the main cavity pulse the constructive addition occurs in the pulse centres and destructive addition in pulse wings, the same effect can also be achieved if the return pulse is chirped by dispersion. Such a thought has led some research workers to conclude that what is important in the control cavity is not the presence of nonlinearity but introducing a frequency chirp, and thus if the nonlinear element is replaced by a purely dispersive medium mode locking enhancement can still be obtained (Zook *et al* 1991). This is a mistaken concept because it must be remembered that, unlike the chirp induced by SPM, the GVD-contributed frequency chirp does not depend on optical intensity and so it will not contribute to any spectral extension. Such a feature, which represents a key difference between the frequency chirps produced by SPM and GVD effects, determines that an avalanche increase of lasing modes will not

occur for the coupled cavities if no nonlinear medium is incorporated in the control cavity. It is thus believed that a significant coupled-cavity mode locking enhancement is most unlikely to be achieved with a linear dispersive control cavity[3].

The highlight of coupled-cavity mode locking is that it represents a mode locking where the interplay between the gain of the lasing medium and the nonlinearity (in particular, the self-phase modulation) in the nonlinear element has a key function. The two-cavity arrangement is important in a sense that these two nonlinear effects (gain and self phase modulation) can be separately adjusted and controlled, and so an appropriate combination of (or interaction between) them can be established that favours generation and coupling of a large number of lasing modes. It can thus be readily understood why the operation of a CCM laser directly depends upon the selection of proper power level in the main cavity and suitable peak intensity in the control cavity for exploiting the optical nonlinearity[4].

It is believed that future research on coupled-cavity mode locking would involve the development of the corresponding laser systems into commercial products and meanwhile more complete theoretical analyses of general performances for a CCM laser are needed. As an improtant supplement to the other pulse generation techniques more exploitations of coupled-cavity mode locking are expected in the lasers where practical limitations arise when conventional mode-locking methods are applied. Femtosecond laser sources constructed with coupled-cavity mode locking will undoubtedly find many applications in the studies of ultrafast dynamic processes. This would be especially true for time-domain spectroscopic research into molecular and bulk/multi-quantum-well semiconductor systems on the picosecond and femtosecond regimes.

---

[3] Up to now, there has not been any experimental results showing that coupled-cavity mode locking can be achieved with a linear, dispersive external cavity. We have conducted an experiment on the KCl:Tl laser with a 20 cm length of glass rod in the control cavity but no mode locking enhancement was observed under the various conditions that have been tried.

[4] It is possible that for some laser system(s) where the gain medium itself also provides a noticeable nonlinear Kerr effect, the balance between the roles played by the gain medium and that by optical Kerr effect may be reached automatically. In this case a special type of self mode locking can occur even for a single cavity laser. This could be the situation for self mode-locked Ti:Al_2O_3 laser (Spence *et al* 1991). A theoretical investigation on this issue has recently been reported by Krausz *et al* (1991).

Appendices

Appendix A Fundamental equations

It is known that the classical description of optical phenomena is based on the *Maxwell Equations*, which in MKS units can be written as

$$\nabla \times \mathbf{E} = -\frac{\partial \mathbf{B}}{\partial t} \tag{A.1}$$

$$\nabla \cdot \mathbf{D} = \rho \tag{A.2}$$

$$\nabla \times \mathbf{H} = \frac{\partial \mathbf{D}}{\partial t} + \mathbf{J} \tag{A.3}$$

$$\nabla \cdot \mathbf{B} = 0 \tag{A.4}$$

The scalar ρ is the free charge density, all the other quantities are vectors and have the physical meanings: $\mathbf{E}(\mathbf{r}, t)$ —— the electric field, $\mathbf{B}(\mathbf{r}, t)$ —— the magnetic induction, $\mathbf{D}(\mathbf{r}, t)$ —— the electric displacement, $\mathbf{H}(\mathbf{r}, t)$ —— the magnetic field, $\mathbf{J}(\mathbf{r}, t)$ —— the current density. Eqs. (A.1- 4) should be supplemented by the so-called *material equations*:

$$\mathbf{D} = \varepsilon_0 \mathbf{E} + \mathbf{P} \tag{A.5}$$

$$\mathbf{H} = \frac{\mathbf{B}}{\mu_0} - \mathbf{M} \tag{A.6}$$

$$\mathbf{J} = \sigma \mathbf{E} \tag{A.7}$$

These describe the behaviour of media under the influence of the incident electromagnetic field. **P** and **M** are the electric and magnetic polarizations of the medium, σ is the specific conductivity and ε_0, μ_0 are the electric and magnetic permeabilities in vacuum.

Classification of media

For different media Eqs (A.5-7) can be reduced into more convenient forms. As far as Eq. (A.5) is concerned, it can always be written as

$$\mathbf{D} = \varepsilon_g \mathbf{E} \tag{A.8}$$

where ε_g is a generalized dielectric coefficient, which is usually a function of space, frequency and also the incident field,

$$\text{i. e.} \quad \varepsilon_g = \varepsilon_g(\mathbf{r}, \omega, \mathbf{E}) \tag{A.9}$$

According to the different forms of Eq. (A.9), The following classification of media can be made.

1) Homogeneous media — ε_g has no dependence on the spatial position,

$$\text{i. e.} \quad \varepsilon_g = \varepsilon_g(\omega, \mathbf{E}) \tag{A.9a}$$

2) Linear media — ε_g is independent of the amplitude of incident field,

$$\text{i. e.} \quad \varepsilon_g = \varepsilon_g(\mathbf{r}, \omega, \mathbf{k}_o) \tag{A.9b}$$

where $\mathbf{k}_o = \mathbf{E}/|\mathbf{E}|$ is the unit directional vector of the electromagnetic field.

3) Isotropic media — ε_g is not a function of the transformation direction of the incident field,

$$\text{i.e.} \quad \varepsilon_g = \varepsilon_g(\mathbf{r}, \omega, |\mathbf{E}|) \tag{A.9c}$$

Note that otherwise ε_g will be a tensor with the order $\nu \geq 2$.

4) Inertialless media — ε_g is not a function of frequency,

$$\text{i.e.} \quad \varepsilon_g = \varepsilon_g(\mathbf{r}, \mathbf{E}) \tag{A.9d}$$

Similar discussions also apply to Eq. (A.6), which can be written in the form of

$$\mathbf{B} = \mu_g \mathbf{H} \tag{A.10}$$

where μ_g is a generalized tensor coefficient. However, for most optical problems the effects of ferroelectricity and ferromagnetism are not involved so $\mathbf{M} = 0$. Therefore μ_g is simply a scalar constant, which is equal to the vacuum magnetic permeability μ_o.

Reduction of Maxwell equations

(i) Linear media

For a charge-free, linear and isotropic medium, we have

$$\rho = 0, \quad \mathbf{D} = \varepsilon \mathbf{E}, \quad \mathbf{B} = \mu \mathbf{H}, \quad \mathbf{J} = \sigma \mathbf{E}. \tag{A.11}$$

where $\varepsilon = \varepsilon_o(1 + \chi)$ is a scalar and independent of incident field $\mathbf{E}$. Combining these equations with Maxwell Eqs. (A.1-4) and using the relationship $\partial\mu/\partial t = 0$ and $\nabla \cdot \mathbf{E} = -(\nabla \lg\varepsilon) \cdot \mathbf{E}$ give

$$\nabla^2 \mathbf{E} - \mu \frac{\partial^2(\varepsilon \mathbf{E})}{\partial t^2} + \nabla \lg\mu \times (\nabla \times \mathbf{E}) + \nabla(\nabla \lg\varepsilon \cdot \mathbf{E}) - \mu \frac{\partial(\sigma \mathbf{E})}{\partial t} = 0 \tag{A.12}$$

If $\nabla\mu = 0$, Eq. (A.12) reduces to

$$\nabla^2\mathbf{E} - \mu\frac{\partial^2(\varepsilon\mathbf{E})}{\partial t^2} + \nabla(\mathbf{E}\cdot\nabla\lg\varepsilon) - \mu\frac{\partial(\sigma\mathbf{E})}{\partial t} = 0 \qquad \text{(A.13)}$$

For a homogeneous dielectric medium, $\sigma = 0$ and $\nabla\lg\varepsilon = 0$, so Eq. (A.13) becomes

$$\nabla^2\mathbf{E} - \mu\frac{\partial^2(\varepsilon\mathbf{E})}{\partial t^2} = 0 \qquad \text{(A.14a)}$$

If ε can be approximated to be time-independent, we then have

$$\nabla^2\mathbf{E} - \frac{1}{v}\frac{\partial^2\mathbf{E}}{\partial t^2} = 0 \qquad \text{(A.15)}$$

where $v = 1/\sqrt{\mu\varepsilon}$, is the light velocity in the medium. Eq. (A.15) is a familiar form of the so-called wave equation, but it should remember that, strictly speaking, it only applies to a single frequency wave (or Fourier frequency component). A more general formula that describes the feature of an arbitrary electromagnetic field propagating in a dispersive medium should be Eq. (A.14a). Assuming $\mu = \mu_o$, another form of Eq. (A.14a) is:

$$\nabla^2\mathbf{E} - \mu_o\varepsilon_o\frac{\partial^2\mathbf{E}}{\partial t^2} = \mu_o\frac{\partial^2\mathbf{P}}{\partial t^2} \qquad \text{(A.14b)}$$

where $\mathbf{P} = \mathbf{P}_L \equiv \chi\varepsilon_o\mathbf{E}$, is the linear electric polarization of the medium. If some loss mechanism is of importance the specific conductivity-related term can be used to represent the function of it, and so Eq. (A.14b) may be amended to

$$\nabla^2\mathbf{E} - \mu_o\varepsilon_o\frac{\partial^2\mathbf{E}}{\partial t^2} - \mu_o\sigma\frac{\partial\mathbf{E}}{\partial t} = \mu_o\frac{\partial^2\mathbf{P}}{\partial t^2} \qquad \text{(A.14c)}$$

(ii) Nonlinear media

For a nonlinear optical medium all the relations given in Eq. (A.11) still hold except $\mathbf{D} = \varepsilon\mathbf{E}$. In this case, the polarization $\mathbf{P}$ is no longer a linear function of the field $\mathbf{E}$. Therefore, instead of $\mathbf{D} = \varepsilon\mathbf{E}$, we have

$$\mathbf{D} = \varepsilon_o\mathbf{E} + \mathbf{P} = \varepsilon_o\mathbf{E} + \mathbf{P}_L + \mathbf{P}_{NL} = \varepsilon\mathbf{E} + \mathbf{P}_{NL} \qquad \text{(A.16)}$$

where $\mathbf{P}_{NL}$ is a function of all the higher-order power items ($n \geq 2$) of $\mathbf{E}$. With Eq. (A.16) and the other associated ones in Eq. (A.11), following the similar procedure in deriving Eq. (A.12) leads to

$$\nabla^2\mathbf{E} - \mu\frac{\partial^2(\varepsilon\mathbf{E})}{\partial t^2} - \nabla(\nabla\cdot\mathbf{E}) - \mu\frac{\partial(\sigma\mathbf{E})}{\partial t} = \mu\frac{\partial^2\mathbf{P}_{NL}}{\partial t^2} \tag{A.17}$$

When the variation of ε and σ with time are neglected, Eq. (A.17) can be rewritten as

$$\nabla\times(\nabla\times\mathbf{E}) + \mu\varepsilon\frac{\partial^2\mathbf{E}}{\partial t^2} + \mu\sigma\frac{\partial\mathbf{E}}{\partial t} = \mu\frac{\partial^2\mathbf{P}_{NL}}{\partial t^2} \tag{A.18}$$

(iii) Resonant (gain and absorption) media

Once the frequencies of an incident beam are close to or matched with some atomic transition bands of a medium, this medium must be treated as a resonant medium. For a resonant medium, the electric displacement can be expressed as

$$\mathbf{D} = \varepsilon_o\mathbf{E} + \mathbf{P} + \mathbf{P}_{tran} \tag{A.19}$$

It can be seen that the polarization is split into two items: one for the nonresonant component $\mathbf{P}$ (the one we ordinarily use) and the other, $\mathbf{P}_{tran}$, is specially assigned to the contributions arising from the atomic transitions. Suppose the medium itself is linear despite of the resonant effect, we then have

$$\varepsilon_o\mathbf{E} + \mathbf{P} = \varepsilon\mathbf{E} \tag{A.20}$$

Thus, Eq. (A.19) can be reexpressed as

$$\mathbf{D} = \varepsilon\mathbf{E} + \mathbf{P}_{tran} \tag{A.21}$$

which has the same form as Eq. (A.16). Therefore, as for Eq. (A.17), we now have

$$\nabla^2\mathbf{E} - \mu\frac{\partial^2(\varepsilon\mathbf{E})}{\partial t^2} - \nabla(\nabla\cdot\mathbf{E}) - \mu\frac{\partial(\sigma\mathbf{E})}{\partial t} = \mu\frac{\partial^2\mathbf{P}_{tran}}{\partial t^2} \tag{A.22}$$

Through making a comparison of Eq. (A.22) with Eq. (A.17), it is clear that the resonant interaction is actually a kind of nonlinear process. Of course, in an alternative description we may regard the nonlinearity in the media as a special type of radiative source[1].

Slowly-varying-amplitude-approximation (SVA)

When the ratio of bandwidth $\Delta\omega$ to the central frequency ω_c of the field is so small that it satisfies $\Delta\omega << \omega_c$, the electric field $\mathbf{E}(\mathbf{r},t)$ can be expressed in a form of a wave packet,

---

[1] Although these two types of nonlinear processes have completely different physical origins, they do, however, present some very common features in the aspect of affecting propagating optical fields. Sometimes, in the literature, the special technical terms "resonant nonlinearity" and "nonresonant nonlinearity" are used to specify them.

$$\mathbf{E}(\mathbf{r}, t) = \mathcal{A}(\mathbf{r},t)e^{i(\mathbf{k}_c\cdot\mathbf{r} - \omega_c t)} \tag{A.23}$$

where $\mathcal{A}(\mathbf{r},t)$ is a complex term, describing the profile of the field and $e^{i(\mathbf{k}_c\cdot\mathbf{r} - \omega_c t)}$ represents the corresponding carrier wave. Similarly, we may write **P** as

$$\mathbf{P}_{NL} = \mathcal{P}_{NL}(\mathbf{r}, t)e^{i(\mathbf{k}_c\cdot\mathbf{r} - \omega_c t)} \tag{A.24}$$

With the expressions of **E** and **P** given by Eqs. (A.23) and (A.24) respectively, the following slowly-varying-amplitude approximations can be established (supposing only the variation in one spatial dimension is considered).

$$\nabla^2\mathbf{E} \approx (2ik_c\frac{\partial\mathcal{A}}{\partial z} - k_c^2\mathcal{A})e^{i(\mathbf{k}_c\cdot\mathbf{r} - \omega_c t)}$$

$$\frac{\partial^2(\varepsilon\mathbf{E})}{\partial t^2} \approx [\,(2\frac{\partial\varepsilon}{\partial t} - 2i\varepsilon\omega_c)\frac{\partial\mathcal{A}}{\partial t} - (\omega^2\varepsilon + 2i\omega_c\frac{\partial\varepsilon}{\partial t})\mathcal{A}]\, e^{i(\mathbf{k}_c\cdot\mathbf{r} - \omega_c t)}$$

$$\mu\frac{\partial^2\mathbf{P}_{NL}}{\partial t^2} \approx -\mu\omega_c^2\mathcal{P}_{NL}(\mathbf{r},t)e^{i(\mathbf{k}_c\cdot\mathbf{r} - \omega_c t)}$$

$$\frac{\partial\mathbf{E}}{\partial t} \approx -i\omega_c\mu\sigma\mathcal{A}(\mathbf{r},t)e^{i(\mathbf{k}_c\cdot\mathbf{r} - \omega_c t)} \tag{A.25}$$

Substitution of Eq. (A.25) into Eq. (A.17) leads to

$$\frac{\partial\mathcal{A}}{\partial z} + i\frac{\mu}{k_c}(\frac{\partial\varepsilon}{\partial t} - i\varepsilon\omega_c)\frac{\partial\mathcal{A}}{\partial t} + (\frac{\omega_c\mu\sigma}{2k_c} - \frac{\omega_c}{k_c}\frac{\partial\varepsilon}{\partial t})\mathcal{A} = i\frac{\mu\omega_c^2}{2k_c}\mathcal{P}_{NL} \tag{A.26}$$

If the dispersive effect of the medium can be neglected, i. e. $\partial\varepsilon/\partial t = 0$, Eq. (A.26) reduces to

$$\frac{\partial\mathcal{A}}{\partial z} + \frac{1}{v}\frac{\partial\mathcal{A}}{\partial t} + \frac{v\mu\sigma}{2}\mathcal{A} = i\frac{v\mu\omega_c}{2}\mathcal{P}_{NL} \tag{A.27}$$

Eq. (A.27) can be used to analyse the supercontinua phenomena contributed by the nonlinearities in any material.

Similarly, under the SVA approximation and without any dispersion, Eq. (A.22) can be approximated as

$$\frac{\partial\mathcal{A}}{\partial z} + \frac{1}{v}\frac{\partial\mathcal{A}}{\partial t} + \frac{v\mu\sigma}{2}\mathcal{A} = i\frac{v\mu\omega_c}{2}\mathcal{P}_{tran} \tag{A.28}$$

Eq. (A.28) is the equation that is often quoted in the theoretical treatment of laser action. $\mathcal{P}_{tran}$, which is related to the populations of atomic levels, also appears in two additional equations derived from quantum mechanics (Yariv 1978), regarding the atomic transition process. These two equations are:

$$\frac{d\Delta N}{dt} = -\frac{i}{2(h/2\pi)}(\mathcal{A}^*\mathcal{P}_{tran} - \mathcal{A}\mathcal{P}_{tran}^*) + W_p(N_o - \Delta N) - \frac{N_o+\Delta N}{T_1} \qquad (A.29)$$

$$\frac{d\mathcal{P}_{tran}}{dt} = -i(\omega_c - \omega_a)\mathcal{P}_{tran} - i\frac{\mu^2\Delta N\mathcal{A}}{(h/2\pi)} - \frac{\mathcal{P}_{tran}}{T_2} \qquad (A.30)$$

$\Delta N = N_2 - N_1$, is the population difference for a two-level atomic system, $N_o = N_2 + N_1$, the total atomic density, W_p, the atomic pump rate, T_1, T_2, the relaxation times for ΔN and $\mathcal{P}_{tran}$ respectively, ω_a, the resonant frequency, and μ relates to the atomic dipole, which is the same one used in Eq. (5.38) in Ch. 5. With Eqs. (A.28-30) the three quantities $\mathcal{A}$, $\mathcal{P}_{tran}$ and ΔN can be solved at least in principle.

Appedix B Miscellanies

Physical meaning of $g_1(\tau)$

It is known that $|g_1(\tau)|$ also describes the spatial interfering pattern on the reception screen of a Michelson interferometer, i. e.

$$|g_1(\tau)| = \gamma(\tau) \qquad (B.1)$$

where $\gamma(\tau)$ is the visibility of the coherent pattern achieved at a time delay τ, defined as

$$\gamma(\tau) \equiv \left(\frac{I_{max} - I_{min}}{I_{max} + I_{min}}\right)_\tau \qquad (B.2)$$

Eq. (B.1) is only valid for the cases where the two recombined beams have equal intensity, otherwise

$$|g_1(\tau)| = \frac{2\sqrt{I_1}\sqrt{I_2}}{I_1 + I_2}\gamma(\tau) \qquad (B.3)$$

in which I_1, I_2 are the average intensities for the two interfering beams. However, it may be noted that the defination of $\gamma(\tau)$ dose not hold for one specified point in space, instead, it describes the contrast of a spatially distributed fringes.

The line width of a single mode $\Delta\omega_m$

In a simplified situation where the lasing medium is approximated as a two energy level gain system, it has been shown that (Yariv 1976; chapter 10)

$$\Delta\omega_m = \frac{h\omega_o(\Delta\omega_l)^2}{2\pi P}\left(\frac{N_2}{N_2 - N_1}\right) \tag{B.4}$$

where h is Plank's constant, P is laser output power, N_1, N_2 are the population densities of the lower and upper energy levels, and $\Delta\omega_l$ is the bandwidth related to the cavity photon lifetime t_c, given by

$$\Delta\omega_l = \frac{1}{t_c} \tag{B.5}$$

It is known that

$$t_c = \frac{1}{c\alpha} \tag{B.6}$$

where c is the velocity of light and α is the average loss per unit length for the cavity. Substituting Eqs. (B.5), (B.6) into Eq. (B.4), we obtain

$$\frac{\Delta\omega_m}{\omega_o} = \frac{h(c\alpha)^2}{2\pi P}\left(\frac{N_2}{N_2 - N_1}\right) \tag{B.7}$$

$\Delta\omega_m$ determined from Eq. (B.7) is also called *quantum limitation of a laser mode linewidth*. In practice, for many laser systems, other disturbing effects such as vibrations or thermal effect can easily lead to an linewidth much greater than the value given by Eq. (B.7). As an example, suppose the cavity length drifts for a laser operating at 1.5 μm is in an order of 1/10 of a wavelenth, i.e. $\Delta L = 0.15$ μm, this attributes to a frequency flunctuation of $\Delta\omega = (\Delta L/L)(2\pi/T) = 5.6$ Hz (for L = 2m). Such a value is at least 2 orders greater than that obtained from Eq. (B.7) assuming P = 100 mW, $\alpha = 0.125$ m^{-1} and $N_2/(N_2-N_1) \approx 1$.

Dynamic spectrogram (sonagram) of optical pulses

Characterization of optical pulses can be also performed by a method of displaying both their duration and bandwidth in a two-dimensional frequency-time diagram. Two examples of them, one for chirp-free pulses and one for frequency-chirped pulses are shown in Fig. B1, where the bandwidth of the pulses for the two cases are assumed to be the same. Such a graph is called dynamic spectrogram, or sonagram (Bradley and New 1974) which is especially useful for demonstrating the properties of chirped pulses. Note

that the projections of a spectragram trace onto the frequency and time axes give the bandwidth and the temporal duration for the associated pulses respectively.

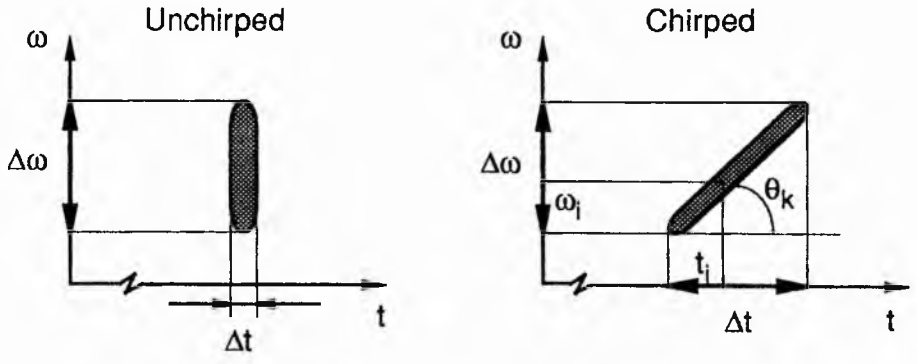

Fig. B1. Spectragrams for chirp-free and chirped pulses.

As clearly shown in Fig. B1 for the unchirped pulses, every portion of the temporal profile has contributions from all of the spectral components. In a contrast, for the chirped pulses different frequencies are only related to the particular parts of the pulses. Therefore, it can be said that the unchirped pulses are frequency homogeneous but the chirped pulses are not. The tilting angle of the spectrogram track is a direct indication of both the sign and magnitude of the chirp in the pulses. Under the condition of a fixed bandwidth, the larger the chrip, the smaller the tilting angle will be. This represents a good illustration of why pulses with frequency chirp generally have greater duration than those of chirp-free pulses. (Further interpretation of this may be deduced by recognizing that for chirped pulses different spectral components are not properly phase-correlated and so they do not lead to bandwidth-limited pulses). Compared with the chirp-free pulses, the chirped pulses are frequency inhomogeneous. In general, a spectrogram track may not be linear or have a uniform width. This is expected to occur if the phase relations within different spectral sections are not the same.

The dynamic spectrogram of ultrashort pulses can be directly and conveniently obtained experimentally by using a streak camera in combination with a spectrometer (Hamaide and Emplit 1989). In this system, the spectrometer is placed in front of a streak camera and with its exit slit orthogonal to the input slit of the streak camera. Therefore,

from the top to the bottom of a streak different spectral components can be displayed. If the optical pulses to be measured are chirped, which means that these different frequency components arrive at the camera slit at a slightly different time, the scanning action of the photoelectrons will lead to the formation of streaks which have exactly the same structure as dynamic spectrograms. Two examples of the original results obtained by Hamaide and Emplit (1989) are reproduced in Fig. B2. These two dynamic spectrograms are for the cw mode-locked Nd:YAG laser pulses following their propagation through a 960 meter long single-mode fibre. There is no doubt that the data in Fig. B2 are excellent and very instructive. When the optical power coupled into the fibre increases, the nonlinear phase modulation enhances, which causes the change of the dynamic spectrogram. It is, however, unfortunate that because of the limited time resolution of the streak cameras spectrograms for subpicosend pulses are not obtainable at the current stage.

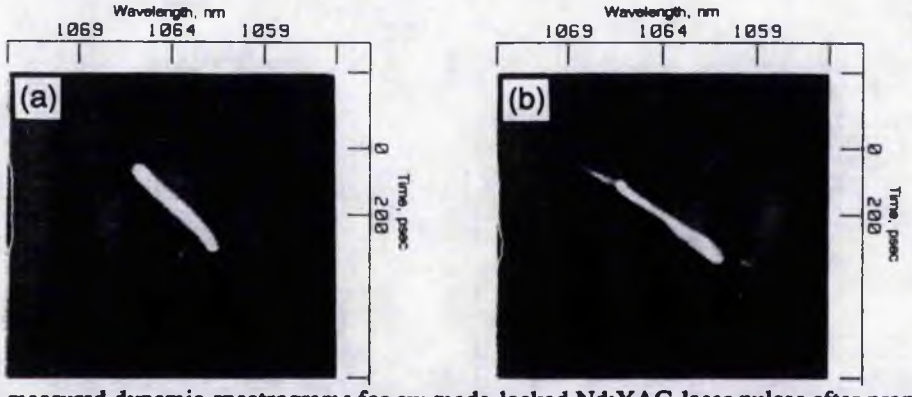

Fig. B2. The measured dynamic spectrograms for cw mode-locked Nd:YAG laser pulses after propagating through a 960 meter long single-mode fibre at two different coupling peak powers: (a) P = 102W (b) P = 166W (from Hamaide and Emplit 1989).

Appendix C Analyses of birefringent plates

Jones vector and Jones matrix

When the polarization characteristics of coherent light need to be considered, Jones vectors and matrices can be used (Gerrard and Bruch 1975). In general, an optical field which does not necessarily have a simple linear polarization can be expressed as

$$\mathbf{E} = \begin{bmatrix} E_x \\ E_y \end{bmatrix} = \begin{bmatrix} |E_x| e^{i\delta_x} \\ |E_y| e^{i\delta_y} \end{bmatrix} \tag{C.1}$$

where E_x, E_y are the two orthogonal components of **E**, both being complex variables. When $|E_x| = 0$ (or $|E_y| = 0$), this means that **E** is a linearly polarized beam with its polarization direction parallel to the y axis (or x axis). When $|E_x| = |E_y| \neq 0$ and $\delta_x - \delta_y = \pi/4$, **E** would be circularly polarized. In more general cases $|E_x| \neq |E_y|$ or $\delta_x - \delta_y \neq \pi/4$, **E** is an elliptically polarized beam.

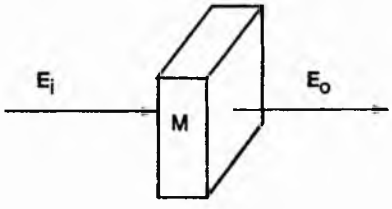

Fig. C.1. A general polarization medium.

Corresponding to Eq. (C.1), the characteristics for a medium whose transformation feature is polarization-dependent can be described by a Jones matrix

$$M = \begin{bmatrix} m_{11} & m_{12} \\ m_{21} & m_{22} \end{bmatrix} \tag{C.2}$$

where all the elements of the matrix are complex. The transformation process of a beam passing through a section of such a medium (see Fig. C.1), can be expressed as

$$\begin{bmatrix} E_{xo} \\ E_{yo} \end{bmatrix} = \begin{bmatrix} m_{11} & m_{12} \\ m_{21} & m_{22} \end{bmatrix} \begin{bmatrix} E_{xi} \\ E_{yi} \end{bmatrix} = \begin{bmatrix} m_{11}E_{xi} + m_{12}E_{yi} \\ m_{21}E_{xi} + m_{22}E_{yi} \end{bmatrix} \tag{C.3}$$

where E_{xo}, E_{yo} are the components of emerging light, E_{xi}, E_{yi} are those of incident light. It can be seen that the matrix elements m_{12}, m_{21} represent the amount of energy transferred from one polarization to another polarization due to the action of the birefringence of the medium. The matrix M given by Eq. (C.2) can thus be regarded as an expression for a generalized "polarization transformer," three particular forms of which, associated with the most commonly used polarzation devices, are listed in Table C.1.

For a retardation plate, if its eigenvectors are not coincident with the x and y axes, the associated transformation matrix becomes

$$M_b = R(-\phi)M_dR(\phi) \tag{C.4}$$

where the argument ϕ is the azimuth angle (see Fig. C.2), $R(\phi)$ is the rotation matrix given by,

$$R(\phi) = \begin{bmatrix} \cos\phi & \sin\phi \\ -\sin\phi & \cos\phi \end{bmatrix} \qquad (C.5)$$

That is, in this case M_b has a general form of Eq. (C.2). Through some simple manipulations on Eq. (C.4), we can obtain,

$$M_b = \begin{bmatrix} \cos^2\phi e^{i\delta_e} + \sin^2\phi e^{i\delta_o} & \sin\phi\cos\phi(e^{i\delta_e} - e^{i\delta_o}) \\ \sin\phi\cos\phi(e^{i\delta_e} - e^{i\delta_o}) & \sin^2\phi e^{i\delta_e} + \cos^2\phi e^{i\delta_o} \end{bmatrix} \qquad (C.6)$$

Eq. (C.6) is the Jones transformation matrix of a birefringent plate when the plate is placed normal to the beam path. Note that the optic axis of the crystal is assumed to lie in the plane of the plate.

Table C.1. Transform matrices for three typical polarization devices

(1)	**Ideal linear polarizer** (oriented with its transmission axis parallel to the y-axis).	$M_o = \begin{bmatrix} 0 & 0 \\ 0 & 1 \end{bmatrix}$
(2)	**General partial polarizer** (e.g. for a Brewster-angled surface $t_s = 2n/(1+n^2)$, $t_p = 1$).	$M_t = \begin{bmatrix} t_s & 0 \\ 0 & t_p \end{bmatrix}$
(3)	**Retardation plate*** (with its Eigen vectors parallel to the x and y-axes respectively).	$M_d = \begin{bmatrix} e^{i\delta_e} & 0 \\ 0 & e^{i\delta_o} \end{bmatrix}$

* $\delta_e = 2\pi n_e l/\lambda$ and $\delta_o = 2\pi n_o l/\lambda$ (l is the thickness of the plat are the phase shifts of extraordinary and ordinary light respectively.

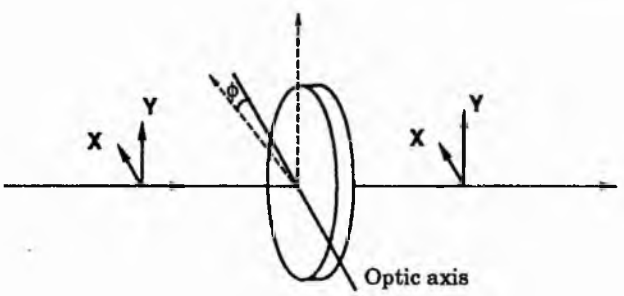

Fig. C.2. A retardation plate with azimuth angle ϕ.

Derivation of the Jones transformation matrix for a tilted birefringent plate

We start here from the more general situation where the optic axis of the birefringent crystal does not lie in the plane of the BP (see Fig. C.3). For clarity, the meanings of various symbols used in the derivation are listed in the following:

θ_i — the incident angle of the ray ($\theta_i = \pi/2 - \theta$),

θ_e, θ_o — the angles of refraction of the extraordinary and ordinary waves respectively,

β — the angle between the optic axis and the plane of the plate,

γ — the angle between normal of the extraordinary wave and the optic axis,

ϕ — the angle between the plane of incidence and projection of the optics axis onto the surface of the plate, usually referred to as the rotation angle,

α — the angle between the plane of incidence and the major plane of the birefringent plate,

n_e, n_o — the major indices of refraction for extraordinary and ordinary waves respectively,

n — the refractive index of extraordinary wave $n = n(\theta_e)$,

δ_e, δ_o — the phase shifts for the extraordinary and ordinary waves respectively,

δ — the phase difference between the extraordinary and ordinary waves $\delta = \delta_e - \delta_o$,

Δ — the effective refractive index difference between extraordinary and ordinary wave, satisfying $\delta = \frac{2\pi}{\lambda}\ell\Delta$,

ℓ — the thickness of birefringent plates

Some relationships between these parameters can be readily obtained (Born and Wolf 1980), such as

$$\sin\theta_e = \frac{\sin\theta_i}{n} \tag{C.7}$$

$$\delta = \frac{2\pi}{\lambda}\left(\sqrt{n^2 - \sin^2\theta_i} - \sqrt{n_o^2 - \sin^2\theta_i}\right)\ell \tag{C.8}$$

$$\frac{1}{n^2} = \left[\frac{1}{n_o^2} - \frac{1}{n_e^2}\right]\cos^2\gamma + \frac{1}{n_e^2} \tag{C.9}$$

and

$$\cos\gamma = \sin\theta_e \cos\beta \cos\phi + \sin\beta \cos\theta_e \tag{C.10}$$

$$\cos\alpha = \frac{\cos\theta_e \cos\beta \cos\phi - \sin\beta \sin\theta_e}{\sqrt{1 - \cos^2\gamma}} \tag{C.11}$$

If the optic axis lies in the plane of plate, i. e. $\beta = 0$, Eqs. (C.10), (C.11) and (C.9) can be respectively reduced to

$$\cos\gamma = \sin\theta_e \cos\phi \tag{C.12}$$

$$\cos\alpha = \frac{\cos\theta_e \cos\phi}{\sqrt{1 - \sin^2\theta_e \cos^2\phi}} \tag{C.13}$$

$$\frac{1}{n^2} = \left[\frac{1}{n_o^2} - \frac{1}{n_e^2}\right] \cos^2\phi \sin^2\theta_e + \frac{1}{n_e^2} \tag{C.14}$$

(i) Matrix expressions

A general form of the transformation matrix for a birefringent plate having the geometrical structure described in Fig. C.3 is (Bloom 1974)

$$M_b = \begin{bmatrix} \cos^2\alpha\, e^{i\delta_e} + \sin^2\alpha\, e^{i\delta_o} & \sin\alpha\cos\alpha(e^{i\delta_e} - e^{i\delta_o}) \\ \sin\alpha\cos\alpha\,(e^{i\delta_e} - e^{i\delta_o}) & \sin^2\alpha\, e^{i\delta_e} + \cos^2\alpha\, e^{i\delta_o} \end{bmatrix} \tag{C.15}$$

Substituting Eq. (C.13) into Eq. (C.15) yeilds

$$M_b = (1 - \cos^2\phi\sin^2\theta_e)^{-1}$$

$$\begin{bmatrix} \cos^2\theta_e\cos^2\phi e^{i\delta_e} + \sin^2\phi e^{i\delta_o} & \cos\theta_e\sin\phi\cos\phi(e^{i\delta_e} - e^{i\delta_o}) \\ \cos\theta_e\sin\phi\cos\phi(e^{i\delta_e} - e^{i\delta_o}) & \sin^2\phi e^{i\delta_e} + \cos^2\theta_e\cos^2\phi e^{i\delta_o} \end{bmatrix} \tag{C.16}$$

If the approximation used by Preuss and Gole (1980) applies, i. e., the birefringent beam splitting is negligible, then:

$$\sin\theta_e \approx \sin\theta_o = \frac{\sin\theta_i}{n_o} \tag{C.17}$$

Eq. (C.16) will change to

$$M_b = \left[1 - \cos^2\phi \frac{\sin^2\theta_i}{n_o^2}\right]^{-1}$$

$$\begin{bmatrix} \left[1 - \frac{\sin^2\theta_i}{n_o^2}\right] \cos^2\phi e^{i\delta_e} + \sin^2\phi e^{i\delta_o} & \sqrt{1 - \frac{\sin^2\theta_i}{n_o^2}}\, \sin\phi\cos\phi(e^{i\delta_e} - e^{i\delta_o}) \\ \sqrt{1 - \frac{\sin^2\theta_i}{n_o^2}}\, \sin\phi\cos\phi(e^{i\delta_e} - e^{i\delta_o}) & \sin^2\phi e^{i\delta_e} + \left[1 - \frac{\sin^2\theta_i}{n_o^2}\right] \cos^2\phi e^{i\delta_o} \end{bmatrix} \tag{C.18}$$

For the above equation, substitution of $\theta_i = \pi/2 - \theta$ leads to Eq. (7.1). This is the same as that given by Preuss and Gole (1980).

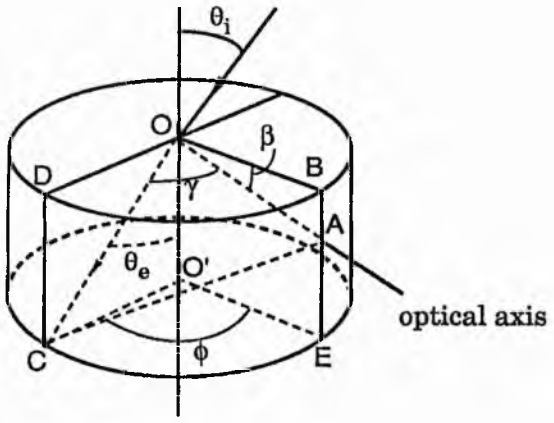

Fig. C.3. Geometrical structure of a birefringent plate. OO' - normal to the plate surface; ODO'C - plane of incidence of the ray; OB - projection of optical axis on the plate surface; OAC - principal plane of the plate.

However, it is noted that when $\beta = 0$, an explicit function of n with respective to n_o, n_e, θ_i, and ϕ can be found. From Eqs. (C.14) and (C.7) we obtain

$$n = n_e \sqrt{1 - \left(\frac{1}{n_o^2} - \frac{1}{n_e^2}\right) \sin^2\theta_i \cos^2\phi} \tag{C.19}$$

$$\sin\theta_e = \frac{\sin\theta_i}{n_e \sqrt{1 - \left(\frac{1}{n_o^2} - \frac{1}{n_e^2}\right) \sin^2\theta_i \cos^2\phi}} \tag{C.20}$$

Substituting Eq. (C.20) into Eq. (C.16), the transformation matrix of a tilted BP with its optic axis lying in the plane of plate can be derived without the approximation given in Eq. (C.17), that is

$$M_b = \left[1 - \frac{\cos^2\phi\cos^2\theta}{qn_e^2}\right]^{-1}$$

$$\begin{bmatrix} \left[1 - \frac{\cos^2\theta}{qn_e^2}\right]\cos^2\phi e^{i\delta_e} + \sin^2\phi e^{i\delta_o} & \sqrt{1 - \frac{\cos^2\theta}{qn_e^2}}\sin\phi\cos\phi(e^{i\delta_e} - e^{i\delta_o}) \\ \sqrt{1 - \frac{\cos^2\theta}{qn_e^2}}\sin\phi\cos\phi(e^{i\delta_e} - e^{i\delta_o}) & \sin^2\phi\, e^{i\delta_e} + \left[1 - \frac{\cos^2\theta}{qn_e^2}\right]\cos^2\phi\, e^{i\delta_o} \end{bmatrix} \tag{C.21}$$

where $\theta = \frac{\pi}{2} - \theta_i$ and

$$q = 1 - \left[\frac{1}{n_o^2} - \frac{1}{n_e^2}\right]\cos^2\theta\cos^2\phi \tag{C.22}$$

Note that combination of Eq. (C.20) and (C.22), leads to

$$n_e^2 q = \frac{\sin^2\theta_i}{\sin^2\theta_e}$$

Using the approximation given by Eq. (C.17), the above equation gives rise to $n_e^2 q \approx n_o^2$ and therefore, Eq. (C.21) will reduce to the approximate form Eq. (C.18).

(ii) Phase shift

As for the phase shift δ_e and δ_o, referring to Fig. C.4, it can be deduced that

$$\begin{aligned}\delta_e &= \frac{2\pi}{\lambda}\left[\, n(\theta_e)\, \underline{OC} \,+\, \underline{DC}\,\right] \\ &= \frac{2\pi}{\lambda}\ell\left[\frac{n(\theta_e)}{\cos\theta_e} + (\mathrm{tg}\theta_o - \mathrm{tg}\theta_e)\sin\theta_i\right] \\ &= \frac{2\pi}{\lambda}\ell\left[n\cos\theta_e - n_o\cos\theta_o + \frac{n_o}{\cos\theta_o}\right] \end{aligned} \tag{C.23}$$

$$\delta_o = \frac{2\pi}{\lambda} n_o\, \underline{OB} = \frac{2\pi}{\lambda}\ell\frac{n_o}{\cos\theta_o} \tag{C.24}$$

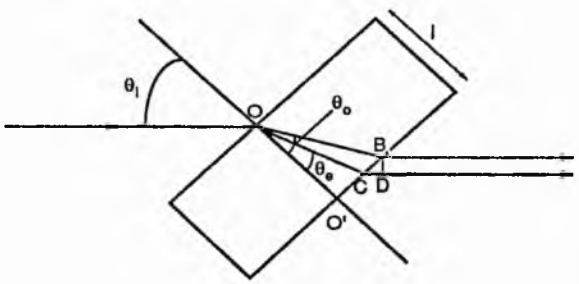

Fig. C.4. Beam splitting inside a birefringent plate.

Using Eqs. (C.19) and (C.20), both δ_e and δ_o can be expressed in terms of n_o, n_e, θ and ϕ:

$$\delta_e = \frac{2\pi}{\lambda}\left[n_e\sqrt{1 - \frac{\cos^2\theta\sin^2\phi}{n_e^2} - \frac{\cos^2\theta\cos^2\phi}{n_o^2}} - n_o\sqrt{1 - \frac{\cos^2\theta}{n_o^2}} - \frac{n_o}{\sqrt{1 - \frac{\cos^2\theta}{n_o^2}}}\right]\ell \tag{C.25}$$

$$\delta_o = \frac{2\pi}{\lambda}\frac{n_o\ell}{\sqrt{1 - \frac{\cos^2\theta}{n_o^2}}} \tag{C.26}$$

If the distance DC which corresponds to the birefringent splitting is neglected, Eq. (C.23) becomes

$$\delta_e = \frac{2\pi}{\lambda}\mathfrak{L}\left[\frac{n(\theta_e)}{\cos\theta_e}\right] = \frac{2\pi}{\lambda}n_e\mathfrak{L}\left[\frac{1+\frac{\cos^2\theta\cos^2\phi}{n_e^2}-\frac{\cos^2\theta\cos^2\phi}{n_o^2}}{\sqrt{1-\frac{\cos^2\theta\sin^2\phi}{n_e^2}-\frac{\cos^2\theta\cos^2\phi}{n_o^2}}}\right] \qquad (C.27)$$

This is the same as Eq. (7.2) in Ch. 7.

From Eqs. (C.23) and (C.24) a general expression of the phase difference can be obtained, which is

$$\delta = \frac{2\pi}{\lambda}(n\cos\theta_e - n_o\cos\theta_o) \qquad (C.28)$$

If the birefringent splitting is neglected the phase difference will be

$$\delta = \frac{2\pi}{\lambda}\left[\frac{n(\theta_e)}{\cos\theta_e} - \frac{n_o}{\cos\theta_o}\right] \qquad (C.29)$$

Using Eqs. (C.14) and (C.7), Eqs. (C.28) and (C.29) can be rewritten respectively as

$$\delta = \frac{2\pi}{\lambda}\left[n_e\sqrt{1-\frac{\cos^2\theta\sin^2\phi}{n_e^2}-\frac{\cos^2\theta\cos^2\phi}{n_o^2}} - n_o\sqrt{1-\frac{\cos^2\theta}{n_o^2}}\right]\mathfrak{L} \qquad (C.30)$$

$$\delta = \frac{2\pi}{\lambda}\left[n_e\frac{1+\frac{\cos^2\theta\cos^2\phi}{n_e^2}-\frac{\cos^2\theta\cos^2\phi}{n_o^2}}{\sqrt{1-\frac{\cos^2\theta\sin^2\phi}{n_e^2}-\frac{\cos^2\theta\cos^2\phi}{n_o^2}}} - n_o\frac{1}{\sqrt{1-\frac{\cos^2\theta}{n_o^2}}}\right]\mathfrak{L} \qquad (C.31)$$

Expressions (C.21), (C.25) and (C.30) are the accurate forms of (C.18), (C.27) and (C.31) respectively. (The latter three are denoted as Eqs. (7.1), (7.2) and (7.13a) in Ch. 7).

If $\beta \neq 0$, the basic equations (C.8) for the phase difference and (C.15) for the transformation matrix must be used. In this situation, from Eqs. (C.10), (C.7) and (C.9) an implicit relation between n and n_o, n_e, θ_i, β, ϕ can be found. Substituting the value of n obtained numerically from these three equations into Eq. (C.8) to find δ, and to Eq. (C.11) to find $\cos\alpha$ (both δ and α are also implicit functions of n_e, n_o, θ_i, β, and ϕ) so that all the elements of matrix Eq. (C.15) may be determined.

A birefingent plate located between two partial polarizers

A tilted BP, with the effect of its two Brewster-angled surfaces taken into account, can be modelled as a BP sandwiched between two partial polarizers (see Fig. C.5). We thus have

$$\begin{bmatrix} E_{xo} \\ E_{yo} \end{bmatrix} = M_{t_2} M_b M_{t_1} \begin{bmatrix} E_{xi} \\ E_{yi} \end{bmatrix} \tag{C.32}$$

where

$$M_{t_1} = M_{t_2} = \begin{bmatrix} t_s & 0 \\ 0 & t_p \end{bmatrix} \tag{C.33}$$

A simple multiplication of Eq. (C.32) results in

$$\begin{bmatrix} E_{xo} \\ E_{yo} \end{bmatrix} = \begin{bmatrix} t_s^2 m_{11} & t_p t_s m_{12} \\ t_p t_s m_{21} & t_p^2 m_{22} \end{bmatrix} \begin{bmatrix} E_{xi} \\ E_{yi} \end{bmatrix} \tag{C.34}$$

If $E_{xi} = 0$, from Eq. (7.8) the transmissivity of the system is given by

$$T = t_s^2 | m_{12} |^2 + | m_{22} |^2 \tag{C.35}$$

where $| m_{22} |^2 = 1 - A\sin^2\frac{\delta}{2}$ (see Sec. 7.2), which is the transmissivity for the case of $t_s = 0$. Utilizing Eq. (C.21), it can be derived that

$$| m_{12} |^2 = A\sin^2\frac{\delta}{2} \tag{C.36}$$

Therefore, Eq. (C.35) can be rewritten as

$$T = 1 - A'\sin^2\frac{\delta}{2} \tag{C.37}$$

where the extinction coefficient A' is equal to

$$A' = (1 - t_s^2)A \tag{C.38}$$

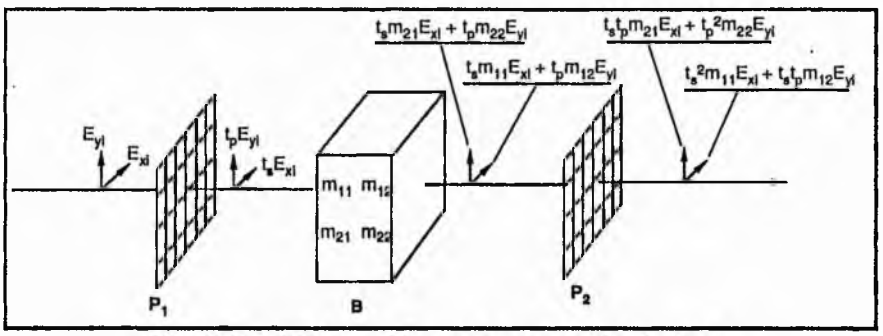

Fig. C.5. A BP located between two partial polarizers.

Appendix D Compression of optical pulses

It has been shown in subsection. 5.1.4 that frequency chirp within an optical pulse can be removed after the pulse propagates some distance in a dispersive medium. At the particular position where the chirp is just cancelled by dispersion, the pulse possesses the shortest possible duration for the spectral bandwidth available. In other words, it becomes bandwidth limited. Such an important feature simply implies that if a pulse can first be frequency chirped (assuming that the associated temporal profile change during this chirping process does not degrad the pulse peak intensity severely), it can then be compressed by letting it pass through a controllable dispersive delay line. Therefore, a general scheme for optical pulse compression can have a schematic as illustrated in Fig. D.1. It comprises two stages: stage I for spectral stretching or pulse chirping and stage II for temporal pulse compression or frequency-chirp compensation. From the discussions in Subsection 5.2.3, it can be recognized that a pure SPM medium makes a good candidate for performing the stage-I task although other types of spectral stretching devices such as a phase modulator (Kobayashi *et al* 1988) or a atomic resonant vapour (Grischkowsky 1974) can be also used. Nowadays, the most popular spectral stretching device is an optical fibre with an appropriately selected length. The dispersive delay line is usually a grating pair where the spatial separation between the two gratings can be conveniently altered[2].

Suppose the pulses after Stage I have a form of $A(t)e^{i\phi(t)}$, the corresponding Fourier spectral counterpart is $\upsilon(\omega)e^{i\phi(\omega)}$ then for an ideal dispersive delay line (compressor) its transform function given by $h(\omega) = |h(\omega)|e^{i\Phi(\omega)}$ should satisfy

$$|h(\omega)| = 1$$

$$\Phi(\omega) = -\phi(\omega) + \phi_o \qquad \text{(D.1)}$$

---

[2] An all-fibre pulse compression has also been realized by Blow *et al* (1985). In this case the second fibre has a zero-dispersion wavelength shorter than that of the incident wave. This enables the fibre to act as a dispersive delay line, like a grating pair that provides negative dispersion for the working wavelength. And therefore the spectrally-stretched pulses exiting from the first fibre can be compressed during the propagation in the second fibre.

where ϕ_0 is a frequency-independent constant phase shift. Because $\phi(\omega)$ varies for different input pulses it is therefore almost impossible to have a dispersive delay line that can make the second condition in Eq. (D.1) hold for any $\phi(\omega)$. However, in practice an approximate quadratic compressor such as a grating pair can be readily obtained. The phase term in the transform function of the quadratic compressor has the form

$$\Phi(\omega) = \Phi_0 + \Phi_1 (\omega - \omega_0) + \Phi_2 (\omega - \omega_0)^2 \qquad (D.2)$$

where the coefficients Φ_0, Φ_1 and Φ_2 are independent of frequency. The quadratic dispersive delay line is ideal for compressing linear chirped pulses.

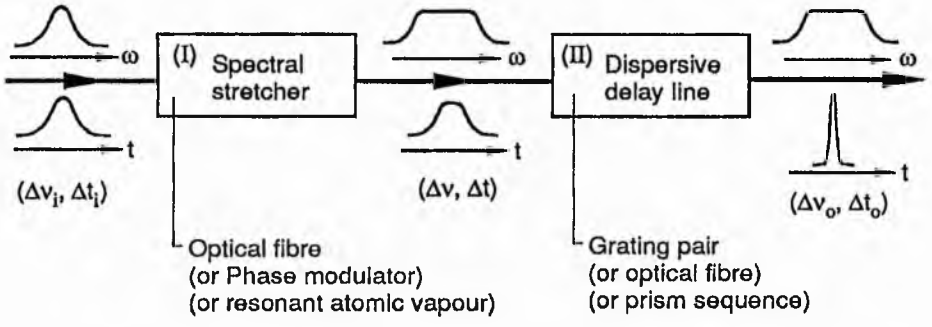

Fig. D.1. Schematic for the temporal compression of optical pulse. (For pure SPM-induced spectral stretching $\Delta t = \Delta t_i$).

In the cases where only pure self-phase modulation is present[3], as shown by Eq. (5.68b) the amount of frequency chirp introduced to the pulses during the first stage is approximately proportional to the maximum nonlinear phase shift $\Delta\phi_{max}$. Under such circumstances, from Eq. (5.18) the optimum compression ratio at the second stage will be

$$\frac{\Delta t_i}{\Delta t_o} = \sqrt{1 + (b/a)^2} \qquad (D.3)$$

This can be achieved if the second-order differential of the spectral phase shift generated by grating pair [Eq. (5.27)] satisfies

$$\phi''(\omega) = \frac{-b}{2(a^2 + b^2)} \qquad (D.4)$$

---

[3] For the situations where the condition L_f, Z_s, << Z_D is satisfied so that the changes in the temporal feature of the pulses can be ignored in the spectral stretching stage [L_f is the fibre length, Z_s, Z_D are the SPM and dispersion characteristic distances respectively (see Eqs. (5.72a) and (5.14b))].

Then by combining Eq. (D.4) and Eq. (5.27), the optimum grating separation can be determined, namely,

$$B = C_g \frac{b}{a^2 + b^2} \tag{D.5}$$

where $C_g = \phi''(\omega)/B = \frac{\omega^3 d^2 \cos^3\gamma}{4\pi^2 c}$. If $b >> a$, Eqs. (D.3) and (D.5) reduce into

$$\frac{\Delta t_j}{\Delta t_o} \approx \frac{b}{a} \approx 2\Delta\phi_{max} \tag{D.6}$$[4]

$$B = C_g \frac{1}{b} = C_g \frac{\Delta t_i^2}{4\ln 2 \Delta\phi_{max}} \tag{D.7}$$

Eq. (D.3) or (D.6) indicates that the maximum compression ratio is independent of the initial pulse duration but Eq. (D.7) shows that the optimum grating separation between the grating pair is proportional to the square of the initial pulse duration.

From Eq. (D.6) it can be concluded that apart from the methods of increasing the peak power of the input pulses the longer the fibre length, the greater the compression ratio would be. However, this will not be the case if the dispersive effect in the first stage is significant. For such situations, in addition to the spectral stretching the temporal duration of the pulses is also enlarged in the first stage. This will lead to a gradual decrease of peak intensity for the propagating pulses and so the spectral broadening process will be frustrated. On another hand, as it is mentioned in Ch.5, the existence of positive GVD helps to linearize the SPM-induced frequency chirp, which means that pulse compression at the second stage with a quadratic compressor can become more effective. Because of all these reasons, in practice, an optimum fibre length exists. Based on the results from numericaly sulutions of the nonlinear Schrodinger equation [Eq. (5.115)], the optimum fibre length used for the purpose of spectral stretching was shown to be (Stolen and Shank 1986, Weiner *et al* 1988),

---

[4] The factor 2 in Eq. (D.6) is due to the quotation of Eq. (5.68b), which means the linear chirp at the central part of a pulse has been used to represent the whole SPM-induced chirp. Obviously, this is not a very valid approximation. To be more precise, Eq. (5.71c) should be used, which leads to

$$\frac{\Delta t_j}{\Delta t_o} \approx \sqrt{1 + (\Delta\phi_{max})^2} \approx \Delta\phi_{max}$$

Thus the temporal compression ratio at the second stage is equal to the spectral extension ratio achieved in the first stage.

$$z_{opt1} = \frac{1.6}{A} z_o \tag{D.8}$$

where $A = \sqrt{P/P_1} = \sqrt{I/I_1}$ is the normalized amplitude [I_1 is the N = 1 soliton intensity (see Eq. (5.112b)], z_o is the soliton period given by Eq. (5.110a). For the fibre length equal to z_{opt1}, the compression ratio is

$$\frac{\Delta t_i}{\Delta t_o} = 0.63A \tag{D.9}$$

provided that the grating separation is selected as

$$B = 84C_2 \frac{(\Delta t_i[ps])^2}{A} [cm] \tag{D.10}$$

where

$$C_2 = \left[\frac{d[cm]}{5.56x10^{-5}}\right]^2 \left[\frac{600}{\lambda[nm]}\right]^2 \cos^3\gamma \tag{D.11}$$

Finally, it should be stressed that all the above discussions have excluded the existence of other types of nonlinear effects. Nevertheless, in the experiments where the propagation of high intensity pulses is involved it is very likely that stimulated Raman scattering may occur. [The influence of SRS on light pulse compression has been studied by many authors e.g. Tomlinson *et al* (1984), Kuchartz and Harde (1988)]. To avoid the occurrence of SRS in the spectral stretching stage in a pulse compression experiment, the fibre length may be chosen much shorter than z_{opt1}. In this case, if the grating pair separation is equal to

$$B = 13C_2 \left[\frac{\Delta t_i[ps]}{A}\right]^2 \frac{z_o}{z} \quad [cm] \tag{D.12}$$

the corresponding optimum compression ratio will be given by (Stolen and Shank 1986)

$$\frac{\Delta t_i}{\Delta t_o} \approx 1 + 0.9A^2 z/z_o \tag{D.13}$$

References

Aechtner, P., Heinz, P. and Laubereau, A., 1986, "Collective modes - an analytical model for active mode locking in the transient case," *Ultrafast Phenomena V, Springer Series in Chemical Physics* Vol. 46, eds G. R. Fleming and A. E. Siegman, Berlin: Springer-Verlag, 1986, 27-29.

Ainslie, B. J. and Day, C. R., 1986, "A review of single-mode figbers with modified dispersion characteristics," *J. Lightwave Technology*, Vol. LT-4, 967-979.

Akhmanov, S. A., Vysloukh, V. A. and Chirkin, A. S., 1986, "Self-action of wave packets in a nonlinear medium and femtosecond laser pulse generation," *Sov. Phys. Usp*, Vol. 29, 642-677.

Alfano, R. R. (ed), 1982, *Biological events probed by ultrafast laser spectroscopy*, Academic Press, Inc., New York.

Alfano, R. R. and Ho, P. P., 1989, "Self- and coupled-phase modulations of ultrashort laser pulses," *Optics News*, No.8, 13-18.

Anderson, D. and Lisak, M., 1982, "Nonlinear asymmetric pulse distortion in long optical fibers," *Opt. Lett.* Vol. 7, 394-396.

Anderson, D. and Lisak, M., 1984, "Modulational instability of coherent optical-fiber transmission signals," *Opt. Lett.* Vol. 9, 468-470.

Armstrong, J. A., 1967, "Measurement of picosecond laser pulse widths," *Appl. Phys. Lett.* Vol. 10, 16-18.

Ausschnitt, C. P., Jain, R. K. and Heritage, J. P., 1979, "Cavity length detuning characteristics of the synchronously mode-locked cw dye laser," *IEEE J. Quantum Electron.* Vol. QE-15, 912-917.

Auston, D. H., 1968, "Transverse mode locking," *IEEE J. Quantum Electron.* Vol. QE-4, 420-422.

Auston, P. H., 1977, "Picosecond nonlinear optics," *Ultrashort light Pulses, Topics in Applied Physics* Vol. 18, ed S. L. Shapiro, Berlin: Springer-Verlag (1977), 123-194.

Auston, D. H., Smith, P. R., Johnson, A. M., Augustiniak, W. M., Bean, J. C. and Fraser, D. B., 1980, "Recent advances in picosecond optoelectronics," *Picosecond Phenomena II, Springer Series in Chemical Physics* Vol. 14, ed R. M. Hochstrasser, W. Kaiser and C. V. Shank, Berlin: Springer-Verlag (1980), 71-74.

Auston, D. H. and Eisenthal, K. B. (ed), 1984, *Ultrafast Phenomena IV, Springer Series in Chemical Physics* Vol. 38, Berlin: Springer-Verlag.

Ausubel, J. H. and Langford, H. D. (ed), 1987, *Lasers-Invention to Application*, National Academy Press, Washington, D. C..

Bado, P., Squier, J., Salin, F., Coe, J. S., Chien, C.-Y., Tapie, J.-L. and Mourou, G. A., 1990, "Ultrahigh peak power generation - present and future," *Picosecond Phenomena VII, Springer Series in Chemical Physics* Vol. 53, eds. C. B. Harris, E. P. Ippen, G. A. Mourou and A. H. Zewail, Berlin: Springer-Verlag, (1990), 92-95.

Baker, R., 1990, "Optical amplification," *Physics World*, Vol. 3, No. 3, 41-44.

Barbara, P. F., 1990, "Ultrafast studies on intramolecular charge transfer and solvation dynamics," *Picosecond Phenomena VII, Springer Series in Chemical Physics* Vol. 53, eds. C. B. Harris, E. P. Ippen, G. A. Mourou and A. H. Zewail, Berlin: Springer-Verlag, (1990), 393-396.

Barr, J. R. M., Hanna D. C. and Hughes, D. W., 1989, "Coupled cavity mode locking of a Nd:YAG laser using second-harmonic generation," Paper FQ-5, Technical Digest of CLEO'89 (April 24-28, 1989, Baltimore, USA).

Barr, J. R. M. and Hughes, D. W., 1989, "Coupled cavity mode locking of a Nd:YAG laser using second-harmonic generation," *Appl. Phys. B* , Vol. 49, 323-325.

Beaud, P., Hodel, W., Zysset, B. and Weber, H. P., 1987, "Ultrashort pulse propagation, pulse breakup, and fundamental soliton formation in a single-mode optical fiber," *IEEE J. Quantum Electron.* Vol. QE-23, 1938-1946.

Beaud, P., Bi, J. Q., Schutz, J., Hodel, W. and Weber, H. P., 1990, "Clean subpicosecond pulses by coupling resonantly to a linear high loss cavity," *Ultrafast Phenomena VII, Springer Series in Chemical Physics*, Vol. 53, ed. C. B. Harris, E. P. Ippen, G. A. Mourou, A. H. Zewail, Berlin: Springer-Verlag (1990), 23-25.

Belanger, P. A., 1988, "Soliton laser. I: A simplified model," *J. Opt. Soc. Am. B*, Vol. 5, 793-798.

Bendow, B., Gianino, P. D., Tzoar, N. and Jain, M., 1980, "Theory of nonlinear pulse propagation in optical waveguides," *J. Opt. Soc. Am.* Vol. 70, 539-546.

Bloom, A. L., 1974, "Modes of a laser resonator containing tilted birefringent plates," *J. Opt. Soc. Am.* Vol. 64, 447-452.

Blow, K. J. and Doran, N. J., 1983, "Nonlinear limits on bandwidth at the minimum dispersion in opticas fibres," *Opt. Commun.* Vol. 48, 181-184.

Blow, K. J., Doran N. J. and Nelson, B. P., 1985, "All-fiber pulse compression at 1.32 μm," *Opt. Lett.* Vol. 10, 393-395.

Blow, K. J. and Wood, D., 1986, "Stability and compression of pulses in the soliton laser," *IEEE J. Quantum Electron.*, Vol. QE-22, 1109-1116.

Blow, K. J. and Doran, N. J., 1987, "Nonlineadr effects in optical fibres and fibre devices," *IEE. Pro.* Vol. 134, 138-144.

Blow, K. J. and Wood, D., 1988, "Mode locked lasers with nonlinear external cavities," *J. Opt. Soc. Am. B*, Vol 13, 1026-1028.

Blow, K. J., Doran, N. J. and Wood, D., 1988, "Suppression of the soliton self-frequency shift by bandwidth-limited amplification," *J. Opt. Scc. Am. B*, Vol. 5, 1301-1304.

Blow, K. J. and Nelson, B. P., 1988, "Improved modelocking of a F-center laser with a nonlinear non-soliton external cavity," *Opt. Lett.*, Vol. 13, 1026-1028.

Blow, K. J. and Wood, D., 1988, "Modelocked lasers with nonlinear external cavities," *J. Opt. Soc. Am. B*, Vol.5, 629-632.

Bonarev, B. V. and Kobtsev, S. M., 1986, "Calculation and optimization of a birefringent filter for a cw dye laser," *Opt. Spectrosc.* (USSR) Vol. 60, 501-504.

Bor, Z., Muller, A., Racz, B., Schafer, F. P., 1982, "Ultrashort pulse generation by distributed feedback dye lasers. I," *Appl. Phys.* Vol. 27B, 9-14.

Bor, Z. and Rácz, B., 1985, "Dispersion of optical materials used for picosecond spectroscopy," *Appl. Opt.* Vol. 24, 3440-3441.

Born, M. and Wolf, E., 1980, "Principles of optics", 6th cor. ed. Oxford, Pergamon, 694-702.

Bourkoff, E., Zhao, W. and Joseph, R. I., 1987, "Intensity-dependent spectra of pulses propagating in optical fibers," *Opt. Commun.* Vol. 62, 284-288.

Boyer, G. R. and Carlotti, X. F., 1988, "Pulse-spread minimization in single-mode optical fibers," *Phys. Rev. A*, Vol. 38, 5140-5148.

Boyer, G. R. and Franco, M. A., 1989, "Numerical and experimental comparison of spectral broadening of femtosecond optical asymmetric pulses in a monomode fiber," *Opt. Lett.* Vol. 14, 465-467.

Bradley, D. J., 1970, UK Patent Spec. 31167/70.

Bradley, D. J. and New, G. H. C., Caughey, S. J., 1970, "Amplitude and phase structure of picosecond pulses from Nd: glass lasers," *Phys. Lett.* Vol. 32A, 313-314.

Bradley, D. J., Liddy, B. and Sleat, W. E., 1971, "Direct linear measurement of ultrashort light pulses with a picosecond streak camera," *Opt. Common.* Vol. 2, 391-395.

Bradley, D. J. and New, G. H. C., 1974, "Ultrashort pulse measurements," *Proc. IEEE*, Vol. 62, 313-345.

Bradley, D. J., 1977, "Methods of generation," *Ultrashort light Pulses, Topics in Applied Physics* Vol. 18, ed S. L. Shapiro, Berlin: Springer-Verlag (1977), 17-81.

Bulushev, A. G., Dianov, E. M. and Okhotnikov, O. G., 1990, "Passive mode locking of a laser with a nonlinear fiber reflector," *Opt. Lett.*, Vol. 17, 968-970.

Burleigh Instruments, Inc., 1980, "Instruction manuals Tech Memo for F-centre lasers."

Campillo, A. J. and Shapiro, S. L., 1977, "Picosecond relaxation measurements in biology," *Ultrashort light Pulses, Topics in Applied Physics* Vol. 18, ed S. L. Shapiro, Berlin: Springer-Verlag (1977), 317-376.

Carruthers, T. F. and Duling III, I, N., 1990, "Passive laser mode locking with an antiresonant nonlinear mirror," *Opt. Lett.*, Vol. 15, 804-806.

Chee, J. K. and Liu, J. M., 1989, "Raman-assisted parametric frequency and polarization conversion in a birefringent fiber," *Opt. Lett.* Vol. 14, 820-822.

Chee, J. K., Cheung, E. C., Kong, M. N. and Liu, J. M., 1990, "Generation of ultrashort Nd:YLF pulses by cw passive mode locking with a nonlinear external cavity," *Ultrafast Phenomena VII, Springer Series in Chemical Physics*, Vol. 53, eds. C. B. Harris, E. P. Ippen, G. A. Mourou, A. H. Zewail, Berlin: Springer-Verlag (1990), 8-10.

Chen, J., 1985, "Mode locking of a Nd:glass laser with LiF:F_2^-," *Appl. Opt.* Vol. 24, 1073-1075.

Chen, Y., 1989, "Four-wave mixing in optical fibers: exact solution," *J. Opt. Soc, Am. B*, Vol. 6, 1986-1993.

Chilla, J. L. A. and Martinez, O. E., 1991, "Direct determination of the amplitude and the phase of femtosecond light pulses," Opt. Lett., Vol. 16, 39-41.

Chong, T. W. and Lindasay, P. A., 1978, "The generation of picosecond pulses in actively mode-locked cw solid-state lasers: IV, The pulse formation," *Int. J. Electronics*, Vol. 45, 573-608.

Christov, I. P. and Tomov, I. V., 1986, "Large bandwidth pulse compression with diffraction gratings," *Opt. Commun.* Vol. 58, 338-342.

Christov, I. P., 1988, "Propagadtion of short optical pulses in dispersive medium," *IEEE J. Quantum. Electdron.* Vol. 24, 1548-1553.

Cotter, D., 1984, "Technique for highly stable active mode-locking," *Ultrafast Phenomena IV, Springer Series in Chemical Physics* Vol. 38, eds D. H. Auston, and K. B. Eisenthal, Berlin: Springer-Verlag (1984), 78-80.

Cox, A. J., Damschen, D. E., Merritt, C. D., Scott, G. W. and Talley, L. D., 1978, "Evidence for nearly transform-limited pulses from a short cavity blue dye laser," *Picosecond Phenomena, Springer Series in Chemical Physics* Vol. 4, eds C. V. Shank, E. P. Ippen and S. L. Shapiro, Berlin: Springer-Verlag (1978), 63-66.

Crosignani, B., Papas, C. H., and Porto, P. Di., 1981, "Coupled-mode theory approach to nonlinear pulse propagation in optical fibers," *Opt. Lett.* Vol. 6, 61-63.

Crowell, M. H., 1965, "Characteristics of mode-coupled lasers," *IEEE J. Quantum Electron.* Vol. QE-1, 12-20.

Curley, P. F. and Ferguson, A. I., 1991, "Resonant frequency doubling of a self-starting, coupled-cavity, mode-locked Ti:Al_2O_3 laser," *Opt. Lett.* Vol. 16, 321-323.

Dantus, M., Bowman, R. M., Zewail, A. H., 1990, "Femtosecond laser observations of molecular vibration and rotation," *Nature*, Vol. 343, 737-739.

Davis, L. W. and Lin, Y. S., 1973, "Propagation of optical pulses in a saturable absorber," *IEEE J. Quantum Electron.* Vol. QE-9, 1135-1138.

Dawson, M. D., Boggess, T. F., Garvey, D. W. and Smirl, A. L., 1986, "Generation of 55-fs pulses and variabale spectral windowing in a linear-cavity synchronously pumped cw dye laser," *Picosecond Phenomena, Springer Series in Chemical Physics* Vol. 46, eds. G. R. Fleming and A. E. Siegman, Berlin: Springer-Verlag (1978), 5-7.

Defonzo, A. P., 1988, "Femtosecond characterization of semiconductor lasers," *Opt. Eng.* Vol. 27, 696-700.

DeMaria, A. J., Stetser, D. A. and Heynau, H., 1966, "Self mode-locking of lasers with saturable absorbers," *Appl. Phys. Lett.* Vol. 8, 174-176.

Demokan, M. S., 1982, "Mode-locking in solid-state and semiconductor lasers," Chichester: Research Studies Press, Acousto-optic modulators: 107-119; Multipulse generation: 141-143; Broadening and compression of pulses: 85-95; Gain switching: 201-208.

Demtroder, W., 1981, "Laser spectroscopy, Basic concepts and instrumentation," *Springer Series in Chemical Physics*, Vol. 5, Berlin: Springer-Verlag, 71-76.

Dianov, E. M., Karasik, A. Ya., Mamyshev, P. G., Onishchukov, G. I., Prokhorov, A. M., stel'makh, M. F. and Fomichev, A. A., 1984, "100-fold compression of picosecond pulses from a parametric light source in single-mode optical fibers at wavelengths 1.5-1.65 μm," *JETP Lett.* Vol. 40, 903-905.

Dianov, E. M., Karasik, A. Ya., Mamyshev, P. G., Prokhorov, A. M. and Serkin, V. N., 1985, "Generation of ultrashort pulses by spectral filtering during stimulated Raman scattering in an optical fiber," *Sov. Phys. JETP*. Vol. 62, 448-455.

Dianov, E. M., Konstantinov, K. K., Luchnicov, A. V., Pilipetskii, A. N. and Starodumov, A. N., 1990, "Femtosecond soliton pulses amplification and Raman self-frequency shift suppression in fibers with complex profile of gain and losses," to be published.

DiDomenico, M. Jr., 1964, "Small-signal analysis of internal (coupling-type) modulation of lasers," *J. Appl. Phys.* Vol. 35, 2870-2876.

Diels, J. -C., Van Stryland, E. W. and Gold, D., 1978, "Investigation of the parameters affecting subpicosecond pulse durations in passivly mode-locked dye lasers," *Picosecond Phenomena, Springer Series in Chemical Physics* Vol. 4, ed C. V. Shank, E. P. Ippen and S. L. Shapiro, Berlin: Springer-Verlag (1978), 117-120.

Diels, J. C., Dietel, W., Fontaine, J. J., Rudolph, W. and Wilhelmi, B., 1985, "Analysis of a mode-locked ring laser: chirped-solitary-pulse solutions," *J. Opt. Soc. Am. B*, Vol. 2, 680-686.

Diels, J. -C., Fontaine, J. J., McMichael, I. C. and Simoni, F., 1985, "Control and measurement of ultrashort pulse shapes (in amplitude and phase) with femtosecond accuracy," *Appl. Opt.* Vol. 24, 1270-1282.

Dietel, W., Fontaine, J. J. and Diels, J.-C., 1983, "Intracavity pulse compression with glass: a new method of generating pulses shorter than 60 fsec," *Opt. Lett.* Vol. 8, 4-6.

Dominic, V., Yao, X. S., Pierce, R. M. and Feinberg, J., 1990, "Measuring the coherence length of mode-locked laser pulses in real time," *Appl. Phys. Lett.* Vol. 56, 521-523.

Doukas, A. G., Buchert, J. and Alfano, R. R., 1982, "Picosecond laser techniques and design," *Biological events probed by ultrafast laser spectroscopy*, eds. R. R. Alfano, Academic Press, Inc., New York (1982), 387-416.

Doust, T. A. M. and West, M. A. (ed) 1983, *Picosecond Chemistry and Biology*, Science Reviews Limited, England.

Downey, P. M., Bowers, J. E., Burrus, C. A., Mitschke, F. and Mollenauer, L. F., 1986, "A high spped, hybrid In GaAs PIN/photoconductor circuit," *Appl. Phys. Lett.*, Vol. 49, 430-431.

Duguay, M. A., Shapiro, S. L. and Rentzepis, P. M., 1967, "Spontaneous appearance of picosecond pulses in ruby and Nd:glass lasers," *Phys. Rev. Lett.* Vol. 19, 1014-1016.

Duguay, M. A. and Hfansen, J. W., 1971, "Ultrahigh-speed photograph of picosecond light pulses", *IEEE J. Quantum. Electron.* Vol. 7, 37-39.

Duling III, I. N., Carruthers, T. F., 1990, "Antiresonant nonlinear mirror for passive mode locking of solid state lasers," Paper CFR4, Technical Digest of CLEO'90 (May 21-25, 1990, Anaheim, USA).

Eisenthal, K. B., 1977, "Picosecond relaxation processes in chemistry," *Ultrashort light Pulses, Topics in Applied Physics* Vol. 18, ed S. L. Shapiro, Berlin: Springer-Verlag (1977), 275-315.

Eisenthal, K. B., Hochstrasser, R. M., Kaiser, W. and Laubereau, A. (ed), 1982, *Picosecond Phenomena III, Springer Series in Chemical Physics* Vol. 23, Berlin: Springer-Verlag.

Fehrenbach, G., W., and Salour, M. M., 1982, "Polarition-induced compensation of picosecond pulse broadening in optical fibers," *Picosecond Phenomena III, Springer Series in Chemical Physics* Vol. 23, eds. K. B. Eisenthal, R. M. Hochstrasser, W. Kaiser and A. Laubereau, Berlin: Springer-Verlag (1982), 126-127.

Fermann, M. E., Hofer, M. Haberl, F., Schmidt, A. J. and Turi, L., 1991, "Additive-pulse-compression mode locking of a neodymium fiber laser," *Opt. Lett.*, Vol. 16, 244-246.

Finch, A., Liu, Y., Niu, H., Sibbett, W., Sleat, W. E., Walker, D. R., Yang, H. and Zhang, R., 1988, "Recent advances towards a 100 fs - resolution streak camera," *Ultrafast Phenomena VI: Springer Series in Chemical Physics* Vol. 48, Berlin: Springer-Verlag (1988), 159-161.

Finch, A., Chen, G., Sleat, W. and Sibbett, W., 1988, "Pulse asymmetry in the colliding pulse mode-locked laser," *J. Mod. Optics* Vol. 35, 345-354.

Finch, A., 1989, "Linear and nonlinear optical pulse characterisation" Ph.D. thesis, University of St.Andrews, U. K..

Finch, A., Zhu, X., Kean, P. N. and Sibbett, W., 1990, "Noise characterization of mode-locked color-center laser sources," *IEEE J. Quantum Electron.* Vol. 26, 1115-1123.

Fisher, R. A. and Kelley, P. L. and Gustafson, T. K., 1969, "Subpicosecond pulse generation using the optical Kerr effect," *Appl. Phys. Lett.* Vol. 14, 140-143.

Fisher, R. A. and Bischel, W. K., 1975, "Numerical studies of the interplay between self-phase modulation and dispersion for intense plane-wave laser pulses," *J. Appl. Phys.* Vol. 46, 4921-4934.

Fleck, J. A., 1970, "Ultrashort pulse generation by Q-switched lasers," *Phys. Rev. B*, Vol. 1, 84-100.

Fleming, J. W., 1978, "Material dispersion in lightguide glasses," *Electron. Lett.* Vol. 14, 326-328.

Fleming, G. R. and Siegman, A. E. (ed), 1986, *Ultrafast Phenomena V, Springer Series in Chemical Physics* Vol. 46, Berlin: Springer-Verlag.

Fleming, G. R. and Wolynes, P. G., 1990, "Chemical dynamics in solution," *Phys. Today*, Vol. 43, No. 5, 36-43.

Fork, R. L. and Beisser, F. A., 1978, "Real-time intensity autocorrelation interferometer," *Appl. Opt.* Vol. 17, 3534-3535.

Fork, R. L., Greene, B. I. and Shank, C. V., 1981, "Generation of optical pulses shorter than 0.1 psec by colliding pulse mode locking," *Appl. Phys. Lett.* Vol. 38, 671-672.

Fork, R. L., Shank, C. V., Yen, R., Hirlimann, C. A., 1983, "Femtosecond optical pulses," *IEEE J. Quantum Electron.* Vol. QE-19, 500-506.

Fork, R. L., Maratinez, O. E. and Gordon, J. P., 1984, "Negative dispersion using pairs of prisms," *Opt. Lett.* Vol. 9, 150-152.

Fork, R. L., 1986, "Optical frequency filter for ultrashort pulses," *Opt. Lett.* Vol. 11, 629-631.

Fork, R. L., Cruz, C. H. B., Becker, P. C. and Shank, C. V., 1987, "Compression of optical pulses to six femtoseconds by using cubic phase compensation," *Opt. Lett.* Vol. 12, 483-485.

Fox, A. G., Schwarz, S. E. and Smith, P. W., 1968, "Use of neon as a nonlinear absorber for mode locking a He-Ne laser," *Appl. Phys. Lett.*, Vol. 12, 371-373.

French, P. M. W. and Taylor, J. R., 1986, "Femtosecond pulse generation from passively mode locked continuous wave dye lasers 550-700 nm," *Ultrafast Phenomena V, Springer Series in Chemical Physics* Vol. 46, eds G. R. Fleming and A. R. Siegman, Berlin: Springer-Verlag (1986) 11-13.

French, P. M. W., Williams, J. A. R. and Taylor, J. R., 1989, "Femtosecond pulse generation from a titanium-doped sapphire laser using nonlinear external cavity feedback," *Opt. Lett.*, Vol. 14, 686-688.

Fritz, B. and Menke, E., 1965, "Laser effect in KCl with F_A(Li) centres," *Solid State Commun.* Vol. 3, 61-63.

Gaddy, O. L. and Schaefer, E. M., 1966, "Self locking of modes in the argon ion laser," *Appl. Phys. Lett.* Vol. 9, 281-282.

Garrett, C. G. B. and McCumber, D. E., 1970, "Propagation of a Gaussian light pulse through an anomalous dispersion medium," *Phys. Rev. A.* Vol. 1, 305-313.

Garth, S. J. and Pask, C., 1986, "Four-photon mixing and dispersion in single-mode fibers," *Opt. Lett.* Vol. 11, 380-382.

Gellermann, W., Luty, F. and Pollack, C. R., 1981, "Optical properties and stable, broadly tunable cw laser operation of new F_A-type centres in Tl^+-doped alkali halides," *Opt. Commun.* Vol. 39, 391-395.

Gellermann, W., Koch, K. P. and F. Luty, 1982, "Recent progress in color center lasers," Laser Focus, April, 1982, 71-75.

German, K. R., 1979, "Polarization beam splitters for pumping of F(II)-center lasers," *Opt. Lett.* Vol. 4, 68-69.

Gerrard, A. and Bruch, J. M., 1975, "Introduction to matrix methods in optics," Wiley, New York.

Giordmaine, J. A., Rentzepis, P. M., Shapiro, S. L., Wecht, K. W., 1967, "Two-photon excitation of fluorescence by picosecond light pulses," *Appl. Phys. Lett.* Vol. 11, 216-218.

Glenn, W. H., 1975, "The fluctuation model of a passively mode-locked laser," *IEEE J. Quantum. Electron* Vol. 11, 8-17.

Golovchenko, E. A., Dianov, E. M., Mamyshev, P. V. and Prokhorov, A. M., 1988, "Optical fibre-grating pulse compression," *Opt. and Quantum Electron.* Vol. 20, 343-355.

Gomes, A. S. L., Gouveia-Neto, A. S. and Taylor, J. R., 1985, "Direct measurement of chirped optical pulses with picosecond resolution," *Electron. Lett.* Vol. 22, 41-42.

Gomes, A. S. L., Sibbett, W. and Taylor, J. R., 1986, "Spectral and temporal study of picosecond-pulse propagation in a single-mode optical fibre," *Appl. Phys. B*, Vol. 39, 43-46.

Gomes, A. S. L., Gouveia-Neto, A. S. and Taylor, J. R., 1988, "Optical fibre-grating pulse compressors," *Opt. & Quantum Electron.* Vol. 20, 95-112.

Goodberlet, J., Wang, J., Fujimoto, J. G., Schulz, P. A. and Henion, S., 1989, "Mode-locked Ti:Al_2O_3 laser with a nonlinear coupled external cavity," *Paper FQ-4, Tech. Digest of CLEO'89* (April 24-28, 1989, Baltimore USA).

Goodberlet, J., Wang, J., Fujimoto, J. G., 1989, "Mode-locked Ti:Al_2O_3 laser with a nonlinear coupled external cavity," *Opt. Lett.*, Vol. 14, 1125-1127.

Goodberlet, J., Jacobson, J., Wang, J., Schulz, P. A., Fan, T. Y. and Fujimoto, J. G., 1990, "Ultrashort pulse generation with additive pulse modelocking in solid state lasers: Ti:Al_2O_3, diode pumped Nd:YAG and Nd:YLF," *Ultrafast Phenomena VII, Springer Series in Chemical Physics*, Vol. 53, ed. C. B. Harris, E. P. Ippen, G. A. Mourou, A. H. Zewail, Berlin: Springer-Verlag (1990), 11-13.

Goodberlet, J., Wang, J., Fujimoto, J. G. and Schulz, P. A., 1990, "Self-starting additive pulse mode-locking characterization with a Ti:Al_2O_3 laser," *Paper CFN1, Technical Digest of CLEO'90* (May 21-25, 1990, Anaheim, USA).

Goodberlet, J., Jacobson, J., Fujimoto, J. G., Schulz, P. A. and Fan, T. Y., 1990, "Self-starting additive pulse mode-locking of a diode pumped Nd:YAG laser," *Paper CFN5, Technical Digest of CLEO'90* (May 21-25, 1990, Anaheim, USA).

Goodwin, D. W. (ed), 1974, *Advances in Quantum Electronics*, Vol. 2, Willian Clowes and Sons, Limited.

Gordon, J. P. and Fork, R. L., 1984, "Optical resonator with negative dispersiono," *Opt. Lett.* Vol. 9, 153-155.

Gordon, J. P., 1986, "Theory of the soliton self-frequency shift," *Opt. Lett.* Vol. 11, 662-664.

Gouveia-Neto, A. S., Gomes, A. S. L. and Taylor, J. R., 1987, "High-order soliton pulse compression and splitting at 1.32 μm in a single-mode optical fiber," *IEEE J. Quantum Electron.* Vol. QE-23, 1193-1197.

Gowar, J., 1984, "Optical Communication Systems," *Prentice-Hall International Series in Optoelectronics*, ed. P. J. Dean (1984).

Grant, R. S., Kean, P. N., Burns, D. and Sibbett, W., 1990, "Enhanced mode locking of a color center laser using an InGaAsP semiconductor amplifier," *Paper CTUH38, Technical Digest of CLEO'90* (May 21-25, 1990, Anaheim, USA).

Grant, R. S., Kean, P. N., Burns, D. and Sibbett, W., 1991, "Passive coupled-cavity mode-locked color-center lasers," *Opt. Lett.* Vol. 16, 384-386.

Grigor'yants, V. V., Smirnov, V. I. and Chamorovshii, Yu. K., 1982, "Generation of wide-band optical continuum in fiber waveguides," *Sov. J. Quantum Electron.* Vol. 12, 841-847.

Grischkowsky, D. and Balant, A. C., 1982, "Optical pulse compression based on enhanced friquency chirping," *Appl. Phys. Lett.* Vol. 41, 1-3.

Grischkowsky, D. and Balant, A. C., 1982, "Optical pulse compression with reduced wings," *Ultrafast Phenomena VII, Springer Series in Chemical Physics*, Vol. 23, eds. K. B. Eisenthal, R. M. Hochstrasser, W. Kaiser and A. Laubereau, Berlin: Springer-Verlag (1982), 123-125.

Grischkowsky, D., Fork, R. L., Shank, C. V., Mourou, G. A., Diels, J.-C., 1985, LF/E-O Technology Symposium on "Frontiers of Femtosecond Research," *Laser Focus/Electro-Optics* Vol. 21, No. 4, 65-76.

Grudinin, A. B., Dianov, E. M., Korobkin, D. V., Prokhorov, A. M., Serkin, V. N. and Khaidarov, D. V., 1987, "Stimulated-Raman-scattering excitation of 18-fs pulses in the 1.6-μm region during pumping of a single-mode optical fiber by the beam from a Nd:YAG laser (λ=1.064 μm)," *JETP Lett.* Vol. 45, 260-263.

Gruebele, M. and Zewail, A. H., 1990, "Ultrafast reaction dynamics," *Phys. Today*, Vol. 43, No. 5, 24-33.

Hamaide, J. -P. and Emplit, P., 1989, "Spectrotemporal measurement of picosecond pulses propagating in nonlinear single-mode fibers," *Opt. Lett.* Vol. 14, 689-691.

Hargrove, L. E., Fork, R. L. and Pollack, M. A., 1964, "Locking of He-Ne laser modes by synchronous intracavity modulation," *Appl. Phys. Lett.* Vol. 5, 4-5.

Harris, S. E., 1966, "Stabilization and modulation of laser oscillators by internal time-varying perturbation," *Proc. IEEE* Vol. 54, 1401-1413.

Harris, C. B., Ippen, E. P. Mourou, G. A. and Zewail, A. H. (ed), 1990, *Ultrafast Phenomena VII, Springer Series in Chemical Physics* Vol. 53, Berlin: Springer-Verlag.

Hasegawa, A. and Tappert, F., 1973, "Transmission of stationary nonlinear optical pulses in dispersive dielictric fibers. 1. Anomalous dispersion," *Appl. Phys. Lett.* Vol. 23, 142-144.

Hasegawa, A. and Brinkman, W. F., 1980, "Tunable coherent IR and FIR sources utilizing modulational instability", *IEEE J. Quantum Electron.* Vol. QE-16, 694-697.

Hasegawa, A., 1983, "Amplification and reshaping of optical solitons in a glass fiber IV: Use of the stimulated Raman process," *Opt. Lett.* Vol. 8, 650-652.

Haus, H. A., 1975, "Theory of mode locking with a slow saturable absorber," *IEEE J. Quantum. Electron.* Vol. 11, 736-746.

Haus, H. A. and Islam, M. N., 1985, "Theory of the soliton laser," *IEEE J. Quantum Electron.*, Vol. QE-21,1172-1188.

Haus, H. A. and Nakazawa, M., 1987, "Theory of the fiber Raman soliton laser," *J. Opt. Soc. Am. B*, Vol. 4, 652-660.

Hercher, M., 1967, "An analysis of saturable absorbers," *Appl. Opt.* Vol. 6, 947-954.

Heritage, J. P., Weiner, A. M. and Thurston, R. N., 1985, "Picosecond pulse shaping by spectral phase and amplitude manipulation," *Opt. Lett.* Vol. 10, 609-611.

Heritage, J. P., Weiner, A. M. and Thurston, R. N., 1986, "Fourier transform picosecond pulse shaping and spectral phase measurement in a grating pulse-compressor," *Ultrafast Phenomena V, Springer Series in Chemical Physics* Vol. 46, eds. G. R. Fleming and A. R. Siegman, Berlin: Springer-Verlag (1986), 34-37.

Herrmann, J. and Wilhelmi, B., 1987, "Lasers for ultrashort light pulses," Berlin: Akademie-Verlag (1987); (Distributed feedback dye laser: 88-90; Passive mode locking of dye lasers: 159-190; Passive mode locking of solid state lasers: 191-224).

Hochstrasser, R. M., Kaiser, W. and Shank, C. V. (ed), 1980, *Picosecond Phenomena II, Springer Series in Chemical Physics* Vol. 14, Berlin: Springer-Verlag.

Hodgkinson, I. J. and Vukusic, J. I., 1978, "Birefrigent filters for tuning flashlamp - pumped dye lasers: simplified theory and design," *Appl. Opt.* Vol. 17, 1944-1948.

Holtom, G. and Teschke, O., 1974, "Design of a birefringent filter for high power dye lasers", *IEEE J. Quantum Electron.* Vol. QE-10, 577-579.

Hutchinson, M. H. R., 1989, "Terawatt laser," *Contem. Phys.* Vol. 30, 355-365.

Huxley, J. M. , Liu, L. Y., Ippen, E. P. and Haus, H. A., 1990, "Self-starting additive pulse mode-locking of 1.06- and 1.32 μm Nd:YAG lasers," *Paper CFN3, Technical Digest of CLEO'90* (May 21-25, 1990, Anaheim, USA).

If, F., Christiansen, P. L., Elgin, J. N., Gibbon, J. D. and Skovgaard, O., 1986, "A theoretical and computational study of the soliton laser," *Opt. Commun.*, Vol. 57, 350-354.

Ippen, E. P. and Shank, C. V. and Dienes, A., 1972, "Passive mode locking os the cw dye laser," *Appl. Phys. Lett.*, Vol. 21, 348-350.

Ippen, E. P. and Shank, C. V., 1977, "Techniques for measurement," *Ultrashort light Pulses, Topics in Applied Physics* Vol. 18, ed S. L. Shapiro, Berlin: Springer-Verlag (1977), 82-122.

Ippen, E. P., Haus, H. A., and Liu, L. Y., 1989, "Additive pulse mode locking," *J. Opt. Soc. Am. B* , Vol. 6, 1736-1745.

Islam, M. N., Mollenauer, L. F. and Stolen, R. H., 1986, "Fiber Raman amplification soliton laser (FRASL)," *Ultrafast Phenomena V, Springer Series in Chemical Physics* Vol. 46, eds. G. R. Fleming and A. R. Siegman, Berlin: Springer-Verlag (1986),

Islam, M. N., Sucha, G., Bar-Joseph, I., Wegener, M., Gordon, J. P. and Chemla, D. S., 1989, "Broad bandwidths from frequency-shifting solitons in fibers," *Opt. Lett.* Vol. 14, 370-372.

Jackson, J. D., 1975, "classical electrodynamics," 2nd Ed. New York: John Wiley & Sons, Inc., 353-356.

Javan, A., 1967, "The optical properties of materials," *Laser and Light, Reading from Scientific America*, W. H. Freeman and Company, Sanfrancisco, 27-33.

Johnson, A. M., Stolen, R. H. and Simpson, W. M., 1986, "The observation of chirped stimulated Raman scattered light in fibers," *Ultrafast Phenomena V, Springer Series in Chemical Physics* Vol. 46, eds. G. R. Fleming and A. R. Siegman, Berlin: Springer-Verlag (1986), 161-163.

Johnson, A. M., Stolen, R. H. and Simpson, W. M., 1984, "Generation of 0.41-Picosecond pulses by the single-stage compression of frequency doubled Nd: YAG laser pulses," *Ultrafast Phenomena IV, Springer Series in Chemical Physics* Vol. 38, eds. D. H. Auston and K. B. Eisenthal, Berlin: Springer-Verlag (1984), 16-18.

Johnston, C. I., Spence, D. E., Grant, R. S. and Sibbett, W., 1989, "Femtosecond pulse generation in the 900-950 nm region from a pasively modelocked LiF:F_2^+ colour centre laser," *Opt. Commun.* Vol. 73, 370-374.

Jones, J., 1974, "On the propagation of a pulse through a dispersive medium," *Am. J. Phys.* Vol. 42, 43-46.

Jones, W. B. Jr., 1988, "Introduction to optical fiber communication system," New York: Holt, Rinehart and Winston, Inc., 11-19.

Kachanov, A. A., 1982, "Birefringent selector of the emission wavelength for a cw dye laser", *Sov. J. Quantum Electron.* Vol. 12, 927-929.

Kafka, J. D., Kolner, B. H., Baer, T., Bloom, D. M., 1984, "Compression of pulses from a continuous-wave mode-locked Nd:YAG laser," *Opt. Lett.* Vol. 9, 505-506.

Kafka, J. D. and Baer, T. M., 1987, "Peak power fluctuations in optical pulse compression," *IEEE J. Quantum Electron.* Vol.24, 341-350.

Kean, P. N., Smith, K. and Sibbett, W., 1987, "Spectral and temporal investigation of self-phase modulation and stimulated Raman scattering in a single-mode optical fibre," *IEE Proc.* Vol.134, 163-170.

Kean, P. N., Smith, K., Sinclair, B. D. and Sibbett, W., 1987, "Characterisation of a fibre raman oscillator using fibre grating reflectors," *Electron. Lett.* Vol. 23, 1241-1242.

Kean, P. N., Grant, R. S., Zhu, X., Crust, D. W., Burns, D. and Sibbett, W., 1988, "Enhanced mode locking of colour-centre lasers by coupled-cavity feedback control," *Paper PD7, Technical Digest of CLEO'88* (May 21-25, 1988, Anaheim, USA).

Kean, P. N., 1989, "Generation and nonlinear propagation of ultrashort near infrared laser pulses," Ph. D thesis, University of St. Andrews, U. K..

Kean, P. N., Zhu, X., Crust, D. W., Grant, R. S., Langford, N. and Sibbett, W., 1989, "Enhanced mode-locking of color center lasers," *Opt. Lett.*, Vol. 14, pp. 39-41, 1989.

Keller, U., Knox, W. H. and Roskos, H., 1990, "Coupled-cavity resonant passive modelocked (RPM) Ti:Sapphire laser," *Ultrafast Phenomena VII, Springer Series in Chemical Physics*, Vol. 53, ed. C. B. Harris, E. P. Ippen, G. A. Mourou, A. H. Zewail, Berlin: Springer-Verlag (1990), 69-71.

Knox, W. H., Fork, R. L., Downer, M. C., Stolen, R. H. and Shank, C. V. and Valdmanis, J. A., 1985, "Optical pulse compression to 8fs at a 5-kHz repetition rate," *Appl. Phys. Lett.* Vol. 46, 1120-1121.

Kobayashi, S., Shibata, S., Shibata N. and Izawa, T., 1977, "Refractive-index dispersion of doped fused silica," IOOC'77 B8-3.

Kobayashi, T., Guo, F. C., Morimoto, A., Sueta, T. and Cho, Y., 1984, "Novel method of waveform evaluation of ultrashort optical pulses," *Picosecond Phenomena, Springer Series in Chemical Physics* Vol. 38, eds. D. H. Auston and K. B. Eisenthal, Berlin: Springer-Verlag (1984), 93-95.

Kobayashi, T., Morimoto, A., Fujita, T., Amano, K., Uemura, T. and Sueta, T., 1986, "Direct generation of picosecond to subpicosecond optical pulses using electrooptic modulation methods,"*Ultrafast Phenomena V, Springer Series in Chemical Physics* Vol. 46, eds. G. R. Fleming and A. E. Siegman, Berlin: Springer-Verlag (1986), 134-135.

Kobayashi, T., Yao, H., Amano, K., Fukushima, Y., Morimoto, A. and Sueta, T., 1988, "Optical pulse compression using high-frequency electrooptic phase modulation," *IEEE J. Quantum Electron.* Vol. 24, 382-387.

Kobayashi, T., Morimoto, A., Lee, B. Y. and Sueta, T., 1990, "A new method of ultrashort pulse generation - modified Fabry-Perot electrooptic modulator," *Ultrafast Phenomena VII, Springer Series in Chemical Physics*, Vol. 53, eds. C. B. Harris, E. P. Ippen, G. A. Mourou, A. H. Zewail, Berlin: Springer-Verlag (1990), 41-44.

Kong, M. N., Chee, J. K. and Liu, J. M., 1991, "Passive mode locking with a nonlinear external coupled cavity at high pulse repetition rates," *Opt. Lett.* Vol. 16, 73-75.

Krause, W., Sleat, W. E. and Sibbett, W., 1984, "Circular-scan photochron streak camera for spaceborne laser ranging applications," *Proc. ESA Workshop on Space Laser Applications and Technology* (Les Diablerets, Switzerlland, 26-30 March 1984), ESA SP-202, (1984), 171-175.

Krausz, F., Spielmann, Ch., Brabec, T., Wintner, E. and Schmidt, A. J., 1990, "Subpicosecond pulse generation from a Nd:glass laser using a nonlinear external cavity," *Opt. Lett.* Vol. 15, 737-739 .

Krausz, F. and Spielmann, Ch., 1991, "Self-starting passive mode locking," *Opt. Lett.*, Vol. 16, 235-237.

Kuckartz, M., Schulz, R. and Harde, H., 1987, "Theoretical and experimental studies of combined self-phase modulation and stimulated Raman-scattering in single-mode fibres," *Opt & Quantum electron.* Vol. 19, 237-246.

Kuckartz, M., Schulz, R. and Harde, H., 1988, "Operation of a fiber-grating compressor in the Raman regime," *J. Opt. Soc. Am. B*, Vol. 5, 1353-1359.

Kuhlke, D., Rudoph, W. and Wilhelmi, B., 1983, "Calculation of the colliding pulse mode locking in cw dye ring lasers," *IEEE J. Quantum Electron.* Vol. 19, 526-533.

Kuizenga, D. and Siegman, A. E., 1970, "FM and AM mode locking of the homogeneous laser -part I: theory," *IEEE J. Quantum Electron.* Vol. 11, 694-708. "FM and AM mode locking of the homogeneous laser -part II: experimental results in a Nd:YAG laser with inernal FM modulation," *IEEE J. Quantum Electron.* Vol. 11, 709-715.

Lamb, W. E., Jr., 1964, "Theory of an optical laser," *Phys. Rev. Series II*, Vol. 134, 1429-1450.

Letokhov, V. S., 1969, "Generation of ultrashort light pulses in lasers with a nonlinear absorber," *Sov. Phys. JETP* Vol. 28, 562-568.

Lin, C. and Nguyen, V. T. and French, W. G., 1978, "Wideband near-I.R. continuum (0.7-2.1 μm) generated in low-loss optical fibres," *Electron.* **Lin**, C., Kogelnik, H. and Cohen, L. G., 1980, "Optical-pulse equalization of low-dispersion transmission in single-mode fibers in the 1.3-1.7 μm spectral region," *Opt. Lett.* Vol. 5, 476-478.

Lin, C., Reed, W. A., Pearson, A. D. and Shang, H.-T., 1981, "Phase matching in the minimum-chromatic-dipersion region of single-mode fibers for stimulated four-photon mixing," *Opt. Lett.* Vol. 6, 493-494.

Lin, C. and Glodis, P. F., 1982, "Tunable fibre Raman oscillator in the 1.32-1.41 μm spectral region using a low-loss, low OH^- single-mode fibre," *Electron. Lett.* Vol. 18, 696-697.

Lin, C., 1986, "Nonlinear optics in fibers for fiber measurements and special device functions," *J. Lightwave Technology*, Vol. LT-4, 1103-1115.

Linde, D. von der, 1973, "Mode-locked lasers and ultrashort light pulses," *Appl. Phys.* Vol. 2, 281-296.

Liu, J. M. and Chee, J. K., 1990, "Passive mode locking of a cw Nd:YLF laser with a nonlinear external coupled cavity," *Opt. Lett.*, Vol. 15, 685-687.

Liu, L. Y., Mark, J., Haus, H. A. and Ippen, E. P., 1989, "Additive pulse mode locking: a mechanism for femtosecond pulse generation with coupled nonlinear resonators," *Paper FQ-2, Technical Digest of CLEO'89* (April 24-28, 1989, Baltimore USA).

Maier, M., Kaiser, W. and Giordmaine, J. A., 1966, "Intensity light bursts in the stimulated Raman effect," *Phys. Rev. Lett.* Vol. 17, 1275-1277.

Maiman, T. H., 1960, "Stimulated optical radiation in ruby," *Nature*, Vol. 187, 493-494.

Maimistov, A. I. and Manykin, E. A., 1983, "Propagation of ultrashort optical pulses in resonant nonlinear light guides," *Sov. Phys. JETP.* Vol. 58, 685-687.

Manassah, J. T., Mustafa, M. A., Alfano, R. R. and Ho, P. P., 1986, "Spectral extent and pulse shape of the supercontinuum for ultrashort laser pulse," *IEEE. J. Quantum Electron.* Vol. QE-22, 197-204.

Marcuse, D., 1980, "Pulse distortion in single-mode fibers," *Appl. Opt.* Vol. 19, 1653-1660.

Marcuse, D. and Lin, C., 1981, "Low dispersion single-mode fiber transmission-the question of practical versus theoreticas maxemum transmission bandwidth," *IEEE J. Quantum. Electron.* Vol. QE-17, 869-877.

Mark, J., Liu, Y. L., Hall, K. L., Haus, H. A. and Ippen, E. P., 1989, "Femtosecond pulse generation in a laser with a nonlinear external resonator," *Opt. Lett.*, Vol. 14, 48-50.

Martinez, O. E. and Chilla, J. L. A., 1990, "Direct measurement of femtosecond pulses in amplitude and phase," *Paper CTUA2, Technical Digest of CLEO'90* (May 21-25, 1990, Anaheim, USA).

McDonald, D. B., Rossel, J. L. and Fleming, G. R., 1981, "Temporal and spectral studies of a synchronously pumped dye laser: detailed interpretation of autocorrelation measurements," *IEEE J. Quantum. Electron.* Vol. 17, 1134-1138.

Menyuk, C. R., 1987, "Nonlinear pulse propagation in birefringent optical fibers," *IEEE J. Quantum Electron.* Vol. QE-23, 174-176.

Miller, A. and Sibbett, W., 1988, "A perspective on ultrafast phenomena," *J. Mod. Opt.*, Vol. 35, 1871-1890.

Mindl, T., Hefferle, P., Schneider, S. and Dorr, F., 1983, "Characterisation of a train of subpicosecond laser pulses by fringe resolved autocorrelation measurements," *Appl. Phys. B.* Vol. 31, 201-207.

Mitschke F. M. and Mollenauer, L. F., 1986, "Discovery of the soliton self-frequency shift," *Opt. Lett.* Vol. 11, 659-661.

Mitschke, F. M. and Mollenauer, L. F., 1986, "Stabilizing the soliton laser," *IEEE J. Quantum. Electron.*, Vol. QE-22, 2242-2250.

Mitschke, F. M. and Mollenauer, L. F., 1987, "Ultrashort pulses from the soliton laser," *Opt. Lett.*, Vol. 12, 407-409.

Miyazoe, Y. and Maeda, M., 1971, "On the spiking phenomenon in organic dye lasers," *IEEE J. Quantum Electron.* Vol. 7, 36-37.

Mocker, H. W. and Collins, R. J., 1965, "Mode competition and self-lockiing effects in a Q-switched ruby laser," *Appl. Phys. Lett.* Vol. 7, 270-273.

Mollenauer, L. F. and Stolen, R. H., 1982, "Solitons in optical fibers," *Fiberoptic Technology*, Vol. 4, 193-198.

Mollenauer, L. F., Vieira, N. D. and Szeto, L., 1982, "Mode locking by synchronous pumping using a gain medium with microsecond decay times," *Opt. Lett.* Vol. 7, 414-416.

Mollenauer, L. F., Stolen, R. H., Gordon, J. P., and Tomlinson, W. J., 1983, "Extreme picosecond pulse narrowing by means of soliton effect in optical fibers," *Opt. Lett.* Vol. 8, 289-291.

Mollenauer, L. F., Vieira, N. D. and Szeto, L., 1983, "Optical properties of the $Tl^0(1)$ center in KCl," *Phys. Rev. B*, Vol. 27, 5332-5346.

Mollenauer, L. F. and Stolen, R. H., 1984, "The soliton laser," *Opt. Lett.* Vol. 9, 13-15.

Mollenauer, L. F. and Stolen, R. H., 1984, "The soliton laser," *Ultrafast Phenomena IV, Springer Series in Chemical Physics*, Vol. 38, eds. D. H. Auston and K. B. Eisenthal, Berlin: Spinger-Verlag (1984), 2-6 .

Mollenauer, L. F., 1985, "Colour centre laser," *Laser Handbook*, Vol.5, ed. by M. I. Stitch and E. M. Bass, North-Holland, Amsterdam: Elsevier Science Publisher, 143-228.

Mollenauer, L. F., 1985, "Solitons in optical fibers and the soliton laser," *Phil. Trans. Roy. Soc. Lond.*, Vol. A315, 437-450.

Mollenauer, L. F., Stolen, R. H. and Islam, M. N., 1985, "Experimental demonstration of soliton propagation in long fibers: loss compensated by Raman gain," *Opt. Lett.* Vol. 10, 229-231.

Mollenauer, L. F., Gordon, J. P. and Islam, M. N., 1986, "Soliton propagation in long fibers with periodically compensated loss," *IEEE J. Quantum Electron.* Vol. QE-22, 157-173.

Mollenauer, L. F., 1987, "Color center lasers," *Tunable lasers: Topics in Applied Physics*, Vol. 59, eds. L. F. Mollenauer and J. C. White, Springer-Verlag: Berlin, 225-277.

Morin, M. and Piché, M., 1989, "Interferential mode locking: Gaussian analysis", *Opt. Lett.*, Vol. 14, 1119-1121.

Morin, M., Champagne, Y., Martin, F., Vallee, R., McCarthy, N. and Piché, M., 1990, "Physical properties of coupled cavity lasers used for ultrashort pulse generation," *Ultrafast Phenomena VII, Springer Series in Chemical Physics*, Vol. 53, ed. C. B. Harris, E. P. Ippen, G. A. Mourou, A. H. Zewail, Berlin: Springer-Verlag (1990), 54-56.

Morin, M. and Piché, M., 1990, "Dynamics of mode-locked lasers coupled to a nonlinear cavity," *Paper CTUH27, Technical Digest of CLEO'90* (May 21-25, 1990, Anaheim, USA).

Mourou, G. A., 1990, "Modulators and Q-switches serve varity of laser applications," *Laser Focus World*, Vol. 26, No. 4, 109-112.

Nakatsuka, H., Grischkowsky, D., and Balant, A. C., 1981, "Nonlinear picosecond-pulse propagation through optical fibers with positive group velocity dispersion," *Phys. Rev. Lett.* Vol. 47, 910-913.

Nakazawa, M., "Propagation and amplification of ultrashort optical soliton pulses in Erbium-doped fibers for very high speed communication," *Picosecond Phenomena VII, Springer Series in Chemical Physics* Vol. 53, eds. C. B. Harris, E. P. Ippen, G. A. Mourou and A. H. Zewail, Berlin: Springer-Verlag (1990), 179-183.

Nelson, B. P., Cotter, D., Blow, K. J. and Doran, N. J., 1983, "Large nonlinear pulse broadening in long lengths of monomode fiber," *Opt. Commun.* Vol. 48, 292-294.

New, G. H. C., 1974, "Pulse evolution in mode-locked quasi-continuous lasers," *IEEE J. Quantum. Electron.* Vol. 10, 115-124.

New, G. H. C., 1983, "The generation of ultrashort laser pulses," *Rep. Prog. Phys.* Vol. 46, 877-971.

New, G. H. C., 1990, "Femtofascination," *Physics World*, Vol. 3, No. 7, 33-37.

Niu, H., Degtyareva, V. P., Platonov, V. N., Prokhorov, A. M. and Schelev, M. Y., 1988, "Specially designed femtosecond streak image tube with temporal resolution of 50 fs," *18th ICHSPP*, Xian (1988), SPIE Vol. 1032, 79-86.

Nuckolls, J., Wood, L., Thiessen, A., Zimmerman, G., 1972, "Laser compresion of matter to super-high densities: thermonuclear (CTR) applications," Nature, Vol. 239, 139-142.

Okada, T., Nishikawa, S., Kanaji, K. and Mataga, N., 1990, "Dynamics of intramolecular electron transfer in polar solvents," *Picosecond Phenomena VII, Springer Series in Chemical Physics* Vol. 53, eds. C. B. Harris, E. P. Ippen, G. A. Mourou and A. H. Zewail, Berlin: Springer-Verlag (1990), 397-401.

Ou, Z. Y., Gage, E. C., Magill, B. E. and Mandel, L., 1989, "Fourth-order interference technique for determining the coherence time of a light beam," *J. Opt. Soc. Am. B.* Vol. 6, 100-103.

Oullette, F. and Piché, M., 1988, "Passive mode locking with a nonlinear Michelson interferometer: transient and steady-state characteristics", *Can. J. Phys.*, Vol. 66, 903-913.

Parker, D., 1990, "Optical detectors: research to reality," *Physics World*, Vol. 3, No. 3, 52-54.

Penzkofer, A. and Kaiser, W., 1977, "Generation of picosecond light continua by parametric four-photon interactions in liquids and solids," *Opt. and Quantum Electron.* Vol. 9, 315-349.

Piche, M. and Quellette, F., 1986, "Compression of mode-locked pulses using nonlinear Fabry-Perot interferometers," *Opt. Lett.* Vol. 11, 15-17.

Pike, H. A. and Hercher, M., 1970, " Basis for picosecond structure in mode-locked laser pulses," *J. Appl. Phys.* Vol. 41, 4562-4565.

Pinto, J. F., Yakymyshyn, C. P. and Pollock, C. R., 1988, "Acousto-optic mode-locked soliton laser," *Opt. Lett.*, Vol. 13, 383-385.

Pollock, C. R., Pinto, J. F. and Georgion, E., 1989, "Recent progress in color center lasers," *Appl. Phys. B*, Vol. 48, 287-292.

Preuss, D. R. and Gole, J. L., 1980, "Three - stage birefringent filter tuning smoothly over the visible region: the theoretical treatment and experimental design," *Appl Opt.* Vol.19, 702-710.

Rand, S. C. and DeShazer, L. G., 1985, "Visible color-center laser in diamond," *Opt. Lett.*, Vol. 10, 481-483.

Reekie, L., Ruddock, I. S. and Illingworth, R., 1983, "The synchronously mode-locked F_A(II) KCl:Li colour centre laser," *Picosecond Chemistry and Biology*, eds. T. A. M. Doust and M. A. West, Science Reviews Limited (1983), 188-196.

Reynaud, F., Salin, F. and Barthelemy, A., 1989, "Measurement of phase shifts introduced by nonlinear optical phenomena on subpicosecond pulses," *Opt. Lett.* Vol. 14, 275-277.

Robbin, R. J., Millar, D. P. and Zewail, A. H., 1980, "Picosecond torsional dynamics of DNA," *Picosecond Phenomena II, Springer Series in Chemical Physics* Vol. 14, ed R. M. Hochstrasser, W. Kaiser and C. V. Shank, Berlin: Springer-Verlag (1980), 331-335.

Robertson, N. A., Hoggan, S., Mangan, J. B. and Hough, J., 1986, "Intensity stabilisation of an argon laser using an electro-optic modulator - performance and limitataions," *Appl. Phys. B* Vol. 39, 149-153.

Rothenberg, J. E. and Grischkowsky, D., 1985, "Measurement of the phase of a frequency-swept ultrashort optical pulse," *J. Opt. Soc. Am. B.* Vol. 2, 626-633.

Rothenberg, J. E., 1986, "Measurement of optical phase with subpicosecond resolution by time domain interferometry," *Picosecond Phenomena, Springer Series in Chemical Physics* Vol. 46, eds. G. R. Fleming and A. E. Siegman, Berlin: Springer-Verlag (1986), 78-81.

Rush, D. W., Ho, P. -T., 1984, "The coherence time of a mode-locked pulse train," *Opt. Commun.* Vol. 52, 41-45.

Sala, K. L., Kenney-wallace, G. A. and Hall, G. E., 1980, "CW autocorrelation measurements of picosecond laser pulses, " *IEEE J Quantum Electron.* Vol. 16, 990-996.

Saleh, B., 1978, "Photoelectron statistics," *Springer Series in Optical Science*, Vol. 6, Berlin: Springer-Verlag.

Sammut, R. A. and Garth, S. J., 1989, "Multiple-frequency generation on single-mode optical fibers," *J. Opt. Soc. Am. B*. Vol. 6, 1732-1735.

Sargent, M., Scully, M. O. and Lamb, W. E., 1974, "Laser Physics," New York: Addison-Wesley.

Satsuma, J. and Yajima, N., 1974, "Initial value problems of one-dimensional self-modulation of nonlinear waves in dispersive media," *Supplement of the Progress of Theoretical Physics*, No. 55, 284-306.

Schadt, D., Jaskorzynska, B. and Osterberg, U., 1986, "Numerical study on combined stimulated Raman scattering and self-phase modulation in optical fibers influenced by walk-off between pump and Stokes pulses," *J. Opt. Soc. Am. B*, Vol.3, 1257-1262.

Schadt, D. and Jaskorzynska, B., 1987, "Frequency chirp and spectra due to self-phase modulation and stimulated Raman scattering influenced by pulse walk-of in optical fibers," *J. Opt. Soc. Am. B*, Vol.4, 856-862.

Schneider, I. and Moss, S. C., 1983, "Color-center laser continuously tunable from 1.67 to 2.46 μm," *Opt. Lett.* Vol. 8, 7-8.

Shank, C. V., Ippen, E. P. and Shapiro, S. L. (ed), 1978, *Picosecond Phenomena, Springer Series in Chemical Physics* Vol. 4, Berlin: Springer-Verlag.

Shank, C. V., Fork, R. L., Leheny, R. F. and Shah, J., 1979, "Dynamics of photoexcited GaAs band-edge absorption with subpicosecond resolution," *Phys. Rev. Lett.* Vol. 42, 112-115.

Shank, C. V., Fork, R. L., Yen, R., Stolen, R. H. and Tomlinson, W. J., 1982, "Compression of femtosecond optical pulses," *Appl. Phys. Lett.* Vol. 40, 761-763.

Shank, C. V., Fork, R. L. and Yen, R. T., 1982, "Moving from the picosecond to the femtosecond time regine," *Picosecond Phenomena III, Springer Series in Chemical Physics* Vol. 23, eds. K. B. Eisenthal, R. M. Hochstrasser, W. Kaiser and A. Laubereau, Berlin: Springer-Verlag (1982), 2-5.

Shank, C. V., 1983, "Measurement of ultrafast phenomena in the femtosecond time domain," *Science*, Vol. 219, 1027-1031.

Shank, C. V., 1987, "Investigations in the world of ultrafast events with femtosecond optical pulses," *Journal de Physique*, Tome 48, Colloque C7, 13-16 (France).

Shapiro, S. L. (ed), 1977, *Ultrashort Light Pulses, Topics in Applied Physics* Vol. 18, Berlin: Springer-Verlag.

Sibbett, W., 1982, "Synchroscan streak camera systems," *SPIE* Vol. 348, High speed photography (San Diego 1982) 15-26.

Sibbett, W., Sleat, W. E. and Taylor, J. R., 1983, "Application of synchronously scanning streak cameras to picosecond time resolved luminescence measurements," *Picosecond Chemistry and Biology*, ed T. A. M. Doust and M. A. West, Science Reviews Limited (1983), 197-226.

Sibbett, W., 1987, "The new science of 'Photonics' - photons where electrons used to be," British Association for the Advancement of Science, Annual Meeting, No. A1, Belfast.

Sibbett, W., 1991, "Ultrashort pulses for nonlinear optical techniques," *Non-linear Optics in Signal Processing*, eds. R. W. Eason and A. Miller, to be published by Chapman & Hall, London (1991).

Sibbett, W., 1989, "Exploitation of optical nonlinearities for enhanced mode locking in coupled cavity lasers," *Paper FQ-1, Tech. Digest of CLEO'89* (April 24-28, 1989, Baltimore USA).

Sibbett, W., "Hybrid and passive mode locking in coupled-cavity lasers," *Ultrafast Phenomena VII, Springer Series in Chemical Physics*, Vol. 53, eds. C. B. Harris, E. P. Ippen, G. A. Mourou, A. H. Zewail, Berlin: Springer-Verlag (1990), 2-7.

Siegman, A. E. and Kuizenga, D. J., 1974, "Active mode-coupling phenomena in pulsed and continuous lasers," *Opto-electronics*, Vol. 6, 43-66.

Siegman, A. E., 1986, "Lasers" University Science Books, Mill Valley, California.

Siegman, A. E., 1987, "The laser: still young at 25?," *Lasers-Invention to Application*, eds. J. H. Ausubel and H. D. Langford, National Academy Press, Washington, D. C. (1987), 1-16.

Silberberg, Y., Smith, P. W., Eilenberger, D. J., Miller, D. A. B., Gossard, A. C. and Wiegmann, W., 1984, "Passive mode locking of a semiconductor diode laser," *Opt. Lett.* Vol. 9, 507-509.

Silvestri, S. D., Laporta, P. and Svelto, O., 1984, "The role of cavity dispersion in CW mode-locked lasers," *IEEE J. Quantum Electron.* Vol. QE-20, 533-539.

Statz, H. and Tang, C. L., 1965, "Phase locking of modes in lasers," *J. Appl. Phys.* Vol. 36, 3923-3927.

Smith, R. G., 1972, "Optical power handling capacity of low loss optical fibers as determined by stimulated Raman and brillouin scattering," *Appl. Opt.* Vol. 11, 2489-2494.

Smith, P. W., 1968, "Simultaneous phase-locking of longitudinal and transverse laser modes," *Appl. Phys. Lett.* Vol. 13, 235-237.

Smith, P. W., 1972, "Mode selection in lasers," *Proc. IEEE.* Vol. 60, 422-440.

Smith, P. W., Duguay, M. A. and Ippen, E. P., 1974, "Mode-locking of lasers," *Progress in Quantum Electronics*, Vol. 3, Part 2, eds. J. H. Sanders and S. Stenholm, Oxford: Pergamon Press (1974), 107-229.

Smith, K., Sibbett, W. and Langford, N., 1985, "Streak camera study of ultrashort pulse propagation in aweakly multimode opticass fibre," *Electron. Lett.* Vol. 21, 1068-1069.

Soffer, B. H. and Linn, J. W., 1968, "Continuously tunable picosecond-pulse organic-dye laser," *J. Appl. Phys.* Vol. 39, 5859-5860.

Spence, D. E., Kean, P. N. and Sibbett, W., 1991, "60-fsec pulse generation from a self-mode-locked Ti:sapphire laser," *Opt. Lett.*, Vol. 16, 42-44.

Spielmann, Ch., Krausz, F., Wintner, E. and Schmidt, A. J., 1990, "Self-starting additive pulse mode-locking of a Nd:glass laser," *Ultrafast Phenomena VII, Springer Series in Chemical Physics*, Vol. 53, eds. C. B. Harris, E. P. Ippen, G. A. Mourou, A. H. Zewail, Berlin: Springer-Verlag (1990), 72-74.

Stolen, R. H. and Ippen, E. P., 1973, "Raman gain in glass optical waveguides," *Appl. Phys. Lett.* Vol. 22, 276-278.

Stolen, R. H., Bjorkholm, J. E. and Ashkin, A., 1974, "Phase-matched three-wave mixing in silica fiber optical waveguides," *App, Phys. Lett.* Vol. 24, 308-310.

Stolen, R. H. and Lin, C. L., 1978, "Self-phase-modulation in silica optical fibers," *Phys Rev. A* , Vol. 17, 1448-1453.

Stolen, R. H., 1979, "Nonlinear properties of optical fibers," *Optical Fibre Telecommunications*, eds. E. M. Stewart and A. G. Chynoweth, New York: Academic (1979), 125-150.

Stolen, R. H., 1980, "Nonlinearity in fiber transmission," *Proc. IEEE*, Vol. 68, 1232-1236.

Stolen, R. H. and Bjorkholm, J. E., 1982, "Parametric amplification and Frequency conversion in optical fibers," *IEEE J. Quantum Electron.* Vol. QE-18, 1062-1072.

Stolen, R. H. Lee, C. and Jain, R. K., 1984, "Development of the stimulated Raman spectrum in single-mode silica fibers," *J. Opt. Soc. Am. B*, Vol. 1, 652-657.

Stolen, R. H., Shank, C. V. and Tomilinson, W. J., 1984, "Procedure for calculating optical pulse compression from fiber-grating combination," *Picosecond Phenomena IV, Springer Series in Chemical Physics* Vol. 38, eds. D. H. Auston and K. B. Eisenthal, Berlin: Springer-Verlag (1984),46-48.

Suzuki, K., Nakazawa, M. and Haus, Hermann. A., 1989, "Parametric solitonlaser," *Opt. Lett.* Vol. 14, 320-322.

Svelto, O., 1982, "Principles of lasers," 2nd Ed. Plenum Press, 128-132.

Tajima, K. and Washio, K., 1985, "Generalized view of Gaussian pulse-transmission characteristics in single-mode optical fibers," *Opt. Lett.* Vol. 10, 460-462.

Tai, K., Hasegawa, A. and Tomita, A., 1986, "Observation of Modulational Instability in optical fibers," *Phys. Rev. Lett.* Vol. 56, 135-138.

Tai, K. and Tomita, A., 1986, "1100X optical fiber pulse compression using grating pair and soliton effect at 1.319 μm," *Appl. Phys. Lett.* Vol. 48, 1033-1035.

Tai, K., Hasegawa, A. and Bekki, N., 1988, "Fission of optical solitons induced by stimulated Raman effect," *Opt. Lett.* Vol. 13, 392-394.

Takahashi, H., Chang, J., Nakamura, K., Sugimoto, I., Takabayashi, T. and Oyobe, A. and Fujii, Y., 1986, "Efficient single-pass Raman generation in a GeO_2 optical fiber and its application to measurement of chromatic dispersion," *Opt. Lett.* Vol. 11, 383-385.

Tan, W. S., 1987, "Optical soliton propagation in an idealmonomode fiber," *Chin. J. Lasers.* Vol. 14, 625-627.

Thomas, S. W., Griffith, R. L. and McDonald, W. R., 1984, "Improvements in avalanche-transistor sweep circuitry for electrooptic streak cameras," *SPIE* Vol. 491, High Speed Photography (Strasbourg, 1984) 101-107.

Tomlinson, W. J, 1989, "Curious features of nonlinear pulse propagation in single-mode optical fibers," *Optics News*, No. 1, 7-11.

Tomlinson, W. J., Hawkins, R. J., Weiner, A. M., Heritage, J. P. and Thurston, R. N., 1989, "Dark optical solitons with finite-width background pulses," *J. Opt. Soc. Am. B*, Vol. 6, 329-334.

Tomlinson, w. J., Stolen, R. H. and Shank, C. V., 1984, "Compression of optical pulses chirped by self-phase modulation in fibers," *J. Opt. Soc. Am. B*, Vol. 1, 139-149.

Treacy, E. B., 1969, "Optical pulse compression with diffraction gratings," *IEEE J. Quantum. Electron.* Vol. QE-5, 454-458.

Valdmanis, J. A., 1978, "Real time picosecond optical oscilloscope," *Picosecond Phenomena, Springer Series in Chemical Physics* Vol. 4, ed C. V. Shank, E. P. Ippen and S. L. Shapiro, Berlin: Springer-Verlag (1978), 82-85.

Valdmams, J. A. and Fork, R. L., 1986, "Design consederation for a femtosecond pulse laser balancing self phase modulation, group velocity dispersion, saturable absorption and saturable gain," *IEEE J. Quantum Elentron.* Vol. QE-22, 112-118.

Valk, B., Hodel, W. and Weber, H. P., 1985, "Stimulated Raman spectra generated by ps-pulses in a single-mode fiber," *Opt. Commun.* Vol. 54, 363-368.

Vanherzeele, H., 1990, "Picosecond laser system continuously tunable in the 0.6-4 μm range," *Appl. Opt.* Vol. 29, 2246-2258.

Vodop'yanov, K. L., Grudinin, A. B., Dianov, E. M., Kulevskii, L. A., Prokhorov, A. M. and Khaidarov, D. V., 1987, "Generation of pulses of 100-200 fsec duration by stimulated Raman scattering in a single-mode fiber waveguide at wavelengths 1.5-1.7 μm," *Sov. J. Quantum Electron.* Vol. 17, 1311-1313.

Wai, P. K. A., Menyuk, C. R., Chen, H. H. and Lee, Y. C., 1986, "Solitons at the zero dispersion wavelength of single-mode fibers," *Ultrafast Phenomena V, Springer Series in Chemical Physics*, Vol. 46, eds. G. R. Fleming and A. E. Siegmen,Berlin: Springer-Verlag (1986), 65-67.

Walker, C. T., 1975, "Light scattering," *Laser applications to optics and spectroscopy, Physics of Quantum Electronics* Vol. 2, eds. S. F. Jacobs, M. O. Scully, and M. Surgent III, London: Addison-Wesley Publishing Company (1975), 281-350.

Van Stryland, E. W., 1979, "The effect of pulse to pulse variation on ultrashort pulsewidth measurements," *Opt. Commun.* Vol. 31, 93-96.

Washio, K., Inoue, K. and Tanigawa, T., 1980, "Efficient generation of near-I. R. stimulated light scattering in optical fibres pumped in low-dispersion region at 1.3 μm," *Electron. Lett.* Vol. 16. 331-333.

Weber, H. P., 1967, "Method for pulsewidth measurement of ultrashort light pulses generated by phase-locked lasers using nonlinear optics," *J. Appl. Phys.* Vol. 38, 2231-2234.

Weber, H. P. and Danielmeyer, H. G., 1970, "Multimode effects in intensity correlation measurements," *Phys. Rev. A*, Vol. 2, 2074-2079.

Weiner, A. M. and Ippen, E. P., 1984, "Novel transient scattering technique for femtosecond dephasing," *Opt. Lett.* Vol. 9, 53-55.

Weiner, A. M., Heritage, J. P. and Thurston R. N., 1986, "Synthesis os phase-coherent, picosecond optical square pulses," Opt. Lett. Vol. 11, 153-155.

Weiner, A. M., Heritage, J. P. and Kirschner, E. M., 1988, "High-resolution femtosecond pulse shaping," *J. Opt. Soc. Am. B*, Vol. 5, 1563-1572.

Weiner, A. M., Heritage, J. P., Hawkins, R. J., Thurston, R. N., Kirschner, E. M., Leaird, D. E. and Tomlinson, W. J., 1988, "Experimental observation of the fundamental dark soliton in optical fibers," *Phys. Rev. Lett.* Vol. 61, 2445-2448.

Weiner, A. M., Heritage, J. P. and Stolen, R. H., 1988, "Self-phase modulation and optical pulse compression influenced by stimjlated Raman scattering in fibers," *J. Opt. Soc. Am. B*, Vol. 5, 364-372.

Wilbrandt, R. and Weber, H., 1975, "Fluctuations in mode-locking threshold due to statistics of spontaneous emission," *IEEE J. Quantum. Electron.* Vol. 11, 186-190.

Yajima, T., Yoshihara, K., Harris, C. B. and Shionoya, S. (ed), 1988, *Ultrafast Phenomena VI, Springer Series in Chemical Physics* Vol. 48, Berlin: Springer-Verlag.

Yakymyshyn, C. P. and Pollock, C. R., 1989, "Frequency-doubled, additive-pulse, mode-locked NaCl:OH^- laser," *Opt. Lett.* Vol. 14, 791-793.

Yakymyshyn, C. P., Pinto, J. F. and Pollock, C. R., 1989, "Additive pulse mode-locked NaCl:OH^- laser," *Paper FQ-3, Technical Digest of CLEO'89* (April 24-28, 1989, Baltimore USA) and also *Opt. Lett.*. Vol. 14, 621-623, 1989.

Yang, G. and Shen. Y. R., 1984, "Spectral broakening of ultrashort pulses in a nonlinear medium," *Opt. Lett.* Vol. 9, 510-512.

Yarborough, J. M. and Hobart, J., 1973, Post-Deadline Paper presented at IEEE / OSA *Conf. on Laser Engineering and Applications*, Washington, D. C..

Yariv, A., 1975, "Quantum electronics," 2nd Ed. New York: John Wiley & Sons. Inc..

Yariv, A., 1976, "Introduction to optical electronics," 2nd Ed. New York: Holt Rinehart and Winston.

Yariv, A. and Yen, P., 1984, "Optical waves in crystals," A Wiley-Interscience Publication, John Wiley & Sons, New York.

Yariv, A. and Yen, P., 1984, "Optical waves in crystals," Wiley Series in Pure and Applied Optics, New York: John Wiley & Sons, Inc. Chapters 8, 9.

Zakharov, V. E. and Shabat, A. B., 1972, "Exact theory of two-eimensional self-focusing and one-dimensional self-modulation of waves in nonlinear media," *Soviet Physics jetp.* Vol. 34, 62-69.

Zavoiskii, E. K. and Fanchenko, S. D., 1957, "Physical fundamentals of electron-optical chronographs," Sov. Phys. Doklady 1, 285-288.

Zhang, H., Dai, J., Wang, P. and Wu, L., 1989, "Self-focusing and self-trapping in new types of Kerr media with large nonlinearities," *Opt. Lett.* Vol. 14, 695-696.

Zhao, W. M. and Bourkoff, E., 1988, "Femtosecond pulse propagation in optical fibers: Higher order effects," *IEEE J. Quantum Electron.* Vol. 24, 365-372.

Zhu, X., Kean, P. N. and Sibbett, W., 1989, "Coupled-cavity mode-locking of a KCl:Tl laser using an erbium-doped optical fiber," *Opt. Lett.* Vol. 14, 1192-1194.

Zhu, X., Kean, P. N. and Sibbett, W., 1989a, "Spectral and temporal characterizations of coupled-cavity mode locking in a KCl:Tl color center laser," *IEEE J. Quantum Electron.*, Vol. 25, 2445-2453.

Zhu, X., Kean, P. N. and Sibbett, W., 1989b, "Coupled-cavity mode-locking of a KCl:Tl laser using an erbium-doped optical fiber," *Opt. Lett.*, Vol. 14, 1192-1194.

Zhu, X., Finch, A. and Sibbett, W., 1989c, "Intracavity and extracavity chirp compensation in a CCM KCl:Tl laser," *Paper 41, 9th National Quantum Electronics Conference (QE-9)* (September 18-22, 1989, Oxford, UK).

Zhu, X., Finch, A. and Sibbett, W., 1990a, "Frequency-chirp compensation in a CCM KCl:Tl laser,"*J. Opt. Soc. Am. B.* Vol. 7, 187-192.

Zhu, X., Finch, A. and Sibbett, W., 1990b, "Pulse shaping effect in a coupled-cavity mode-locked KCl:Tl laser," *J. Opt. Soc. Am. B.* Vol. 7, 1221-1224.

Zhu, X. and Sibbett, W., 1990c, "Experimental study of the primary mode-locking parameters of a coupled-cavity KCl:Tl color-center laser," *Paper CFN4, Technical Digest of CLEO'90* (May 16-18, 1990, Anaheim USA), and also *J. Opt. Soc. Am. B.* Vol. 7, 2187-2191.

Zhu, X. and Sibbett, W., 1990d, "Intracavity characterisation of erbium-doped fiber using a coupled-cavity mode-locked KCl:Tl color center laser," *Opt. Commun.* Vol. 76, 340-344.

Zhu, X., Sleat, W., Walker, D. and Sibbett, W., 1990e, "Pulse evolution in a coupled-cavity mode-locked KCl:Tl color-center laser," *Ultrafast Phenomena VII, Springer Series in Chemical Physics*, Vol. 53, ed. C. B. Harris, E. P. Ippen, G. A. Mourou, A. H. Zewail, Berlin: Springer-Verlag (1990), 87-89.

Zhu, X. and Sibbett, W., 1991, "Propagation characteristics of femtosecond pulses in erbium doped monomode optical fibers," *IEEE J. Quantum Electron.* Vol. 27, 101-113.

Zook, B. J., Yakymyshyn, C. P. and Pollock, C. R., 1991, "Numerical optimization of the additive-pulse mode-locked laser," to be published.

Publications

[1] P. N. Kean, X. Zhu, D. W. Crust, R. S. Grant, N. Langford and W. Sibbett, "Enhanced mode-locking of color center lasers," *Opt. Lett.* Vol. 14, 39-41, 1989.

[2] X. Zhu, P. N. Kean and W. Sibbett, "Spectral and temporal characterizations of coupled-cavity mode locking in a KCl:Tl color center laser," *IEEE J. Quantum Electron.* Vol. 25, 2445-2453, 1989.

[3] X. Zhu, P. N. Kean and W. Sibbett, "Coupled-cavity mode-locking of a KCl:Tl laser using an erbium-doped optical fiber," *Opt. Lett.* Vol. 14, 1192-1194, 1989.

[4] X. Zhu, A. Finch and W. Sibbett,"Frequency-chirp compensation in a coupled-cavity mode-locked KCl:Tl laser," *J. Opt. Soc. Amer. B.* Vol. 7, 187-192, 1990.

[5] X. Zhu, A. Finch and W. Sibbett, "Pulse shaping effect in a coupled-cavity mode-locked KCl:Tl laser." *J. Opt. Soc. Amer. B.* Vol. 7, 1221-1224, 1990.

[6] X. Zhu and W. Sibbett, "Experimental study of the primary mode-locking parameters of a coupled-cavity KCl:Tl color center laser," *J. Opt. Soc. Amer. B.* Vol. 7, 2187-2191, 1990.

[7] X. Zhu and W. Sibbett, "Intracavity characterisation of erbium-doped fiber using a coupled-cavity mode-locked KCl:Tl color center laser," *Opt. Commun.* Vol. 76, 340-344, 1990.

[8] A. Finch, X. Zhu, P. N. Kean and W. Sibbett, "Noise characterization of mode-locked color-center laser sources," *IEEE J. Quantum Electron.* Vol. 26, 1115-1123, 1990.

[9] X. Zhu and W. Sibbett, "Propagation characteristics of femtosecond pulses in erbium doped monomode optical fibers," *IEEE J. Quantum Electron.* Vol. 27, 101-113, 1991.

[10] X. Zhu, W. Sleat, D. Walker and W. Sibbett, "Pulse evolution in a coupled-cavity mode-locked KCl:Tl color-center laser," *Picosecond Phenomena VII, Springer Series in Chemical Physics* Vol. 53, eds. C. B. Harris, E. P. Ippen, G. A. Mourou and A. H. Zewail, Berlin: Springer-Verlag, 87-89, 1991.

[11] J. Chen, X. Zhu and W. Sibbett, "Derivation of threshold pump power of erbium doped fibre laser," accepted for publication in *Opt. Lett.* 1991.

[12] J. Chen, X. Zhu and W. Sibbett, "An analytical expression for the output power characteristics of erbium-doped fiber lasers," submitted to *J. Opt. Soc. Amer. B.*